CHARACTERIZATION OF THE ELECTROPHYSIOLOGICAL PROPERTIES OF HUMAN PLURIPOTENT STEM CELL DERIVED NEURONS (HPSC) FROM FRAGILE X SYNDROME PATIENTS

A THESIS TO BE SUBMITTED TO

THE UNIVERSITY OF TRANS-DISCIPLINARY HEALTH SCIENCES AND TECHNOLOGY

FOR THE AWARD OF THE DEGREE OF
DOCTOR OF PHILOSOPHY
BY

SHREYA PARTHADAS SHARMA

UNDER THE GUIDANCE OF

PROF. SUMANTRA CHATTARJI
GKVK-POST,
BELLARY ROAD,
BANGALORE-560065

PROF. DAVID WYLLIE
HUGH ROBSON
BUILDING, 15 GEORGE SQUARE, EDINBURGH
EH8,9XD

INSTITUTE FOR STEM CELL SCIENCE AND REGENERATIVE MEDICINE

FEBRUARY-2021

THE UNIVERSITY OF TRANS-DISCIPLINARY HEALTH SCIENCES AND TECHNOLOGY
Private University Established in Karnataka by ACT 35 of 2013
BENGALURU - 560064

THE UNIVERSITY OF TRANS-DISCIPLINARY HEALTH SCIENCES AND TECHNOLOGY

Private University Established in Karnataka by ACT 35 of 2013
BENGALURU - 560064

CERTIFICATE

This is to certify that the work incorporated in this thesis **"Characterization of the electrophysiological properties of human pluripotent stem cell derived neurons (hPSC) from fragile X Syndrome patients"** submitted by Shreya Parthadas Sharma was carried out under my supervision. No part of this thesis has been submitted for a degree or examination at any university. References, help and material obtained from other sources have been duly acknowledged. I hereby confirm the originality of the work and that there is no plagiarism in any part of the dissertation.

S. Chattarji

Research Supervisor

Date: 3-9-2021

Prof. Sumantra Chattarji,

Director, Centre for Brain Development and Repair (CBDR)

Institute for Stem Cell Science and Regenerative Medicine (inStem)

GKVK – Post, Bellary Road,

Bangalore 560065,

Karnataka, India

THE UNIVERSITY OF TRANS-DISCIPLINARY HEALTH SCIENCES AND TECHNOLOGY

Private University Established in Karnataka by ACT 35 of 2013
BENGALURU - 560064

CERTIFICATE

This is to certify that the work incorporated in this thesis **"Characterization of the electrophysiological properties of human pluripotent stem cell derived neurons (hPSC) from fragile X Syndrome patients"** submitted by Shreya Parthadas Sharma was carried out under my supervision. No part of this thesis has been submitted for a degree or examination at any university. References, help and material obtained from other sources have been duly acknowledged. I hereby confirm the originalitiy of the work and that there is no plagiarism in any part of the dissertation.

Co-Supervisor

Name, designation & address details

Prof. David Wyllie,

Professor of Ion Channel Physiology and Pharmacology; Director, Centre for Discovery Brain Sciences

Hugh Robson Building

15 George Square

Edinburgh, EH8 9XD

February-2021

Fragile X Syndrome (FXS) is an X-linked disorder and the most common form of inherited intellectual disability and autism. It is caused by an increased CGG triplet repeat mutation in the 5' UTR of the Fragile X mental retardation 1 (FMR1) gene, thereby silencing the gene and subsequent loss of its product. Data from animal models suggest that FMRP expression is necessary for proper neuronal development and normal synaptic physiology. Clinical investigations to develop FXS specific treatments based on the above preclinical findings have limited success.
Thus, it is imperative to look into more human-based FXS *in vitro* models using neural progenitor cells and compare them with the existing animal models of FXS. The neurons derived from human stem cells of patients with FXS can therefore serve as an invaluable model to study the progression of the symptoms of FXS in vitro and subsequently help in developing new therapies. In my PhD, I focused on studying the functional properties of human stem cell derived FXS neurons and rescuing the potential defects.

Results:

• Neurons lacking FMRP exhibit aberrant network activity when co-cultured with primary mouse astrocytes – high frequency bursts but shorter duration than control neurons.

• Neurons lacking FMRP display reduced persistent sodium channel current (I_{NaP}) and reduced persistent big conductance calcium-activated potassium (BKCa) current.

• Human astrocytes derived from pluripotent stem cells modulate the network activity of hPSC derived cortical neurons, mediated through the astrocyte conditioned medium (ACM).

• ACM mediates these effects is through the molecule S100β, which potentiates the persistent sodium channel.

Conclusion:

• Co-culturing the hPSC derived cortical neurons with primary mouse astrocytes led to the development of spontaneous neuronal network activity.

• Loss of FMRP led to aberrant network activity of neurons characterized by high frequency, short duration bursts.

• I_{NaP} is reduced in neurons lacking FMRP. Potentiating I_{NaP} with veratridine, "rescues" the aberrant network activity of FMRP-lacking neurons.

• Astrocytes modulate the neuronal network activity as shown by co-culturing the hPSC derived cortical neurons with hPSC derived astrocytes. This effect is mediated by the ACM.

• The ACM could be modulating the neuronal activity via the S100β molecule which is secreted by the astrocytes.

Fragile X Syndrome (FXS) is an X-linked disorder and the most common form of inherited intellectual disability and autism. It is caused by an increased CGG triplet repeat mutation in the 5' UTR of the Fragile X mental retardation 1 (FMR1) gene, thereby silencing the gene and subsequent loss of its product. Data from animal models suggest that FMRP expression is necessary for proper neuronal development and normal synaptic physiology. Clinical investigations to develop FXS specific treatments based on the above preclinical findings have limited success.
Thus, it is imperative to look into more human-based FXS *in vitro* models using neural progenitor cells and compare them with the existing animal models of FXS. The neurons derived from human stem cells of patients with FXS can therefore serve as an invaluable model to study the progression of the symptoms of FXS in vitro and subsequently help in developing new therapies. In my PhD, I focused on studying the functional properties of human stem cell derived FXS neurons and rescuing the potential defects.

Results:

• Neurons lacking FMRP exhibit aberrant network activity when co-cultured with primary mouse astrocytes – high frequency bursts but shorter duration than control neurons.

• Neurons lacking FMRP display reduced persistent sodium channel current (I_{NaP}) and reduced persistent big conductance calcium-activated potassium (BKCa) current.

• Human astrocytes derived from pluripotent stem cells modulate the network activity of hPSC derived cortical neurons, mediated through the astrocyte conditioned medium (ACM).

• ACM mediates these effects is through the molecule S100β, which potentiates the persistent sodium channel.

Conclusion:

• Co-culturing the hPSC derived cortical neurons with primary mouse astrocytes led to the development of spontaneous neuronal network activity.

• Loss of FMRP led to aberrant network activity of neurons characterized by high frequency, short duration bursts.

• I_{NaP} is reduced in neurons lacking FMRP. Potentiating I_{NaP} with veratridine, "rescues" the aberrant network activity of FMRP-lacking neurons.

• Astrocytes modulate the neuronal network activity as shown by co-culturing the hPSC derived cortical neurons with hPSC derived astrocytes. This effect is mediated by the ACM.

• The ACM could be modulating the neuronal activity via the S100β molecule which is secreted by the astrocytes.

DECLARATION BY THE CANDIDATE

I declare that this thesis entitled "**Characterization of the electrophysiological properties of human pluripotent stem cell derived neurons (hPSC) from fragile X Syndrome patients**" submitted for the award of Doctor of Philosophy to THE UNIVERSITY OF TRANS-DISCIPLINARY HEALTH SCIENCES AND TECHNOLOGY, Bengaluru, is my original work, conducted under the supervision of my guides Prof. Sumantra Chattarji and Prof. David Wyllie. I also wish to inform that no part of the research has been submitted for a degree or examination at any university. References, help, and material obtained from other sources have been duly acknowledged.

I hereby confirm the originality of the work and that there is no plagiarism in any part of the dissertation.

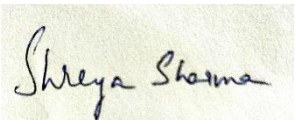

Place: Bengaluru **Signature of the Candidate**

Date: 3-9-2021

Name of candidate: Shreya Parthadas Sharma

Reg. No.: 21117020493
(10/11/2017) Pre-registration
(12/6/2019) Registration

Acknowledgements

The course of pursuing a PhD degree in biological sciences is a fulfilling albeit a demanding task. I take this opportunity to express my gratitude to everyone who has helped me in this journey.

This project would not have been possible at all without Dr. Rakhi Pal, Bharath Reddy, Krishna Kumar Samaga, Durga Jeyalakshmi and Nikhita Aannaiyappa. Their consistent efforts made sure that the cells were successfully generated and healthy for my electrophysiology experiments. I extend my immense gratitude towards them.

I would like to thank my research supervisors, Prof. Sumantra Chattarji and Prof. David Wyllie for giving me the opportunity to pursue this doctoral research. Without Shona's and David's persistent guidance this thesis would not have shaped up. Shona has always made sure that the resources to conduct the experiments are always available. He has allowed me the freedom to follow the science wherever it may lead. This has helped me to develop a self-sufficiency that is necessary to continue in this field. From the start, David has consistently provided feedback on all the electrophysiology experiments. Despite geographical barriers, he made sure that the experiments are always discussed at length, which has been instrumental in maintaining the CBDR-Edinburgh collaboration. His critical feedback on how best to communicate the science has made me more confident.

I have also had the pleasure of interacting with Prof. Siddharthan Chandran and I am very grateful for his constant support and insights into the stem cell biology. I would like to thank my doctoral advisory committee member, Prof. Gaiti Hasan for her valuable help and advice over the years.

I would like to thank Dr. Bhuvaneish Selvaraj for all the isogenic cell lines. I've had the pleasure of discussing my work with him and his feedback has always been very helpful. I would also like to extend my gratitude to Dr. Matthew Livesey. Without his help, I would not have been able to standardize the various electrophysiology protocols.

I am deeply grateful to Giselle Fernandes and Farhana Yasmin for helping me with the basics of whole-cell patch clamp technique. I also wish to thank Zubin Rashid for helping me troubleshoot whenever any noise issue cropped up in the patch-clamp rig. I also wish to acknowledge the entire BliSc community, laboratory kitchen, library facility, administration, and purchase and accounts departments.

These years at the BliSc campus have been both very fun and also very frustrating especially when experiments flopped. I would not have been able to survive the crazy hours without the support and

companionship of my friends. I would especially like to thank Vidya, Durga, Lavanyaa, Rashmi, Parul, Calvin, Neel, Deepanjali, Rohini and Suranjana and many more. I would also like to acknowledge the present and past lab members. They have always been ready with help and support and made sure working in the lab was fun and stimulating.

Lastly and most importantly, I would like to thank my family whose constant love and support has made this journey possible. My father and my brother, Arnav have always provided me with helpful suggestions in dealing with stress and anxiety during the bad days. Finally, I thank my mom who is my greatest support and cheerleader. She always made sure that I know what my priorities are. Without her constant love and encouragement, I would not have been able to pursue and complete this thesis.

Table of Contents

List of tables

List of figures

List of abbreviations

AP	Action potential
ATP	adenosine tri phosphate
ALDH1L1	Aldehyde dehydrogenase 1 family, member L1
ACM	Astrocyte conditioned medium/media
AD	Alzheimer's disease
ALS	Amyotrophic lateral sclerosis
AMPA	α-amino-3-hydroxy-5-methyl-4-isoxazolepropionic acid
APC	Astrocyte progenitor cell
AP5	D-2-amino-5-phosphonopentanoate
ASD	Autism Spectrum Disorders
BK_{Ca}	Big conductance calcium-activated potassium channel
BDNF	Brain derived neurotrophic factor
CNS	Central nervous system
DKK1	dickkopf protein
DS	Down's syndrome
DMEM	Dulbecco's modified eagle medium
ESC	Embryonic stem cell
ERP	Event related potential
EPSC	Excitatory postsynaptic current
FBS	Fetal bovine serum
FGF	Fibroblast growth factor
FXTAS	Fragile X associated tremor/ataxia syndrome
FMRP	Fragile X mental retardation protein
FXS	Fragile X Syndrome
GABA	Gamma-aminobutyric acid
GDNF	Glial cell line derived neurotrophic factor
GFAP	Glial fibrillary acidic protein
GLAST	Glutamate-aspartate transporter
gRNA	guide RNA
HITS-CLIP	High-throughput sequencing of RNAs isolated by crosslinking immunoprecipitation
hNA	Human nuclear antigen
hPSC	Human pluripotent stem cell
iPSC	Induced pluripotent stem cell
ICM	Inner cell mass
IL	Interleukin
I_{BKCa}	Big conductance, calcium activated potassium current
I_{NaP}	Persistent sodium current
I_{NaT}	Transient sodium current
KO	Knockout

K_{Na}	Slack Na^+ activated K^+ channel
LTD	Long-term depression
LTP	Long-term potentiation
mGluR	Metabotropic glutamate receptor
Map2	Microtubule associated protein
mEPSC	Miniature excitatory postsynaptic current
miPSC	Miniature inhibitory postsynaptic current
MEF	Mouse embryonic fibroblast
MEA	Multiple ekectrode array
MBP	Myelin binding protein
mRNA	messenger RNA
NPC	Neural precursor cell
NO	Nitric oxide
NMDA	N-methyl-D-aspartate
NMR	Nuclear magnetic resonance
NEAA	Non-essential amino acid
NaP	Persistent sodium channel
PAR-CLIP	Photoactivable ribonucleoside-enhanced crosslinking and immunoprecipitation
PSC	Pluripotent stem cell
PET	Positron Emission Tomography
PND	Post natal day
PM	Pre mutation
PGD	Preimplantation genetic diagnosis
POI	Premature ovarian failure
RMP	Resting membrane potential
RT-qPCR	Reverse transcriptase quantitative polymerase chain reaction
RNA	Ribonucleic acid
SCID	Severe combined immunodeficiency disease
STR	Short tandem repeat
SK_{Ca}	Small conductance calcium-activated potassium channel
Shh	Sonic hedgehog signaling
TSC	Tenascin
TEA	Tetraethyammonium
TTX	Tetrodotoxin
TSP-1	Thrombospondin-1
TMS	Transcranial magnetic stimulation
TGFβ	Transforming growth factor β
WT	Wild-type

DECLARATION BY THE CANDIDATE

I declare that this thesis entitled "**Characterization of the electrophysiological properties of human pluripotent stem cell derived neurons (hPSC) from fragile X Syndrome patients**" submitted for the award of Doctor of Philosophy to THE UNIVERSITY OF TRANS-DISCIPLINARY HEALTH SCIENCES AND TECHNOLOGY, Bengaluru, is my original work, conducted under the supervision of my guides Prof. Sumantra Chattarji and Prof. David Wyllie. I also wish to inform that no part of the research has been submitted for a degree or examination at any university. References, help, and material obtained from other sources have been duly acknowledged.

I hereby confirm the originality of the work and that there is no plagiarism in any part of the dissertation.

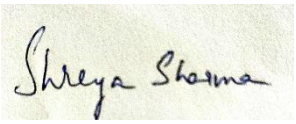

Place: Bengaluru **Signature of the Candidate**

Date: 3-9-2021

Name of candidate: Shreya Parthadas Sharma

Reg. No.: 21117020493
(10/11/2017) Pre-registration
(12/6/2019) Registration

Acknowledgements

The course of pursuing a PhD degree in biological sciences is a fulfilling albeit a demanding task. I take this opportunity to express my gratitude to everyone who has helped me in this journey.

This project would not have been possible at all without Dr. Rakhi Pal, Bharath Reddy, Krishna Kumar Samaga, Durga Jeyalakshmi and Nikhita Aannaiyappa. Their consistent efforts made sure that the cells were successfully generated and healthy for my electrophysiology experiments. I extend my immense gratitude towards them.

I would like to thank my research supervisors, Prof. Sumantra Chattarji and Prof. David Wyllie for giving me the opportunity to pursue this doctoral research. Without Shona's and David's persistent guidance this thesis would not have shaped up. Shona has always made sure that the resources to conduct the experiments are always available. He has allowed me the freedom to follow the science wherever it may lead. This has helped me to develop a self-sufficiency that is necessary to continue in this field. From the start, David has consistently provided feedback on all the electrophysiology experiments. Despite geographical barriers, he made sure that the experiments are always discussed at length, which has been instrumental in maintaining the CBDR-Edinburgh collaboration. His critical feedback on how best to communicate the science has made me more confident.

I have also had the pleasure of interacting with Prof. Siddharthan Chandran and I am very grateful for his constant support and insights into the stem cell biology. I would like to thank my doctoral advisory committee member, Prof. Gaiti Hasan for her valuable help and advice over the years.

I would like to thank Dr. Bhuvaneish Selvaraj for all the isogenic cell lines. I've had the pleasure of discussing my work with him and his feedback has always been very helpful. I would also like to extend my gratitude to Dr. Matthew Livesey. Without his help, I would not have been able to standardize the various electrophysiology protocols.

I am deeply grateful to Giselle Fernandes and Farhana Yasmin for helping me with the basics of whole-cell patch clamp technique. I also wish to thank Zubin Rashid for helping me troubleshoot whenever any noise issue cropped up in the patch-clamp rig. I also wish to acknowledge the entire BliSc community, laboratory kitchen, library facility, administration, and purchase and accounts departments.

These years at the BliSc campus have been both very fun and also very frustrating especially when experiments flopped. I would not have been able to survive the crazy hours without the support and

companionship of my friends. I would especially like to thank Vidya, Durga, Lavanyaa, Rashmi, Parul, Calvin, Neel, Deepanjali, Rohini and Suranjana and many more. I would also like to acknowledge the present and past lab members. They have always been ready with help and support and made sure working in the lab was fun and stimulating.

Lastly and most importantly, I would like to thank my family whose constant love and support has made this journey possible. My father and my brother, Arnav have always provided me with helpful suggestions in dealing with stress and anxiety during the bad days. Finally, I thank my mom who is my greatest support and cheerleader. She always made sure that I know what my priorities are. Without her constant love and encouragement, I would not have been able to pursue and complete this thesis.

Table of Contents

List of tables

List of figures

List of abbreviations

AP	Action potential
ATP	adenosine tri phosphate
ALDH1L1	Aldehyde dehydrogenase 1 family, member L1
ACM	Astrocyte conditioned medium/media
AD	Alzheimer's disease
ALS	Amyotrophic lateral sclerosis
AMPA	α-amino-3-hydroxy-5-methyl-4-isoxazolepropionic acid
APC	Astrocyte progenitor cell
AP5	D-2-amino-5-phosphonopentanoate
ASD	Autism Spectrum Disorders
BK_{Ca}	Big conductance calcium-activated potassium channel
BDNF	Brain derived neurotrophic factor
CNS	Central nervous system
DKK1	dickkopf protein
DS	Down's syndrome
DMEM	Dulbecco's modified eagle medium
ESC	Embryonic stem cell
ERP	Event related potential
EPSC	Excitatory postsynaptic current
FBS	Fetal bovine serum
FGF	Fibroblast growth factor
FXTAS	Fragile X associated tremor/ataxia syndrome
FMRP	Fragile X mental retardation protein
FXS	Fragile X Syndrome
GABA	Gamma-aminobutyric acid
GDNF	Glial cell line derived neurotrophic factor
GFAP	Glial fibrillary acidic protein
GLAST	Glutamate-aspartate transporter
gRNA	guide RNA
HITS-CLIP	High-throughput sequencing of RNAs isolated by crosslinking immunoprecipitation
hNA	Human nuclear antigen
hPSC	Human pluripotent stem cell
iPSC	Induced pluripotent stem cell
ICM	Inner cell mass
IL	Interleukin
I_{BKCa}	Big conductance, calcium activated potassium current
I_{NaP}	Persistent sodium current
I_{NaT}	Transient sodium current
KO	Knockout

K_{Na}	Slack Na^+ activated K^+ channel
LTD	Long-term depression
LTP	Long-term potentiation
mGluR	Metabotropic glutamate receptor
Map2	Microtubule associated protein
mEPSC	Miniature excitatory postsynaptic current
miPSC	Miniature inhibitory postsynaptic current
MEF	Mouse embryonic fibroblast
MEA	Multiple ekectrode array
MBP	Myelin binding protein
mRNA	messenger RNA
NPC	Neural precursor cell
NO	Nitric oxide
NMDA	N-methyl-D-aspartate
NMR	Nuclear magnetic resonance
NEAA	Non-essential amino acid
NaP	Persistent sodium channel
PAR-CLIP	Photoactivable ribonucleoside-enhanced crosslinking and immunoprecipitation
PSC	Pluripotent stem cell
PET	Positron Emission Tomography
PND	Post natal day
PM	Pre mutation
PGD	Preimplantation genetic diagnosis
POI	Premature ovarian failure
RMP	Resting membrane potential
RT-qPCR	Reverse transcriptase quantitative polymerase chain reaction
RNA	Ribonucleic acid
SCID	Severe combined immunodeficiency disease
STR	Short tandem repeat
SK_{Ca}	Small conductance calcium-activated potassium channel
Shh	Sonic hedgehog signaling
TSC	Tenascin
TEA	Tetraethyammonium
TTX	Tetrodotoxin
TSP-1	Thrombospondin-1
TMS	Transcranial magnetic stimulation
TGFβ	Transforming growth factor β
WT	Wild-type

1.1 Fragile X Syndrome

In 1938, Lionel Penrose studied 1280 cases of intellectual disability and observed that more males are afflicted with intellectual disability than females (Penrose, 1938). This observation has been strengthened across the years by numerous studies across countries like USA, Canada, Australia and Europe (Baird & Sadvonick, 1985; McLaren & Bryson, 1987; Stevenson *et al.,* 1996). In 1943, Martin and Bell provided the first definitive evidence of X-linked intellectual disability based on a pedigree where mental retardation appeared to follow an X-linked inheritance pattern (Martin & Bell, 1943). Lubs, in 1969 first observed a "fragile" site on the X chromosome after karyotyping cultured leucocytes from families with X-linked mental retardation (Lubs, 1969). The intellectual disorder with this cytogenetic marker was appropriately named as Fragile X Syndrome.

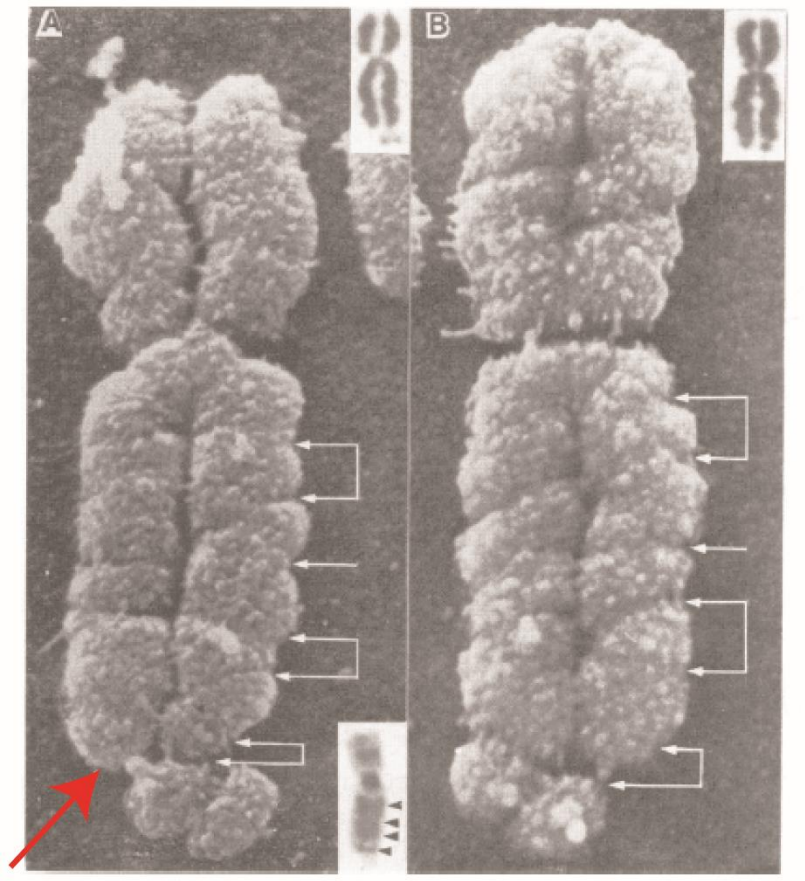

Figure 1.1 The scanning micro electrograph image (× 9500) of fragile X chromosomes. The "fragile" site (red arrow) can be easily identified *Adapted from Harrison et al., 1983.*

FXS is caused by the CGG repeat expansion in the 5' untranslated region (5' UTR) of the fragile X mental retardation (*FMR1*) gene. The *FMR1* gene maps at the Xq27.3 band (Bell *et al.,* 1991; Verkerk *et al.,* 1991)

and due to this FXS is more prevalent in males (1:4000) than females (1:6000-8000). The normal CGG repeat size ranges from 5 to 44. Repeat numbers of 55-200 is considered as a pre mutation (PM). The pathophysiology of PM is different than FXS – premature ovarian failure (POI) in females and Fragile X associated tremor/ataxia syndrome (FXTAS) in males. FXS is associated with a CGG repeat expansion more than 200. The consequence of this repeat expansion is hypermethylation of the *FMR1* promoter, inhibiting the *FMR1* transcription which leads to loss of expression of FMRP (the protein product of *FMR1* (Crawford *et al.,* 2001, Hagerman, 2008, Ciaccio *et al.,* 2017). The disorder usually manifests at an early age and individuals exhibit a wide variety of symptoms like - learning disabilities, anxiety, unstable mood, attention deficit, hyperactivity, seizures and altered social behavior. Physical abnormalities in males include long face, large protruding ears and macroorchidism. (Hagerman *et al.,* 1986, Freund & Reiss, 1992). The behavioral abnormalities are usually less severe in females (Nussbaum & Ledbetter, 1986; Bagni *et al.,* 2012). Autism Spectrum Disorders (ASD) occurs as a common comorbidity with FXS. It is estimated that about 30-50% males and 25% females suffering from FXS also show autistic behaviour (Hagerman *et al.,* 1986; Miles 2011), thus making FXS the most common monogenic cause of ASD.

1.2 FMRP – role in translational regulation

Since the identification of the *FMR1* gene, considerable efforts have been made over the years to undertand the structure and function of its protein product. Studies showed presence of RNA binding sites on FMRP suggesting a potential role in translation. The amino acid sequence of FMRP revealed three RNA-binding motifs - two KH domains and arginine-glycine-glycine (called RGG boxes) (Ashley *et al.,* 1993; Siomi *et al.,* 1993). A patient with a point mutation in one of the KH domains but normal CGG repeat length showed severe mental retardation (De Boulle *et al.,* 1993) indicating that mRNA binding to FMRP is a critical step in the proper functioning of the protein. FMRP has been shown to associate with actively translating polyribosomes (Corbin *et al.,* 1997; Stefani *et al.,* 2004) and acts as a translational repressor by stalling the ribosome translocation (Darnell *et al.,* 2011). The loss of FMRP thus leads to an increase in protein synthesis (Bakker *et al.,* 1994, Zalfa *et al.,* 2003). High-throughput sequencing of RNAs isolated by crosslinking immunoprecipitation (HITS-CLIP) identified ≈800 neuronal mRNAs that were regulated by FMRP in the mouse brain (Darnell *et al.,* 2011). A study using photoactivable ribonucleoside-enhanced crosslinking and immunoprecipitation (PAR-CLIP) identified ≈6000 mRNAs that could potentially bind to FMRP (Ascano *et al.,* 2012). A recent study has identified *FMR1* targets in human dorsal and ventral forebrain neural progenitor cells (Li *et al.,* 2020). FMRP has been known to regulate transport, stability

and regulation of neuronal mRNAs encoding proteins that are involved in maintaining and regulating synaptic structure and function (Bagni & Greenough, 2005, Neves-Pereira *et al.,* 2009, Darnell *et al.,* 2011).

1.3 *Fmr1* KO mouse model

Many animal models have been developed to study the pathophysiology of FXS including zebrafish, drosophila, mouse and rat (Tucker *et al.,* 2004; McBride *et al.,* 2012; Bakker *et al.,* 1994; Hamilton *et al.,* 2014). Much of the FXS pathophysiology now understood is derived from studies using the *Fmr1* KO mice. The *Fmr1* KO mouse model was developed and characterized initially by the Dutch-Belgian Fragile X Consortium. It was developed using a homologous recombination targeting vector containing a disrupted *Fmr1* DNA sequence with an insertion of a neomycin casette in exon 5 (KO allele). This was inserted into embryonic stem cells which were then transferred to a pseudo-pregnant female mice of the C57BL/6 mouse strain (Bakker *et al.,* 1994). The resultant *Fmr1* KO mice were unable to produce FMRP protein, but did contain detectable levels of *Fmr1* mRNA (Yan *et al.,* 2004). Since its development, the *Fmr1* KO mouse model has provided us with extensive mechanistic details about the role of FMRP in maintaining neuronal function. However inspite of their advantage as a tool to elucidate the molecular and signalling pathways involved in FXS, the animal models are not without their limitations. One of the major limitation is these animal models mimicking the CGG-repeat expansion mediated silencing do not show the hypermethylation pattern seen in humans (Brouwer *et al.,* 2007). These limitations associated with the animal models make it necessary to study FXS in more human relevant models.

1.4 FMRP and cortex

Event related potential recordings (ERP) and transcranial magnetic stimulation (TMS) studies have suggested that there are deficits in the cortical activity and plasticity in patients suffering from FXS (Molen *et al.,* 2012; Oberman *et al.,* 2010, Kogan *et al.,* 2004). Whole-cell patch clamp studies from *Fmr1* KO mice show an increase in neuronal excitability in different regions of the cortex. This increase in neuronal hyperecxitability is characterized by an increase in firing frequency of the FXS neurons (Deng *et al.,* 2013; Deng *et al.,* 2016; Zhang *et al.,* 2014). Consequently this also leads to an increase in the circuit excitability (Gibson *et al.,* 2008; Hays *et al.,* 2011; Goncalves *et al.,* 2013). The hyperexcitability of the cortical neurons have been a hallmark of FXS. Recent studies however have shown that this hyperexcitability phenotype is not uniform. A study using primary mouse cortical neurons has shown that loss of FMRP has no impact on the baseline firing frequency and the synaptic activity (Bulow *et al.,* 2019). Another study suggests a hypoexcitabilty phenotype of the visual cortex in the *Fmr1* KO mice (Berzhanskaya *et al.,* 2016). FMRP is

ubiquitously expresed in the CNS of mammals throughtout development (Gholizadeh *et al.,* 2015). Thus understanding the role of FMRP in regulation of neuronal development in the cortex is crucial. FMRP influences both function and morphology of neurons. Studies on cortical post-mortem tissues from adult FXS patients show abnormalities in density, length and morphology of the dendritic spines (Churchill *et al.,* 2002; Greco *et al.,* 2002). The dendritic spines in the neocortex and visual cortex of FXS patients show an immature morphology (Hinton *et al.,* 1991; Irwin *et al*., 2001). Interestingly, dendritic spine studies in *Fmr1* KO mouse models also show a similar phenotype. The spines from the layer V visual cortex and the occipital cortex of an *Fmr1* KO mouse shows significantly higher number of longer spines (more filopodia like and thin-headed) which are known to be immature than shorter spines (mushroom-headed/stubby). The overall spine density was also greater in the *Fmr1* KO animals (Irwin *et al.,* 2002; McKinney *et al.,* 2006, Grossman *et al.,* 2006). The overall changes in the number of neurons and glial cells across the neocortex absence of FMRP further reiterates the importance of FMRP during cortical development (Lee *et al.,* 2019). While considerable insights have been gleaned into the FXS pathophysiology in the cortex using animal models, it is very important to study FXS in human cortical neurons. In this thesis, we will provide an in-depth analysis of how loss of FMRP leads to functional deficits in human cortical neurons.

1.5 FMRP and ion channels

Voltage-gated sodium channels play a critical role in generation and propagation of action potentials. In addition to the fast activating and inactivating sodium current (I_{NaT}), some cells also possess an inactivating component called as the persistent sodium current (I_{NaP}) (reviewed in Kiss, 2008). Some of FMRP's targets include mRNAs that encode proteins for ion channels or their regulation (Darnell *et al.,* 2011). Several ion channels have been reported to be dysregulated in the absence of FMRP. Studies investigating prefrontal and entorhinal cortical neuron dysfunction in *Fmr1*$^{-/y}$ mice concluded that the hyperexcitability displayed by these neurons was due to an increase in transient (I_{NaT}) (Routh *et al.,* 2017) and persistent (I_{NaP}) (Deng & Klyachko, 2016) sodium currents. FMRP has also been known to interact with mRNAs encoding potassium channels. Voltage gated potassium channels Kv3.1 b and Kv4.2 mRNA are confirmed targets of FMRP (Darnell *et al.,* 2011, Gross *et al.,* 2011). Kv3.1 b plays an important role in neurons that have a high spike rate with spike frequencies > 300 Hz (Gan & Kaczmarek, 1998). Loss of FMRP leads to altered levels of Kv3.1 b and an aberration in the sound detection by *Fmr1* KO mice (Strumbos *et al.,* 2010). Kv4.2 is one of the major channels that regulates neuronal excitability in hippocampal neurons. FMRP acts as a positive regulator of the Kv4.2 mRNA. Consequently, loss of FMRP leads to reduced levels of Kv4.2 and a concomitant increase in neuronal excitability (Gross *et al.,* 2011). Deng and colleagues observed a

broadening of action potentials (AP) in the CA3 and cortical pyramidal neurons of *Fmr1* KO mice. This modulation of AP duration by FMRP is via big conductance calcium-activated potassium (BK_{Ca}) channels. FMRP directly interacts with the β4 subunit of the BK_{Ca} channel and loss of FMRP leads to a decrease in the BK_{Ca} current conductance (Deng *et al.,* 2013). Genetic upregulation of the BK_{Ca} channels can correct the AP duration defects even in the absence of FMRP (Deng & Klyackho, 2016). FMRP also interacts directly with the Slack Na^+ activated K^+ channel (K_{Na}) via the channel's cytoplasmic C-terminal domain and enhances the channel activity (Brown *et al.,* 2010; Zhang *et al.,* 2012). Other ion channels modulated by FMRP and thereby influencing spiking activity of the neurons also include small conductance calcium-activated potassium (SK_{Ca}) channels and HCN channels (Deng *et al.,* 2019; Brager *et al.,* 2012). Ligand-gated ion channels are also involved in the pathophysiology of FXS. Of these, the main ligand-gated channels affected in FXS are, NMDARs, AMPARs and $GABA_A$Rs. Studies using *Fmr1* KO mice have shown that the expression of GluA1 (AMPAR subunit) in the cortex is decreased, which leads to impaired LTP. The effect of FMRP on AMPARs is dependent on the brain region and the cell types (Deng & Klyachko, 2021). Studies have also shown that loss of FMRP leads to dysregulated NMDAR signaling in the hippocampus of mouse models (Toft *et al.,* 2016). There are very few studies that have looked at the effect of FMRP on NMDAR regulation. However, there are reports of reduced NMDA currents in the anterior piriform cortex of *Fmr1* KO mice (Gocel & Larson, 2012). In *Fmr1* KO mice, the NMDAR signaling is impaired in the layer IV stellate cells of the cortex (Booker et al., 2019). Thus, similar to AMPARs, the effect of FMRP on NMDARs is also brain region/cell specific. Studies on human patients and animal models have shown that in FXS, the function and expression of $GABA_A$R is impaired (Van der Aa & Kooy, 2020). This loss of $GABA_A$R leads to the hyperexcitability phenotype observed in FXS patients and animal models (Morin-Parent et al., 2019). Thus, loss of FMRP leads to deficits in voltage-gated and ligand-gated ion channels.

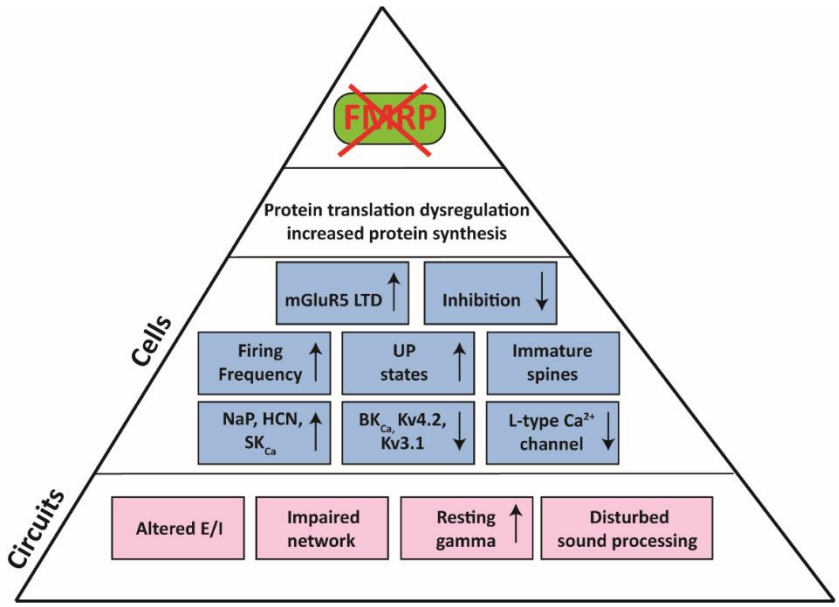

Figure 1.5 Summary of the cellular and behavioral impairments in the absence of FMRP.

1.6 Targeted treatments of FXS

Studies predominantly using the *Fmr1* KO mouse models have revealed several molecular signaling pathways which are affected in FXS. The key and most widely studied signaling pathway is the mGluR theory put forward by Mark Bear in 2004. According to this theory, absence of FMRP leads to an increased glutamatergic signaling through metabotropic glutamate receptor 5 (mGluR5) with a concomitant increase in protein synthesis and deficits in synaptic plasticity including enhanced long term depression (LTD) in the hippocampus (Bear *et al.,* 2004). In the amygdala *Fmr1* KO mice, absence of FMRP leads to impaired mGluR-dependent long term potentiation (LTP) and deficits in synaptic activity (Suvrathan *et al.,* 2010). The mGluR theory led to several clinical trials (reviewed in Ligsay & Hagerman, 2016) with mGluR anatagonists – fenobam (Berry-Kravis *et al.,* 2009), mavoglurant (Jacquemont *et al.,* 2011; Berry-Kravis *et al.,* 2016) and basimglurant (Quiroz *et al.,* 2016). Fenobam, mavoglurant and basimglurant showed good safety profiles but failed the efficacy tests. Thus though mGluR antagonists alleviated FXS symptoms in preclinical models, trials with human patients produced less favourable results indicating that the pathophysiology of FXS is more complicated.

The major inhibitory neurotransmitter in the brain is γ-aminobutyric acid (GABA). The GABA receptors are classified as $GABA_A$ (ionotropic) and $GABA_B$ (metabotropic). The binding of GABA to the receptors leads to an influx of chloride (Cl^-) into the cell, thus hyperpolarizing and ultimately inhibiting the postsynaptic neuron. In 2006, D'Hulst and colleagues reported a decrease in the expression levels of $GABA_A$ receptor in

the cortex of *Fmr1* KO mice (D'Hulst *et al.,* 2006). Many studies since then have corroborated this result and have also shown a decrease in $GABA_A$ receptor levels in the hippocampus and amygdala in the absence of FMRP with a concomitant decrease in inhibitory post synaptic currents and an overall increase in the excitability of the circuit (Olmos-Serrano *et al.,* 2010; Paluszkiewicz *et al.,* 2010). Positron Emission Tomography (PET) imaging also showed significant decrease in the $GABA_A$ levels in various parts of the brain of FXS patients (D'Hulst *et al.,* 2015). These promising results led to clinical trials using agonists of $GABA_A$ to potentiate its effects. Ganoxolone which improved the FXS symptoms like seizures, repetitive behaviours in *Fmr1* KO mice (Heulens *et al.,* 2012; Braat *et al.,* 2015) when tried on FXS patients of ages ranging from 6-17 years, failed to show any significant improvement (Ligsay *et al.,* 2017) when compared to the placebo group.

All the clinical trials summarized above, were conducted after obtaining successful results using the drugs in *Fmr1* KO mouse models. But these drugs did not fare very well in the clinical trials. While the FXS pathophysiology have been studied over the years in considerable details it is still poorly understood till date because of limitations of the model systems. It has been shown that despite the similarities in biochemical, phenotypical, and neuropathological features of *Fmr1* KO mice with those of humans, the abnormal methylation status observed in humans is not captured in *Fmr1* KO mice (Brouwer *et al.,* 2008). Moreover, data from primary human cell culture studies suggest that in humans, CGG amplification does not inhibit FMR1 transcription and production of FMRP in the absence of DNA methylation (Pietrobono *et al.,* 2005; Smeets *et al.,* 1995). Studies have also shown that the actual timing of FMR1 silencing is critical in the development of the symptoms (Eiges *et al.,* 2007). Thus, to fully understand the pathophysiology of FXS in humans, it is imperative to characterize FXS in more human – based models. Human pluripotent stem cell (hPSC) derived neurons are an attractive platform for studying the underlying mechanism of FXS because they can be obtained from the FXS patients (iPSCs) and the FXS mutation can be preserved during the reprogramming process. In addition, because hPSC derived neurons are usually present at early developmental stages, they provide insights into the role of FMRP in early neural development.

1.7 Human pluripotent stem cells

Stem cells are self-renewing cells present in the embryo and adult tissue. These cells can differentiate into any other cell type of the organism. Stem cells can be totipotent or pluripotent. Totipotent stem cells can give rise to the entire organism, e.g. the zygote. These cells can give rise to the three germ layers and the

extraembryonic membranes. Pluripotent stem cells (PSCs) can give rise to the three germ layers but not the extraembryonic membranes (reviewed in Zakrzewski *et al.,* 2019).

Human pluripotent stem cells (hPSCs) include embryonic stem cells (ESCs) and induced pluripotent stem cells (iPSCs). Because stem cells can be differentiated into several neural cell types, including neurons and astrocytes, they have become an invaluable platform to model neurodevelopmental diseases.

Human embryonic stem cells are isolated from the inner-cell mass (ICM) of the preimplantation embryo (reviewed in Vazin & Freed, 2010). Following the establishment of first stable mouse embryonic stem cell lines (Martin, 1981; Evans & Kauffman, 1981), Thomson and colleagues, in 1998 successfully isolated hESC lines from human embryos. These isolated cells retained the two most important features critical to stem cells – self renewal and pluripotency (Thomson *et al.,* 1998). Karyotyping of these cells when grown on mouse embryonic fibroblast (MEF) feeders revealed them to be karyotypically normal. These cells could also generate large cell tumors comprising of several types tissue (teratoma) when grafted into immunodeficient (SCID) mice (Bosma *et al.,* 1983; reviewed in Vazin & Freed, 2010). In a set of pioneering experiments, Sir John Gurdon in 1962, reported the generation of tadpoles from enucleated fertilized frog ova that had been transplanted with nuclei from intestinal epithelial cells of tadpoles. This was the first example of cellular reprogramming of somatic cells (Gurdon, 1962). The iPSC technology was developed by Shinya Yamanaka and Kazutoshi Takahashi in 2006. They generated mouse iPSC lines by reprogramming a mouse fibroblast by retroviral delivery of four reprogramming transcription factors, Oct3/4, Sox2, Klf4 and c-Myc (together known as Yamanaka factors) (Takahashi & Yamanaka, 2006). In 2007, Yamanaka and colleagues applied the same technology to generate human induced pluripotent stem cells (reviewed in Omole & Fakoya, 2018). The iPSCs are self-renewing in culture and like the ESCs can give rise to cells from the three germ layers. Unlike the ESCs, use of iPSCs do not warrant as much ethical considerations, hence use of iPSCs in disease modelling has been very appealing. The ability of self-renewal renders the hPSCs as an invaluable tool for basic as well as translational research purposes. However, because of the tumorigenic capacity of the pluripotent stem cells, these cells in an undifferentiated stage cannot be used for patient-specific treatment. Hence, over the years several strides have been made to develop protocols for differentiating the pluripotent stem cells into specific cell types.

1.8 Generation of cortical neurons from hPSCs

The cortex is a target for many neurodevelopmental diseases like autism spectrum disorders (ASD), Down's syndrome and several neurodegenerative diseases such as Alzheimer's, Parkinson's, Huntington's.

The human cerebral cortex is an incredibly complex and stratified structure. Different areas of the cortex are responsible for integration of sensory and motor information and memory formation. The arrangement and diverse cell types present in the different layers are crucial for proper functioning of the cortex. These cell types can be excitatory or inhibitory and differ in their gene expression profiles, morphology and functional properties (Molyneaux *et al.,* 2007).

Most of the studies investigating cortical development and neuronal function have used rodent models. However, the development of human cortex distinctly differs in several aspects from rodent cortex. These include the micro cytoarchitecture, tangential expansion of the frontal cortex and gyrencephaly (Defelipe, 2011; Liu *et al.,* 2011). This makes it difficult to model neurodevelopmental disorders in rodent. As discussed in the above section, pluripotent stem cells can differentiate into several cell types. Recently, several labs have developed sophisticated protocols to differentiate the hPSCs into cortical neurons, primarily pyramidal neurons which are the chief excitatory neurons in the cortex (reviewed in Yap & Winkler, 2015).

Neural differentiation of hPSCs is dependent on a complex interplay of activation and inhibition of several molecular signaling pathways controlled by morphogens, cytokines, and growth factors. Over several years better understanding of the various signaling pathways involved in development has led to refining of neural differentiation protocols. One of the most widely used process of neural induction is dual inhibition of SMAD signals, developed by Chambers and colleagues in 2009. Several studies on *Xenopus laevis* demonstrated that inhibition of bone morphogenetic protein (BMP) by Noggin, Follistatin and Chordin is an important process in neural development of the embryo via the SMAD signaling pathways (Smith & Harland, 1992; Smith *et al.,* 1993). SMAD proteins are components of the TGFβ signaling pathway (reviewed in Moustakas *et al.,* 2001). Chambers and colleagues used two SMAD inhibitors, Noggin and SB431542 (Chambers *et al.,* 2009) and reported successful neural conversion of hPSCs in an adherent cell culture condition. Early development comprises of the formation of the forebrain from the anterior neuroectoderm (Wilson & Houart, 2007). Morphogen gradient based dorso-ventral patterning of the forebrain leads to the development of the dorsally positioned telencephalon, which included the cerebral cortex (Wilson & Rubenstein, 2000). The telencephalon has several multipotent precursor (NPCs) cells which are very important for corticogenesis (Azzarelli *et al.,* 2015). The dorsal NPCs predominantly express the transcription factor, PAX6 (reviewed in Osumi *et al.,* 2008). The neuroepithelia derived from hPSCs are organized radially, called “neural rosettes” (Zhang *et al.,* 2001). These rosettes assume a primitive anterior identity by default (Pankratz *et al.,* 2007). Protocols have evolved to derive specific neural

subtypes by modulating pathways such as WNT signaling under dual-SMAD inhibition conditions. Activation of WNT signaling pathway, leads to the generation of cells from the neural crest lineage (Mica *et al.,* 2013, Menendez *et al.,* 2011), whereas inhibition of WNT signaling results enhances formation of forebrain precursors using small molecule antagonists like DKK1, confirmed by the expression of forebrain fate marker, FOXG1 (Maroof *et al.,* 2013; Qi *et al.,* 2017). The FOXG1 positive telencephalic progenitors can be patterned to dorsal or ventral precursors, and subsequently to mature glutamatergic or GABAergic cortical neurons. Dorsal fate of the precursors can be achieved by external treatment with retinoic acid or inhibiting Sonic hedgehog (Shh) signaling. The resultant dorsal telencephalic precursors (NPCs) are positive for PAX6 and terminal differentiation into cortical glutamatergic neurons can be achieved by removal of fibroblast growth factor (FGF2) from the culture medium (reviewed in McCaughey-Chapman & Connor, 2018).

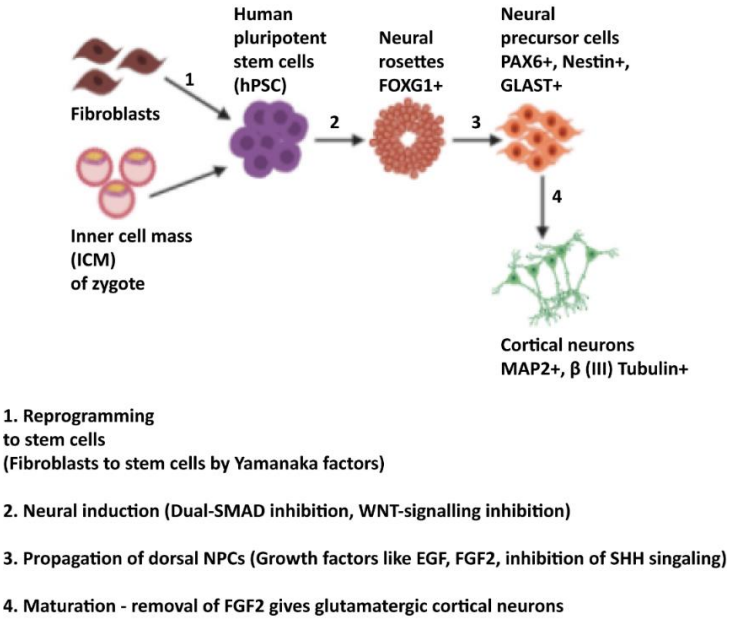

Figure 1.8 Schematic showing the different steps for the generation of cortical neurons from hPSCs.

1.9 Astrocytes

Astrocytes are a type of glial cell and the most abundant cell in the central nervous system (Volterra & Meldolesi, 2005). Ramon y Cajal published two seminal papers in 1897 and 1913, focusing on neuroglia. Cajal proposed the “insulation theory” which is that astrocytes function as cellular insulators separating the activity of neurons around them (reviewed in Navarrete & Araque, 2014). This is probably the first-time astrocytes were thought of as active components in modulation of neuronal function. This theory, however, did not gain traction until recently, over hundred years later. The predominant view of the

function of astrocytes has been their role in providing nourishment and support to the neurons. This "nutrition theory" was originally proposed by Golgi in 1903. This theory relegated astrocytes to a passive role without any direct involvement in the processing of information in the brain. Astrocytes are not electrically excitable cells and because the information transfer in the brain is via passage of electricity, the neurons emerged as the champions. Subsequently all the studies aimed at understanding the structure and function of the neurons. Similarly, understanding of neurodevelopmental and neurodegenerative diseases was restricted to studying neuronal dysfunction.

Astrocytes are divided into two types depending on their morphology and location – 1) protoplasmic astrocytes are found in the grey matter with long, thick, and highly ramified processes, located near the periphery of the blood vessels and 2) fibrous astrocytes, found in the white matter where their processes pass between the nerve fibres (reviewed in Kettenmann & Verkhratsky, 2008, 2011). A number of immunological markers have been used to study the morphology of astrocytes. Of these, the predominant marker for astrocytes was glial fibrillary acidic protein (GFAP), however GFAP only marks the primary branches which represents only ≈ 15% of the total astrocyte volume (Bushong *et al.,* 2002). Other markers like Glt-1 (glial glutamate transporter), GLAST (glutamate-aspartate transporter) and ALDH1L1 (aldehyde dehydrogenase 1 family, member L1) (Rothstein *et al.,* 1994; Cahoy *et al.,* 2008) show significant promise in elucidating the complex morphology of mammalian astrocytes though a specific marker for mature astrocytes doesn't exist yet.

Advancement in fluorescent dyes and microscopy in 1990s led to several studies that reported astrocytes displaying cellular excitability through variations in their intracellular calcium concentrations (Cornell-Bell *et al.,* 1990; Charles *et al.,* 1991; Perea & Araque, 2006). These calcium transients occurred spontaneously, but could also be evoked by synaptic activity and sensory stimuli (Wang *et al.,* 2006; Perea *et al.,* 2009; Takata *et al.,* 2011; Araque *et al.,* 2014) thus challenging the passive role of the astrocytes. A number of neurotransmitters such as glutamate, GABA, acetylcholine, dopamine, serotonin, adenosine tri phosphate (ATP) and nitric oxide (NO) are able to elicit calcium response from astrocytes (reviewed in Perea *et al.,* 2009; Araque *et al.,* 2014). Several studies conducted by Ben Barres in 1990s showed that the astrocytes also displayed several ligand and voltage-gated ion channels (reviewed in Barres *et al.,* 1990). In an isolated culture of astrocytes from optic nerve of rats, he showed the presence of voltage-gated potassium channels like inward rectifying potassium channel (K_{IR}) and delayed rectifier potassium channels (K_D) (Barres *et al.,* 1990). Although astrocytes are non-excitable, there are multiple evidences of them possessing voltage-gated sodium channels. The earliest evidence came from studies on cultured

astrocytes from rats (Bevan *et al.,* 1985) which shows fast-inactivating, TTX sensitive sodium currents. Subsequent whole-cell patch clamp studies have corroborated the presence of functional voltage-gated sodium channels in astrocytes (Barres *et al.,* 1988, 1989; Sontheimer *et al.,* 1992).

Astrocytes are secretory cells. Many of the physiological functions are performed by the proteins secreted by them. These include:- thrombospondins for regulation of synapse formation (Christopherson *et al.,* 2005), metallothionein for axonal regeneration (Chung *et al.,* 2008), TGF-β for prevention of apoptosis (Dhandapani & Brann, 2003), several cytokines, chemokines, and protease inhibitors (Lafon-Cazal *et al.,* 2003; Moore *et al.,* 2009; Delcourt *et al.,* 2005; Keene *et al.,* 2009). All the above studies have provided ample evidence to establish the role of astrocytes in modulating neuronal function and vice-versa, thus it is important to study the astrocyte dysfunction in disorders of the CNS.

1.10 Astrocytes in FXS

In healthy CNS tissue, astrocytes maintain homeostasis of extracellular ions, neurotransmitters, provide glucose metabolites to neurons, regulate local blood flow, modulate synapse development and plasticity and play an essential role in neural circuit function and behaviour (see reviews, Verkhratsky & Nedergaard, 2018; Magistretti & Allaman, 2018; MacVicar & Newman, 2015; Khakh, 2019). However, during injury or disease of the CNS, the astrocytes become reactive and the process is termed reactive astrogliosis. Astrocyte reactivity can lead to a diver change in the astrocyte morphology with a concomitant change in its physiological functions (reviewed in Sofroniew & Vinters, 2010).

FMRP was thought to be expressed predominantly in the neurons with negligible expression in the mature glial cells, rendering studies examining FXS pathophysiology to focus solely on the neurons (Bakker *et al.,* 2000; Devys *et al.,* 1993). In 2004, Wang and colleagues reported expression of FMRP in oligodendrocyte precursor cells (OPC) but not in mature oligodendrocytes. They suggested that during OPC development, FMRP binds the mRNA of myelin binding protein (MBP) and suppresses its translation. Post differentiation, FMRP expression is downregulated resulting in increase of MBP (Wang *et al.,* 2004). Pacey and Doering observed co-expression of FMRP and GFAP in differentiated neurospheres isolated from mouse brain suggesting the presence of FMRP in glial lineage (Pacey & Doering, 2007). Immunohistochemical studies of cingulate cortex, hippocampus, striatum, corpus callosum and cerebellum of wild-type mice revealed FMRP to be expressed until post natal day (PND) 10, and a decrease in FMRP expression thereafter. However, in corpus callosum FMRP expression continued until adulthood (Gholizadeh *et al.,* 2015). From these studies it is clear that *in vitro* and *in vivo*, FMRP is expressed in developing astrocytes. The pioneering

experiments that established the role of astrocytes in FXS pathophysiology came from Laurie Doering's group. Using a co-culture system consisting of mouse primary hippocampal neurons and astrocytes form *Fmr1* KO mice, they demonstrated that the hippocampal neurons exhibited abnormal dendritic morphology. To further cement their observations, they studied the dendritic morphology of *Fmr1* KO neurons plated on WT and *Fmr1* KO astrocytes. The *Fmr1* KO neurons when plated with WT astrocytes displayed normal dendritic phenotype suggesting that WT astrocytes can "rescue" the FXS phenotype (Jacobs & Doering, 2010).

Astrocytes exert their effect through secretions and contact-mediated (reviewed in Cheng *et al.,* 2012). Several studies have shown that neurons with media conditioned by astrocytes enhances synapse efficacy (Pfrieger & Barres, 1997; Nagler *et al.,* 2001; Ullian *et al.,* 2001). Recent studies have started looking at how the loss of FMRP affects the astrocyte secretome. Doering's group showed downregulation of the secreted thrombospondin-1 (TSP-1) protein in astrocytes cultured from *Fmr1* KO mouse, (Cheng *et al.,* 2016), and enhanced expression of Tenascin (TSC) and its downstream target interleukin-6 (IL-6) in *Fmr1* KO astrocytes (Krasovka & Doering, 2018). Astrocyte secretory protein S100β which also serves as a marker for astrocytes (Raponi *et al.,* 2009) was elevated in the cerebellum of *Fmr1 KO* mice (Pacey *et al.,* 2015). Interestingly S100β is a calcium-binding protein, and it is implicated in modulating the network activity of neurons (Morquette *et al.,* 2015). S100β overexpression and concomitant aberrant calcium signaling and neuronal dysfunction has also been found in hPSC model of Down's syndrome which can be rescued by addition of astrocyte conditioned media from control astrocytes (Chen *et al.,* 2014; Mizuno *et al.,* 2018). Indeed, children with autism spectrum disorder show an increase S100β levels in the serum (Al-Ayadhi & Mostafa, 2012; Guloksuz *et al.,* 2017; Ayaydin *et al.,* 2020). Thus there is clear evidence of the astrocytes being affected by the loss of FMRP. Furthermore, above studies suggest that healthy astrocytes or the secretome from healthy astrocytes can aid in correcting the FXS phenotype, thereby providing a host of new therapeutic targets to explore. In this thesis, we will study the impact of astrocytes on synapse and network efficacy of the hPSC derived cortical neurons. We will also provide a mechanistic basis of FMRP modulation of neuronal network activity through the astrocytes.

1.11 Modelling FXS in hPSC derived neurons

FXS hESCs- Verlinsky and colleagues in 2005 were the first to isolate FXS hESCs from preimplantation embryos carrying the FXS mutation identified by preimplantation genetic diagnosis (PGD) (Verlinsky *et al.,* 2005, reviewed in Bhattacharyya & Zhao, 2016). In 2007, Rachel Eiges and colleagues, generated and characterized FXS hESCs. They showed that even though the FXS hESCs retained full mutation in the *FMR1*

gene, the promotor region is unmethylated and in the undifferentiated state, the *FMR1* gene could still be transcribed and translated (Eiges *et al.,* 2007). This is in agreement with reports by Sutherland and colleagues in 1992, who had observed hypermethylation and lack of *FMR1* translation in embryonic tissue but found that the chorionic villi of 13-week-old fetus still retained *FMR1* expression (Sutherland *et al.,* 1991). Subsequent establishment of multiple FXS hESC lines however have shown that hypermethylation and loss of *FMR1* expression can also be acquired in undifferentiated cells (Avitzour *et al.,* 2014). Thus, the actual timing of epigenetic silencing of *FMR1* gene is still debatable and more studies are needed to arrive at a conclusion.

The generation and characterization of cortical neurons derived from FXS hESCs was from Dalit Ben-Yosef's group in 2013. They reported abnormal gene expression (low expression of PAX6 and SOX1, β III tubulin) and neurogenesis in the early stages of development. The neurons derived from FXS hEPSCs had less firing frequency than control neurons and did not show considerable response to glutamate (Telias *et al.,* 2013). In a more comprehensive study, they reported that neurons derived from FXS hEPSCs could fire single action potential in response to depolarizing current steps. The synaptic activity of the FXS neurons was diminished as compared to controls and the FXS neurons displayed low sodium and potassium currents (Telias *et al.,* 2015). In the subsequent chapters of this thesis, we will look at the action potential, synaptic and network properties of cortical neurons derived from FXS hESCs.

FXS hiPSCs – Studies describing FXS hiPSCs are relatively few (reviewed in Bhattacharyya & Zhao, 2016). Sheridan and colleagues generated iPSCs from fibroblasts of three FXS patients, of which one was a mosaic donor. The *FMR1* gene was methylated and epigenetically silenced in the iPSCs (Sheridan *et al.,* 2011) in contrast to what was seen in the FXS hESCs. Thus, until the differences in FXS-hESCs and hiPSCs are delineated it is necessary to study the two together. The neuronal progenitor cells derived from from the FXS-iPSCs exhibited shorter and fewer processes than controls. Another study reported downregulation of several genes related to neuron differentiation, axogenesis, and axon guidance pathway in the FXS-iPSC derived neurons (Halevy *et al.,* 2015). Doers and colleagues reported defects in neurite outgrowths in the FXS iPSC derived neurons (Doers *et al.,* 2014). Recently a study using a micro-raft culture method, showed pre-synaptic vesicle recycling is reduced in FXS-hiPSC derived neurons (Niedringhaus *et al.,* 2015). Another recent study reported an increase in spontaneous recordings using multiple electrode array (MEA) recordings. Transient transfection of WT *FMR1* mRNA into the FXS cultures resulted in partial rescue of the aberrant spontaneous activity of the FXS-hiPSC derived neurons (Graef *et al.,* 2020). The diversity in the results obtained from FXS-hESC and hiPSC studies and the limited number of such studies highlight

the acute need to study FXS in hESC and hiPSC together and comprehensively analyze the effect of loss of FMRP on cortical neuronal development and function.

1.12 Differences between mouse and human astrocytes

In this thesis we will show results of co-culturing hPSC derived neurons with both primary mouse astrocytes (Chapter 4) and hPSC derived astrocytes (Chapters 5 and 6). To understand the profound effect exerted by the human astrocytes on the human neurons discussed in the later chapters, it is first important to discuss the differences between mouse and human astrocytes. In the human cortex, the ratio of astrocytes to neurons is ≈ 1.6 times than that of mice, making astrocytes the most abundant cell in the human cortex (Nedergaard *et al.,* 2003). Oberheim and colleagues published a seminal study detailing the structural and functional differences between human and mouse astrocytes. They showed that human cortical astrocytes are larger ≈ 3 times and extend ≈ 10 times the number of processes than the mouse astrocytes. The microanatomy of the end-feet (specialized structures that contact the vasculature) of protoplasmic astrocytes differed between humans and mice. The speed of the calcium wave transmission was significantly higher in human cortical astrocytes (43.4 ± 4.7 μm/s) than mouse astrocytes (8.6 ± 0.6 μm/s). Human astrocytes respond to ATP and glutamate through rises in intracellular calcium similar to rodents, however the rate of signal transmission is greater in humans than their rodent counterpart (Oberheim *et al.,* 2009). Thus several differences in morphology and function between rodent and human astrocytes necessitate the use of human astrocytes in conjunction with human astrocytes.

The first human astrocytes were cultured in 1990s from fetal and adult post-mortem tissues however these cultures were contaminated with other cell types (Ennas *et al.,* 1992; Lee *et al.,* 1993). The advent of stem cell technology in recent years has made it possible to derive astrocytes from human pluripotent stem cells. Lee and colleagues were the first group to generate GFAP+ astroglia from hESC by inhibition of sonic hedgehog (SHH) signaling at the neural induction stage. The first chemically-defined protocol for developing astrocytes from hPSCs was reported by Su-Chun Zhang's group (Krencik *et al.,* 2011). Their protocol consisted of three stages – induction of neuroepithelium, generation of astrocyte progenitor cells and maturation of astrocytes by maintaining the astrospheres. Several protocols since then have been developed to generate functional astrocytes from human pluripotent stem cell cells.

In this thesis, we have used stem cell derived neurons (iPSC and ESC) to study the role of FMRP in the regulation of neuronal function. The several aims of this thesis are:

- To analyze the effect of loss of FMRP on the firing and synaptic activity of hPSC derived neurons.

- Understanding FMRP's function in maintaining proper neuronal network activity.
- Glial modulation of neuronal function.

The findings detailed in this study show for the first time the role of FMRP in modulating the network activity of human neurons. Another novel feature of this thesis is an in-depth analysis of glia-neuron crosstalk and how glial cells are key modulators of neuronal function hence providing a new framework for studying FXS and other neurodevelopmental diseases.

2.1 Culture and propagation of hIPSC and hESC:

The materials and methods outlined here, have been published in

Das Sharma S, Pal R, Reddy BK, Selvaraj BT, Raj N, Samaga KK, Srinivasan DJ, Ornelas L, Sareen D, Livesey MR, Bassell GJ, Svendsen CN, Kind PC, Chandran S, Chattarji S & Wyllie DJA (2020). Cortical neurons derived from human pluripotent stem cells lacking FMRP display altered spontaneous firing patterns. *Mol Autism* **11** 52. doi: 10.1186/s13229-020-00351-4. PMID: 32560741

In this study, the hiPSC (human induced pluripotent stem cell) lines used were:

SC 176 (healthy male), SC 128 (fragile X syndrome male) hereby will be referred to as **CON1** and **FXS1** respectively. These were obtained from Dr. Philip H. Schwartz at Children's Hospital of Orange County's National Human Neural Stem Cell Resource (http://nhnscr.org/). Fibroblast lines were reprogrammed at the Laboratory for Translational Cell Biology at Emory University (Atlanta, GA) using established protocols and under institutional approval.

Early passage fibroblasts were cultured in fibroblast medium ((10% ES-qualified FBS, 0.1 mM NEAA, 55 µM β-mercaptoethanol, high glucose DMEM with Glutamax) for two days. On day 0, fibroblasts were transduced with a cocktail of KOS, hc-Myc, hKlf4 (Yamanaka factors) using Sendai virus. Cells were fed with the fibroblast medium every alternate day for one week.

Day 7 – Cells were passaged onto vitronectin (Thermofisher) coated coverslips at a density of 250,000 – 500,000 cells/well.

Day 8 onwards cells were fed with fibroblast medium every day and colonies began to emerge after 7-10 days.

Individual hiPSCs were picked manually and transferred to a vitronectin or Matrigel (BD Biosciences) coated dish. These colonies were expanded as clonal lines. These were fed everyday with complete mTesR1 medium (Stem Cell Technologies) and passaged every 5-7 days with complete mTesR1 medium (Stem Cell Technologies).

ND30625 (healthy male), GM07072 (fragile X syndrome male), GM05848 (fragile X syndrome male) hereby will be referred to as **CON2**, **FXS2** and **FXS3** respectively. These fibroblasts were obtained from the Coriell Institute of Medical Research under their consent and privacy guidelines as described on their website (http://catalog.coriell.org/). The generation of hIPSCs was carried out at Cedar-Sinai Medical Centre (LA, CA).

Fibroblasts were re-programmed into non-integrating and virus free hIPSCs by nucleofecting them with episomal plasmids that expressed the reprogramming factors OCT4, SOX2, KLF4, L-MYC, LIN28 and shRNA to TP53. Using a battery of characterization tests for pluripotency like hiPSC Scorecard Assay, PluriTest, and RT-qPCR, the newly reprogrammed hiPSCs were confirmed to be pluripotent. Further authentication of the iPSCs were also performed by matching the short tandem repeat (STR) profiles with the parental tissue source (fibroblasts) to ensure the correct identity of the cell lines.

The hESC (human embryonic stem cell) Shef 4, hereafter called *FMR1*$^{+/y}$ was obtained from UK stem cell bank. From Shef 4 using CRISPR-Cas9 technology (D'Souza *et al.,* 2019), *FMR1* was deleted to yield the Shef 4 null line hereafter called *FMR1*$^{-/y}$*.*

Xeno-free and feeder free medium, Essential 8 (Thermo Fisher Scientific) was used to culture and propagate the stem cells. The cultures were done using 6-well plates (Nunc Nunclon delta surface, Thermo Fisher Scientific) coated with reduced growth-factor Matrigel (Corning Inc, New York, NY) at 37°C, 5% CO_2 in a humidified incubator. The cells were cultured till 90% confluence and then enzymatically passaged for propagation and cryopreservation.

ID in manuscript	**ID at source**	**Age (years)**	**Sex**	**Reprogrammed cell line name**	**Re-programming method**	**Starting cell type**	**G band karyotype**
CON1	SC176	14	M	SC176	Sendai virus	Fibroblast	Normal
CON2	ND30625	76	M	CS25iCTR-18nxx	Episomal vectors	Fibroblast	Normal
FXS1	SC128	23	M	SC128	Sendai virus	Fibroblast	Normal
FXS2	GM07072	22	M	CS072iFXS-n4	Episomal vectors	Fibroblast	Normal
FXS3	GM05848	4	M	CS8488iFXS-n5	Episomal vectors	Fibroblast	Normal
FMR1$^{+/y}$	SHEF 4	ESC	M	NA	NA	-	Normal
FMR1$^{-/y}$	SHEF 4-*FMR1* null	ESC	M	ESC- CRISPR Cas 9 edited	NA	-	cNormal

Table 2.1 Details of cell lines used in this study.

2.2 Generation of NPCs and neurons:

Cortical NPCs were derived from the hESC and hIPSC cells using previously published protocols. Human cortical neurons were then generated from NPCs.

- NPCs were plated on to 13 mm glass coverslips (VWR, Radnor, PA) coated with poly-L-ornithine, laminin, fibronectin (Sigma, St. Louis, MO) and reduced growth-factor Matrigel at 30,000 cells / coverslip in default medium; maintained at 3% O_2, 5% CO_2, 37°C for 1 week (days 1-7)
- For further 2 weeks (day 8-21) default + forskolin (Tocris, UK) was added.
- Default + forskolin media was supplemented with BDNF and GDNF and added to the cells for further 5 weeks (days 22-56)
- At the 8th week, neurons were used for electrophysiology experiments.

2.3 Generation of primary rodent astrocytes:

Astrocytes were isolated from the cerebral cortex of E18.5 CD1 mice. Cortices were dissected, enzymatically digested and mechanically dissociated. Astrocytes were plated on poly-D-lysine and laminin (Sigma) coated plates in medium containing DMEM supplemented with 10% FBS (Thermo Fisher Scientific) and passaged twice prior to co-culturing with neurons on a 24 well- plate. For co-cultures, human NPCs (30,000 cells/cover-slip) were plated on to a layer of astrocytes and differentiated into neurons in a humidified incubator (5% CO2) at 37°C for 8 weeks.

2.4 Generation of astrocytes from iPSC and ESC

IPSCs and ESCs were neuralized and then converted to spheres as described earlier (Bilican et al., 2012; Serio et al., 2013). Next, to induce astrogliogenesis spheres were subjected to glial enrichment medium for 2 weeks before being cultured in glial maturation medium for 4 weeks. At the end of this conversion phase, medium was switched to glial enrichment medium to maintain the proliferation of astrocyte progenitor cells (APCs) in spheres. These astrospheres were dissociated into single cells using the Papain Dissociation System (Worthington Biochemical) and plated onto 6-well Matrigel (BD Biosciences, 1:80 diluted) coated plates to obtain monolayers of APCs, which were subsequently differentiated into astrocytes by switching the medium to astrocyte differentiation medium for 2 weeks. All media were changed every 2–3 days during the astrocyte generation process.

2.5 Gene-correction of FXS iPSC lines

CRISPR/Cas9 genome editing to remove pathogenic CGG repeats from FXS iPSC lines were performed by Ms. Tuula Ritakari, a PhD student in Prof Chandran lab, University of Edinburgh (UK). Briefly, two guide

RNAs flanking the *FMR1* 5'UTR CGG repeat were used to excise the repeat from the genome (gRNA-1: 5'-GACGGAGGCGCCGCTGCCAG-3'; gRNA-2: 5'-GCCCGCAGCCCACCTCTCGG-3'). The gRNAs were cloned into pSpCas9-2A-GFP (Addgene: px458) vector and 2 ug of each plasmid together with 1 ug of an eGFP-puromycin resistance plasmid were transfected into iPSC. Four hundred individual clones for each line were picked and screened for FMRP re-expression by antibody staining for FMRP. Successful clones were further screened for deletion of the CGG repeat by PCR flanking the CGG repeats (Fw: 5'-tgcgctactttgaaccggacc-3'; Rev: 5'-gactccgagaggccctagcg-3') and repeat primed PCR (South East Scotland Genetics Service, Western General Hospital, Edinburgh). Demethylation of the FMR1 promoter site upstream of the 5'UTR was confirmed with bisulphite sequencing and *FMR1* mRNA re-expression was confirmed in FMRP-positive clones with qPCR.

2.6 Western Blotting:

Pellets of hiPSC and hESC were lysed using lysis buffer (50 mM Tris-HCL, pH 7.4, 2mM EDTA, 0.1% SDS, 1% Triton-X 100, 0.5% Na-deoxycholate, 150mM NaCl, protease and phosphatase inhibitor cocktails) followed by sonication (10 cycles of 30 s on/30 s off) and centrifugation at 13,000 rpm for 10 min. The supernatant was collected and using a BCA assay kit (Thermo Fisher Scientific), protein estimation was performed. On a precast NuPAGE 4–12% Bis-Tris Protein gel (Thermo Fisher Scientific), 20 mg/sample protein was loaded, followed by protein transfer to a PVDF membrane (GE Healthcare, Life science, Chicago, IL). The blot was blocked in 1:1 TBST (0.2M Trizma base, 0.15M NaCl, 0.1% Tween-20) and Odyssey blocking buffer (Li-COR Bioscience, Lincoln, NE) for 1 h at room temperature. The membrane was incubated with primary antibodies FMRP (1:1000, AbCam, Cambridge, UK) and β-actin (1:5000, Sigma), in blocking buffer for overnight at 4 °C, washed with TBST and incubated in secondary antibodies with IRDye 680RD and IRDye 800CW (Li-COR Bioscience) respectively for 1 h at room temperature. After multiple washes, the blot was dried and imaged using Li-COR Odyssey FC infrared system.

2.7 Immunohistochemistry:

hiPSCs, hESCs, NPCs and neurons were stained as per standard immunocytochemistry protocols. Cells were fixed with 4% PFA for 10 min followed by permeabilization for 5 min using 0.3% Triton X (USB Corporation, Cleveland, Ohio, OH). To block nonspecific antibody binding, cells were incubated in 3% BSA (Sigma) for 30 min. Following this, cells were incubated in primary antibody (Oct 4, 1:250, Santa Cruz

Biotechnology; Nanog, 1:100, R&D Systems; GFAP, 1:500, Sigma; Human nuclear antigen, 1:1000, Merck Millipore; MAP2, Sigma; Beta tubulin, Sigma) at room temperature and secondary antibody (1:1000) consecutively for 1 h each and then mounted on glass slides using Fluorsave (Sigma) and stored at 4 °C in the dark till imaging. Images were acquired using a confocal laser scanning microscope (Fluoview 3000 Olympus, Japan). hiPSC and ESC imaging was done using a × 40 (1.3 NA) oil immersion objective, and NPCs and co-culture images were captured using × 60 (1.4 NA) oil immersion objective with diode lasers 405 nm, 488 nm, 561 nm, and 640 nm. All images were captured at 512 × 512 pixels per inch; Z step size was set at 0.5 µm with 1 airy unit of pinhole diameter.

2.8 Electrophysiology:

Whole-cell patch clamp experiments were performed at room temperature (23 – 24°C). 13mm coverslips containing the human cortical neurons cultured for 8 weeks were transferred onto the electrophysiology chamber. Cells were perfused with an external recording solution comprising:

Ingredients	Concentration (in mM)
NaCl	152
KCl	2.8
HEPES	10
$CaCl_2$	2
Glucose	10
pH	7.3-7.4
Osmolarity	300-320 mOsm

Table 2.6 Composition of the external recording solution.

with a flow rate of approximately **1.35 ml per minute.** The liquid junction potential was calculated to be +14 mV (JPCalc, Clampex) and the values for membrane potential reported here do not take liquid junction potential into consideration.

The cells were viewed under an inverted microscope (Scientifica, UK) with a 40X, water-immersion objective (Olympus, Japan). Whole-cell current or voltage-clamp recordings were made using a Molecular Devices MultiClamp 700B amplifier (Molecular Devices, San Jose, CA).

Recording patch-pipettes, fabricated from thick-walled borosilicate glass, with a resistance of 3-4 MΩ were filled with an internal recording solution.

Current clamp internal solution:

Ingredients	Concentration (in mM)

K-gluconate	155
$MgCl_2$	2
HEPES	10
Na-PiCreatine	10
Mg_2-ATP	2
Na_3-GTP	0.3
pH	7.3
Osmolarity	280-290 mOsm

Table 2.6.1. Composition of the current clamp internal recording solution.

Voltage-clamp internal solution:

Ingredients	Concentration (in mM)
Cs-gluconate	110
CsCl	20
HEPES	10
NaCl	4
QX-314	5
EGTA	0.2
Na-PiCreatine	10
Mg_2-ATP	2
Na_3-GTP	0.3
pH	7.3
Osmolarity	280-290 mOsm

Table 2.6.2 Composition of the voltage clamp internal recording solution.

Data were filtered at either 3 kHz or 10 kHz, for voltage-clamp and current-clamp recordings, respectively, and digitized, via a Digidata 1550, at 20 kHz. Stimulation protocols were generated using pClamp 10.5 software and subsequent offline analysis was conducted using Clampfit 10.5 software.

2.9 Intrinsic properties

For calculation of the active and passive electrical properties, in current-clamp mode, the neurons were clamped at a voltage of -60 mV. Depolarizing steps of current were injected into the neurons. The protocol followed was: 500 ms long current steps ranging from -10 to +65 pA, with a step interval of 5pA. Passive properties calculated were: -

Resting membrane potential (RMP) – the membrane voltage of the neuron at rest.

Input resistance – input resistance was calculated in current – clamp mode from the sub-threshold current and the corresponding change in voltage steps using Ohm's law: **R = V/I**

Capacitance – The plasma membrane of the neuron acts as a capacitor. Whole- cell capacitance was measured from the capacitance cap on the pClamp software.

Rheobase – The minimum current required to elicit an action potential from the neuron.

The action potential parameters calculated were: -

Threshold – The potential to which a neuron must be depolarized to be able to fire an action potential.

Amplitude – Amplitude is measured from the baseline to the peak of the action potential. An immature neuron fires action potentials with lower amplitude.

Half-width – AP width at half the amplitude. As the neuron matures, AP half-with decreases.

Maximum number of Action potentials – The maximum number of action potentials fired by the neuron in response to any current step was calculated.

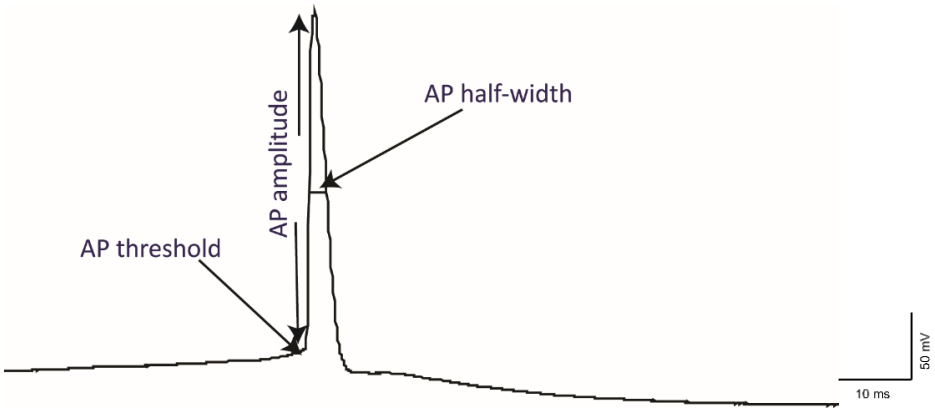

Fig 2.9 AP properties of a hPSC derived cortical neuron.

2.10 Synaptic properties

Spontaneous miniature synaptic responses are called excitatory postsynaptic currents (mEPSCs). These were recorded in voltage-clamp mode. The external recording solution was supplemented with tetrodotoxin (TTX; 500 nM) to block the sodium channels and hence the action potential dependent events. $MgCl_2$ (1.3 mM) was also added to block the NMDA receptor-component of synaptic events. Neurons were clamped at -60 mV and the events were recorded in the gap-free mode. Analysis of the amplitude and frequency of the mEPSC events were done offline.

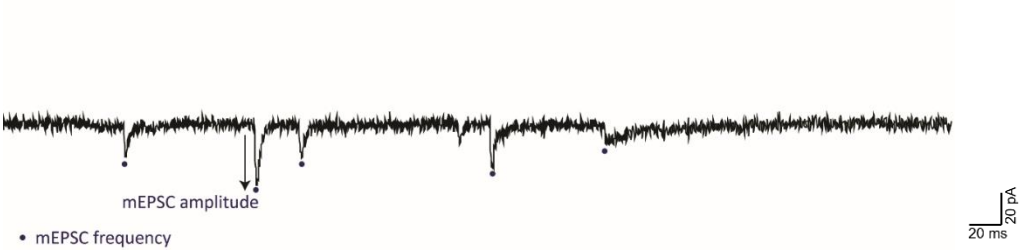

Fig 2.10 A voltage clamp recording showing the mEPSCs from a hPSC derived cortical neuron.

2.11 Burst properties

Spontaneous burst recordings were performed in current and voltage-clamp. The neurons were clamped at -70 mV. Bursts were defined as two or more action potentials occurring during a period of depolarization followed by a quiescent phase. The duration of action potential bursts were measured from the start of the first action potential to the time of the last action potential with bursts. The burst number was defined as the number of bursts in a 10 min recording.

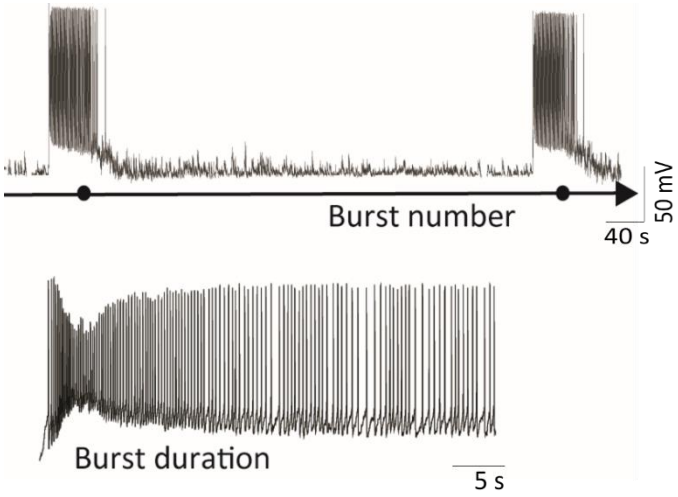

Fig 2.11 Trace from a hPSC derived control neuron displaying the characteristic burst activity.

2.12 Pharmacology

- **Riluzole** – For studying the effect of riluzole on the spontaneous burst activity of the neurons, baseline burst recordings were performed for 10 mins, and for further 10 mins bursts were recorded in the presence of 0.1 µM riluzole.
- **Paxiline** – Effect of paxilline was studied by recording the baseline bursts for 10 min, and then for further 10 min bursts were recorded in presence of 10 µM paxilline.

- **Veratridine**:

  Neuron- rodent astrocyte co-culture – 10 min baseline bursts + 10 min in presence of 0.5 µM veratridine.

  Human co-cultures – 10 min baseline bursts + 20 min burst recordings in presence of 0.5µM veratridine. The bursts in the last 10 min of the recording was taken for analysis to see the effect of veratridine.

- **S100β** – Two concentrations of S100β were used – 100 µM and 1 mM. 10 min baseline bursts + 20 min burst recordings in presence of S100β. The bursts in the last 10 min of the recording was taken for analysis to see the effect of S100β.

Culture	Baseline recording time (min)	Drug/Protein	Recording time (min) in presence of drug/protein
Rodent co-culture	10	Riluzole	10
Rodent co-culture	10	Paxilline	10
Rodent co-culture	10	Veratridine	10
Human co-culture	10	Veratridine	20
Human co-culture	10	S100β 100 µM/ 1 mM	20

Table 2.12 Recording protocols for analysing the effect of the drugs on burst activity.

2.13 Current measurements

Persistent sodium current (I_{NaP}) - To record the persistent sodium current (I_{NaP}), neurons were clamped at –80 mV, then stepped to –100 mV and a depolarizing voltage ramp [30] to –20 mV (20 mV/s) was applied. I_{NaP} was isolated by subtracting the current recorded in the presence of TTX (1 µM) from current recorded immediately prior in the same neuron but in the absence of TTX. To see the effect of veratridine and S100β on I_{NaP}, current was measured in their presence.

BK current - To record the Ca^{2+}-activated BK current (I_{BKCa}), neurons were clamped at –60 mV, then stepped to –110 mV and a depolarizing voltage ramp to +40 mV (100 mV/s) was applied, with neurons being held at +40 mV for a further 50 ms. During these recordings the external recording solution was supplemented with TTX (0.5 µM) and with I_{BKCa} being isolated by subtracting the current recorded in the presence of paxilline (10 µM) from current recorded immediately prior in the same neuron but in the absence of paxilline.

2.14 Statistical Analysis

All values are expressed as mean ± standard error of the mean (SEM) and each data set was assessed for normality. For the analysis of intrinsic membrane properties, mEPSC and network recordings, one-way repeated analysis of variance (ANOVA) followed by post-hoc Tukey's and Bonferroni's test were used. Paired statistical tests were used for data sets before and after drug application. Paired t-test was used for data sets that passed the normality test, and Wilcoxon test was used for data sets that failed the normality test. Two –way repeated measures ANOVA, followed by post-hoc Tukey's or Bonferroni test were used for I_{NaP} and I_{BKCa} current – voltage relationships. GraphPad Prism (GraphPad software Inc., La Jolla, CA, RRID: SCR_002798) was used for all the statistical tests. In all the experiments, 'n' denotes the number of cells while 'N' represents number of *de novo* preparations of batches of culture from which 'n' is obtained.

Summary

Modelling neurodevelopmental diseases using human pluripotent stem cell derived neurons, provides a wonderful platform to understand the fundamental properties of developing neurons and studying the molecular underpinnings involved in the disease pathology. The basic techniques to derive neurons from stem cells are now established (Benninger *et al.,* 2003; Wernig *et al.,* 2004). Increase in the refinement of culture protocols now make it possible to generate region specific neurons from embryonic or induced pluripotent stem cells (ESC/iPSC). The neurons thus generated are not only able to fire sustained action potentials, but they also establish normal synaptic connections (Moody & Bosma, 2005; Livesey *et al.,* 2014). The neurons derived from the human stem cells of patients suffering from FXS can therefore serve as an invaluable model to study the progression of the symptoms of FXS in vitro and subsequently help in developing new therapies.

Thus, in this chapter protocols for generating ESC and iPSC derived cortical purely neuronal cultures are discussed. The lines used are the isogenic pair *FMR1*$^{+/y}$, *FMR1*$^{-/y}$ (ESC-derived) and CON1 and FXS1 (iPSC-derived).

Whole-cell patch clamp recordings were performed in these neurons when they were 8-week-old *in vitro*. These recordings revealed that the active and passive parameters did not differ between control and FXS neurons. Thus, absence of FMRP did not alter the neurons' ability to fire action potentials. However, in a purely neuronal culture, both the control and FXS neurons did not develop robust synaptic activity.

3.1 Generation of cortical neurons from human pluripotent stem cells

The pathophysiology of FXS in *Fmr1* KO mouse models have revealed that the excitability of the cortical neurons is altered in the absence of FMRP (reviewed in Contractor *et al.,* 2015). However, it is crucial to understand the FXS pathophysiology in human neurons and the advent of stem cell technology makes this possible. The neural conversion of human pluripotent stem cells which mimics mammalian neurogenesis is now well-established (Bouhon *et al.,* 2006; Elkabetz *et al.,* 2008; Vallier *et al.,* 2004; Zhang *et al.,* 2001). In this study, to study the electrical properties of neurons in the *presence* and *absence* of FMRP, we have used fibroblast derived iPSCs generated from a healthy individual (CON1), a FXS patient lacking FMRP (FXS1), and one isogenic embryonic stem cell (*FMR1*$^{+/y}$; *FMR1*$^{-/y}$) (Fig 3.1). Pluripotent stem cells were converted to neurons (Fig 3.1A) and whole-cell patch clamp recordings were performed at 8 weeks. ESC derived *FMR1*$^{-/y}$ was generated by CRISPR/Cas9 mediated deletion (Fig 3.1B) (D'Souza *et al.,* 2019). After PCR amplification, positive clones were around 450 bps and negative clones were about 100 bps (Fig 3.1C). The FMRP western blot of positive clones shows the lack of FMRP. The selected clones are marked by * (Fig 3.1D). Of these the Sanger sequence of the clone G3 is shown because the neurons derived from this hESC clone was used for all the experiments (Fig 3.1E). Next immunohistochemistry experiments were carried out to check the pluripotency of the stem cells. All cell lines expressed pluripotent stem cell marker, Nanog (Fig. 3.1F). NPCs were generated from PSC and further terminally differentiated into neurons using previously published protocols (Bilican *et al.,* 2015). Immunocytochemistry showed high expression of NPC markers, Nestin across all samples (Fig. 3.1G). The cultures at 8 weeks post differentiation were positive for Map2ab and human nuclear antigen (hNA) thereby confirming the human origin of the neurons. Moreover, there was negligible expression of the astrocyte marker, GFAP. (Fig. 3.1H). The development and maturation of neurons from human pluripotent stem cells is not affected by the loss of FMRP.

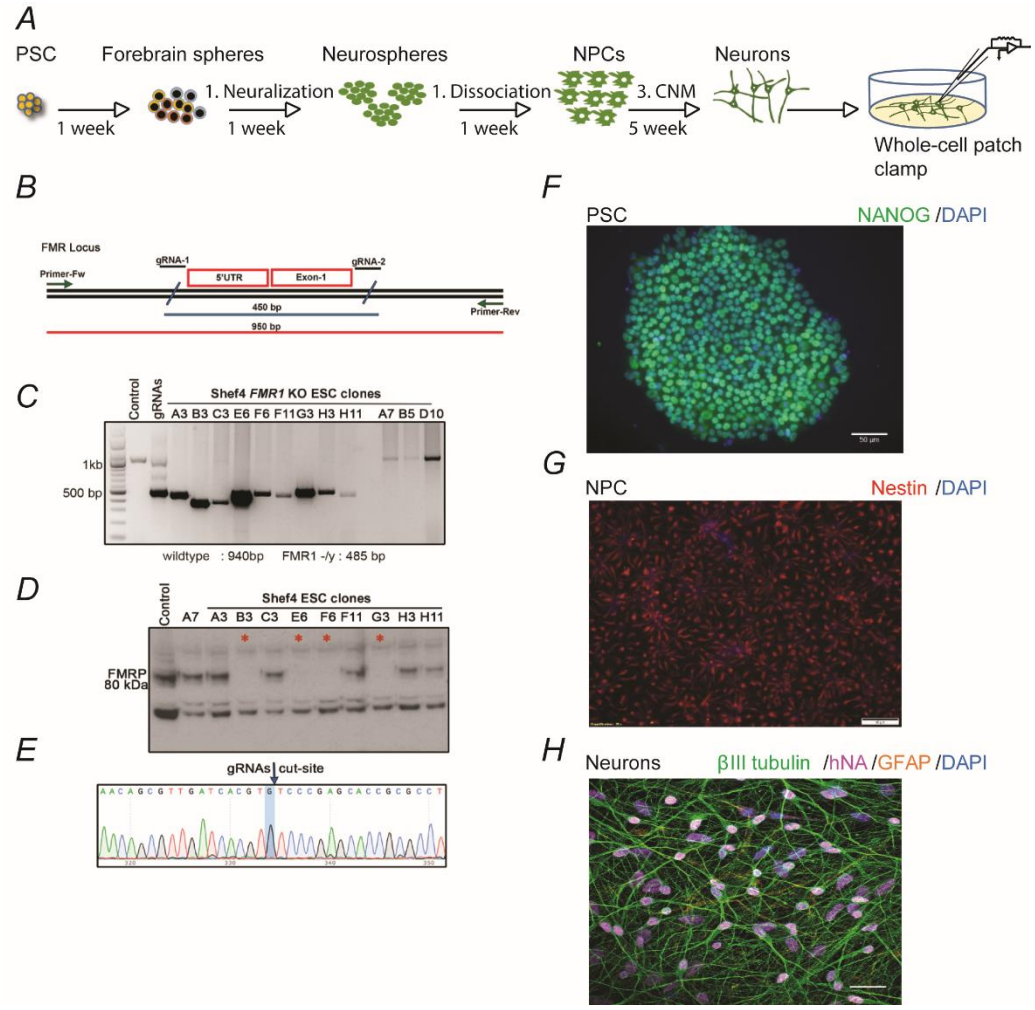

Figure 3.1 Derivation and specification of neurons from human pluripotent stem cell (hPSC)-derived neural progenitor cells (NPCs).

(A): Summary of the protocol used to generate hPSC-derived cortical neurons: **(1)** hPSCs were neuralized via dual-SMAD inhibition. **(2)** dissociated neural rosettes were propagated at 3% O_2 with mitogens. **(3)** Cortical Neuronal Maturation (CNM) was induced by exposure to BDNF, GDNF and **(4)** subsequently co-cultured with/without astrocytes. **(B):** Schematic of the gene targeting strategy used to generate *FMR1* KO hPSC. **(C)** PCR screen illustrating *FMR1* KO positive clones **(D)**: Immunoblot analysis of FMRP protein on positive clones from PCR screen. **(E):** Sanger sequencing of positive *FMR1* KO clone -G3. **(F):** Representative staining of hPSC identifies pluripotent cells expressing Nanog. Scale bar = 50µm. **(G):** Immunofluorescence analysis of dissociated cortical NPCs uniformly express Nestin and OTX2. Scale bar = 50µm. **(H)**: Example images illustrating hPSC derived cortical neurons expressing βIII tubulin, human nuclei antigen. GFAP immunostaining shows no significant presence of astrocytes in the culture. Scale bar = 25 µm. (*Work performed by Rakhi Pal and Bharath Reddy)*

3.2 Passive electrical properties of cortical FXS neurons in a neuron-only culture

Cortical hyperexcitability is a hallmark of FXS. Studies using *Fmr1* KO mouse model have suggested that the hyperexcitability phenotype is linked to changes in the intrinsic membrane properties of the neurons and dysregulation of ion channels (Contractor *et al.,* 2015; Gibson *et al.,* 2008; Goncalves *et al.,* 2013; Gross *et al.,* 2015; Zhang *et al.,* 2014). However, a recent crop of studies using primary mouse cortical neurons and hPSC derived cortical neurons have also shown that loss of FMRP does not alter the passive electrical properties (Bulow *et al.,* 2019; Telias *et al.,* 2015; Zhang *et al.,* 2018). Thus we analysed the passive membrane properties to understand how loss of FMRP affects the neurons generated using our protocols. Whole-cell patch clamp recordings of 8 week old cortical neurons were performed in current-clamp mode. Depolarizing current steps were injected to the neurons (-10 to +65 pA). The passive membrane properties were analysed across all the lines (Fig 3.2). There were no significant differences in these properties between the control and the FXS neurons. The mean resting potential (Fig 3.2A) of these neurons was considerably depolarized and the mean input resistance (Fig 3.2B) was very high. This suggests that despite being in culture for 8 weeks, these neurons were immature. The mean capacitance (Fig 3.3C) and mean rheobase current (Fig 3.4D) also reinforces the immature state of the neurons. Thus in a neuron-only culture, the passive membrane properties were unaffected by the loss of FMRP. Next, we characterized the action potential properties of these neurons to check whether they varied between control and FXS neurons.

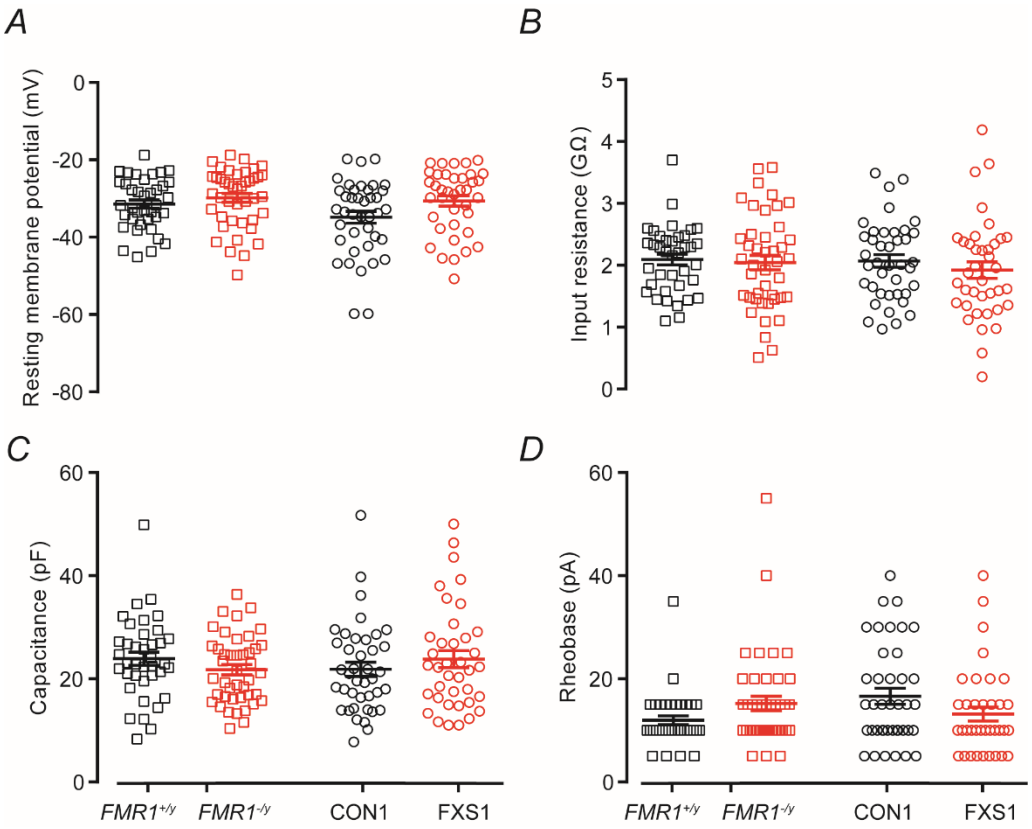

Figure 3.2: Passive electrical properties of FXS neurons is similar to controls in a neuron-only culture. **(A)** Quantification of the resting membrane potential of control neurons (*FMR1*$^{+/y}$, -31.43 ± 1.084, n= 38, N=3; CON1, -34.84 ± 1.526, n = 40, N = 4) and FXS neurons (*FMR1*$^{-/y}$, -29.84 ± 1.148, n = 43, N = 4; FXS1, -30.61 ± 1.345, n = 38, N = 3). **(B)** Quantification of the input resistance of control (*FMR1*$^{+/}$, 2.093 ± 0.087 GΩ; CON1, 2.07 ± 0.1 GΩ) and FXS neurons (*FMR1*$^{-/y}$ 2.04 ± 0.11 GΩ; FXS1, 1.922 ± 0.13 GΩ). **(C)** Capacitance of the controls (*FMR1*$^{+/}$, 23.91 ± 1.27 pA; CON1, 21.86 ± 1.37 pA) and FXS neurons neurons (*FMR1*$^{-/y}$ 21.76 ± 0.99 pA; FXS1, 23.82 ± 1.63 pA). **(D)** Quantification of the rheobase current in controls (*FMR1*$^{+/}$, 11.97 ± 0.63 pA; CON1, 16.63 ± 1.53 pA) and FXS neurons neurons (*FMR1*$^{-/y}$ 15.23 ± 1.39 pA; FXS1, 13.16 ± 1.35 pA). All values are mean ± SEM. Unpaired t-test.

3.3 Action potential properties of cortical FXS neurons in a neuron-only culture

Across several studies conducted using Fragile X mouse models, one of the key consistent feature was the hyperexcitability displayed by the cortical neurons (Gibson *et al.,* 2008, Deng *et al.,* 2013, Zhang *et al.,* 2014). However, a recent study using human embryonic stem cell derived cortical neurons showed that the FXS neurons were hypoexcitable (Telias *et al.,* 2015). They were unable to fire sustained action potentials. In the previous section, we reported that the passive membrane properties of the FXS neurons did not differ from the control neurons. We sought to check if the action potential properties of the FXS neurons neurons (ESC and iPSC) were different. Whole-cell patch clamp recordings were conducted on 8 week old neurons. In current-clamp mode, the neurons were injected with 500 ms long depolarizing current steps ranging from -10 pA to +65 pA. The number of spikes were counted against each current step to yield the firing frequency. A *FMR1*$^{+/y}$ (*black trace*) and *FMR1*$^{-/y}$ neuron (*red trace*) fired similar number of action potentials in response to a depolarized current step (Fig 3.3A-B). The firing frequency (Fig 3.3C) of the FXS neurons was similar to the controls across the iPSC and ESC lines. FXS neurons were able to fire sustained action potentials at higher current steps similar to control neurons. Analysis of the action potential properties (Fig 3.3D-F) - threshold, amplitude, and half-width also did not reveal any significant differences between control and FXS neurons neurons. It should be noted however that like passive membrane properties, these action potential properties exhibited by the 8 week old cortical neurons were immature. These neurons fired short, thick action potentials as indicated by the mean action potential amplitude (Fig 3.3E) and half-width (Fig 3.3F) respectively. Thus, 8 weeks of culture did not yield sufficiently mature hPSC derived neurons, but in these neurons lack of FMRP did not alter the action potential properties.

Next we asked if these neurons display robust synaptic activity and if the synaptic activity is different between control and FXS neurons.

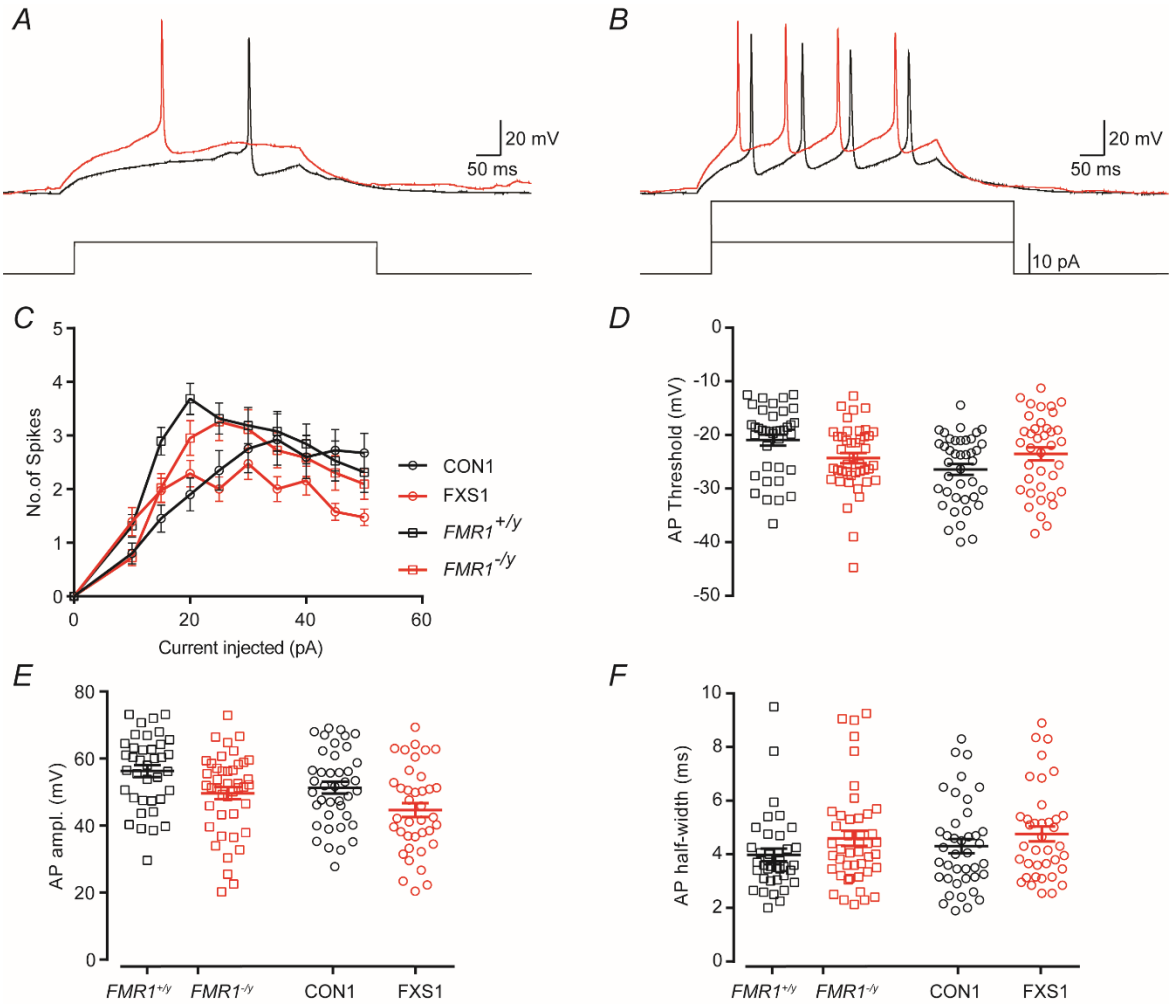

Figure 3.3 FXS neurons display similar action potential properties as control neurons.

(A) Representative current-clamp traces showing action potential firing at rheobase current (500 ms, +10 pA) from either *FMR1*$^{+/y}$ (black) or *FMR1*$^{-/y}$ (red) neuron. **(B)** Sustained action potential firing evoked by depolarizing current pulse (500 ms, +20 pA) from either *FMR1*$^{+/y}$ (black) or *FMR1*$^{-/y}$ (red) neuron. **(C)** Firing frequency plotted as the mean number of spikes elicited by the depolarized current steps (+10 pA to +50 pA). **(D)** Quantification of action potential threshold of control (*FMR1*$^{+/y}$, -20.95 ± 1.029 mV, n= 38, N=3; CON1, -26.43 ± 1.024 mV, n = 40, N = 4) and FXS neurons (*FMR1*$^{-/y}$, -24.31 ± 0.95 mV, n = 43, N = 4; FXS1, -23.52 ± 1.192, n = 38, N = 3). **(E)** The action potential amplitude was similar between controls (*FMR1*$^{+/}$, 56.27 ± 1.76 mV; CON1, 51.33 ± 1.77 mV) and FXS neurons (*FMR1*$^{-/y}$ 49.66 ± 1.84 mV; FXS1, 44.64 ± 2.077 ms). **(F)** The action potential half-width did not differ between controls (*FMR1*$^{+/}$, 3.97 ± 0.23 ms; CON1, 4.303 ± 0.26 ms) and FXS neurons (*FMR1*$^{-/y}$ 4.59 ± 0.28 ms; FXS1, 4.75 ± 0.27 ms). All values are mean ± SEM. Two-way ANOVA with post-hoc Bonferroni's test; Unpaired t-test.

3.4 ESC/iPSC derived cortical neurons in a neuron-only culture failed to develop synaptic activity

Glutamatergic synapses provide the bulk of the excitatory input to all the neurons in the brain. Any alterations in this input would thus result in gross deficits in synapse and network excitability. The effect of loss of FMRP on the synaptic activity of neurons have been studied in FXS mouse models (Pfeiffer & Huber, 2007, Bureau *et al.,* 2008, Gibson *et al.,* 2008, Domanski *et al.,* 2019). Telias *et al.,* 2015 reported a decrease in the frequency of synaptic events in the hESC derived FXS neurons. Thus, we sought to check whether the loss of FMRP led to synaptic dysregulation of the hPSC neurons generated using our protocols. We performed voltage – clamp recordings to record miniature excitatory postsynaptic currents (mEPSCs). Spontaneous mEPSCs were recorded at a holding potential of -60 mV in the *presence* of 0.5 µM TTX, a sodium channel blocker, to block all the action potential dependent events (Fig 3.4A). We found that both control and FXS neurons across the iPSC and ESC lines did not develop robust synaptic activity even after 8 weeks *in vitro* (Fig 3.4B-C). Thus, together with the previous results, it is clear that hPSC cortical neurons in a neuron-only culture did not mature after 8 weeks *in vitro.* Thus, for the proper assessment of the role of FMRP in regulating neuron-only and synaptic excitability, it is imperative to generate cultures where the neuron-only maturity is enhanced.

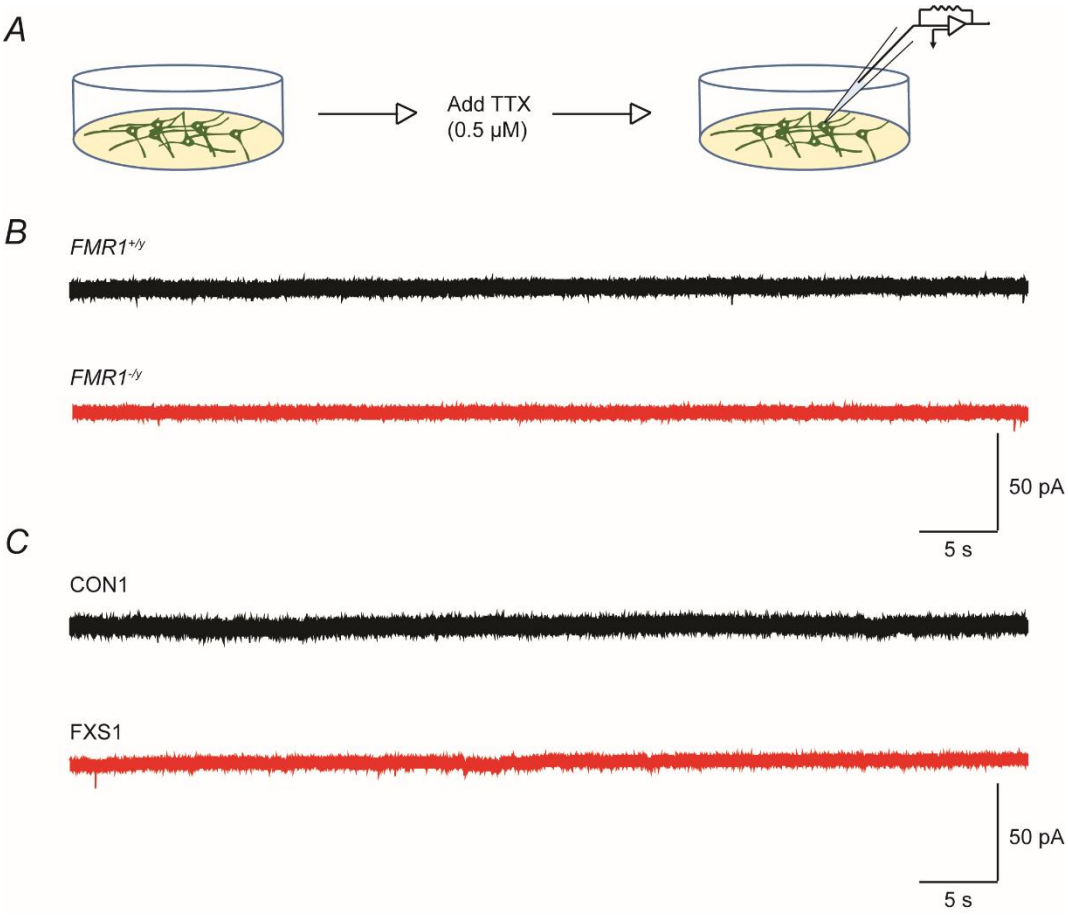

Figure 3.4 Cortical neurons derived from hESC and hiPSC in a neuron-only culture do not develop robust synaptic activity.

(A) Schematic shows the voltage-clamp recordings from the cortical neurons in presence of 0.5 µM TTX. **(B)** Representative traces from a *FMR1*$^{+/y}$ (*black*) and a *FMR1*$^{-/y}$ (*red*) neuron showing little to no synaptic activity. **(C)** Same as **(B)** but the representative traces are from a CON1 (*black*) and a FXS1 (*red*) neuron.

Discussion

Hyperexcitability of cortical neurons has been a key hallmark of the FXS pathophysiology established from various studies using *Fmr1*$^{-/y}$ mouse models (reviewed in Contractor *et al.,* 2015). This hyperexcitabilty manifested as an increase in firing frequency of the neurons (Domanski *et al.,* 2019; Zhang *et al.,* 2014; Deng & Klyachko, 2016). The *Fmr1*$^{-/y}$ neurons displayed an increase in action potential firing following depolarized current injections. FMRP binds to mRNAs and acts as a translational repressor (Darnell *et al.,* 2011). Many of the target mRNAs encode for proteins that are synaptically located and FMRP has been reported to maintain the structural and functional integrity of the synapse (Pfeiffer & Huber, 2007). Indeed, loss of FMRP has been reported to perturb the excitation-inhibition balance in the neocortex (Gibson *et al.,* 2008). Despite the numerous insights into the FXS pathophysiology yielded by rodent and animal studies, to fully understand the details of the onset and progression of the disease in humans, it is important to study this disease in a human-based model.

In this chapter we have described the generation of excitatory cortical neurons from human pluripotent stem cells in a neuron-only culture. We have derived neurons from induced pluripotent stem cell (CON1, FXS1) and an isogenic embryonic stem cell line (*FMR1*$^{+/y}$, *FMR1*$^{-/y}$) wherein the *FMR1* gene has been deleted using CRISPR-Cas9. The use of the isogenic line is crucial because any disease phenotype seen using this line would be attributed to the loss of FMRP and not any other environmental factors. Using whole-cell patch clamp recordings, we have also obtained an exhaustive characterization of the active and passive membrane properties of the control and FXS neurons neurons. The key observations are:-

- Loss of FMRP doesn't affect the development and maturation of the hPSC derived cortical neurons.
- Passive membrane properties of FXS neurons did not differ from the control neurons.
- Action potential properties of the FXS neurons were similar to the control neurons.
- The hPSC derived cortical neurons failed to develop synaptic activity after 8 weeks *in vitro*.

The first study to investigate the role of FMRP in neurogenesis, reported that loss of FMRP in mouse NPCs led to generation of more neurons and loss of glial cells (Castren *et al.,* 2005). Subsequent studies in mice and Drosophila have also shown an increase in the proliferative capacity due to loss of FMRP (Luo *et al.,* 2010; Callan *et al.,* 2010). Loss of FMRP has been reported to cause aberrant differentiation of neural progenitor cells derived from hiPSCs (Sunamura *et al.,* 2018), however, another study found no difference in the human NPCs and the subsequent neurogenesis after the loss of FMRP (Acharyya *et al.,* 2008). Thus,

the effect of FMRP on human stem cells and neural progenitor cells is not uniform. Using our protocols, we did not observe any difference in the differentiation and proliferation of NPCs in the absence of FMRP.

Cortical hyperexcitability is a common phenotype seen in mouse models of FXS. Changes in membrane properties in the absence of FMRP is reported to be one of the causes of this hyperexcitability (Domanski *et al.,* 2019; Gibson *et al.,* 2008, Deng *et al.,* 2013, Zhang *et al.,* 2014). However recent studies have reported that loss of FMRP does not alter the passive membrane properties of cortical neurons (Bulow *et al.,* 2019; Zhang *et al.,* 2018). In this study, we looked at the electrical properties of hPSC derived cortical neurons 8 weeks *in vitro*. Achieving mature neurons in a culture has always been a hurdle. Here we report, that the cortical neurons derived from iPSC and ES lines are able to fire sustained action potentials. We did not find any significant difference in the passive membrane properties analysed between the controls and FXS neurons neurons. However, analysis of passive properties of both control and FXS neurons neurons indicated that the neurons were still immature characterized by high input resistance, low capacitance, depolarized resting membrane potentials. Maturation of neurons is accompanied by changes in the active and passive membrane properties (Wu & Oertel, 1987; Mongiat *et al.,* 2009; Cepeda *et al.,* 2007) which influences the excitability. Thus, these results need to be confirmed in a more mature culture system.

A study using ES derived cortical neurons reported that loss of FMRP led to hypoexcitability. The FMRP-null neurons could only fire a single action potential in response to depolarized current injections (Telias *et al.,* 2015). However, in contrast to what Telias *et al*, reported, the FXS neurons neurons generated by us could fire sustained action potentials similar to the controls in response to increased depolarizing current steps. Analysis of the spike properties – amplitude, half-width, and threshold did not reveal any significant difference between FMRP-null neurons and controls. This is broad agreement with the study by Bulow *et al.,* 2019, which reported that loss of FMRP did not affect the baseline firing frequency of primary mouse cortical neurons. Thus, the cortical hyperexcitability phenotype of FXS is not uniform and depends on the brain region and the type of neurons being studied.

The role of FMRP in modulating glutamatergic synapses has been studied in mice. Loss of FMRP led to impairments in the excitatory drive onto the layer IV cortical neurons (Gibson *et al.,* 2008). In the absence of FMRP, there was a downregulation of NMDA receptor signalling in the cortex of mice (Gocel & Larson, 2013). Studies have reported a change in the AMPA/NMDA ratio in the cortex of mice due to loss of FMRP (Harlow *et al.,* 2010; Pilpel *et al.,* 2009). However, there have been studies that report no change in the baseline synaptic activity after loss of FMRP (Bulow *et al.,* 2019; Zhang *et al.,* 2018). Telias *et al,* also

reported a decrease in the synaptic activity in the absence of FMRP. In our study, we attempted to characterize the synaptic activity of the hPSC derived cortical neurons, however we found that both control and FXS neurons did not develop considerable synaptic activity after 8 weeks *in vitro*. The mEPSCs if present were of extremely small amplitude (< 5 pA) making them very difficult to differentiate from the baseline noise in the recording. The most likely explanation of this diminished synaptic activity is because the percentage of glia in the neuron-only culture is very low. Several studies have shown the importance of glia in the development and maintenance of synaptic transmission (reviewed in Araque & Perea, 2004). Because a neuron-only culture system offered only limited scope, in the subsequent chapters of this thesis we will discuss co-cultures of hPSC derived cortical neurons with astrocytes: mouse and human.

The results reported in this chapter have been published in:

Das Sharma S, Pal R, Reddy BK, Selvaraj BT, Raj N, Samaga KK, Srinivasan DJ, Ornelas L, Sareen D, Livesey MR, Bassell GJ, Svendsen CN, Kind PC, Chandran S, Chattarji S & Wyllie DJA (2020). Cortical neurons derived from human pluripotent stem cells lacking FMRP display altered spontaneous firing patterns. *Mol Autism* **11** 52. doi: 10.1186/s13229-020-00351-4. PMID: 32560741

Summary

Extensive studies in rodent models of FXS, show that FMRP acts as a translational repressor (Zalfa *et al.,* 2005) and loss of FMRP often leads to protein dysregulation (Krueger *et al.,* 2011). Furthermore, many proteins interacting with FMRP, are involved in maintaining synapse integrity and neuronal excitability (Darnell *et al.,* 2011). Indeed, aberrant neuronal excitability has been a consistent finding from rodent and models of FXS (Goncalves *et al.,* 2013; Contractor *et al.,* 2015; Zhang *et al.,* 2014). This aberrant neuronal excitability leads to a concomitant alteration in the network activity of the FXS neurons (Gibson *et al.,* 2008). Studies using rodent models have provided many mechanistic insights into the FXS pathophysiology.

In the previous chapter, using whole-cell patch clamp, we assessed the electrophysiological properties of hPSC derived cortical control and FXS neurons in a neuron-only culture. We reported that the intrinsic and action potential properties of the FXS neurons did not differ significantly from the controls, however both the control and FMRP null neurons, did not develop robust synaptic activity. Multiple studies have reported the prominent role of astrocytes in the development and maintenance of synapses (Araque & Perea, 2004; Hama *et al.,* 2004).

Thus, to assess the effect of the loss of FMRP on the synaptic and network activity of hPSC derived cortical neurons were co-cultured with primary mouse astrocytes. In this study, cell lines used are: CON1, CON2, FXS1, FXS2, FXS3 (iPSC derived) and the isogenic line *FMR1*$^{+/y}$ and *FMR1*$^{-/y}$ (ESC derived). In the absence of FMRP, the neurons develop aberrant network activity characterized by high frequency bursts that last for a shorter duration. We have further delineated the network activity to look at the underlying ion channels modulating the network activity in these neurons and the dysregulation of these channels in the absence of FMRP (Das Sharma *et al.,* 2020).

4.1 Generation of co-cultures of hPSC derived cortical neurons and rodent astrocytes

In the previous chapter, it was seen that the hPSC derived cortical neurons did not develop proper synaptic activity even after 8 weeks *in vitro.* In this chapter, we will see if the loss of FMRP alters the properties of cortical neurons when co-cultured with primary mouse astrocytes. As in the previous chapter, fibroblast derived iPSCs were generated. However, here in addition to CON1, another control (CON2) was used. Three FXS patient lines (FXS1, FXS2, FXS3) and the ES-derived isogenic pair (*FMR1*$^{+/y}$; *FMR1*$^{-/y}$) were also used. Western blot images confirmed the absence of FMRP in the FXS ESC (*FMR1*$^{-/y}$) and iPSC (FXS1, FXS2, FXS3) colonies. Brain lysate from *Fmr1* KO rats were used as a negative control (Fig 4.1A, N=3). The cells lines were stained for the pluripotency stem cell markers, Oct4 and Nanog. All the cell lines were positive for Oct4/Nanog (Fig 4.1B, left panel, n=9; N=3). NPCs were generated from PSCs by dual-SMAD inhibition (Bilican *et al.,* 2014). All the samples were stained with the NPC markers Nestin and Pax6. High expression of both these markers were observed across all the cell lines (Fig 4.1B, middle panel, n=18; N=6). The NPCs were further plated on to a layer of astrocytes and terminally differentiated into neurons in a humidified incubator (5% CO_2) at 37°C for 8 weeks. Immunocytochemistry of the co-cultures at 8 weeks post differentiation confirmed the presence of neurons positive for Map2ab and human nuclear antigen (hNA) confirming all neurons to be of human origin and the astrocytes were positive for GFAP (Figure 4.1B right panel, N=6; n=18). The differentiation efficiency observed across all 7 lines was comparable. Thus this set of data suggests that the loss of FMRP does not affect the differentiation potential of human PSC derived cortical neurons *in vitro*.

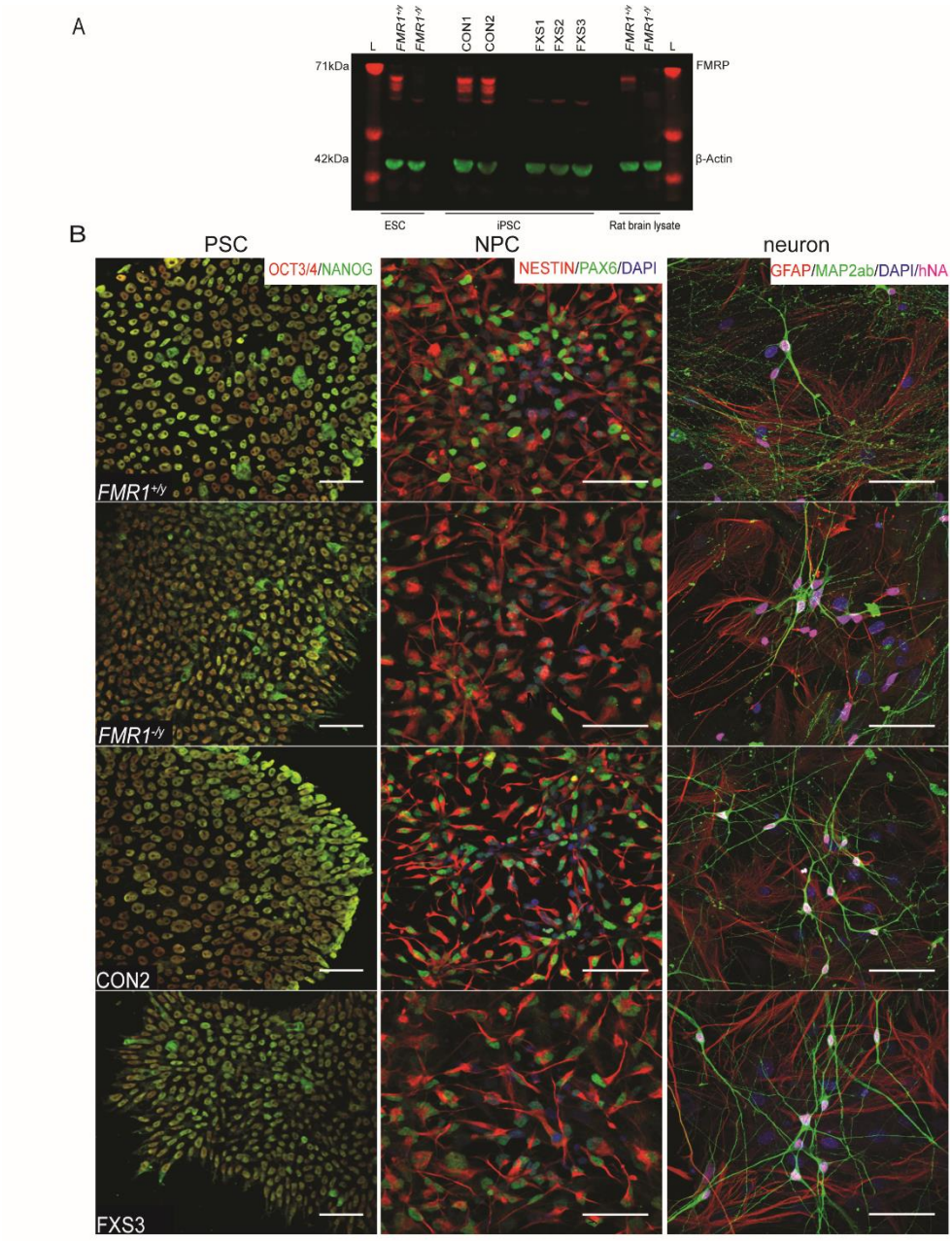

Figure 4.1 Specification of neurons from human stem cell and pluripotent stem cell derived neural progenitor cells.

(A) LI-COR immunoblot image of FMRP obtained from each of the pluripotent stem cell lines examined. The image illustrates that *FMR1*$^{+/y,}$ CON1, CON2 cell lines express FMRP (71 kDa) and *FMR1*$^{-/y}$, FXS1, FXS2 and FXS3 lines lack FMRP. Rat brain lysate from *Fmr1*$^{+/y}$ and *Fmr1*$^{-/y}$ animals were used as positive and negative controls respectively. **(B) Left panel:** Representative confocal images of paraformaldehyde fixed hESC (*FMR1*$^{+/y}$ *and FMR1*$^{-/y}$) and hiPSC (CON2 and FXS3) expressing the pluripotency markers, Nanog and Oct3/4. Scale bar = 50 µm. **Middle panel:** Immunofluorescent staining of NPCs arranged as rosettes (derived from hESC and hiPSC) for the progenitor markers Nestin and PAX6. Scale bar = 50 µm. **Right panel**: Confocal images illustrating hESC and hiPSC derived cortical neurons expressing

Map2ab/DAPI/hNA. The GFAP positive cells are murine astrocytes (negative for human nuclei) with which hESC- and hiPSC-derived neurons were co-cultured. Scale bar = 50 µm. Abbreviations: hESC: human embryonic stem cells; hiPSC: human pluripotent stem cells; *FMR1*$^{+/y}$: human embryonic stem cell line. *FMR1*$^{-/y}$: gene edited isogenic hESC pair lacking *FMR1* gene. L: Ladder. CON1; CON2: control hiPSC line. FXS1, FXS2 and FXS3: hiPSC lines from fragile X syndrome patients. (*Work performed by Rakhi Pal and Bharath Reddy. Reproduced with permission.)*

4.2 Loss of FMRP does not alter the passive membrane and action potential properties

Hyperexcitability exhibited by an increase in neuronal firing and alterations in the membrane properties has been shown in *Fmr1* KO mouse models (Gibson *et al.,* 2008; Zhang *et al.,* 2014; Booker *et al.,* 2019). However recent studies using mouse primary cortical neurons and ES-derived human neurons have found that loss of FMRP doesn't affect the intrinsic properties of the neurons (Bulow *et al.,* 2019; Telias *et al.,* 2015; Zhang *et al.,* 2018). Human FXS neurons have been reported to exhibit a considerably compromised ability to generate trains of action potential firing in response to depolarizing current injections (Telias *et al.,* 2015). Using the protocols discussed in this thesis to generate human excitatory cortical neurons we did not observe differences in either passive or active membranes properties in any of the lines we studied. For obtaining trains of action potentials, we followed the same protocol as described in chapter 3. Briefly, Neurons were injected with 500 ms long depolarizing current steps ranging from -10 pA to +65 pA. As shown in Fig 4.2A, the FXS neurons fired the same number of action potentials as the controls. The passive membrane properties (Fig 4.2B-D) – resting membrane potential, input resistance and capacitance of the FXS neurons were similar to the controls across the iPSC and ES cell lines. The action potential properties – rheobase, AP threshold, amplitude, half-width were analysed from the first action potential fired by the neuron. These were also similar between controls and FXS neurons (Fig 4.2E-H). The maximum number of action potentials fired by the FXS neurons did not differ from the controls (Fig 4.2I). Analysis of these properties show that the intrinsic and firing properties of hPSC derived cortical neurons are not altered by the loss of FMRP.

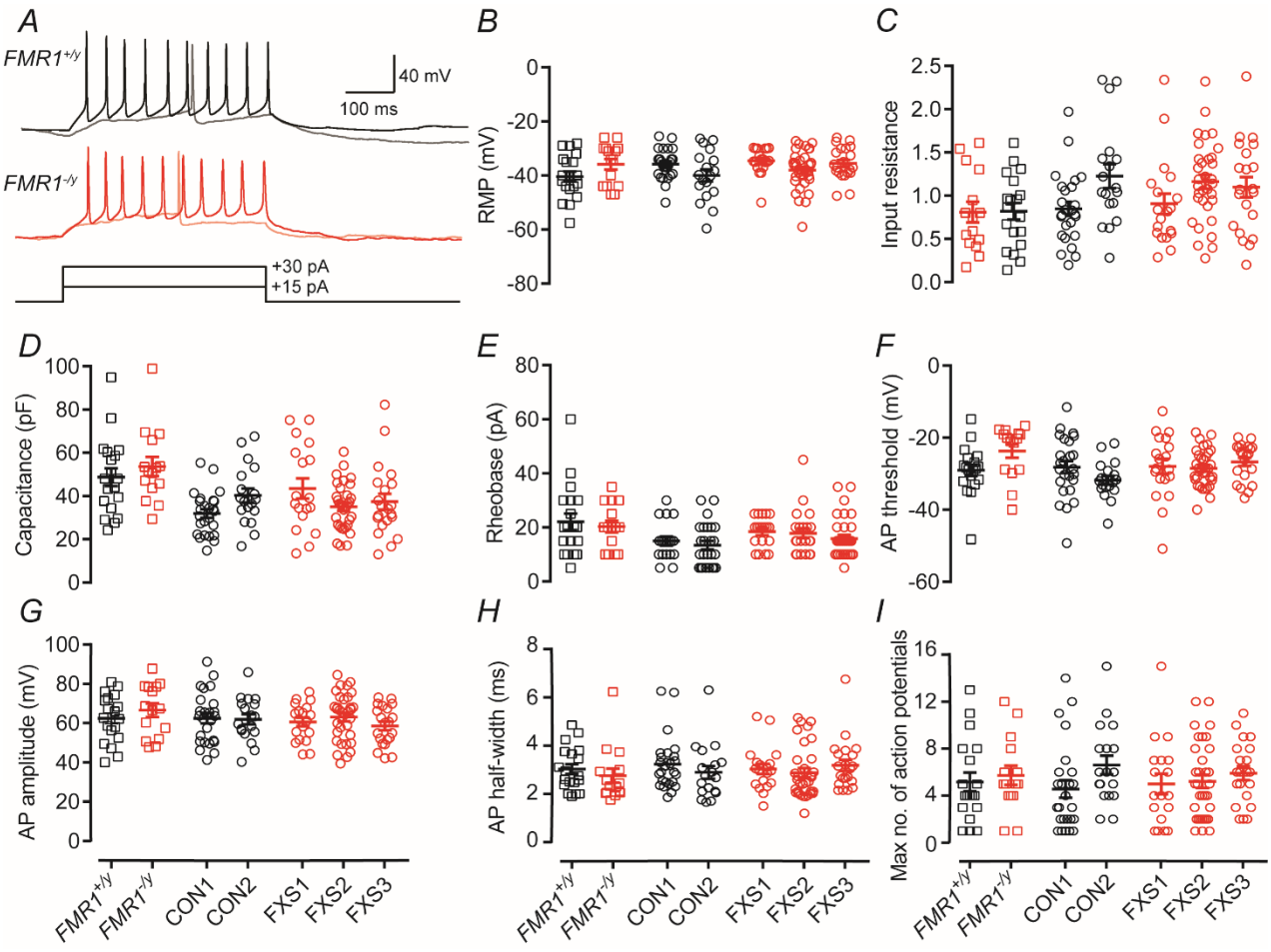

Figure 4.2 Active and passive membrane properties of human pluripotent stem cell derived cortical FXS neurons are similar to the control neurons.

(A) Representative current-clamp traces showing action potential firing in response to two depolarizing current injections (500 ms; +15 pA or +30 pA) from either *FMR1*$^{+/y}$ (black trace) or *FMR1*$^{-/y}$ (red trace) neurons. **(B, C, D, E)** Quantification of the passive membrane properties of hESC (*FMR1*$^{+/y}$, *FMR1*$^{-/y}$) and hiPSC (CON1, CON2, FXS1, FXS2, FXS3) derived cortical neurons illustrating no significant differences between control neurons and FXS neurons in their resting membrane potential (B), input resistance (C), capacitance (D) or rheobase current (E). **(F, G, H, I)** Quantification of action potential parameters in each of the lines indicating no difference in action potential (AP) threshold (F), AP amplitude (G), AP half-width (H) or the maximum number of APs fired in response to depolarizing current injections (I). One-way ANOVA with *post hoc* Tukey's test. *FMR1*$^{+/y}$: n = 19, N = 3; *FMR1*$^{-/y}$: n = 15, N = 3; CON1: n = 25, N = 3; CON2: n = 18, N = 3; FXS1: n = 19, N = 3; FXS2: n = 33, N = 3; FXS3: n = 21, N = 3.

4.3 The synaptic properties of FXS neurons are similar to control neurons

The hPSC derived cortical neurons in a neuronal culture failed to develop robust synaptic activity as reported in Chapter 3. Spontaneous miniature excitatory post synaptic currents (mEPSC) were recorded in voltage-clamp mode, in the presence of 0.5 µM TTX at a potential of -60 mV. For this experiment only one pair of iPSC (CON1, FXS1) and the isogenic (*FMR1*$^{+/y}$, *FMR1*$^{-/y}$) were used. The neurons showed considerable synaptic activity (Fig 4.3A, B). Quantification of the mEPSC frequency and amplitude revealed no difference between the controls and FXS neurons (Fig 4.3C, D). Previous studies of hPSC-derived cortical neurons have suggested that FXS neurons possess low levels of spontaneous synaptic activity (Telias *et al.,* 2013, 2015). However a recent study using a mixed culture iPSC derived neurons, mouse glia and mouse neurons showed that in the absence of FMRP the baseline mEPSC and miPSC frequency and amplitude are unaltered (Zhang *et al.,* 2018). Similarly in primary mouse cortical cultures, the baseline mEPSC properties are similar between controls and *Fmr1* KO neurons (Bulow *et al.,* 2019). Thus all these studies, corroborate our observation that the loss of FMRP doesn't affect the baseline synaptic activity in hPSC derived cortical neurons.

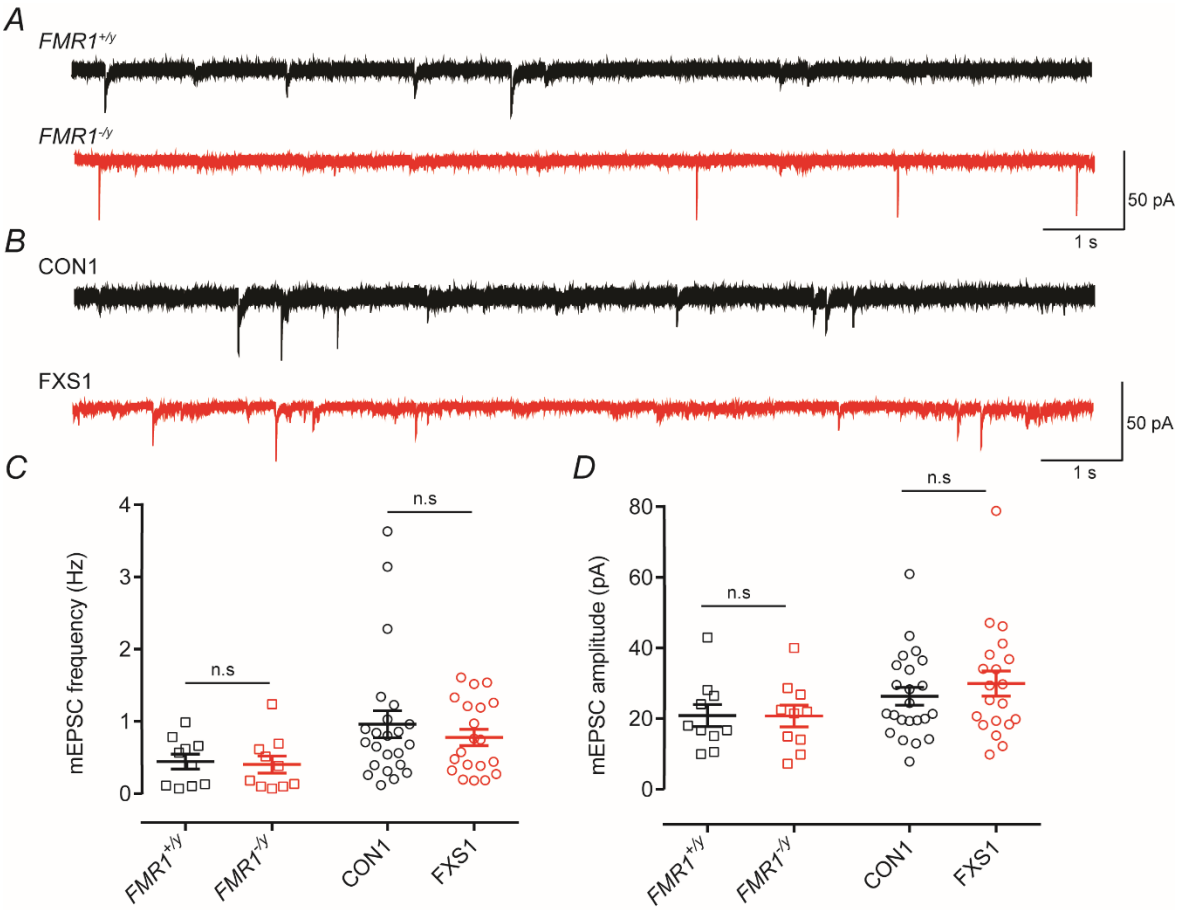

Figure 4.3 Synaptic activity of human cortical FXS neurons is comparable to the control neurons.

(A) Representative voltage-clamp traces of mEPSCs (V_{hold} = –70mV) from either *FMR1*$^{+/y}$ (black) and *FMR1*$^{-/y}$ (red) neurons and recorded in the *presence* of TTX (0.5 µM). **(B)** As in (A) but from CON1 (black) or FXS1 (red) neurons. **(C)** Quantification of mEPSC frequencies indicating that these do not differ between each of the lines examined and had mean values of 0.443 ± 0.10 Hz (*FMR1*$^{+/y}$; n = 10, N = 2); 0.403 ± 0.11 Hz (*FMR1*$^{-/y}$; n =10, N = 2); 0.96 ± 0.18 Hz (CON1; n =23, N =3) and 0.78 ± 0.11 Hz (FXS1, n = 20, N = 3). **(D)** Quantification of mEPSC amplitudes indicating that these do not differ between each of the lines examined and had mean values of 20.85 ± 3.13 pA (*FMR1*$^{+/y}$); 20.72 ± 3.08 pA (*FMR1*$^{-/y}$); 26.3 ± 2.53 pA (CON1) and 29.92 ± 3.54 pA (FXS1). One-way ANOVA with post hoc Tukey's test.

4.4 Loss of FMRP leads to altered spontaneous action potential burst firing of the neurons

Human excitatory cortical neurons derived from iPSC and ES cells develop active neuronal network exhibited by the presence of synchronous burst activity (Heikkila *et al.,* 2009; Weick *et al.,* 2011). Recordings from the principal neurons of somatosensory cortex and hippocampus shows an altered burst firing profile in the *Fmr1* KO mice (Zhang *et al.,* 2014; Deng *et al.,* 2016). Imbalance of excitation and inhibition in the neocortex of *Fmr1* KO mice, led to altered UP states reflecting aberrant network activity (Gibson *et al.,* 2008). Thus, to assess the role of FMRP in maintaining the neuronal network integrity, we examined the spontaneous (action-potential) driven burst activity in the hiPSC and hES derived cell lines. The cortical neurons derived from hPSCs when co-cultured with primary mouse astrocytes displayed robust burst activity. However, the loss of FMRP led to a significantly different bursting profile as shown in Fig 4.4. Recordings from *FMR1*$^{+/y}$ neuron show longer bursts which are less frequent (Fig 4.4A, *black trace*). Similar recordings from *FMR1*$^{-/y}$ neuron show bursts that are more frequent but last for a shorter duration (Fig 4.4A, *red trace*). This difference in bursting profile is also seen in iPSC derived neurons CON1 and FXS1 (Fig, 4.4B). Quantification of the burst activity across the iPSC and ESC cell lines reveal the same difference - in *FMR1*$^{+/y}$, CON1 and CON2 lines bursts of action potentials occur at a low frequency (Fig. 4.4C) but have long durations (Fig. 4.4D) as defined by the interval between the first and last action potential in a burst. In contrast, absence of FMRP in the FXS lines (*FMR1*$^{+/y}$, FXS1, FXS2) led to cells exhibiting bursts of higher frequencies but shorter durations.

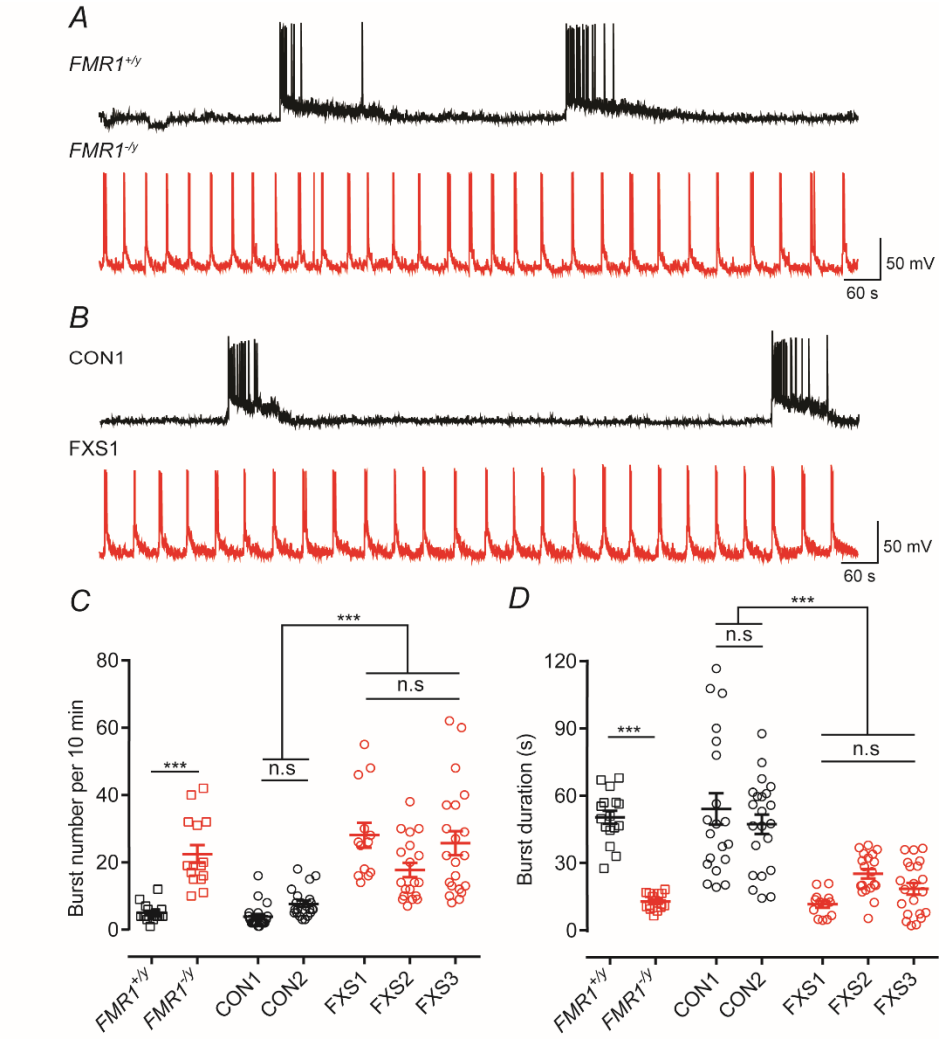

Figure 4.4 Bursts of action potentials occur at high frequencies but with shorter durations in FXS neurons.

(A) Representative current-clamp recording (V_{hold} = –70mV) of spontaneous bursts from either *FMR1*$^{+/y}$ (black) or *FMR1*$^{-/y}$ (red) neuron illustrating the difference in action potential bursting profiles. **(B)** As in (A) but illustration recordings fron hiPSCs lines CON1 (black) and FXS1 (red). **(C)** Mean burst number per 10 minutes of recording for each of the hESC and hiPSC lines. Overall the mean number for bursts (per 10 minutes) are: 5 ± 0.65 (*FMR1*$^{+/y}$; n = 16, N = 3); 22.53 ± 2.63 (*FMR1*$^{-/y}$; n = 15, N = 3); 3.9 ± 0.81 (CON1; n =20, N = 3); 7.727 ± 0.88 (CON2; n = 22, N = 3); 28.07 ± 3.73 (FXS1; n = 13, N = 3); 17.74 ± 2.10 (FXS2; n = 19, N = 3); 25.71 ± 3.56 (FXS3; n = 21, N = 3). **(D)** Mean burst duration for each of the hESC and hiPSC lines. Overall the mean durations are: 50.4228 ± 2.88 s (*FMR1*$^{+/y}$); 12.85 ± 0.92 s (*FMR1*$^{-/y}$); 54.15 ± 7.03 s (CON1); 47.38 ± 4.30 s (CON2); 11.66 ± 1.51 s (FXS1); 25.25 ± 2.1 s (FXS2); 18.55 ± 2.58 s (FXS3). ***p< 0.001, one way ANOVA with post hoc Tukey's test.

4.5 Voltage clamp recordings also shows the aberrant bursting activity of FXS neurons

The bursts of action potentials seen in the current clamp mode can be easily identified as large inward currents in voltage clamp (Fig 4.5). Here also, we found that the frequency of inward currents was higher in the *FMR1*$^{-/y}$ and FXS1 neurons as compared to *FMR1*$^{+/y}$ and CON1 neurons. The duration of the inward current was calculated as the time interval during which the cell remained depolarized. *FMR1*$^{-/y}$ and FXS1 neurons had shorter durations than *FMR1*$^{+/y}$ and CON1 neurons (Fig 4.5A, B). The bursting activity is NMDA receptor dependent as application of the NMDA blocker, AP5 abolished the bursting activity. The expanded traces show the integration of all the synaptic events impinging on the postsynaptic neuron. These synaptic events drive the waves of depolarization and result in bursts of action potentials in current-clamp. Quantification of the number and duration yielded similar values as was seen in voltage clamp (Fig 4.5C, D). The presence of wild-type primary mouse astrocytes was necessary for the development of network activity of the human cortical neurons as we did not observe these bursts in voltage-clamp/current-clamp mode in the neuron-only culture. This is primarily because the network activity is a consequence of synaptic connectivity within the neurons and as we have already seen (chapter 3) neurons in a neuron-only culture have very limited functional synaptic connectivity.

Because the intrinsic properties were not different between the FXS neurons and controls, we hypothesized that the aberrant burst firing activity in the absence of FMRP could be due to altered ionic channel conductances.

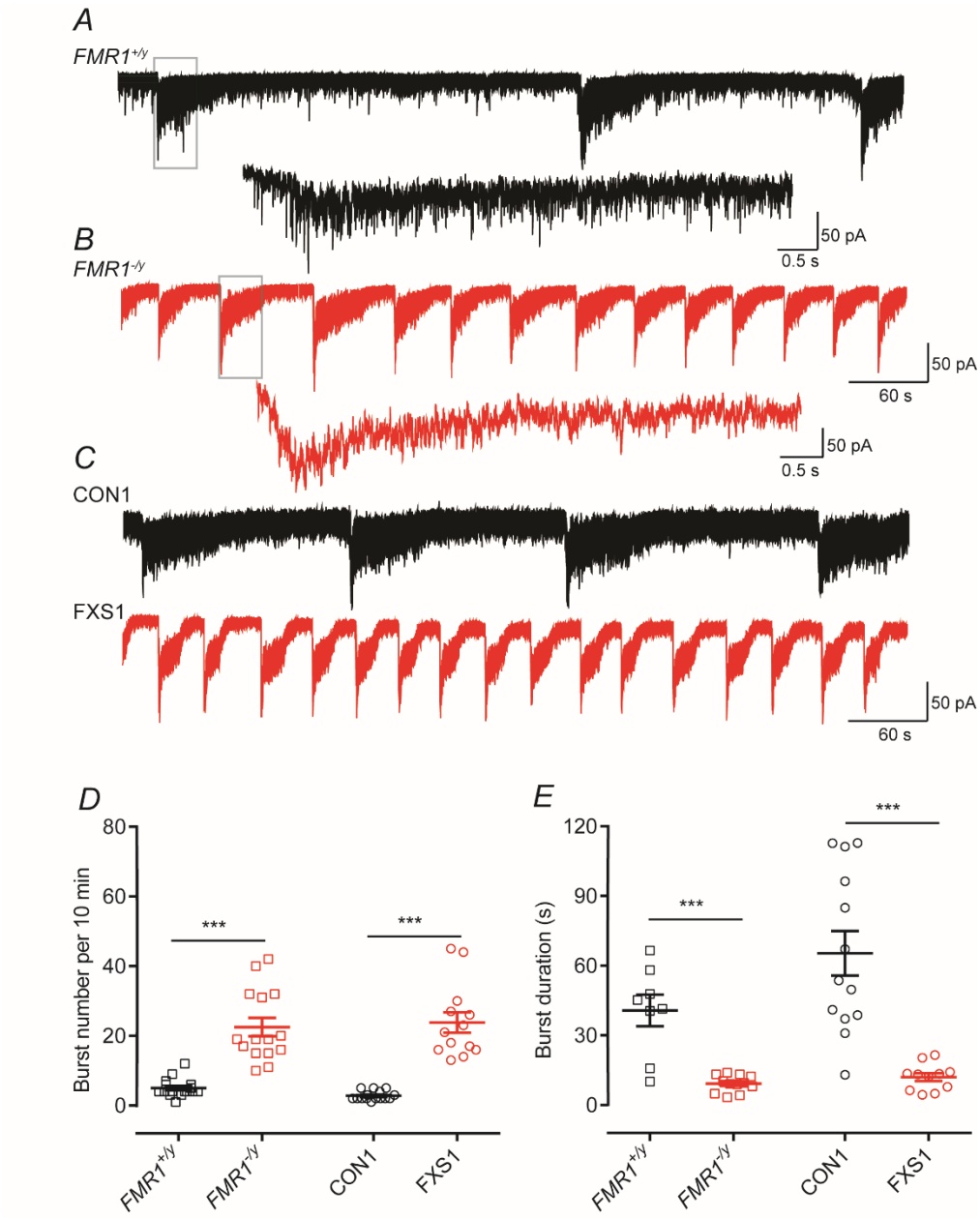

Figure 4.5 FXS neurons display bouts of inward current activity of higher frequencies but of shorter durations compared to control neurons.

(A) Representative voltage-clamp recording (V_{hold} = –70mV) of spontaneous inward currents from either *FMR1*$^{+/y}$ (black) or *FMR1*$^{-/y}$ (red) neurons illustrating the difference in spontaneous events. The insets below each trace illustrate an expanded time-base where evidence of synaptic currents underlying these inward currents can be observed. **(B)** As in (A) but illustration recordings from hiPSCs lines CON1 (black) and FXS1 (red). **(C)** The number of events is higher in neurons lacking *FMR1* than control. Overall the mean number for bursts (per 10 minutes) are: 4.5 ± 0.56 (*FMR1*$^{+/y}$; n = 8, N = 3); 20.67 ± 3.96 (*FMR1*$^{-/y}$; n = 12, N = 3); 2.8 ± 0.34 (CON1; n =13, N = 3); 23.85 ± 2.92 (FXS1; n = 11, N = 3). **(D)** Mean burst durations recorded from FXS neurons are shorter than those from control lines. Overall the mean durations are:

40.72 ± 6.8 s (*FMR1*$^{+/y}$); 9.28 ± 1.05 s (*FMR1*$^{-/y}$); 59.90 ± 9.07 s (CON1); 11.52 ± 1.55 s (FXS1). ***p< 0.001, paired t-test, Wilcoxon test.

4.6 Bursting activity of hPSC derived cortical neurons is dependent on the sodium channel

Recent studies from *Fmr1 KO* mice have shown that the neuronal hyperexcitability in the neurons of entorhinal and prefrontal cortex is due to altered persistent and transient sodium currents (Deng *et al.,* 2016; Routh *et al.,* 2017). The network activity of the hPSC derived cortical neurons is dependent on the sodium current, as the bursts are abolished in the presence of TTX (Fig 4.6). Spontaneous network recordings from a *FMR1*$^{+/y}$ neuron (Fig 4.6A) and *FMR1*$^{-/y}$ neuron (Fig 4.6B) is abolished after addition of 0.5 µM TTX, indicating that the sodium channels play a crucial role in modulation of the network activity.

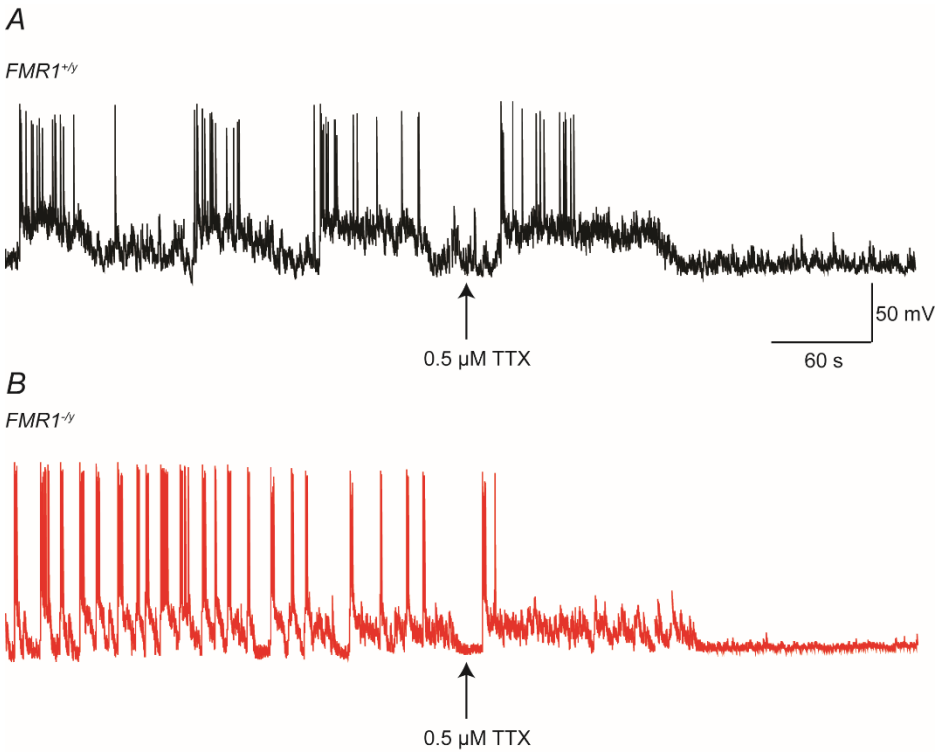

Figure 4.6 TTX abolishes the spontaneous bursting activity in control and FMRP-null neurons

(A) Representative current-clamp trace from a *FMR1*$^{+/y}$ neuron. Burst activity is inhibited after addition of 0.5 µM TTX. **(B)** Representative current-clamp trace from a *FMR1*$^{-/y}$ neuron in the *absence* and *presence* of TTX.

4.7 Loss of FMRP leads to a reduced I_{NaP} magnitude in hPSC derived cortical neurons

We did not quantify the transient sodium current because as we saw in Fig 4.2, there was no difference in the action potential firing between control and FXS neurons after injection of 500 ms depolarizing pulses. However, it is likely that intrinsic properties are altered after prolonged periods of depolarization. One such conductance which is intimately associated with prolonged depolarization is the persistent sodium current (I_{NaP}) and it has been implicated as the major conductance underlying the bursting phenomenon in neurons (Williams & Stuart, 1999; Magistretti & Alonso, 2002; Franceschetti *et al.,* 1995; Parri & Crunelli, 1998; Brumberg *et al.,* 2000). To assess the effect of loss of FMRP on the I_{NaP} of the hPSC derived cortical neurons, we injected a slow depolarizing ramp (20 mV/s) (Fig 4.7A) and recorded the elicited current in the absence and presence of TTX (*traces a* and *b*). The subtracted current (*trace, c*) represented the I_{NaP} . As shown in Fig 4.7A, *FMR1*$^{-/y}$ (*red trace*) neuron showed very less I_{NaP} as compared to *FMR1*$^{+/y}$ neuron (*black trace*). The I_{NaP} current density of *FMR1*$^{-/y}$ and FXS3 neurons is significantly less than *FMR1*$^{+/y}$ and CON2 neurons (Fig 4.7B,C). Given the reduced I_{NaP} of the FXS neurons, we hypothesized that addition of riluzole, a persistent sodium channel antagonist, wouldn't alter the burst profile of the FXS neurons. However, riluzole would change the burst profile of the control neurons. To test this hypothesis, we recorded baseline burst activity (10 min) and added riluzole (0.1 µM) and further recorded for 10 min in *presence* of riluzole. A *FMR1*$^{+/y}$ neuron shows the characteristic long duration, less frequent bursts but the bursting profile changes after addition of riluzole (Fig 4.7D, *black traces*). The frequency of bursts is unaltered, however riluzole significantly shortens the burst duration. In contrast, addition of riluzole doesn't alter the burst frequency or the burst duration of the *FMR1*$^{-/y}$ neuron (Fig. 4.7D, *red traces*). The burst number of *FMR1*$^{+/y}$ and CON2 is not significantly different after addition of riluzole (Fig 4.7E), however the burst duration is significantly reduced in presence of riluzole (Fig 4.7F). Thus, by inhibiting the persistent sodium current, the burst duration of the hPSC derived control neurons can be phenocopied to resemble the short duration bursts of FXS neurons. It should be noted that the reduced I_{NaP} observed in the human FXS neurons is in contrast to the findings from *Fmr1* KO mice, where the neurons from the entorhinal cortex show an increased I_{NaP} conductance (Deng *et al.,* 2016), thus highlighting how the pathophysiology of FXS might vary significantly between rodents and humans.

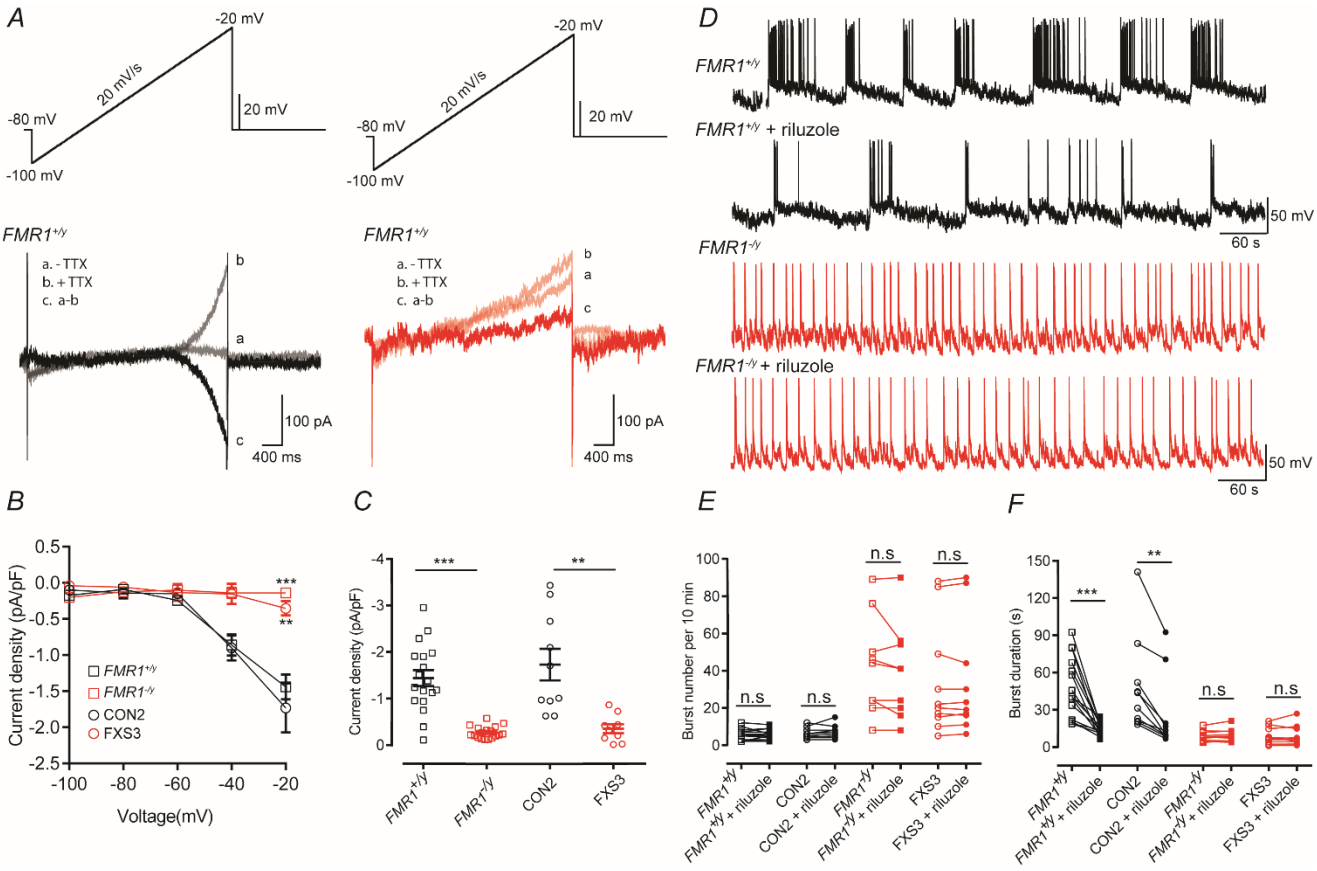

Figure 4.7 FXS neurons have reduced I_{NaP} densities and their burst properties are insensitive to riluzole. **(A)** Persistent sodium currents (I_{NaP}) evoked by a slow depolarizing ramp (−100 mV to −20 mV, 20 mV/s) either before (*traces* a) or during (*traces* b) application of TTX. The TTX-sensitive current (*traces* c) was isolated by subtracting *traces* a and b. **(B)** I-V curves plotted from the ramp-evoked I_{NaP}, showing the decreased I_{NaP} in FXS neurons. Currents are normalized to the corresponding cell capacitance. **(C)** Quantification of current density at −20 mV show significant decrease of the persistent sodium current in FXS neurons. Overall mean current densities are: -1.44 ± 0.17 (*FMR1*$^{+/y}$, n = 18, N=3); -1.73 ± 0.33 (CON2, n = 10, N =3); -0.27 ± 0.03 (*FMR1*$^{-/y}$, n = 18, N=3); -0.35 ± 0.098 (FXS3, n = 9, N = 3). **p< 0.01, ***p< 0.001, two-way repeated measures ANOVA with post hoc Tukey's test, paired t-test, Wilcoxon test. **(D)** Representative traces illustrating spontaneous bursts recorded from either a *FMR1*$^{+/y}$ neuron or a *FMR1*$^{-/y}$ neuron before and after the application of riluzole (0.1 µM). **(E)** Quantification of the number of bursts recorded from *FMR1*$^{+/y}$, CON2, *FMR1*$^{-/y}$ or FXS3 neurons before (open symbols) or after (closed symbols) application of riluzole. Overall the mean number of bursts recorded are: 5.733 ± 0.72 (*FMR1*$^{+/y}$, n = 15, N= 3); 5.733 ± 0.65 (*FMR1*$^{+/y}$ + riluzole, n= 15, N=3); 6.3 ± 0.9 (CON2, n=10, N=3); 7 ± 1.12 (CON2 + riluzole, n=10, N=3); 42.33 ± 8.92 (*FMR1*$^{-/y}$, n = 9, N=3); 38.89 ± 8.49 (*FMR1*$^{+/y}$ + riluzole, n=9, N=3); 34.1 ± 9.52 (FXS3, n=10, N=3); 34.3 ± 9.62 (FXS3 + riluzole, n=10, N=3). **(F)** Quantification of the duration of bursts recorded from *FMR1*$^{+/y}$, CON2, *FMR1*$^{-/y}$ or FXS3 neurons before (open symbols) or after (closed symbols) application of riluzole. Overall the mean burst durations are: 47.86 ± 6.27 s (*FMR1*$^{+/y}$); 14.14 ± 1.33 s (*FMR1*$^{+/y}$ + riluzole); 47.81 ± 12.14 s (CON2); 25.55 ± 9.54 s (CON2 + riluzole); 8.77 ± 1.34 s (*FMR1*$^{-/y}$); 9.43 ± 1.62 s (*FMR1*$^{+/y}$); 8.91 ± 2.19 s (FXS3); 9.01 ± 2.52 (FXS3 + riluzole) **p< 0.01; ***p< 0.001, paired t-test, Wilcoxon test.

4.8 Potassium conductances are affected by the loss of FMRP, contributing to the altered burst firing

FMRP is known to interact with several mRNAs encoding potassium channels (Darnell *et al.,* 2011). Studies have shown several potassium channel conductances to be impaired by the loss of FMRP (reviewed in Ferron, 2016). To test whether potassium conductances are involved in maintaining the spontaneous network activity of the hPSC derived cortical neurons we used a global potassium channel blocker, tetraethyammonium bromide (TEA-Br). The baseline burst activity (10 min) was recorded from controls and FXS neurons. Then 1mM TEA was added and network activity was recorded for another 10 min (Fig 4.8). In the presence of TEA, the bursting profile of *FMR1*$^{+/y}$ neuron was altered to give shorter duration bursts which were more frequent (Fig 4.8A). TEA had no significant effect on the bursting profile of the *FMR1*$^{-/y}$ neuron (Fig 4.8B). Quantification of the burst number and duration (Fig 4.8C-D) shows the significant increase in burst number and decrease in burst duration of *FMR1*$^{+/y}$ and CON2 neurons, following application of TEA. Thus blocking potassium conductances could alter the bursting profile of the control neurons to resemble the FXS neurons, thereby suggesting that potassium conductances of hPSC derived cortical neurons are downregulated by the loss of FMRP. Because TEA is a global potassium blocker, this experiment did not help us to identify the particular potassium channel responsible for altered bursting profiles.

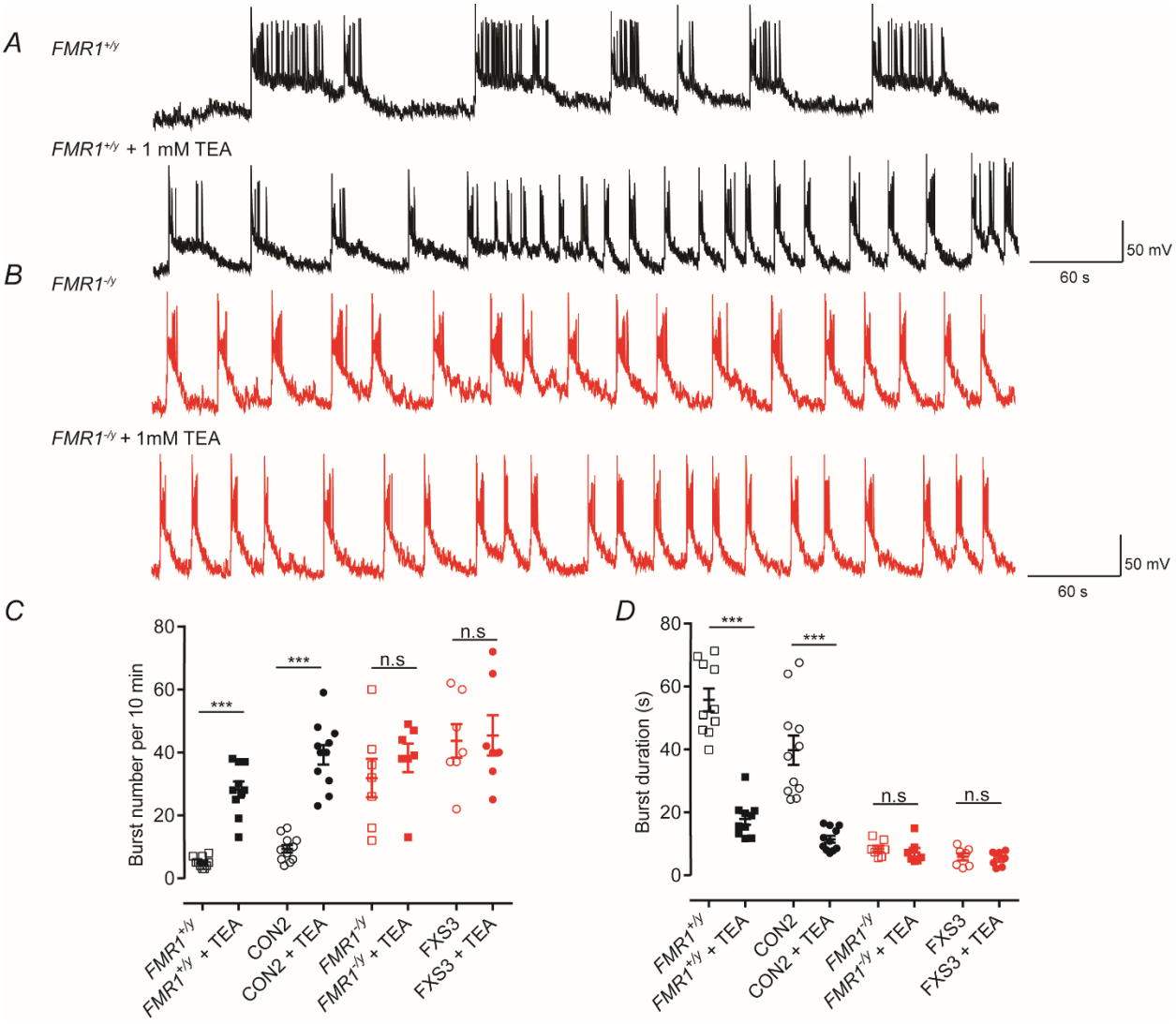

Figure 4.8 Pharmacological blocking of K^+ channels alters the bursting profile of the control neurons making it similar to the neurons lacking FMR1.

(A) Representative traces of a *FMR1*$^{+/y}$ neuron firing spontaneous bursts before the application of TEA. The *bottom* trace shows the change in the burst frequency and duration of the same *FMR1*$^{+/y}$ neuron after the application of 1 mM TEA. **(B)** Representative traces from a *FMR1*$^{-/y}$ neuron before the application of TEA. The *bottom* trace from the same *FMR1*$^{-/y}$ neuron after the application of 1 mM TEA shows no change in the bursting profile. **(C)** Burst frequency of control neurons in *presence* of TEA was significantly higher but the burst frequency of neurons lacking *FMR1* was not significantly altered. **(D)** Burst duration of control neurons in *presence* of TEA was significantly shorter but the burst duration of neurons lacking *FMR1* did not show any significant change. ***p< 0.001, paired t-test, Wilcoxon test. The number of cells were: *FMR1*$^{+/y}$, n = 10; CON2, n = 11; *FMR1*$^{-/y}$, n = 6; FXS3, n = 7.

4.9 FXS neurons show reduced BK_{Ca} currents and the bursting activity is insensitive to paxilline

As seen in the previous section, the bursting activity of the FXS neurons was insensitive to TEA, suggesting a downregulation of potassium channels. However, TEA is not specific to a particular potassium channel. Studies have shown the big conductance calcium activated potassium (BK_{Ca}) channels to be dysregulated by the loss of FMRP and this was the underlying cause of the aberrant network firing in the entorhinal cortex and following genetic upregulation or pharmacological activation of BK_{Ca} channels, the aberrant network activity was restored to normal (Deng *et al.,* 2013, 2016; Zhang *et al.,* 2014). To assess whether BK_{Ca} channels were affected by the loss of FMRP in the hPSC derived cortical neurons, we injected a depolarizing ramp (-110 mV to 40 mV, 100 mV/s) (Fig 4.9A). The currents in response to the depolarizing ramp were recorded in absence and presence of BK_{Ca} specific channel blocker, paxilline (*traces a,b*). Fig 4.9B shows the currents from *FMR1*$^{+/y}$ (*black traces*) and *FMR1*$^{-/y}$ neuron (*red traces*) respectively, elicited by the depolarizing ramp. The subtracted trace (Fig 4.9B, *below*) shows the reduced I_{BKCa} of the *FMR1*$^{-/y}$ neuron. Quantification of the I_{BKCa} current densities (Fig 4.9C, D) shows the significantly reduced I_{BKCa} of the *FMR1*$^{-/y}$ and FXS3 neurons as compared to *FMR1*$^{+/y}$ and CON4. We hypothesized that the reduced I_{BKCa} of the FXS neurons, would render their burst activity insensitive to paxilline whereas it would alter the burst activity of the control neurons. To test this, after baseline burst recordings (10 min), paxilline (10 µM) was washed in and burst activity recorded for further 10 min. Fig 4.9E shows the burst firing from *FMR1*$^{+/y}$ neuron (black traces) before and after addition of paxilline. Paxilline alters the frequency of bursts of the *FMR1*$^{+/y}$ neuron without affecting the burst duration. The bursting activity of *FMR1*$^{-/y}$ neuron doesn't change after addition of paxilline (Fig 4.9E, *red traces*). The burst number (Fig 4.9F) of *FMR1*$^{+/y}$ and CON2 neurons shows a significant increase following application of paxilline whereas the burst number of *FMR1*$^{-/y}$ and FXS3 is not altered. Paxilline doesn't alter the burst duration (Fig 4.9G) of controls and FXS neurons. These results are in agreement with the observations from *Fmr1* KO mice. The pathophysiology of FXS is quite complex and while some aspects maybe similar to that seen in rodent and other animal models, other aspects are starkly different.

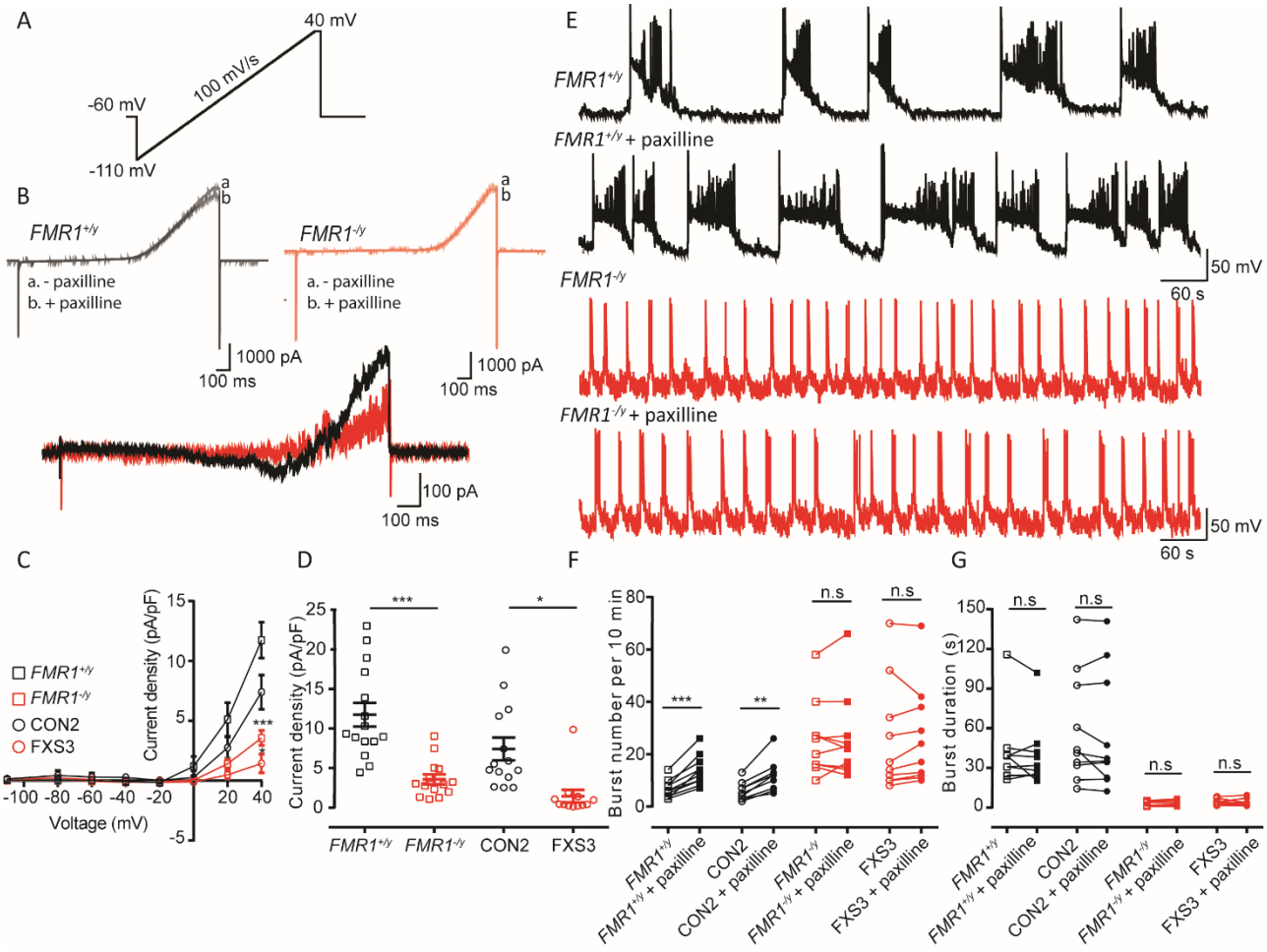

Figure 4.9 FXS neurons have reduced I_{BKCa} densities and their burst properties are insensitive to paxilline.

(A) Large Ca-activated potassium currents (I_{BKCa}) evoked by a depolarizing voltage ramp from −110 mV to +40 mV, 10 mV/s, with a hold of 50ms at +40 mV. **(B)** The I_{BKCa} was isolated by subtracting the currents recorded in the absence and presence of paxilline (10 µM). **(C)** I-V curves plotted from the ramp-evoked I_{BKCa} showing the decreased I_{BKCa} in FXS neurons. Currents are normalized to the corresponding cell capacitance. **(D)** Quantification of current densities at +40 mV show significant decrease of I_{BKCa} in FXS neurons. Overall mean current densities are: 11.73 ± 1.49 (*FMR1*$^{+/y}$, n = 15, N=3); 7.4 ± 1.43 (CON2, n = 14, N =3); 3.57 ± 0.62 (*FMR1*$^{-/y}$, n = 14, N=3); 1.44 ± 0.78 (FXS3, n = 12, N = 3). *p< 0.05, ***p< 0.001, two-way repeated measures ANOVA with post hoc Tukey's test, paired t-test, Wilcoxon test. **(E)** Representative traces illustrating spontaneous bursts recorded from either a *FMR1*$^{+/y}$ neuron or a *FMR1*$^{-/y}$ neuron before and after the application of paxilline (10 µM) and illustrating the increase of action potential burst frequencies in *FMR1*$^{+/y}$ neurons in the presence of paxilline. **(F)** Quantification of the number of bursts recorded from *FMR1*$^{+/y}$, CON2, *FMR1*$^{-/y}$ or FXS3 neurons before (open symbols) or after (closed symbols) application of paxilline. Overall mean number of bursts are: : 6.7 ± 1.086 (*FMR1*$^{+/y}$, n = 10, N= 3); 13.8 ± 1.85 (*FMR1*$^{+/y}$ + paxilline, n= 10, N=3); 5.6 ± 1.08 (CON2, n=10, N=3); 11.3 ± 1.94 (CON2 + paxilline, n=10, N=3); 25.5 ± 4.51 (*FMR1*$^{-/y}$, n = 10, N=3); 26 ± 5.12 (*FMR1*$^{+/y}$ + paxilline, n=10, N=3); 25.4 ± 6.6 (FXS3, n=10, N=3); 26.5 ± 5.95 (FXS3 + paxilline, n=10, N=3). **(G)** Quantification of the duration of bursts recorded from *FMR1*$^{+/y}$, CON2, *FMR1*$^{-/y}$ or FXS3 neurons before (open symbols) or after (closed

symbols) application of paxilline. Overall mean burst duration are: 40.97 ± 8.68 s (*FMR1*$^{+/y}$); 38.47 ± 7.85 s (*FMR1*$^{+/y}$ + paxilline); 58.65 ± 13.12 s (CON2); 56.08 ± 14.04 s (CON2 + paxilline); 2.65 ± 0.53 s (*FMR1*$^{-/y}$); 3.08 ± 0.68 s (*FMR1*$^{+/y}$ + paxilline); 4.107 ± 0.64 s (FXS3); 3.93 ± 0.77 (FXS3 + paxilline). **p< 0.01, ***p< 0.001, paired t-test, Wilcoxon test

4.10 Blocking I_{NaP} and I_{BKCa} simultaneously increases action potential burst frequencies and decreases their duration in control neurons

In the above sections we saw that altering specific conductances (I_{Na} and I_{BKCa}) separately using channel specific blockers in control neurons altered the burst duration and burst number respectively. We assessed whether the effects of blocking I_{NaP} and I_{BKCa} were additive on the action potential burst parameters recorded from *FMR1*$^{+/y}$ and CON2 lines. Figure 4.10A,B illustrates simultaneous application of riluzole and paxilline gave rise to an action potential burst profile that was similar to that seen in *FMR1*$^{-/y}$ or FXS3 neurons albeit that the absolute burst frequencies and burst durations (Fig 4.10C, D) were still different (statistically) from that seen in FXS neurons. Furthermore, application of riluzole and paxilline resulted in no overall change in these parameters in *FMR1*$^{-/y}$ or FXS3 neurons.

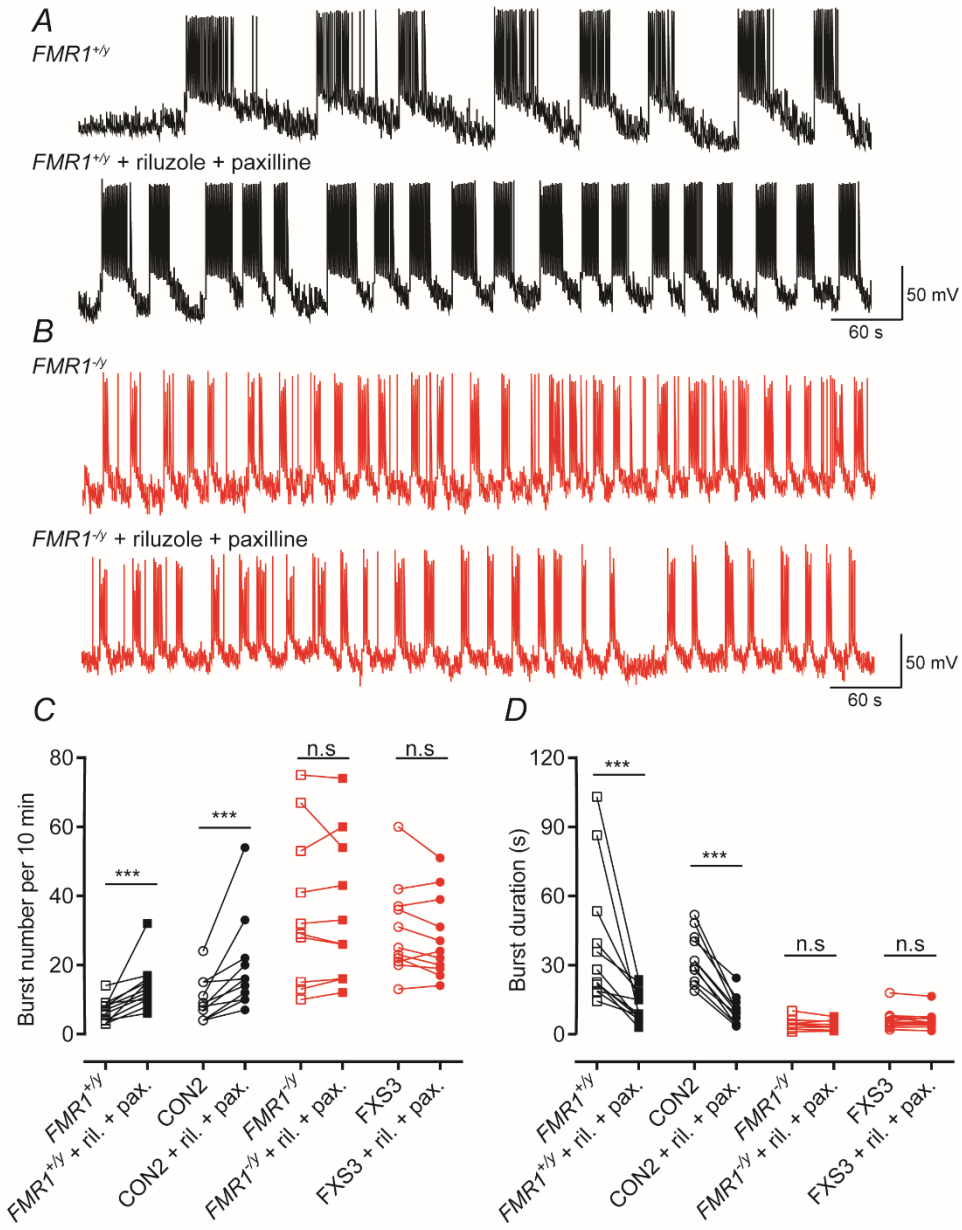

Figure 4.10 Pharmacological block of I_{NaP} and I_{BKCa} increases action potential burst frequencies and decreases their duration in control neurons.

(A) Representative traces of a *FMR1*$^{+/y}$ neuron illustrating spontaneous action potential bursting before and after the application of riluzole (0.1 µM) and paxilline (10 µM). **(B)** As in (A) but illustrating traces obtained from a *FMR1*$^{-/y}$ neuron. **(C)** Quantification of burst number in *FMR1*$^{+/y}$, CON2, *FMR1*$^{-/y}$ and FXS3 lines before and after the application of riluzole and paxilline. For both *FMR1*$^{+/y}$ and CON2 lines the number of bursts recorded in a 10 minute period increased significantly but these drugs did not affect burst frequency in *FMR1*$^{-/y}$ and FXS3. Overall the mean number of bursts are: 6.917 ± 0.91 (*FMR1*$^{+/y}$, n = 12, N= 3); 13.75 ± 1.91 (*FMR1*$^{+/y}$ + riluzole + paxilline, n= 12, N=3); 9.909 ± 1.84 (CON2, n=11, N=3); 19.45 ± 4.07 (CON2 + riluzole + paxilline, n=11, N=3); 36.3 ± 7.12 (*FMR1*$^{-/y}$, n = 10, N=3); 36 ± 6.64 (*FMR1*$^{+/y}$ + riluzole + paxilline, n=10, N=3); 30 ± 3.97 (FXS3, n=11, N=3); 28 ± 3.6 (FXS3 + riluzole + paxilline, n=11, N=3). **(D)** Quantification of action potential burst durations in each of the four lines examined. Simultaneous application of riluzole and paxilline resulted in a significant decrease in the duration of action potential bursts in *FMR1*$^{+/y}$ and CON2 lines but was without effect in *FMR1*$^{-/y}$ and FXS3 lines. Overall the mean burst duration are: 38.68 ± 8.24 s (*FMR1*$^{+/y}$); 12.12 ± 1.96 s (*FMR1*$^{+/y}$ + riluzole + paxilline); 33.3 ± 3.31 s (CON2); 10.32 ± 1.86 s (CON2 + riluzole + paxilline); 4.23 ± 0.81 s (*FMR1*$^{-/y}$); 3.7 ± 0.68 s *FMR1*$^{+/y}$ + riluzole + paxilline); 6.36 ± 1.28 s (FXS3); 6.05 ± 1.16 s (FXS3 + riluzole + paxilline). ***p< 0.001, paired t-test, Wilcoxon test.

4.11 Pharmacological activation of NaP channels partially rescue the bursting profile of FXS neurons to look more like the controls

As seen in section 4.7, hPSC cortical FXS neurons display a decrease in the I_{NaP} magnitude. We hypothesized that activation of the voltage-gated Na^+ channels would "rescue" the aberrant bursting activity of the FXS neurons. To test this hypothesis, in a final set of experiments we tested the effect of the sodium channel opener, veratridine on the bursting activity of the neurons. After recording the baseline burst activity for 10 mins, veratridine (0.5 µM) was washed in and burst activity was recorded for another 10 min. Indeed, the voltage-dependent Na^+ channel activator, veratridine (0.5 µM), has a selective action on the burst firing patterns we recorded. As illustrated in Figure 4.11, it had no significant effect on the burst parameters we measured in *FMR1*$^{+/y}$ and CON2 lines but altered the bursting profile in *FMR1*$^{-/y}$ and FXS3 lines (Fig. 4.11A-B). Veratridine significantly reduced the frequency of action potential bursts and increased the durations of *FMR1*$^{-/y}$ and FXS3 lines (Fig. 4.11C, D). Thus, to some extent activating voltage-dependent Na^+ channels in FXS neurons gave rise to activity that phenocopies that seen in *FMR1*$^{+/y}$ and CON2 lines.

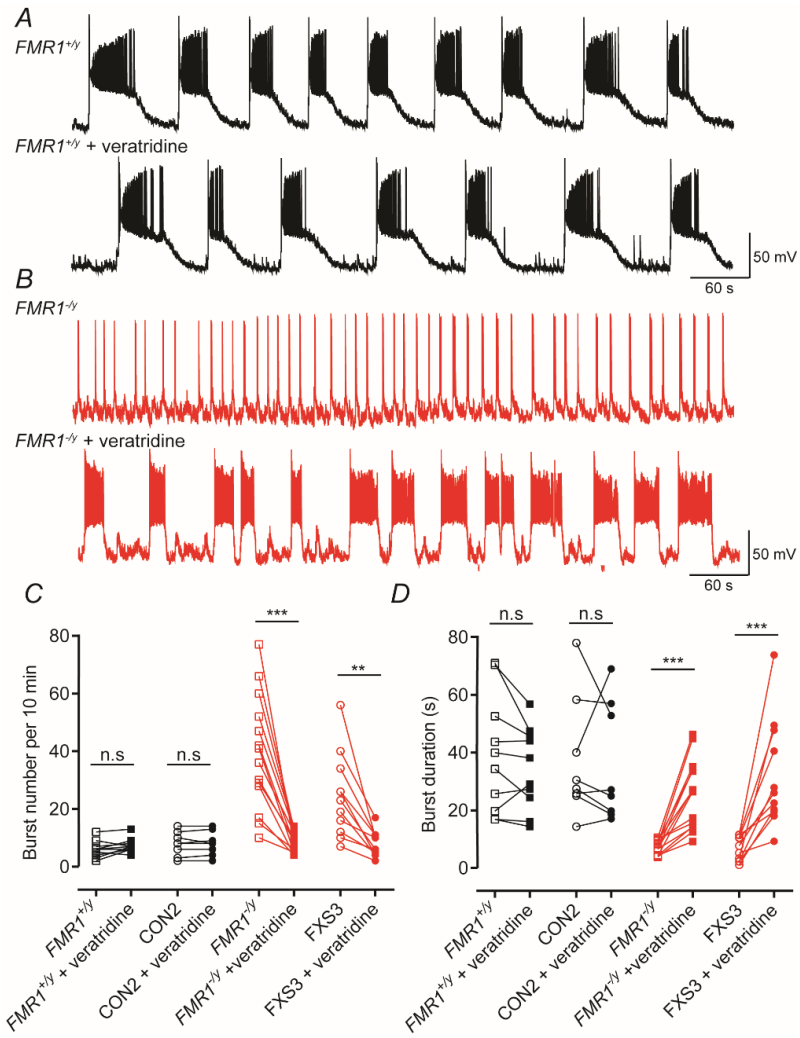

Figure 4.11 In FXS neurons activation of voltage-dependent Na^+ channels decreases action potential burst frequencies but increases their duration.

(A) Representative traces of a *FMR1*$^{+/y}$ neuron illustrating spontaneous action potential bursting before and after the application of veratridine (0.5 µM). **(B)** As in (A) but illustrating traces obtained from a *FMR1*$^{-/y}$ neuron. **(C)** Quantification of burst number in *FMR1*$^{+/y}$, CON2, *FMR1*$^{-/y}$ and FXS3 lines before and after the application of veratridine. Veratridine reduced significantly the frequency of bursts in lines lacking FMRP. Overall the mean number of bursts are: 6 ± 0.92 (*FMR1*$^{+/y}$, n = 10, N= 3); 7.3 ± 0.76 (*FMR1*$^{+/y}$ + veratridine, n= 10, N=3); 7.87 ± 1.46 (CON2, n=8, N=3); 8 ± 1.45 (CON2 + veratridine, n=8, N=3); 39.29 ± 5.27 (*FMR1*$^{-/y}$, n = 14, N=3); 8.857 ± 0.98 (*FMR1*$^{+/y}$ + veratridine, n=14, N=3); 24.45 ± 4.37 (FXS3, n=11, N=3); 7.818 ± 1.32 (FXS3 + veratridine, n=11, N=3) **(D)** Quantification of action potential burst durations in each of the four lines examined. Veratridine increased significantly the duration of bursts in *FMR1*$^{-/y}$ and FXS3 lines and had no overall effect on *FMR1*$^{+/y}$ and CON2 lines. Overall the mean burst durations are: 39.09 ± 6.47 s (*FMR1*$^{+/y}$); 34.34 ± 4.5 s (*FMR1*$^{+/y}$ + veratridine); 37.42 ± 7.39 s (CON2); 35.77 ± 7.25 s (CON2); 7.318 ± 0.64 s (*FMR1*$^{-/y}$); 25.5 ± 3.23 s (*FMR1*$^{+/y}$ + veratridine); 7.004 ± 1.28 s (FXS3); 32.26 ± 5.66 (FXS3 + veratridine). For both (C) and (D) **p< 0.01, ***p< 0.001, paired t-test, Wilcoxon test.

Discussion

Altered cortical network excitability have been described in FXS patients (reviewed in Contractor *et al.,* 2015), however detailed mechanistic studies to reveal the physiological underpinnings of the disease have not been done in the human context. Most of the understanding of the FXS pathophysiology have been from the rodent models of FXS and while it has helped glean many insights, we must also consider that they may not always reflect human-specific physiology. In FXS, the temporal profile of FMRP expression is very critical. Studies demonstrate that despite the CGG repeat expansion, FMRP can be detected in human embryonic tissue till the end of first trimester (Willemsen *et al.,* 2002; Mor-Shaked & Eiges, 2018). This is not seen in genetically engineered rodent models of FXS and hence these models may not be able to capture the full FXS etiology. The ability to model neurodevelopmental disease using human pluripotent stem cells can give us many mechanistic insights into the FXS pathophysiology in humans.

In this chapter, we have reported the presence of spontaneous network activity displayed in the hPSC derived cortical neurons *in vitro* when co-cultured with primary mouse astrocytes. We have also provided detailed mechanistic insights into how loss of FMRP can lead to aberrant network activity. The key findings emerging from this part of the study are:-

- The intrinsic and action potential properties of FXS neurons are not different than control neurons.
- In a neuron-astrocyte co-culture, the neurons are able to develop considerable synaptic activity. The synaptic activity is of FXS neurons is similar to the control neurons.
- hPSC derived neurons in co-culture, develop robust spontaneous network activity characterized by bursts of action potentials.
- FXS neurons display an altered bursting profile – more frequent bursts of shorter duration.
- FXS neurons show reduced persistent sodium current (I_{NaP})
- FXS neurons show reduced big conductance, calcium activated potassium current (I_{BKCa})

All of the observations summarized above have been observed both in the iPSC as well as the ESC derived isogenic lines, thereby unequivocally caused by the loss of FMRP and not any other external factors.

Altered network activity as a consequence of hyperexcitability of cortical neurons have been reported in rodent models of FXS with a concomitant change in the active and passive membrane properties (Gibson *et al.,* 2008; Goncalves *et al.,* 2013; Zhang *et al.,* 2014; Booker *et al.,* Domanski *et al.,* 2019). However the FXS pathophysiology is very complex and diverse. A recent study using mouse primary cortical neuronal

culture showed that the active and passive membrane properties are not different between control and *Fmr1* KO neurons. Moreover loss of FMRP did not alter the synaptic and intrinsic excitability of the neurons. Another study reported neuronal hypoexcitability in the visual cortex of fetal *Fmr1* KO mice (Berzhanskaya *et al.,* 2016). These exemplar studies highlight the diversity of the FXS etiology and how the properties of FXS neurons depend on the developmental stage and neuronal subtype being investigated. One of the first studies using hES derived cortical neurons report the *FMR1* null neurons to be hypoexcitable (Telias *et al.,* 2015). These neurons were able to fire only one action potential following depolarized current injections. In the previous chapter we had reported that the loss of FMRP did not affect the passive and active membrane properties of the hPSC derived neurons in a neuron-only culture. The FXS neurons were able to generate sustained action potentials in response to depolarized current steps. However, as evidenced by the intrinsic membrane parameters and the lack of synaptic activity, these neurons were immature and hence unsuitable for the study. Co-culturing hPSC derived neurons with primary rodent astrocytes led to accelerated maturation of neurons evidenced by a decrease in their resting potential, an increase in the Na+ and K+ currents and an increased propensity to fire action potentials (Johnson *et al.,* 2007). Indeed, we report that co-culturing of the neurons with primary mouse astrocytes led to an enhanced maturation profile. These neurons were able to fire mature action potentials and developed robust synaptic activity. However, we found that loss of FMRP did not alter the intrinsic and synaptic properties of the neurons. This result is in agreement with a recent study using hES derived neurons that shows no change in the baseline synaptic activity in the absence of FMRP (Zhang *et al.,* 2018).

During development, giant depolarizing potentials (GDPs) provide synaptic activity. GDPs are network driven large oscillations and are important to establish proper synchrony between the neurons (Ben-Ari, 2001). In the cerebral cortex these rhythmic oscillations are pervasive and critical for proper cognitive functions (Silva *et al.,* 1991). Co-culturing human iPSC derived neurons with rat astrocytes also led to the development of similar rhythmic network activity *in vitro* (Odawara *et al.,* 2014). Indeed, we report robust development of network bursting activity in the hPSC derived neurons co-cultured with mouse astrocytes after 8 weeks *in vitro.* Several studies have suggested that loss of FMRP led to alterations in the cortical circuits of *Fmr1* KO mice resulting in network activity deficits (Goncalves *et al.,* 2013; Gibson *et al.,* 2008; Testa-Silva *et al.,* 2012). In the hPSC derived neurons, loss of FMRP led to aberrant bursting phenotype characterized by more number of bursts of shorter durations. We found this to be a consistent phenotype across all the ESC and iPSC derived FXS lines. These results suggest that though loss of FMRP doesn't affect

the intrinsic and synaptic properties of individual neurons, the whole neuronal network is dysregulated in FMRP's absence.

FMRP binds to several mRNAs that encode proteins associated with ion channels or their regulation (Darnell *et al.,* 2011). Studies investigating prefrontal and entorhinal cortical dysfunction in the absence of FMRP report an increase in transient (Routh *et al.,* 2017) and persistent sodium current (Deng & Klyachko, 2016). Sodium current is an integral component governing the bursting activity of neurons. Indeed we observe a complete abolishment of bursting activity following addition of TTX. This led us to investigate the effect of loss of FMRP on the persistent sodium current. We report a decrease in the persistent sodium current magnitude in FXS neurons. Due to this reduced I_{NaP} addition of riluzole, a perisistent sodium channel blocker doesn't change bursting profile of the FXS neurons. However, the burst duration of control neurons is significantly reduced in the presence of riluzole. Thus, persistent sodium current plays an important role in determining the burst duration of the hPSC derived cortical neurons and is dysregulated by the loss of FMRP.

Several potassium channels are dysregulated in the absence of FMRP (reviewed in Ferron, 2016). Using a non-specific potassium blocker, tetraethylammonium bromide (TEA) we observe a change in the bursting profile of the control neurons – bursts durations become shorter and frequency increases. Thus, blocking the potassium currents, alters the network activity of the control neurons to resemble that of the FXS neurons. Studies have reported a dysfunction in the big conductance, calcium activated (BK_{Ca}) channel in the absence of FMRP (Deng *et al.,* 2013). FMRP interacts with the auxillary β4 subunit, of BK_{Ca} and loss of FMRP results in a decrease in $I_{BKCa.}$ Genetic upregulation or pharmacological activation of BK_{Ca} rescues the defects in the absence of FMRP (Deng & Klyachko, 2016; Zhang *et al.,* 2014). We also report a decrease in the current conducted by BK_{Ca} channels in FXS neurons. Indeed, blocking BK_{Ca} with specific channel blocker, paxilline doesn't change the bursting profile of FXS neurons, however in controls, paxilline increased the frequency of bursts. Thus, BK_{Ca} together with persistent sodium channel is involved in maintaining the bursting activity of hPSC derived cortical neurons. Blocking NaP and BK_{Ca} channels simultaneously using paxilline and riluzole together, changed the burst number and burst duration of the control neurons while the FXS neurons remained unaffected.

Having seen the dysfunction of the persistent sodium channels in the absence of FMRP, we used the voltage-gated sodium channel activator, veratridine. We observed a significant increase in the burst

duration and decrease in the burst frequency of the FXS neurons. Thus, potentiating the sodium channel current could partially “rescue” the aberrant network activity in the absence of FMRP.

Thus, in this chapter, we have provided a comprehensive analysis of how loss of FMRP leads to aberrant spontaneous network activity of neurons. We have demonstrated that pharmacological manipulations can alter the action potentials burst profiles in both control and FMRP-null human cortical neurons, making them appear like their genetic counterpart. Our study indicates that many of the FMRP targets found to be dysregulated in rodent models are also potential targets in the human-based system. However, we also show the difference in how these FMRP targets are dysregulated in the human context as compared to the rodent models. In combination with previous *Fmr1 KO* mice studies, our data suggest that regulating network activity and the underlying channels is critical in FXS. Thus, future studies should aim to develop potential therapeutics that can selectively target these ion channels and assess these drugs vigorously in hPSC models.

Summary

The cortical neuronal network activity is shaped by a concerted effort of neurons and astrocytes (Lines *et al.,* 2020). Several *in vitro* studies have shown that the human stem cell derived neurons develop spontaneous network activity in the presence of rodent astrocytes (Odawara *et al.,* 2014; Tang *et al.,* 2013; Weick *et al.,* 2011). In chapter 4, we have shown that hPSC derived glutamatergic cortical neurons co-cultured with primary mouse astrocytes develop robust spontaneous network activity.

In our studies, co-culture of hPSC derived FXS neurons with mouse astrocytes still displayed the aberrant network activity indicating that FMRP expressing mouse astrocytes were unable to rescue the network activity impairments of human neurons. Multiple lines of evidence suggest that there are significant differences between rodent and human astrocytes (Oberheim *et al.,* 2009; Zhang *et al.,* 2016). This led us to ask if the presence of human astrocytes would have any non-cell autonomous effects on the neuronal function.

Thus, we generated co-cultures of hPSC derived neurons with hPSC derived astrocytes to investigate the role of human astrocytes in the FXS pathophysiology. In this study, one control (CON2) and two FXS patient lines (FXS2, FXS3) of human cortical neurons and astrocytes derived from iPSCs are used. In addition to these, the ESC derived isogenic pair *FMR1*$^{+/y}$ and *FMR1*$^{-/y}$ is used. For the first time, in specific experiments, astrocytes derived from the gene-corrected iPSC line (FXS2Δ) are used wherein, the *FMR1* gene was reactivated using CRISPR-Cas9. This gene-corrected iPSC line serves as another iPSC control. We find that the network activity of the neurons is dependent on the astrocyte genoptye.

In this chapter, we have also studied the effect of astrocyte conditioned medium (ACM) from iPSC (CON2, FXS2, FXS3) and ESC (*FMR1*$^{+/y}$ and *FMR1*$^{-/y}$) cell lines on the cortical network activity. Further, we have studied the modulation of neuronal persistent sodium channel (NaP) by the astrocytes and ACM to provide a mechanistic basis of the non-cell autonomous modulation of neuronal network activity.

Results

5.1 Co-cultures of hPSC derived neurons with hPSC derived FXS astrocytes does not affect the maturation of the neurons

The morphological and metabolic changes in astrocytes following the loss of FMRP are reminiscent of the astrocyte response to CNS injuries and diseases (reviewed in Boghdadi *et al.,* 2020). Recent studies have also shown that loss of FMRP selectively in the astrocytes leads to spine dysmorphogenesis and impaired learning in the *Fmr1* KO mouse models (Jacobs & Doering, 2010; Hodges *et al.,* 2017). In the previous chapters we observed no significant changes in the morphology of iPSC and ESC derived FXS neurons in a neuron-only culture or in a co-culture with primary mouse astrocytes. To understand the FXS pathophysiology in a completely human system, we generated co-cultures of hPSC derived neurons with hPSC derived astrocytes (Fig 5.1A). After 8 weeks *in vitro* the neurons and astrocytes were stained with Map2ab and GFAP, respectively. We did not observe any significant difference in the morphology of human neurons and astrocytes in the absence of FMRP thus suggesting that loss of FMRP did not significantly disrupt the maturation of the neurons and astrocytes.

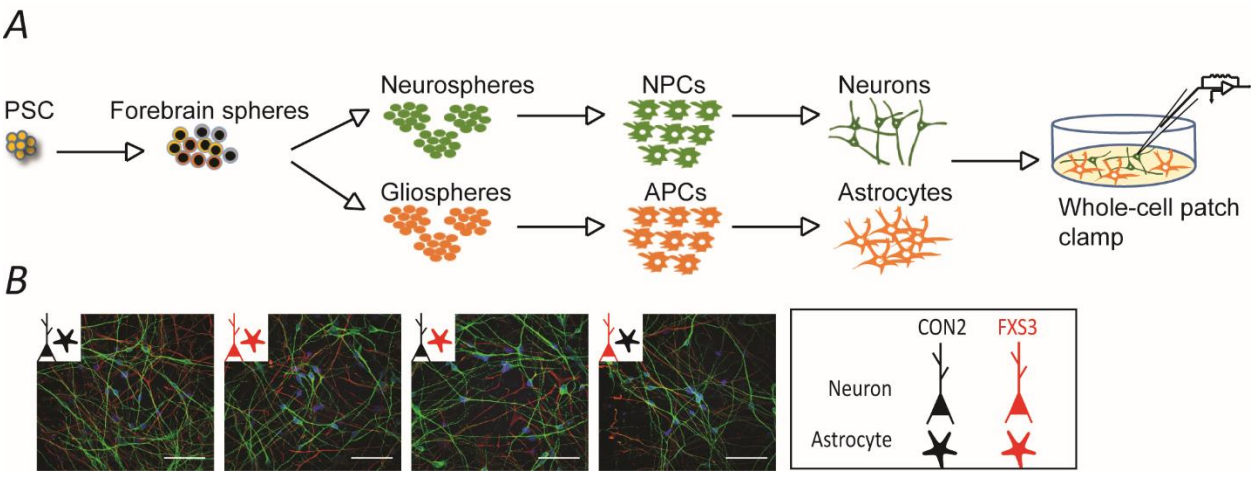

5.1 Loss of FMRP does not affect the morphology of human neurons and astrocytes.

(A) Schematic showing the generation of neurons and astrocytes from human pluripotent stem cells. **(B)** Representative confocal images of hiPSC (CON2 and FXS3) derived cortical neurons expressing Map2ab co-cultured with hiPSC derived astrocytes expressing GFAP. *Left to right*, neurons were co-cultured in four combinations: CON2 neurons with CON2 astrocytes, FXS3 neurons with FXS3 astrocytes, CON2 neurons with FXS3 astrocytes, FXS3 neurons with CON2 astrocytes. Scale bar = 50 µM. *Work done by Rakhi Pal and Bharath Reddy*.

5.2 Human astrocytes derived from pluripotent stem cells modulate the network activity of hPSC derived cortical neurons

Several *in vitro* studies have shown the modulatory effect of astrocytes on the burst firing of neurons (Tukker *et al.,* 2018; Paavilainen *et al.,* 2018). In the previous chapter, we provided a detailed analysis of the bursting properties of hPSC derived cortical neurons when co-cultured with primary mouse astrocytes. In the absence of FMRP, the cortical neurons displayed an aberrant burst firing – more frequent bursts, short burst duration (Das Sharma *et al.,* 2020). This type of burst firing henceforth will be referred to as "FXS bursting". Multiple lines of evidence suggest the presence of FMRP in the astrocytes during early-mid postnatal brain development (Gholizadeh *et al.,* 2015; Pacey & Doering, 2007). Absence of FMRP led to hypertrophy and increased GFAP expression in the astrocytes of the neocortex of *Fmr1* KO mice (Lee *et al.,* 2019). As discussed in Chapter 4, we observed aberrant burst firing of the FMRP-null neurons in the presence of healthy rodent astrocytes. Thus healthy mouse astrocytes were unable to rescue the aberrant network activity of human cortical neurons. This led us to investigate the bursting activity of the neurons co-cultured with human astrocytes. We conducted whole-cell patch clamp recordings from 8 week *in vitro* hPSC derived cortical neurons co-cultured with hPSC derived astrocytes. Recordings from CON2 neurons co-cultured with CON2 astrocytes displayed the control burst firing – low burst number, longer duration (Fig 5.2A). In contrast, FXS3 neurons co-cultured with FXS3 astrocytes displayed FXS bursting profile - higher frequency of bursts, but of lesser duration (Fig 5.2B). Analysis of the number of bursts (Fig 5.2C) and burst duration (Fig. 5.2D) across all the iPSC and ESC derived cell lines showed that FXS neurons co-cultured with FXS astrocytes display the aberrant burst profile.

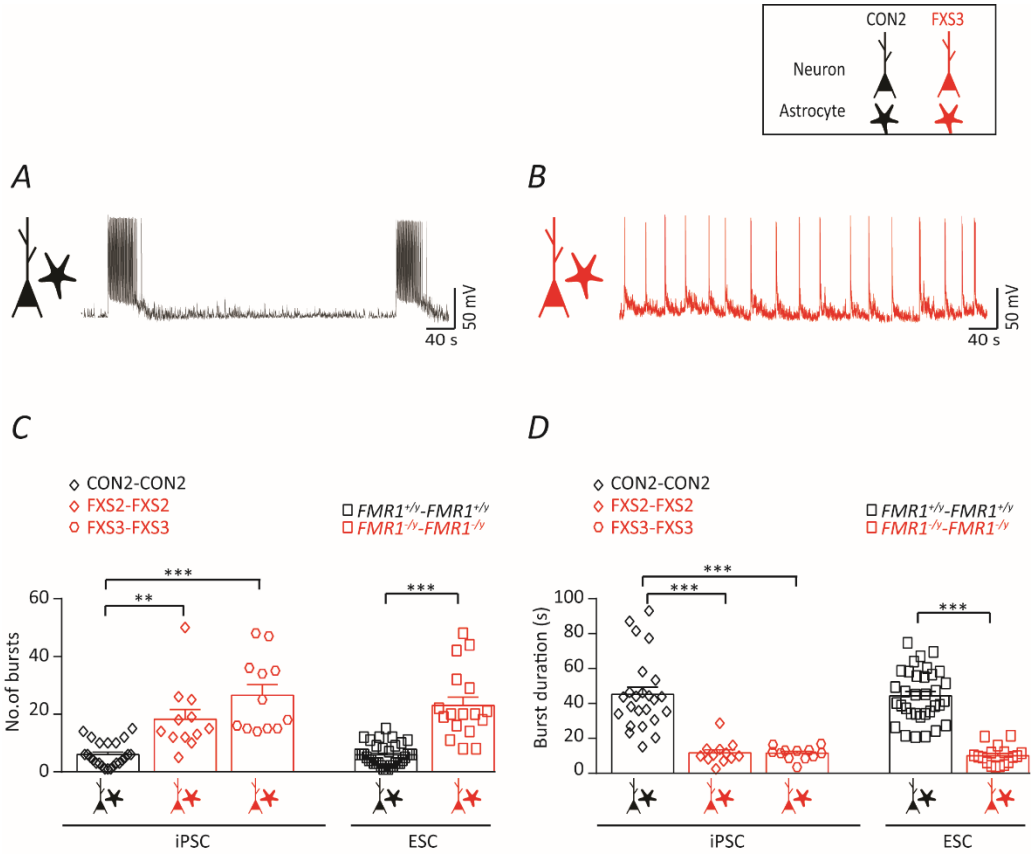

Figure 5.2 hPSC derived FXS neurons co-cultured with FXS astrocytes display aberrant spontaneous burst firing.

(A) Representative current clamp recording (V_{HOLD} = -70 mV) of spontaneous bursts from a CON2 neuron co-cultured with CON2 astrocyte illustrating the low burst number and longer burst duration. **(B)** Representative current clamp recording of spontaneous bursts from a FXS3 neuron co-cultured with FXS3 astrocyte illustrating the aberrant burst firing - significantly higher burst number and shorter burst duration. **(C)** Quantification of the burst number of all the lines. Overall the mean values are: 6 ± 0.87 (CON2 neurons with CON2 astrocytes: n = 24, N = 4); 18.25 ± 3.36 (FXS2 neurons with FXS2 astrocytes: n = 12, N = 3); 26.5 ± 3.73 (FXS3 neurons with FXS3 astrocytes: n = 12, N = 3). **(D)** Quantification of the burst duration of all the combinations. The overall mean burst durations are (in seconds): 45.2 ± 4.24 (CON2 neurons with CON2 astrocytes); 11.76 ± 1.85 (FXS2 neurons with FXS2 astrocytes); 11.55 ± 1.04 (FXS3 neurons with FXS3 astrocytes). Values are ± SEM. ***p< 0.001, **p< 0.01, one way ANOVA with post hoc Bonferroni test.

5.3 Human astrocyte genotype determines the phenotype of bursting activity of human cortical neurons

Studies have shown that selective deletion of FMRP in the astrocytes contribute towards the FXS phenotype in *Fmr1* KO mouse models *in vitro* and *in vivo* (Jacobs & Doering, 2010; Higashimori *et al.,* 2016; Hodges *et al.,* 2017). Interestingly, healthy astrocytes could prevent the abnormal dendrite morphology of the *Fmr1* KO neurons (Jacobs & Doering, 2010). However, in our own studies, we did not observe rescue of the aberrant network activity of human FXS neurons by wild-type mouse astrocytes. This led us to investigate if the spontaneous network activity of the neurons could be modulated by the human astrocytes. In section 5.2, we saw that control neurons co-cultured with control astrocytes led to the neurons displaying control burst phenotype and co-culturing FXS neurons with FXS astrocytes resulted in the neurons exhibiting the FXS bursting phenotype. Here, we co-cultured control neurons with FXS astrocytes and FXS neurons with control astrocytes. Similar to previous experiment, whole-cell patch clamp recordings were performed when the neurons were 8 weeks *in vitro*, to assess the role of astrocyte genotype on the spontaneous network behaviour of the neurons. Strikingly, recordings from CON2 neuron co-cultured with FXS3 astrocytes showed that the bursting profile of the CON2 neurons resembled that of the FXS – with more number of bursts and shorter burst duration (Fig 5.3A). Consequently, when FXS3 neurons were co-cultured with CON2 astrocytes the aberrant bursting activity was rescued to resemble the control neurons with lesser number of bursts and longer burst duration (Fig 5.3B). Analysis of the network activity of the other iPSC derived FXS line and ESC derived neurons and astrocytes showed the same (Fig 5.3C-D) - the genotype of astrocytes determines the bursting phenotype of neurons across all the lines, iPSC and ESC.

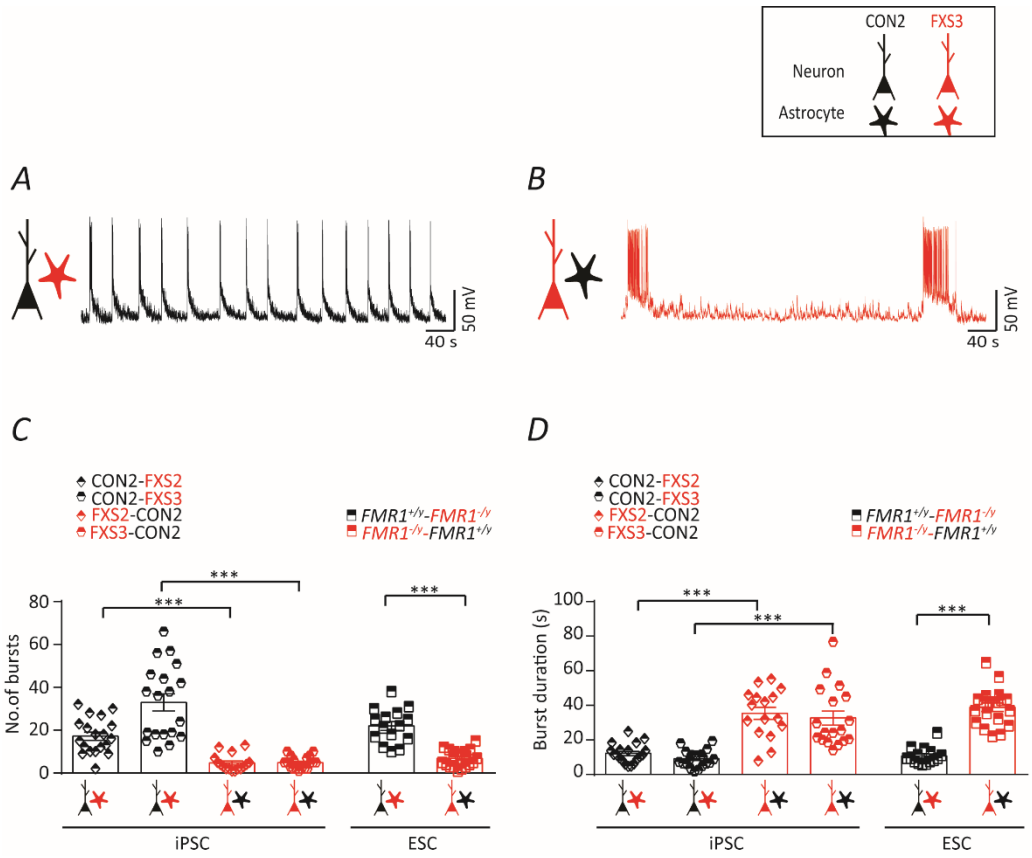

Figure 5.3 Spontaneous bursting activity of hPSC derived cortical neurons is non-cell-autonomous and determined by the genotype of the astrocytes.

(A) Representative current clamp trace from a CON2 neuron co-cultured with FXS3 astrocyte shows the effect of astrocyte on the bursting profile of neuron. CON2 neuron shows the aberrant burst activity like the FXS – high burst number, shorter burst duration. **(B)** Representative trace from a FXS3 neuron co-cultured with CON astrocyte shows the FXS2 neuron bursting like control – low burst number, longer burst duration. **(C)** Quantification of the burst number of all the combinations. Overall the mean values are: 17.21 ± 1.88 (CON2 neurons with FXS2 astrocytes: n = 19, N = 3); 33 ± 3.9 (CON2 neurons with FXS3 astrocytes: n = 19, N = 3); 4.75 ± 0.95 (FXS2 neurons with CON2 astrocytes: n = 16, N = 3); 4.88 ± 0.67 (FXS3 neurons with CON2 astrocytes: n = 18, N = 3); 5.91 ± 0.64 (*FMR1*$^{+/y}$ neurons with *FMR1*$^{+/y}$ astrocytes : n = 34, N = 4); 23.06 ± 2.93 (*FMR1*$^{-/y}$ neurons with *FMR1*$^{-/y}$ astrocytes : n = 17, N = 3); 22 ± 2.08 (*FMR1*$^{+/y}$ neurons with *FMR1*$^{-/y}$ astrocytes : n = 15, N = 3); 6.89 ± 0.95 (*FMR1*$^{-/y}$ neurons with *FMR1*$^{+/y}$ astrocytes : n = 19, N = 3). **(D)** Quantification of the burst duration of all the combinations. The overall mean burst durations are (in seconds): 12.18 ± 1.26 (CON2 neurons with FXS2 astrocytes); 9.12 ± 1.11 (CON2 neurons with FXS3 astrocytes); 35.44 ± 3.4 (FXS2 neurons with CON2 astrocytes); 32.73 ± 4.08 (FXS3 neurons with CON2 astrocytes); 44.46 ± 2.52 (*FMR1*$^{+/y}$ neurons with *FMR1*$^{+/y}$ astrocytes); 10.10 ± 1.31 (*FMR1*$^{-/y}$ neurons with *FMR1*$^{-/y}$ astrocytes); 10.71 ± 1.24 (*FMR1*$^{+/y}$ neurons with *FMR1*$^{-/y}$ astrocytes); 38.94 ± 2.48 (*FMR1*$^{-/y}$ neurons with *FMR1*$^{+/y}$ astrocytes). Values are ± SEM. ***p< 0.001, one way ANOVA with post hoc Bonferroni test.

5.4 Gene-corrected astrocytes can rescue the aberrant network activity of FXS neurons

In the last section, we observed that healthy human astrocytes were able to rescue the aberrant network phenotype of the neurons even in the absence of FMRP. Consequently, selective absence of FMRP in the human astrocytes led to control neurons firing like fragile X neurons. To further confirm, that it is the presence of FMRP in the healthy astrocytes that led to the rescue of aberrant neuronal firing, we generated astrocytes from FXS gene-corrected (FXS2Δ) line wherein FMRP has been genetically re-expressed by correcting the mutation using CRISPR-Cas. We co-cultured iPSC derived control (CON2) and Fragile X (FXS2) neurons with the FXS2Δ astrocytes. At 8 weeks *in vitro*, whole-cell patch clamp recordings were conducted. We hypothesized that the gene-corrected astrocytes would behave similar to control astrocytes and control neurons when co-cultured with the gene-corrected astrocytes would exhibit a control bursting phenotype. However, co-culturing FXS neurons on the gene-corrected astrocytes, would rescue the aberrant spontaneous burst activity and the FXS neurons would display a bursting phenotype resembling the controls (Fig 5.4). As expected, recordings from CON2 neurons plated with FXS2Δ astrocytes displayed the control burst firing – low no of bursts, longer duration (Fig 5.4A). FXS2 neurons co-cultured with FXS2Δ astrocytes also exhibited the control burst firing (Fig 5.4B). The no. of bursts (Fig 5.4C) and burst durations (5.4D) were similar between CON2 neurons co-cultured with FXS2Δ astrocytes and FXS2 neurons co-cultured with FXS2Δ astrocytes, thus confirming that presence of FMRP in the human astrocytes is crucial for the development of the proper network activity of human cortical neurons.

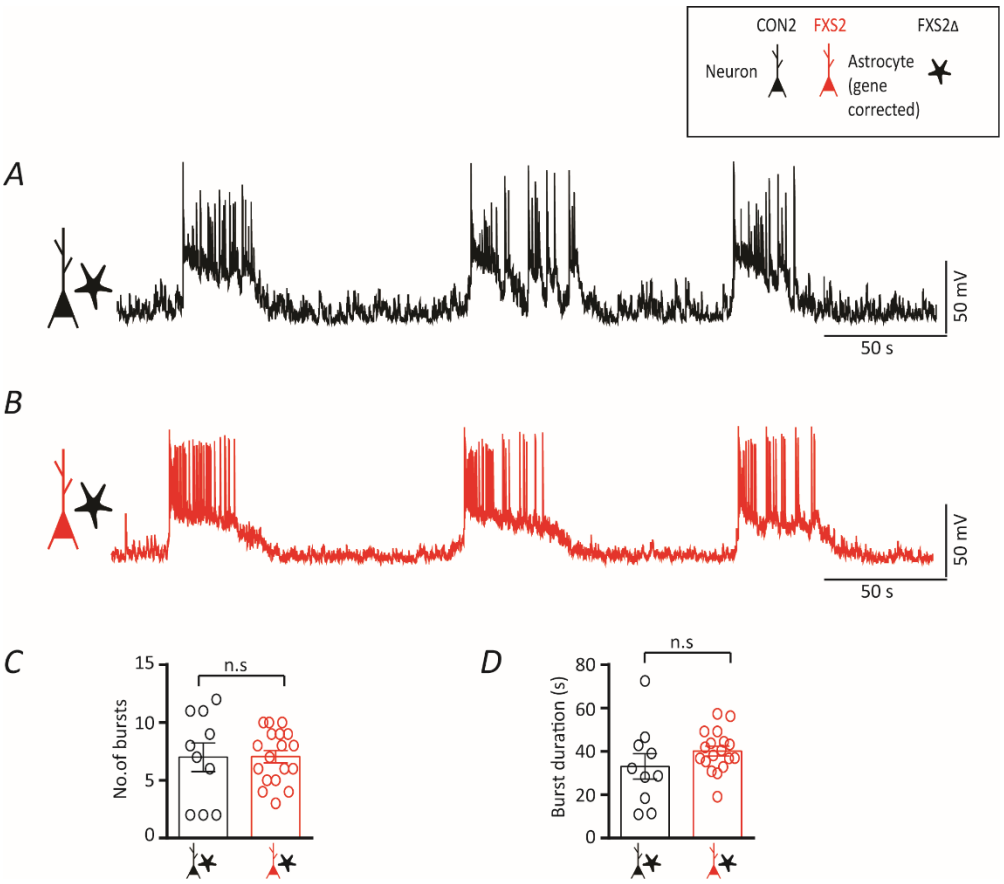

Figure 5.4 Gene-corrected astrocytes can rescue the aberrant burst firing of Fragile X neurons.

(A) Representative current-clamp trace from a CON2 neuron co-cultured with FXS2Δ astrocytes illustrating the control type of burst firing – low number of bursts, longer duration. (B) Representative current-clamp recording from a FXS2 neurons co-cultured with FXS2Δ astrocytes bursting like the control. (C) Quantification of the number of bursts shows no difference between CON2 neurons co-cultured with FXS2Δ astrocytes and FXS2 neurons co-cultured with FXS2Δ astrocytes. Overall, the mean no. of bursts are: 7 ± 1.23 (CON2 neurons with FXS2Δ astrocytes: n = 10, N = 1); 7.056 ± 0.53 (FXS2 neurons with FXS2Δ astrocytes: n = 18, N =2). (D) There was no significant difference in the burst durations between CON2 neurons and FXS2 neurons when co-cultured with FXS2Δ astrocytes. The mean burst durations are: 33.14 ± 5.86 (CON2 neurons with FXS2Δ astrocytes); 40.19 ± 2.22 (FXS2 neurons with FXS2Δ astrocytes). Values are ± SEM. Unpaired t-test.

5.5 Passive membrane properties of FXS neurons are similar to control neurons in a human neuron-astrocyte co-culture

Many studies using *Fmr1* KO mice have reported a change in the passive membrane properties like the input resistance and rheobase current of cortical neurons underlying the hyperexcitability phenotype of FXS (Gibson *et al.,* 2008; Kalmbach *et al.,* 2015). However, recent studies using primary mouse cultures have also observed no change in the baseline passive membrane properties in the absence of FMRP (Bulow *et al.,* 2019). Studies using hPSC derived neurons, have shown that loss of FMRP does not affect the passive membrane properties (Telias *et al.,* 2015; Zhang *et al.,* 2018). In our neuronal and rodent co-culture studies, we did not observe any change in the intrinsic properties of neurons, upon loss of FMRP. Having observed the effect of human astrocytes on the spontaneous network activity of human neurons, we conducted whole-cell patch clamp recordings, to check if the passive membrane properties of the neurons were affected by the astrocyte genotype (Fig 5.5). The passive membrane analyzed were: resting membrane potential (RMP) (Fig 5.5A), input resistance (Fig 5.5B), capacitance (Fig 5.5C) and rheobase current (Fig 5.5D). These parameters were similar between control and FXS neurons across the iPSC and ESC lines. Analysis of the passive membrane properties of neurons co-cultured with the gene-corrected astrocytes were also similar to all the other lines. This suggests that loss of FMRP from the astrocytes and neurons does not significantly alter the intrinsic membrane properties of the hPSC derived neurons.

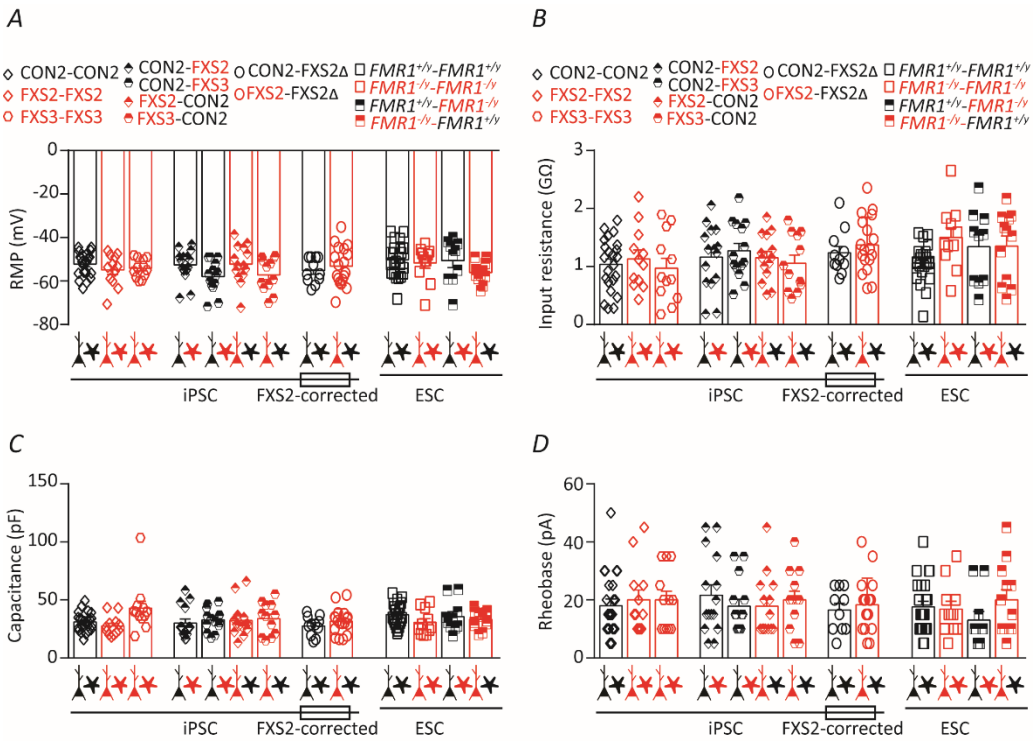

Figure 5.5 Passive membrane properties of hPSC derived neurons co-cultured with hPSC derived astrocytes.

(A) Resting membrane potentials across all the lines. **(B)** Quantification of input resistances. **(C)** Quantification of capacitance across all the lines. **(D)** Quantification of the rheobase currents. All the values are mean ± SEM. One-way ANOVA with *post hoc* Bonferroni's test. CON2 neurons with CON2 astrocytes, n = 23, N = 3; FXS2 neurons with FXS2 astrocytes, n = 12, N = 3; FXS3 neurons with FXS3 astrocytes, n = 12, N = 3; CON2 neurons with FXS2 astrocytes, n = 15, N = 3; CON2 neurons with FXS3 astrocytes, n = 14, N = 3; FXS2 neurons with CON2 astrocytes, n = 14, N = 3; FXS3 neurons with CON2 astrocytes, n = 12, N = 3; CON2 neurons with FXS2Δ astrocytes, n = 11, N = 1; FXS3 neurons with FXS2Δ astrocytes, n = 18, N = 1; *FMR1*$^{+/y}$ neurons with *FMR1*$^{+/y}$ astrocytes, n = 23, N = 3; *FMR1*$^{-/y}$ neurons with *FMR1*$^{-/y}$ astrocytes, n = 11, N = 3; *FMR1*$^{+/y}$ neurons with *FMR1*$^{-/y}$ astrocytes, n = 10, N = 3; *FMR1*$^{-/y}$ neurons with *FMR1*$^{+/y}$ astrocytes, n = 12, N = 3.

5.6 The active properties of FXS cortical neurons co-cultured with hPSC derived astrocytes are similar to control neurons

As already mentioned, neuronal hyperexcitability has been a hallmark of FXS pathophysiology. However, recent studies using both *Fmr1* KO mouse models and hPSC derived neurons have shown that the hyperexcitability phenotype is dependent on the type of neurons, age and the area of brain being examined. Indeed, studies also have reported hypoexcitability and no alteration in the basal firing of the cortical neurons of *Fmr1* KO mice (Berzhanskaya *et al.,* 2016; Bulow *et al.,* 2019). Hypoexcitability was also a key phenotype of the hESC derived cortical neurons (Telias *et al.,* 2015). However, another study using patient derived iPSC FXS neurons showed that the baseline firing frequency between controls and FXS neurons was unaltered (Zhang *et al.,* 2018). In chapter 3 and 4, we showed that hPSC derived glutamatergic cortical neurons when cultured in a neuron-only culture or co-cultured with WT rodent astrocytes, do not show any altered AP properties (Das Sharma *et al.,* 2020). Recent lines of evidence suggest that astrocytes contribute significantly to AP firing in neurons and the metabolic status of human astrocytes is a determining factor (Deemyad *et al.,* 2018; You *et al.,* 2019). In the next step of experiments, we wanted to investigate the role of FMRP in modulating the active AP properties of the human neurons when co-cultured with human astrocytes. Neurons were co-cultured with astrocytes in the following combinations – control neurons with control astrocytes, FXS neurons with FXS astrocytes, control neurons with FXS astrocytes and FXS neurons with control astrocytes. We performed whole-cell patch clamp recordings on neurons at 8 week *in vitro*. In current-clamp mode, 500 ms long depolarizing current steps (-10 to +65 pA) were injected and the AP parameters were calculated from the first AP fired by the neuron (Fig 5.6). Control and FXS neurons could fire sustained action potentials in response to a depolarizing current step in all the four combination of astrocytes (Fig 5.6A, B). We calculated the AP properties – rheobase, spike amplitude and spike half-width and did not find any difference between control and FXS neurons across all the lines (iPSC and ESC) and four combinations. Analysis of the AP properties of CON2 neurons co-cultured with FXS2Δ astrocytes and FXS2 neurons co-cultured with FXS2Δ astrocytes also did not reveal difference (Fig 5.6C-E). To see if the firing frequency was affected by the absence of FMRP, we calculated the maximum number of APs fired by the neurons and found no difference between control and FXS neurons across the lines and four combinations. CON2 neurons and FXS2 neurons when co-cultured with FXS2Δ astrocytes also did not exhibit any difference in the maximum number of APs fired (Fig 5.6F). Thus, absence of FMRP does not affect the basal active properties of hPSC neurons when co-cultured with hPSC derived astrocytes.

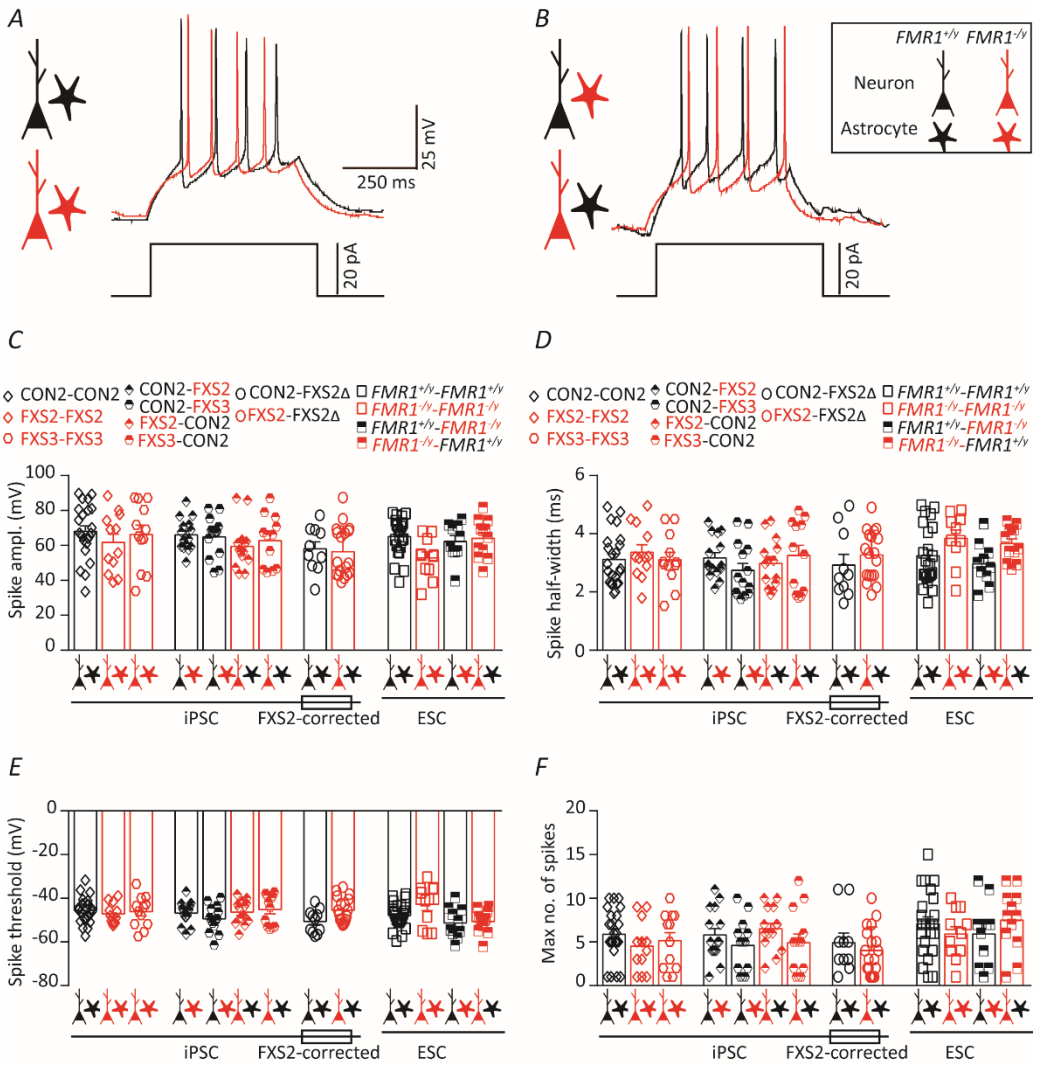

Fig 5.6 In a human neuron-astrocyte co-culture, active properties of FXS neurons are similar to controls.

(A) Representative current-clamp recordings of AP firing by a *FMR1*$^{+/y}$ neurons co-cultured with *FMR1*$^{+/y}$ astrocyte (black trace) and a *FMR1*$^{-/y}$ neurons co-cultured with *FMR1*$^{-/y}$ astrocyte (red trace) in response to a depolarizing current step (500ms, 20 pA). **(B)** Representative AP traces by a *FMR1*$^{+/y}$ neurons co-cultured with *FMR1*$^{-/y}$ astrocyte (black trace) and a *FMR1*$^{-/y}$ neurons co-cultured with *FMR1*$^{+/y}$ astrocyte (red trace) in response to a depolarizing current step (500ms, 20 pA). **(C, D, E)** Quantification of AP properties- spike amplitude, half-width, threshold across the iPSC and ESC and all the four combinations – control neurons with control astrocytes, FXS neurons with FXS astrocytes, control neurons with FXS astrocytes and FXS neurons with control astrocytes did not reveal any significant differences. **(F)** Maximum number of APs by the neurons was similar between control and FXS neurons neurons. One-way ANOVA with *post hoc* Bonferroni's test.

5.7 FXS neurons co-cultured with FXS astrocytes display reduced persistent sodium current (I_{NaP})

As already discussed, I_{NaP} is a sub-threshold, slowly-inactivating, TTX-sensitive sodium current. In section 2.5, we showed that I_{NaP} was critical for proper burst activity of the human cortical neurons and neurons

which lacked FMRP displayed reduced I_{NaP}. Blocking the I_{NaP} in control neurons with riluzole resulted in bursts with shorter burst durations resembling the FXS bursting profile. In section 2.9 we showed that pharmacological activation of the voltage-gated sodium channels using an activator, veratridine, could partially rescue the aberrant burst activity of FMRP-null neurons. Several studies have confirmed the crucial role of persistent sodium channels (NaP) in driving the burst activity of cortical networks (Magistretti & Alonso, 2002; Van Drongelen *et al.,* 2006; Astman *et al.,* 2006). Studies on *Fmr1* KO mice have shown that loss of FMRP leads to an increase in I_{NaP} (Deng & Klyachko, 2016) and transient sodium current (Routh *et al.,* 2017) in the entorhinal and prefrontal cortex. However our own studies on hPSC derived cortical neurons suggests a decrease in I_{NaP} in the absence of FMRP (Das Sharma *et al.,* 2020). This is corroborated by the study using human embryonic stem cell derived neurons which showed an overall reduction in the sodium current of the FXS neurons (Telias *et al.,* 2015). Thus it is imperative to study the persistent sodium channel in a total human system – human neurons with human astrocytes. We used both iPSC and ESC derived neurons and astrocytes. As in section 2.5, we injected a slow depolarizing voltage ramp (-100 mV to -20 mV, 20 mV/s) to the neurons in the absence and presence of TTX (Fig 5.7A). Subtraction of the traces obtained in the absence and presence of TTX, yielded the TTX-sensitive $I_{NaP.}$ CON2 neurons when co-cultured with CON2 astrocytes, exhibited a robust inward current which was the I_{NaP} (Fig 5.7A, *black trace*). In contrast FXS2 neurons co-cultured with FXS2 astrocytes displayed an extremely reduced I_{NaP} (Fig 5.7A, *red trace*). To neutralize the effect of cell size on the current observed, the current was divided by capacitance, to give current density. Analysis of the current density across all the iPSC lines revealed that FXS neurons co-cultured with FXS astrocytes exhibited significantly lesser I_{NaP} current densities than control iPSC neurons co-cultured with control iPSC astrocytes (Fig 5.7B-C). Similarly, I_{NaP} current densities of ESC derived $FMR1^{-/y}$ neurons co-cultured with $FMR1^{-/y}$ astrocytes was significantly reduced than $FMR1^{+/y}$ neurons co-cultured with $FMR1^{+/y}$ astrocytes (Fig 5.7D-E). Thus, loss of FMRP from the neurons and astrocytes leads to drastically reduced I_{NaP}.

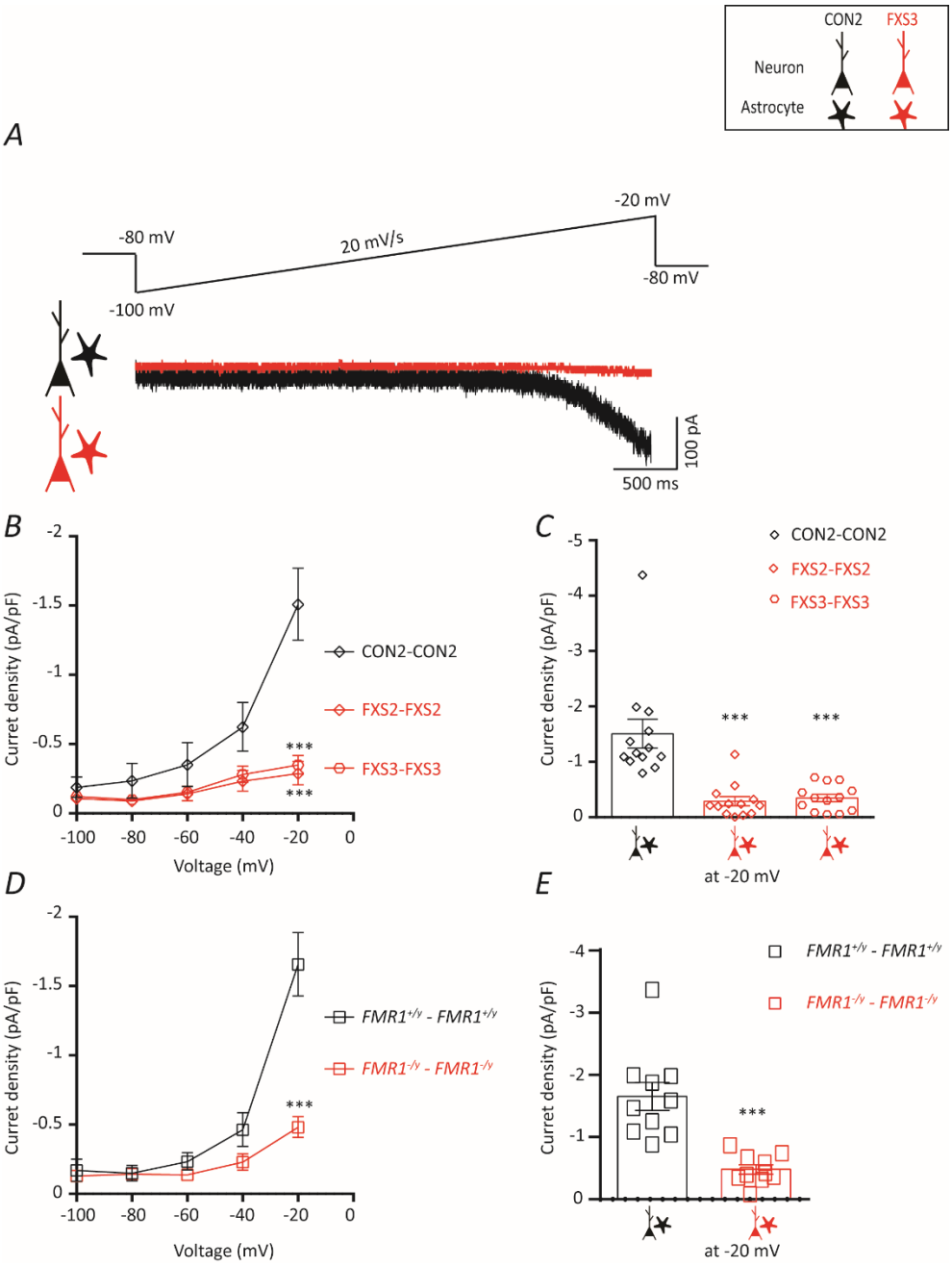

Figure 5.7 hPSC derived FXS neurons co-cultured with hPSC derived astrocytes display reduced I_{NaP} current densities.

(A) I_{NaP} isolated from the neurons co-cultured with human astrocytes in response to a depolarizing voltage ramp (-100 to -20 mV, 20 mV/s). Representative I_{NaP} trace from a CON2 neuron co-cultured with CON2 astrocytes (*black trace*). I_{NaP} was isolated by subtracting the current elicited by the ramp in the *presence* and *absence* of TTX. I_{NaP} from a FXS3 neuron co-cultured with FXS3 astrocytes (*red trace*) is significantly reduced. **(B)** I -V curves plotted from the ramp-evoked $I_{NaP,}$ showing the decreased I_{NaP} in iPSC derived FXS neurons co-cultured with iPSC derived FXS astrocytes. Currents are normalized to the corresponding cell capacitance. **(C)** Quantification of current density at −20 mV show significant decrease of the persistent sodium current in iPSC derived FXS neurons co-cultured with FXS astrocytes. Overall mean current

densities are: -1.508 ± 0.25 (CON2 neurons co-cultured with CON2 astrocytes, n = 13, N = 3); -0.288 ± 0.083 (FXS2 neurons co-cultured with FXS2 astrocytes, n = 13, N = 3); -0.349 ± 0.066 (FXS3 neurons co-cultured with FXS3 astrocytes, n = 13, N = 3). **(D)** I -V curves plotted from the ramp-evoked $I_{NaP,}$ showing the decreased I_{NaP} in *FMR1*$^{-/y}$ neurons co-cultured with *FMR1*$^{-/y}$ astrocytes. Currents are normalized to the corresponding cell capacitance. **(E)** Quantification of current density at −20 mV show significant decrease of the persistent sodium current in *FMR1*$^{-/y}$ neurons co-cultured with *FMR1*$^{-/y}$ astrocytes. Overall the mean current densities are: -1.656 ± 0.22 (*FMR1*$^{+/y}$ neurons co-cultured with *FMR1*$^{+/y}$ astrocytes, n = 10, N = 2); -0.48 ± 0.074 (*FMR1*$^{-/y}$ neurons co-cultured with *FMR1*$^{-/y}$ astrocytes, n = 10, N = 2). Values are ± SEM. ***p< 0.001, two-way repeated measures ANOVA with post hoc Bonferroni test, One-way ANOVA with post hoc Bonferroni test, Wilcoxon test.

5.8 NaP dysfunction of hPSC derived neurons is rescued by co-culturing with control astrocytes

Control human astrocytes could rescue the aberrant burst firing of the FXS neurons as seen in section 5.3. Similarly, FXS astrocytes could alter the bursting pattern of the control neurons to look like the FXS. Thus the human astrocytes are fundamental in the development of proper network activity of the neurons. We asked, if selective absence of FMRP in the astrocytes could lead to a reduction of I_{NaP} in the neurons. The I_{NaP} from control neurons plated with FXS astrocytes and FXS neurons co-cultured with control astrocytes was recorded (Fig 5.8). Recordings from CON2 neurons co-cultured with FXS3 astrocytes showed that the I_{NaP} of CON2 is reduced (Fig 5.8A, *black trace*). A FX3 neuron when co-cultured with CON2 astrocytes however, showed robust I_{NaP} (Fig 5.8A, *red trace*). Analysis of the I_{NaP} current densities across all the iPSC lines revealed the same – control neurons co-cultured with FXS astrocytes showed significantly reduced I_{NaP} whereas FXS neurons when co-cultured with control astrocytes displayed significantly greater I_{NaP} current densities (Fig 5.8B-C). I_{NaP} current densities of *FMR1*$^{+/y}$ neurons co-cultured with *FMR1*$^{-/y}$ astrocytes was significantly less than *FMR1*$^{-/y}$ neurons co-cultured with *FMR1*$^{+/y}$ astrocytes (Fig 5.8D-E). Thus this suggests that selective loss of FMRP from the human astrocytes leads to a reduction in the I_{NaP} magnitude of the cortical neurons. Consequently, FMRP expressed in the healthy astrocytes rescues the I_{NaP} dysfunction seen in cortical FXS neurons.

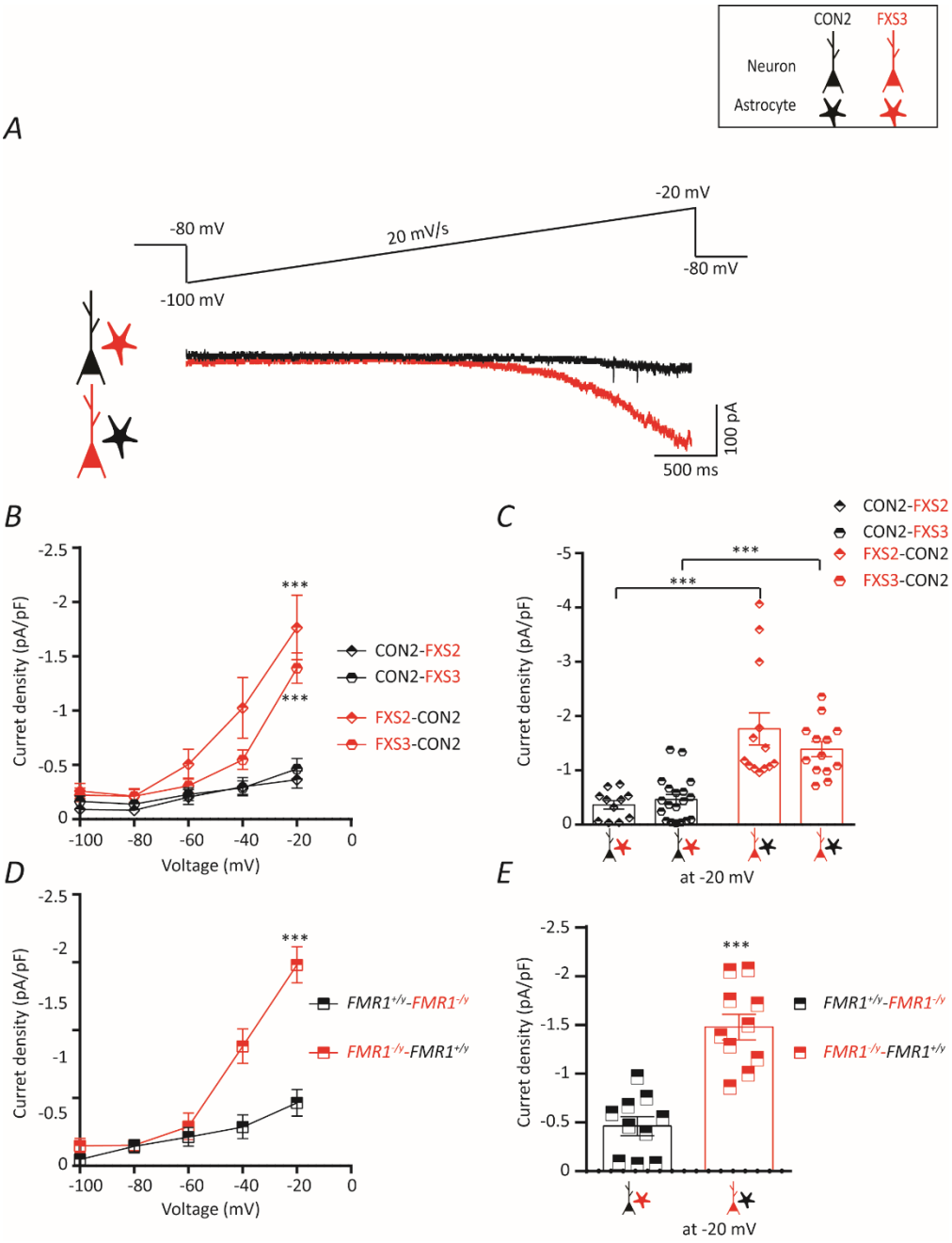

Figure 5.8 hPSC derived control neurons co-cultured with FXS astrocytes display reduced I_{NaP} magnitude. Control astrocytes rescue the I_{NaP} dysfunction of FXS neurons and FXS neurons display robust I_{NaP}.

(A) Reduced I_{NaP} elicited in response to depolarizing ramp from CON2 neuron co-cultured with FXS3 astrocytes (*black trace*). FXS3 neurons co-cultured with CON2 astrocytes displayed a robust I_{NaP} (*red trace*). **(B)** I -V curves plotted from the ramp-evoked $I_{NaP,}$ showing the decreased I_{NaP} in CON2 neurons co-cultured with iPSC derived FXS astrocytes and the increased I_{NaP} of FXS neurons co-cultured with CON2 astrocytes. **(C)** Quantification of I_{NaP} current densities at -20 mV. Overall the mean current densities are: -0.36 ± 0.079 (CON2 neurons co-cultured with FXS2 astrocytes, n = 11, N = 3); -0.46 ± 0.09 (CON2 neurons co-cultured with FXS3 astrocytes, n = 19, N = 3); -1.764 ± 0.29 (FXS2 neurons co-cultured with CON2 astrocytes, n =

13, N = 3); -1.39 ± 0.13 (FXS3 neurons co-cultured with CON2 astrocytes, n = 13, N = 3). **(D)** I-V curves showing the decreased I_{NaP} in *FMR1*$^{+/y}$ neurons co-cultured with *FMR1*$^{-/y}$ astrocytes and significantly greater I_{NaP} of *FMR1*$^{-/y}$ neurons co-cultured with *FMR1*$^{+/y}$ astrocytes. **(E)** Quantification of I_{NaP} current densities at -20 mV. The mean current densities are: -0.46 ± 0.097 (*FMR1*$^{+/y}$ neurons co-cultured with *FMR1*$^{-/y}$ astrocytes, n = 10, N = 2); -1.48 ± 0.13 (*FMR1*$^{-/y}$ neurons co-cultured with *FMR1*$^{+/y}$ astrocytes, n = 10, N = 2). Values are ± SEM. ***p< 0.001, two-way repeated measures ANOVA with post hoc Bonferroni test, One-way ANOVA with post hoc Bonferroni test, Wilcoxon test.

5.9 iPSC derived gene-corrected astrocytes rescue the NaP dysfunction of FXS neurons

In a separate set of experiments to confirm that expression of FMRP in the astrocytes is indeed the critical factor in the modulation of the persistent sodium current of neurons, we recorded I_{NaP} from control and FXS neurons co-cultured with FXS2Δ astrocytes (Fig 5.9). As expected, CON2 neurons co-cultured with FXS2Δ astrocytes displayed robust I_{NaP} (Fig 5.9A, *black trace*). We hypothesized that the expression of FMRP in the gene-corrected astrocytes would rescue the I_{NaP} of the FXS neurons, similar to control astrocytes. Indeed FXS2 neurons co-cultured with FXS2Δ astrocytes exhibited increased I_{NaP} similar to control neurons (Fig 5.9A, *red trace*). I_{NaP} current densities of FXS neurons co-cultured with FXS2Δ astrocytes did not differ from the CON2 neurons co-cultured with FXS2Δ astrocytes (Fig 5.9B-C). Our results with the ESC derived isogenic pair (section 5.8) and these results from the gene-corrected astrocytes confirm that it is indeed the expression of FMRP in the astrocytes and not any other environmental factor that was able to rescue the dysfunction of the persistent sodium channels in FXS neurons.

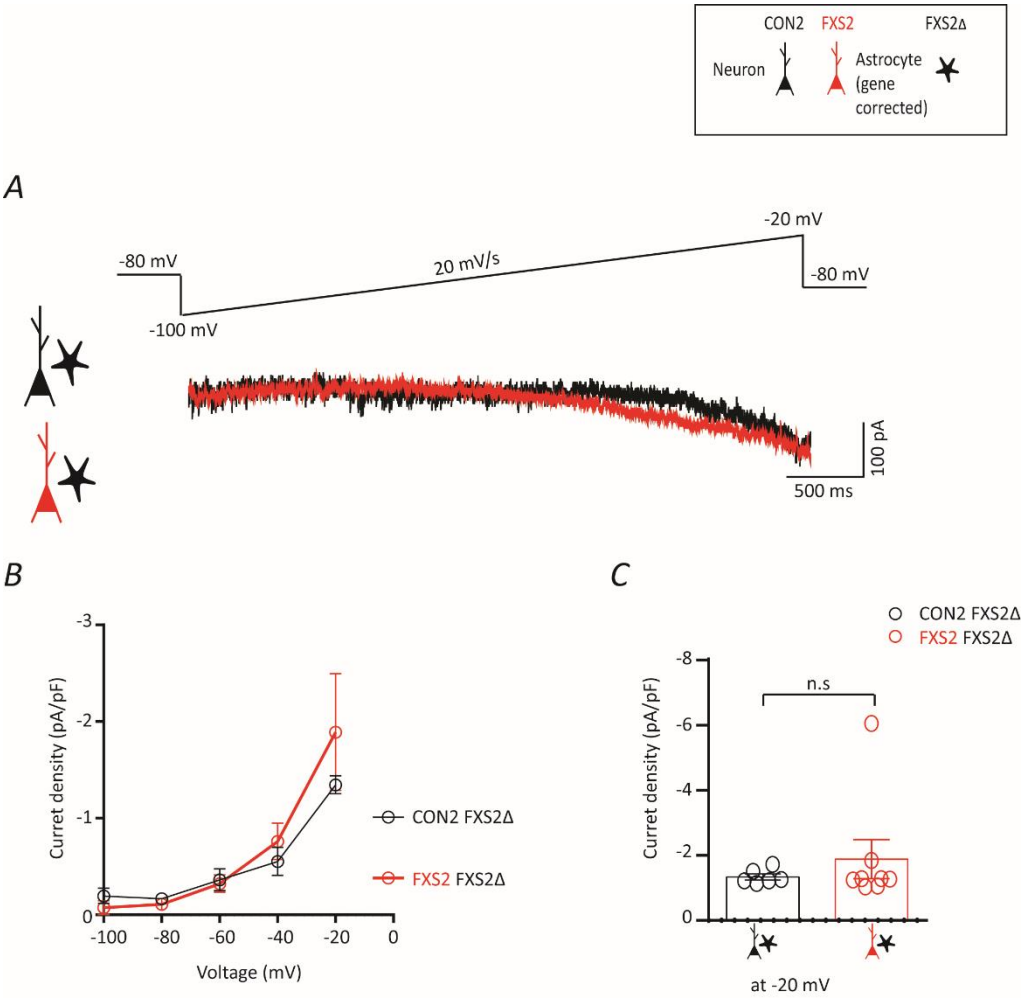

Figure 5.9 Gene-corrected astrocytes (FXS2Δ) can rescue the I_{NaP} defects of FXS neurons.

(A) Robust I_{NaP} elicited by CON2 neurons co-cultured with FXS2Δ astrocytes (*black*). FXS2 neurons co-cultured with FXS2Δ astrocytes also exhibit robust I_{NaP} (*red*) in response to depolarizing voltage ramp (-100 to -20 mV, 20 mV/s). **(B)** I-V curves showing robust I_{NaP} from FXS2 neurons co-cultured with FXS2Δ astrocytes. **(C)** Quantification of the I_{NaP} current densities at -20 mV. I_{NaP} current densities of FXS2 neurons co-cultured with FXS2Δ astrocytes is similar to CON2 neurons with FXS2Δ astrocytes. Overall the mean I_{NaP} are: -1.344 ± 0.091 (CON2 neurons co-cultured with FXS2Δ astrocytes, n = 6, N = 1); -1.89 ± 0.603 (FXS2 neurons co-cultured with FXS2Δ astrocytes, n = 8, N = 1). Values are ± SEM. Repeated measures two way ANOVA with post hoc Bonferroni test, Wilcoxon test.

5.10 Astrocyte conditioned media (ACM) from the human astrocytes has no effect on the maturation of human cortical neurons.

In sections, 5.2 and 5.3, we observed the modulation of network activity of hPSC derived cortical neurons by hPSC derived astrocytes. Indeed, presence of healthy astrocytes expressing FMRP could rescue the aberrant bursting phenotype of FXS neurons. Consequently, FXS astrocytes lacking FMRP, altered the bursting profile of the control neurons to resemble the FXS bursting – high number of bursts, shorter durations. We have also given evidence, of how the human astrocytes exert their influence on the neuronal network bursting via the persistent sodium channels. Control human astrocytes led to the development of robust I_{NaP} in the FXS neurons, whereas FXS astrocytes prevented persistent sodium channel activity in control neurons and led to significantly reduced I_{NaP} (Fig 5.8). The myriad of functions performed by astrocytes are mostly through secreted proteins (Christopherson *et al.,* 2005; Chung *et al.,* 2008) which regulate synapse formation, axonal regeneration and neuronal apoptosis. In the next set of experiment, we asked if the conditioned medium from the hPSC derived astrocytes had any effect on the morphology and function of neurons. We plated neuronal cultures and added astrocyte conditioned medium (ACM) at the 3rd week (Fig 5.10A). The neurons were allowed to grow and mature in the presence of ACM till the 8th week after which stained the neurons with Map2ab. We found that culturing the neurons with ACM did not have any significant effect on the morphology and maturation of neurons (Fig 5.10B).

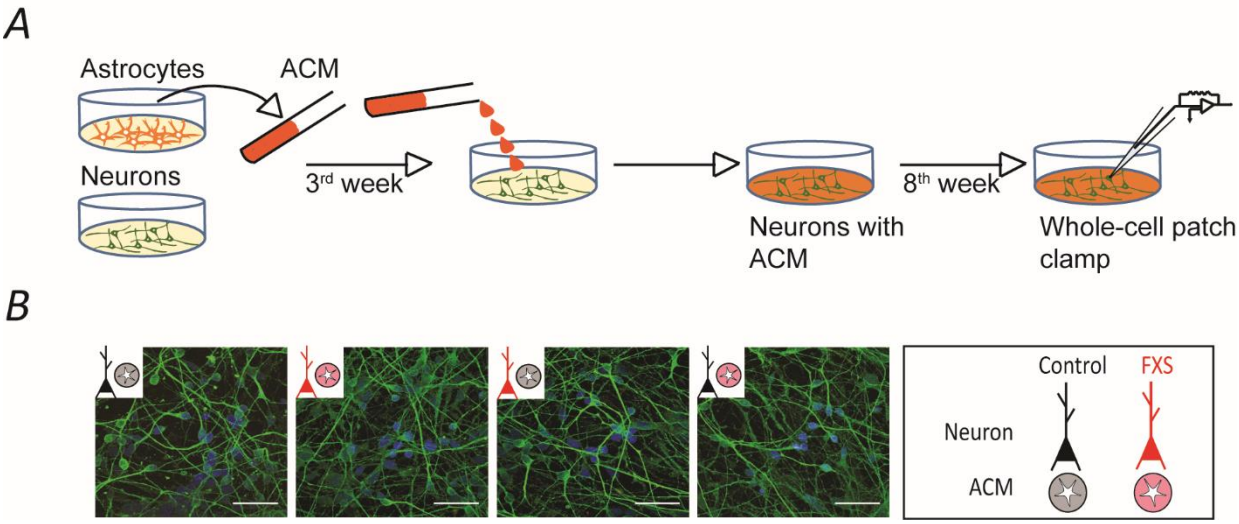

Figure 5.10 Culturing of hPSC derived neurons with FXS ACM does not alter their maturation.

(A) Schematic showing the addition of ACM to the neuron-only culture. **(B)** Representative confocal images of hiPSC (CON2 and FXS3) derived cortical neurons expressing Map2ab. *Left to right*, neurons were plated with ACM in four combinations: CON2 neurons with CON2 ACM, FXS3 neurons with FXS3 ACM, CON2 neurons with FXS3 ACM, FXS3 neurons with CON2 ACM. Scale bar = 50 µM. (*Work done by Rakhi Pal and Bharath Reddy*).

5.11 Astrocyte conditioned media (ACM) from the human astrocytes modulates the spontaneous network activity of human cortical neurons

In the next set of experiments, we asked if the conditioned medium from astrocytes could modulate the spontaneous burst activity of the hPSC derived neurons. Again, neuron-only cultures were allowed to mature in the presence of ACM and at the 8th week, whole-cell patch clamp recordings were performed to assess the spontaneous network activity. Both iPSC and ESC derived neurons and ACM were used in this experiment. In chapter 3, we had demonstrated that hPSC derived control and FXS neurons in a neuron-only culture had failed to develop proper synaptic activity and a concomitant absence of network activity. Presence of rodent and human astrocytes in the cortical neuron-only culture (chapters 2 and 3) led to the development of spontaneous network activity in the form of bursts of action potentials. We found that in presence of ACM, even in a neuron-only culture, the cortical neurons developed robust network activity (Fig 5.11). CON2 neurons which were grown in presence of CON2 ACM had a bursting activity like the controls – low number of bursts, longer durations (Fig 5.11A). Alternatively FXS3 neurons grown in the presence of FXS3 ACM displayed a FXS bursting profile – high number of bursts, shorter durations (Fig 5.11B). Analysis of the bursting activity across all the iPSC and ESC lines revealed the same (5.11C-D). Thus cortical neurons are able to develop spontaneous network activity in the presence of ACM.

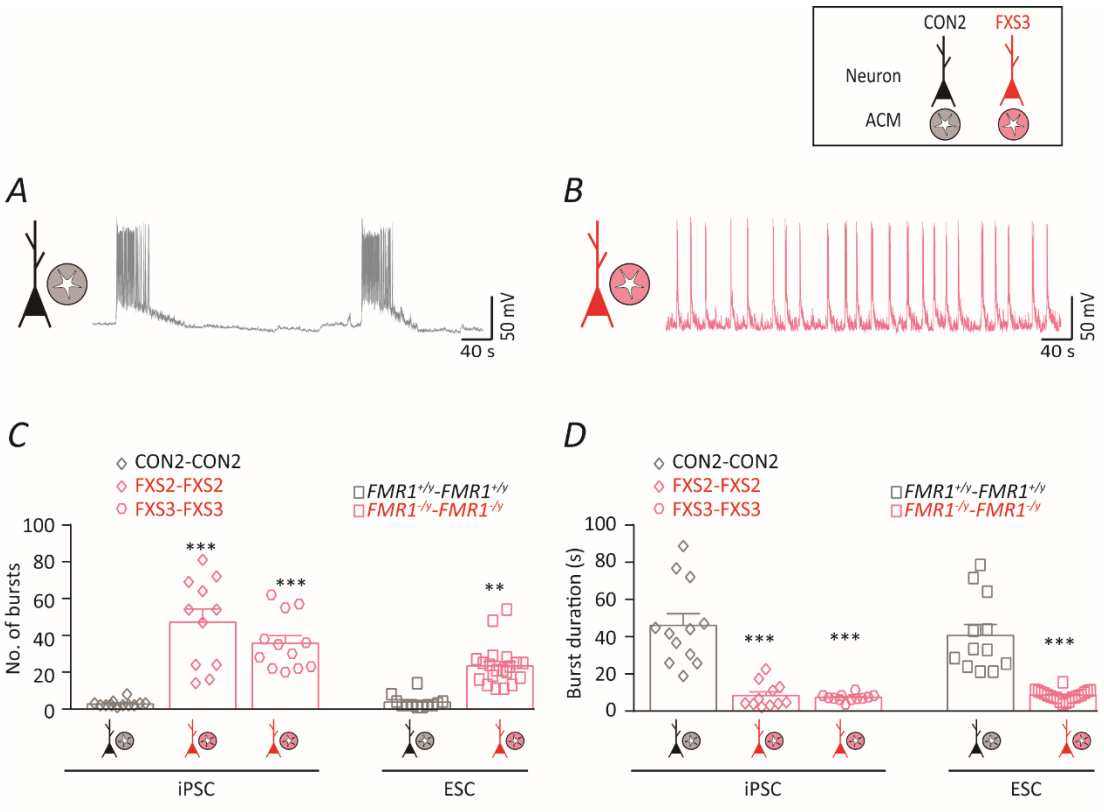

Fig 5.11 Human cortical neurons in presence of hPSC derived ACM developed spontaneous network activity.

(A) Representative current clamp recording (V_{HOLD} = -70 mV) of spontaneous bursts from a CON2 neuron co-cultured with CON2 ACM illustrating the low burst number and longer burst duration. **(B)** Representative current clamp recording of spontaneous bursts from a FXS3 neuron co-cultured with FXS3 ACM illustrating the aberrant burst firing - significantly higher burst number and shorter burst duration **(C)** Quantification of the number of bursts across the iPSC and ESC lines. Over the mean no. of bursts are: 2.83 ± 0.52 (CON2 neurons with CON2 ACM, n = 12, N = 3); 47.18 ± 7.23 (FXS2 neurons with FXS2 ACM, n = 11, N = 3); 35.67 ± 4.23 (FXS3 neurons with FXS3 ACM, n = 12, N = 3); 3.75 ± 1.08 (*FMR1*$^{+/y}$ with *FMR1*$^{+/y}$ ACM, n = 12, N = 3); 23.45 ± 2.45 (*FMR1*$^{-/y}$ with *FMR1*$^{-/y}$ ACM, n = 12, N = 3). **(D)** Quantification of the burst durations across all the lines. The mean burst durations are: 46.1 ± 8.47 (CON2 neurons with CON2 ACM); 8.47 ± 2.01 (FXS2 neurons with FXS2 ACM); 7.34 ± 0.51 (FXS3 neurons with FXS3 ACM); 40.69 ± 5.82 (*FMR1*$^{+/y}$ neurons with *FMR1*$^{+/y}$ ACM); 8.58 ± 0.633 (*FMR1*$^{-/y}$ neurons with *FMR1*$^{-/y}$ ACM).Values are ± SEM. ***p< 0.001, **p< 0.01, One-way ANOVA with post hoc Bonferroni test.

5.12 The ACM genotype determines the bursting phenotype of the hPSC cortical neurons

Several studies on *Fmr1* KO mouse models have shown that selective loss of FMRP from the astrocytes leads to neuronal dysfunction and presence of healthy astrocytes rescue the neuronal dysfunctions

(Higashimori *et al.,* 2016; Jacobs & Doering, 2010; Wallingford *et al.,* 2017). Multiple lines of evidence show that the neuronal abnormalities in *Fmr1* KO mice can be rescued by conditioned media from the astrocytes *in vitro* (Cheng *et al.,* 2016; Krasovska & Doering, 2018; Sourial & Doering, 2016). Having observed bursting of the cortical neurons in the presence of ACM, we asked if the neuronal bursting phenotype depended on the ACM genotype, i.e. do control neurons display a FXS bursting profile in presence of FXS ACM and can control ACM rescue the aberrant bursting phenotype of the FXS neurons (Fig 5.12). To test this, we recorded the spontaneous burst activity of control neurons which were cultured in presence of FXS ACM. Recordings from a CON2 neuron cultured in presence of ACM from FXS3 astrocytes, indeed show a FXS type bursting – high number of bursts, shorter durations (Fig 5.12A). A FXS3 neuron cultured in the presence of CON2 ACM exhibited a control bursting phenotype – low number of bursts, longer durations (Fig 5.12B). Thus the genotype of the ACM determines the neuronal bursting phenotype. This was true across all the iPSC lines and ES lines (Fig 5.12C-D). To further confirm that the ACM derived from iPSC and ESC astrocytes exert the same effects, we cultured iPSC derived CON2 and FXS3 neurons with ES derived *FMR1*$^{-/y}$ and *FMR1*$^{+/y}$ ACM respectively. FXS3 neurons in presence of *FMR1*$^{+/y}$ ACM displayed a decrease in the number of bursts fired (Fig 5.12E) and an increase in the burst duration (Fig 5.12F) as compared to CON2 neurons cultured with *FMR1*$^{-/y}$, thus suggesting that both ESC and iPSC derived astrocytes secrete similar factors that are able to rescue the aberrant network activity of neurons lacking FMRP. These results show that the hPSC derived astrocytes act as a determining factor of the neuronal network activity via its secretome. This is a novel finding and for the first time we have provided evidence of the rescue of FXS phenotype of human cortical neurons through factors secreted by the human astrocytes.

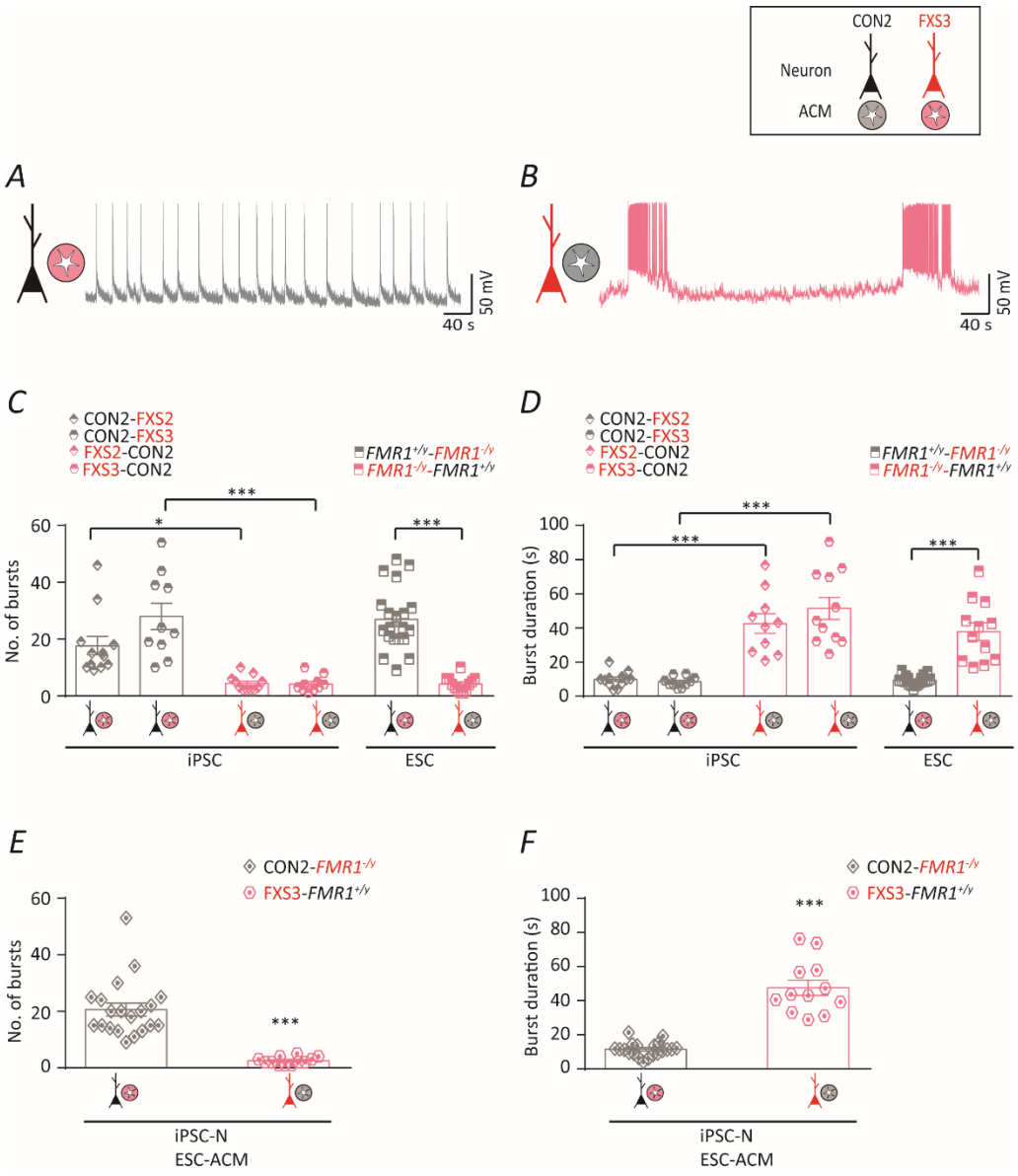

Figure 5.12 The ACM genotype determines the bursting phenotype of human cortical neurons.

(A) Representative current-clamp recording of a CON2 neuron cultured with FXS3 ACM displaying a FXS bursting phenotype. **(B)** Representative trace of a FXS3 neuron cultured with CON2 ACM exhibiting the control bursting phenotype. **(C)** Quantification of number of bursts across all the lines. Overall the means are: 17.67 ± 3.23 (CON2 neurons with FXS2 ACM, n = 12, N = 3); 28 ± 4.67 (CON2 neurons with FXS3 ACM, n = 10, N = 3); 4.36 ± 0.82 (FXS2 neurons with CON2 ACM, n = 10, N = 3); 4.2 ± 0.89 (FXS3 neurons with CON2 ACM, n = 11, N = 3); 26.95 ± 2.46 (*FMR1*$^{+/y}$ neurons with *FMR1*$^{-/y}$ ACM, n = 20, N = 3); 4.167 ± 0.75 (*FMR1*$^{-/y}$ neurons with *FMR1*$^{+/y}$ ACM, n = 12, N = 3). **(D)** Quantification of the burst durations across all the lines. The mean burst durations are: 9.98 ± 1.27 (CON2 neurons with FXS2 ACM); 8.59 ± 0.96 (CON2 neurons with FXS3 ACM); 42.66 ± 5.78 (FXS2 neurons with CON2 ACM); 51.59 ± 6.56 (FXS3 neurons with CON2 ACM); 9.40 ± 0.58 (*FMR1*$^{+/y}$ neurons with *FMR1*$^{-/y}$ ACM); 37.95 ± 5.14 (*FMR1*$^{-/y}$ neurons with *FMR1*$^{+/y}$ ACM). **(E)** Quantification of the number of bursts of iPSC neurons with ES ACM. Mean number of bursts are: 20.65 ± 2.26 (CON2 neurons with *FMR1*$^{-/y}$ ACM, n = 20, N = 2); 2.5 ± 0.38 (FXS3 neurons with *FMR1*$^{+/y}$

ACM, n = 12, N = 2). **(F)** Quantification of the burst durations of iPSC neurons with ES ACM. Mean burst durations are: 11.57 ± 0.93 (CON2 neurons with *FMR1*$^{-/y}$ ACM); 47.63 ± 4.5 (FXS3 neurons with *FMR1*$^{+/y}$ ACM). Values are ± SEM. ****p*< 0.001, **p< 0.01, *p< 0.05, One-way anova with post hoc Bonferroni test.

5.13 Intrinsic properties of FXS neurons are similar to controls in a neuron – ACM culture

In the previous section, we saw that the genotype of ACM determines the phenotype of the neuronal bursting i.e. control neurons in presence of FXS ACM displayed the aberrant FXS bursting phenotype whereas FXS neurons in presence of control ACM bursts like the control. This was true across the ES and the iPSC lines. In section 5.5 and 5.6, we showed that though the astrocyte genotype determined the bursting phenotype of the neurons, absence of FMRP in the neurons or the astrocytes did not have any effect on the active and passive membrane properties of the neurons. To check, if the conditioned media from the astrocytes altered the intrinsic membrane properties of the neurons were analysed. Similar to previous experiments, neurons (iPSC and ESC) were cultured with ACM (iPSC and ESC). The passive membrane properties – resting membrane potential (Fig 5.13A) input resistance (5.13B), capacitance (5.13C) and rheobase current (5.13D) were similar between control and FXS neurons across the iPSC and ESC lines. ACM from control or FXS astrocytes did not affect the basal passive membrane properties of the neurons. This result is in accordance with our earlier observations with human and mouse astrocytes.

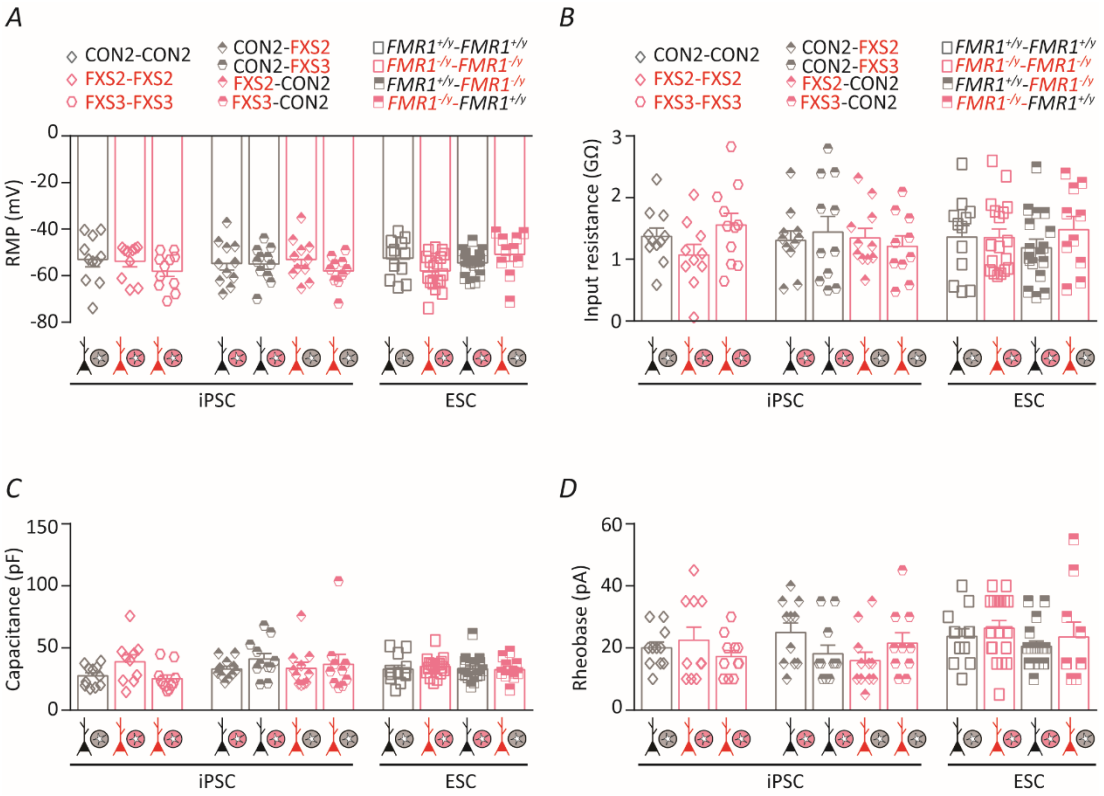

Figure 5.13 Passive membrane properties of hPSC derived neurons cultured with ACM.

(A) Resting membrane potentials across all the lines. **(B)** Quantification of input resistances. **(C)** Quantification of capacitance across all the lines. **(D)** Quantification of the rheobase currents. All the values are mean ± SEM. One-way ANOVA with *post hoc* Bonferroni's test. CON2 neurons with CON2 ACM, n = 11, N = 3; FXS2 neurons with FXS2 ACM, n = 10, N = 3; FXS3 neurons with FXS3 ACM, n = 11, N = 3; CON2 neurons with FXS2 ACM, n = 11, N = 3; CON2 neurons with FXS3 ACM, n = 11, N = 3; FXS2 neurons with CON2 ACM, n = 11, N = 3; FXS3 neurons with CON2 ACM, n = 10, N = 3; *FMR1*$^{+/y}$ neurons with *FMR1*$^{+/y}$ ACM, n = 12, N = 3; *FMR1*$^{-/y}$ neurons with *FMR1*$^{-/y}$ ACM, n = 18, N = 3; *FMR1*$^{+/y}$ neurons with *FMR1*$^{-/y}$ ACM, n = 17, N = 3; *FMR1*$^{-/y}$ neurons with *FMR1*$^{+/y}$ ACM, n = 10, N = 3.

5.14 Action potential properties of FXS neurons are similar to controls in a neuron – ACM culture

In the next step of experiments, we analysed the action potential properties of the hPSC derived neurons cultured with ACM. At 8 weeks *in vitro* depolarized current pulses (-10 to +65 pA) were injected into the neurons. Analysis of the action potential properties from the 1st AP also did not reveal any significant differences (Fig 5.14). Current clamp traces from a *FMR1$^{+/y}$* neuron cultured with *FMR1$^{+/y}$* ACM (Fig 5.14A, *grey trace*) and a *FMR1$^{-/y}$* neuron cultured with *FMR1$^{-/y}$* ACM (Fig 5.14B, *pink trace*), show similar sustained AP firing in response to a depolarized current (20 pA) step. Similarly, current clamp traces from *FMR1$^{+/y}$* neuron cultured with *FMR1$^{-/y}$* ACM (Fig 5.14B, *grey trace*) and a *FMR1$^{-/y}$* neuron cultured with *FMR1$^{+/y}$* ACM (Fig 5.14B, *pink trace*) displayed similar AP firing in response to the depolarized current step. AP properties like – Spike amplitude (Fig 5.14C), Spike half-width (5.14D), Spike threshold (5.14E) were similar across all the lines and combinations. The maximum number of APs fired by the neurons (5.14F) was also similar. Thus, in accordance with our observations on neuronal, rodent astrocyte co-cultures, human neuron astrocyte co-cultures the active membrane properties of control and FXS neurons do not differ in human neurons-ACM cultures.

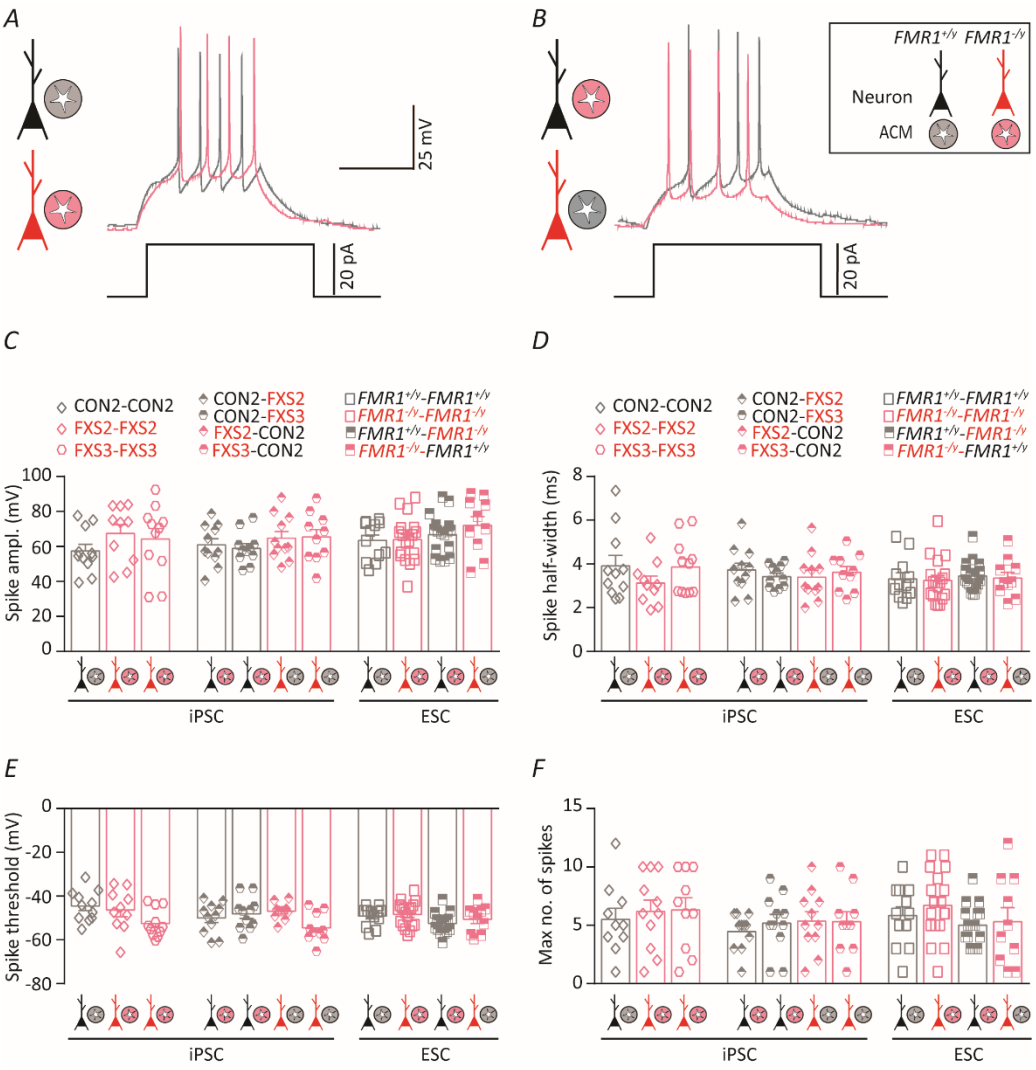

Figure 5.14 AP properties of hPSC derived neurons cultured with ACM.

(A) Representative current-clamp recordings of AP firing by a *FMR1*$^{+/y}$ neurons cultured with *FMR1*$^{+/y}$ ACM (*grey trace*) and a *FMR1*$^{-/y}$ neurons cultured with *FMR1*$^{-/y}$ ACM (*pink trace*) in response to a depolarizing current step (500ms, 20 pA). **(B)** Representative AP traces by a *FMR1*$^{+/y}$ neurons cultured with *FMR1*$^{-/y}$ ACM (*grey trace*) and a *FMR1*$^{-/y}$ neurons cultured with *FMR1*$^{+/y}$ ACM (*pink trace*) in response to a depolarizing current step (500ms, 20 pA). **(C, D, E)** Quantification of AP properties- rheobase, spike amplitude and half-width across the iPSC (CON2, FXS2, FXS3) and ESC (*FMR1*$^{+/y}$, *FMR1*$^{-/y}$ lines and all the four combinations – control neurons with control ACM, FXS neurons with FXS ACM, control neurons with FXS ACM and FXS neurons with control ACM did not reveal any significant differences. **(F)** Maximum number of APs by the neurons was similar between control and FXS neurons neurons. One-way ANOVA with *post hoc* Bonferroni's test.

5.15 FXS neurons cultured with ACM from FXS astrocytes display reduced persistent sodium currents (I_{NaP})

As already discussed, I_{NaP} plays a critical role in the bursting activity of the neurons. In Chapter 4, we saw that addition of voltage-gated sodium channel opener, veratridine rescued the aberrant bursting activity of FXS neurons co-cultured with rodent astrocytes. In section 5.7, we demonstrated that FXS neurons co-cultured with FXS astrocytes displayed significantly less I_{NaP} than control neurons co-cultured with control astrocytes. The hPSC derived astrocytes determined the neuronal network activity through its secretome as evidenced by the ACM experiments in section 5.12. We hypothesized that the aberrant burst activity of FXS neurons cultured with FXS ACM was due to reduced $I_{NaP.}$ To test this hypothesis, we recorded the I_{NaP} using previously described protocols. For this experiment, we used the iPSC derived CON2 and the FXS3 lines. CON2 and FXS3 neurons were cultured with CON2 and FXS3 ACM respectively, and the I_{NaP} was recorded at 8 weeks *in vitro* (Fig 5.15). CON2 neurons cultured with CON2 ACM displayed robust NaP currents (Fig 5.15A, *grey trace*). FXS3 neurons cultured with FXS3 ACM exhibited reduced NaP currents (Fig 5.15A, *pink trace*). Analysis of the current densities at different voltages revealed that the FXS3 neurons cultured with FXS3 ACM had significantly reduced I_{NaP} current densities (Fig 5.15B-C). Thus, similar to FXS neurons – FXS astrocyte c-culture, culturing of FXS neurons with FXS ACM also led to reduced I_{NaP} resulting in an aberrant spontaneous network activity.

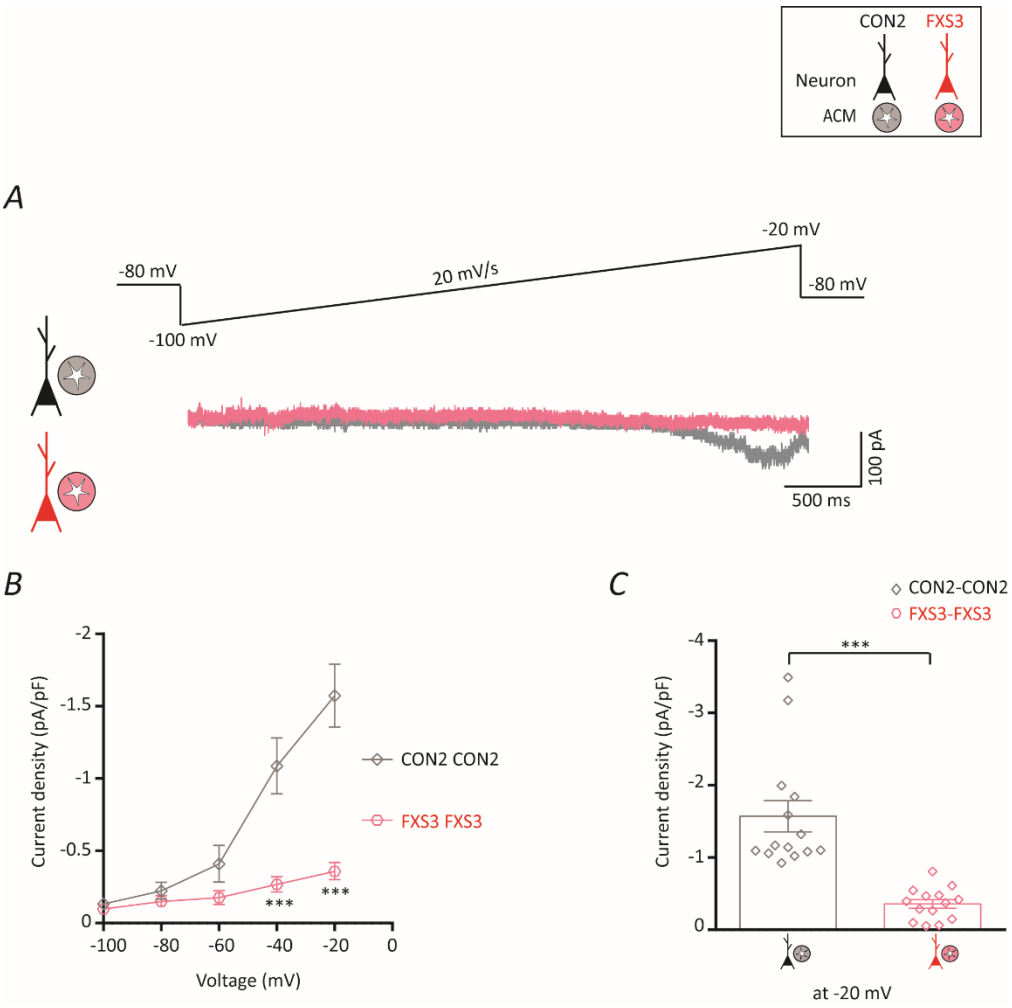

Figure 5.15 hPSC derived FXS neurons cultured with FXS ACM display reduced I_{NaP} current densities.

(A) I_{NaP} isolated from the neurons cultured with ACM in response to a depolarizing voltage ramp (-100 to -20 mV, 20 mV/s). Representative I_{NaP} trace from a CON2 neuron cultured with CON2 ACM (*grey trace*). I_{NaP} was isolated by subtracting the current elicited by the ramp in the *presence* and *absence* of TTX. I_{NaP} from a FXS3 neuron cultured with FXS3 ACM (*pink trace*) is significantly reduced. **(B)** I -V curves plotted from the ramp-evoked $I_{NaP,}$ showing the decreased I_{NaP} in FXS3 neurons cultured with FXS3 ACM. Currents are normalized to the corresponding cell capacitance. **(C)** Quantification of current density at −20 mV show significant decrease of the persistent sodium current in FXS3 neurons cultured with FXS3 ACM. Overall mean current densities are: -1.572 ± 0.217 (CON2 neurons cultured with CON2 ACM, n = 14, N = 3); -0.379 ± 0.059 (FXS3 neurons cultured with FXS3 ACM, n = 14, N = 3). Values are ± SEM. ***p< 0.001, Two-way anova with post-hoc Bonferroni test, Unpaired t-test.

5.16 Control ACM rescues the Na_P dysfunction of FXS neurons and the neurons display robust I_{NaP}

In section 5.8, we showed that control astrocytes rescued the persistent sodium channel dysfunction of FXS neurons. FXS neurons co-cultured with control astrocytes displayed robust persistent sodium currents. However, control neurons co-cultured with FXS astrocytes had significantly reduced I_{NaP}. This modulation of persistent sodium channel by astrocytes led to the determination of bursting patterns of neurons. We hypothesized that culturing of FXS neurons with ACM from control astrocytes would also rescue the sodium channel dysfunction and culturing control neurons in presence of FXS ACM would lead to a drastic reduction of the $I_{NaP.}$ To test this, we isolated and analysed the I_{NaP} CON2 neurons cultured with FXS3 ACM and FXS3 neurons cultured with CON2 ACM (Fig 5.16). Indeed we found that, in response to a depolarizing voltage ramp, CON2 neurons cultured with FXS3 ACM, displayed reduced I_{NaP} (Fig 5.16A, g*rey trace*), while the I_{NaP} magnitude of FXS3 neurons cultured with CON2 ACM was significantly large (Fig 5.16A, *pink trace*). Analysis of the current densities showed that FXS3 neurons cultured with CON2 ACM had significantly increased I_{NaP} as compared to CON2 neurons cultured with FXS3 ACM (Fig 5.16B-C). Thus the secretions from the human astrocytes are able to modulate the persistent sodium channel, thus determining the network activity of the neurons.

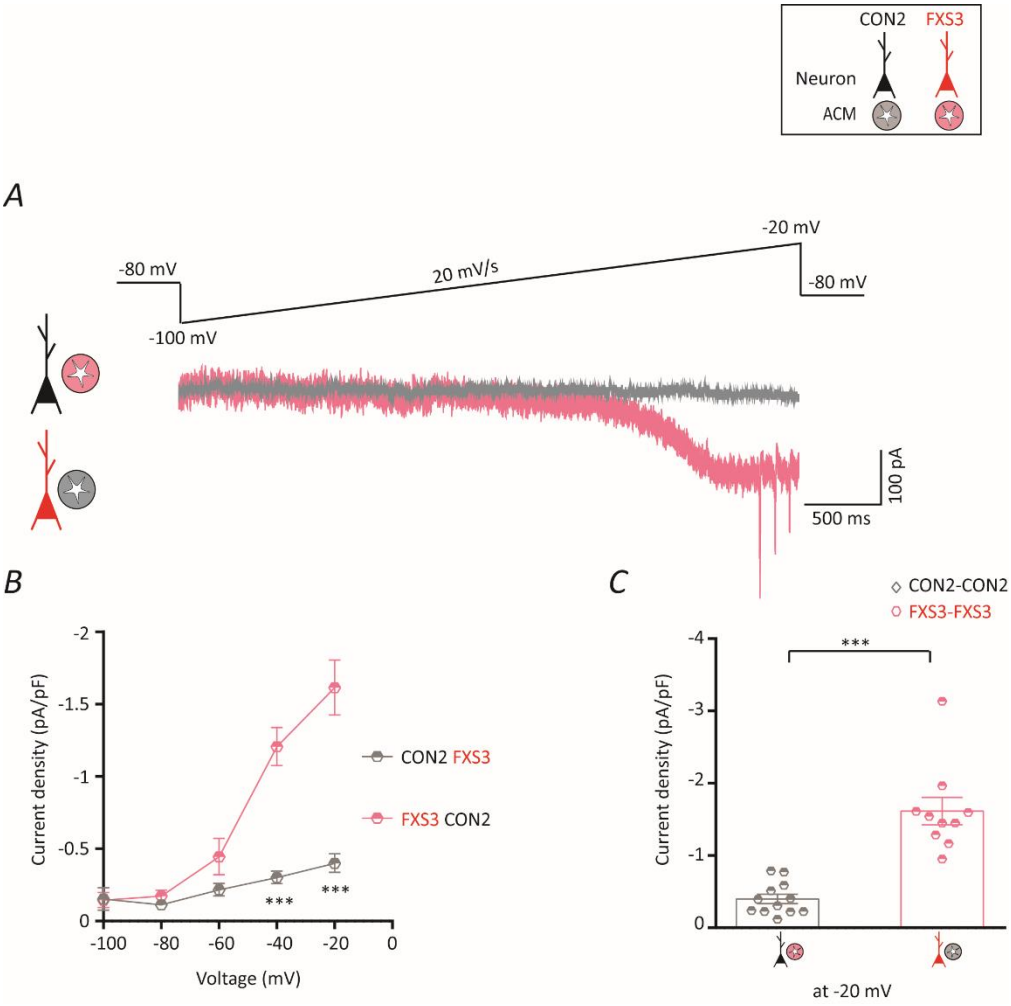

Figure 5.16 Control ACM rescues the NaP dysfunction resulting in robust I_{NaP} densities in FXS neurons.

(A) I_{NaP} isolated from the neurons cultured with ACM in response to a depolarizing voltage ramp (-100 to -20 mV, 20 mV/s). Representative I_{NaP} trace from a CON2 neuron cultured with FXS3 ACM (*grey trace*). I_{NaP} was isolated by subtracting the current elicited by the ramp in the *presence* and *absence* of TTX. I_{NaP} from a FXS3 neuron cultured with CON2 ACM (*pink trace*) is increased. (B) I -V curves plotted from the ramp-evoked $I_{NaP,}$ showing the increased I_{NaP} in FXS3 neurons cultured with CON2 ACM and the reduced I_{NaP} of CON2 neurons cultured with FXS3 ACM. Currents are normalized to the corresponding cell capacitance. (C) Quantification of current density at −20 mV show significant increase of the persistent sodium current in FXS3 neurons cultured with CON2 ACM. Overall mean current densities are: -0.399 ± 0.06 (CON2 neurons cultured with FXS3 ACM, n = 12, N = 3); -1.615 ± 0.19 (FXS3 neurons cultured with CON2 ACM, n = 10, N = 3). Values are ± SEM. ***p< 0.001, Two-way anova with post-hoc Bonferroni test, Unpaired t-test.

Discussion

Periodic spontaneous bursting activity is an important attribute of cortical pyramidal cells and is critical for reliable signal transmission, synaptic plasticity and overall development of the cortex (Wang, 1999; O'Donovan, 1999). Disruptions in the cortical network activity has been observed in rodent models and in human pluripotent stem cell models of FXS (Contractor *et al.,* 2015; Graef *et al.,* 2019; Das Sharma *et al.,* 2020). Understanding the FXS pathophysiology in rodent models and human stem cell derived models have focused exclusively on the neurons, as neurons are the excitable components of the nervous system. However, there is emerging evidence demonstrating that the network activity of the neurons is modulated by the astrocytes (Fellin, 2009; Lines *et al.,* 2020). Hence, to comprehend the complexities of FXS physiology, it is necessary to study the astrocytes and neurons together.

The key findings emerging from our study are:

- hPSC derived cortical neuron co-cultured with hPSC derived astrocytes after 8 weeks in vitro develop spontaneous network activity – neurons fire rhythmic action potentials.
- The genotype of the astrocytes determines the bursting phenotype of the neurons

The aberrant bursting phenotype of FXS neurons can be rescued by control astrocytes. Control neurons display the aberrant FXS bursting in the presence of FXS astrocytes in the culture.

- FXS neurons co-cultured with FXS astrocytes display reduced I_{NaP}. However, co-culturing FXS neurons with control astrocytes rescue the NaP dysfunction leading to an increase in the magnitude of $I_{NaP.}$
- Control neurons co-cultured with control astrocytes display robust I_{NaP}. Co-culturing of control neurons with FXS neurons, leads to significantly reduced I_{NaP}.
- Conditioned media from astrocytes, ACM, can elicit the same effects as the astrocytes i.e. genotype of the ACM determined the bursting phenotype of the neurons

ACM from the control astrocytes can rescue the aberrant bursting phenotype of the FXS neurons. Control neurons in presence of FXS ACM displays the FXS bursting.

- ACM can modulate the NaP. FXS neurons cultured with FXS-ACM show the characteristic reduced $I_{NaP,}$ which is rescued when the neurons are cultured in presence of control ACM. Control neurons in presence of control ACM show robust I_{NaP}, which is significantly reduced when neurons are cultured with FXS ACM.

Studies have predominantly looked at the FMRP expression in the neurons, but the intimate involvement of astrocytes in modulating the neuronal function has led to studies examining the FMRP expression patterns in the astrocytes and other glial cells. Immunocytochemistry studies have shown co-expression of FMRP and astrocyte marker GFAP both in developing mouse brain and differentiating neurospheres suggesting that FMRP is present in the astrocytes during early and mid postnatal brain development (Pacey & Doering, 2007; Gholizadeh *et al.,* 2015). Thus, presence of FMRP in the astrocytes during development is crucial for proper neuronal function. Interestingly, recent studies have shown that selective loss of FMRP from the astrocytes contribute to the FXS phenotype and re-expression of FMRP in the astrocytes can rescue the synaptic deficits and abnormal neuronal development in *Fmr1* KO mouse models (Higashimori *et al.,* 2016; Jacobs & Doering, 2010).

In our study using human cortical neurons with wild-type mouse primary astrocytes, we observed neurons lacking FMRP displaying an aberrant spontaneous network phenotype characterized by more number of bursts and shorter durations (Das Sharma *et al.,* 2020). While presence of rodent astrocytes led to development and maturation of synaptic and network properties of the hPSC derived cortical neurons, the wild-type rodent astrocytes could not correct the network activity deficits of human FXS neurons. Rodent astrocytes have been crucial in studying the astrocytic properties, but emerging studies have shown that there are fundamental differences between human and rodent astrocytes (reviewed in Vasile *et al.,* 2017). Strikingly, transplantation of human astrocyte progenitor cells into the embryonic neocortex of mice, led to adult mice with enhanced synaptic plasticity and learning (Han *et al.,* 2013). Thus in the present study, we used co-cultured hPSC neurons with hPSC derived astrocytes to understand the FXS pathogenesis in a completely human system. We found that human neurons – human astrocytes co-cultures had robust spontaneous network activity. For the first time we show that the genotype of the astrocytes had a profound effect on the burst activity of neurons. FXS neurons when co-cultured with FXS astrocytes had the characteristic aberrant burst activity, but when FXS neurons were co-cultured with control astrocytes, the network activity deficits were rescued and the FXS neurons displayed a control burst phenotype. Consequently, control neurons co-culture with control astrocytes showed control bursting activity, but when co-cultured with FXS astrocytes, the control neurons displayed FXS bursting phenotype. Thus, selective expression of FMRP in the human astrocytes is sufficient for proper neuronal network behaviour. Similarly, loss of FMRP from the astrocytes is enough to give rise to the FXS phenotype. Using gene-corrected astrocytes, we have also shown that reactivation of *FMR1* in the astrocytes, leads to correction of the network deficits of FXS neurons.

FMRP is known to regulate a wide number of ion channels, thereby influencing the neuronal excitability (reviewed in Ferron, 2016). *Fmr1* KO mouse studies have shown that alterations in the neuronal excitability of the entorhinal cortex, is due to increase in the persistent sodium current (Deng & Klyachko, 2016). In section 2.5, we observed that the FXS neurons co-cultured with mouse astrocytes, displayed significantly reduced I_{NaP} and in section 2.9, we partially rescued the aberrant bursting activity of the FXS neurons, by potentiating the voltage-gated sodium channels, using veratridine. This propelled us to look at the I_{NaP} in a human neuron-human astrocyte co-culture. Indeed, we found that human astrocytes determine the bursting phenotype of the neurons by modulating the $I_{NaP.}$ FXS neurons co-cultured with FXS astrocytes displayed the characteristic reduced I_{NaP}, but co-culturing with control astrocytes rescued the NaP deficits and FXS neurons displayed enhanced $I_{NaP,}$ similar to control neurons. Control neurons co-cultured with FXS astrocytes showed reduced I_{NaP} suggesting that loss of FMRP expression from the astrocytes is sufficient to cause dysfunction of the NaP channel in the neurons and selective expression of FMRP in the astrocytes is able to rescue the NaP channel dysfunction of FXS neurons.

Astrocytes are secretory cells and secrete factors that actively regulate neurogenesis, neural function and synapse development (reviewed in Barres, 2008). Recent body of evidence suggest that the astrocyte function can be brought about by its secretome. Several *in vitro Fmr1* KO mouse studies have shown that conditioned medium extracted from the astrocytes can rescue the FXS phenotype displayed by neurons (Sourial & Doering, 2016; Cheng *et al.,* 2016; Wang *et al.,* 2016). Indeed we see a striking effect of ACM derived from hPSC astrocytes on the human neurons. The ACM genotype determined the bursting phenotype of the neurons just like the astrocytes. ACM from control astrocytes could rescue the aberrant bursting phenotype of the FXS neurons and ACM from FXS astrocytes made the control neurons burst like FXS. Thus secretions from healthy astrocytes is able to rescue the network deficits observed in human FXS neurons. Similar to the astrocytes, we found that the ACM also modulated the NaP of the neurons. FXS neurons cultured with control ACM, displayed enhanced I_{NaP} and the control neurons cultured with FXS ACM displayed reduced I_{NaP}. This suggests that the factor/s secreted by the healthy astrocytes are able to potentiate the NaP channel. This result is particularly important because, it gives us clues to further investigate the ACM for factors that modulate the sodium channels.

Thus this study provides important mechanistic insights in understanding the role of human astrocytes in FXS pathophysiology. Astrocyte cell based therapy is a relatively new approach and is being extensively studied for neurodegenerative diseases like ALS (Barbeito, 2018). Astrocyte studies to understand FXS pathogenesis are burgeoning, and studies like ours are an important precursor for

designing such cell based therapies. Our results with astrocyte conditioned medium are significant as the ACM can be screened for factors that interact with FMRP and modulate network behavior which will hopefully translate to new therapeutic drugs.

Summary

In the previous chapter, we have provided comprehensive details of the modulation of network activity of hPSC derived neurons by hPSC derived astrocytes. Conditioned media experiments showed us that this modulation was through the astrocyte secretions. Healthy astrocytes and conditioned media derived from healthy astrocytes rescued the aberrant network activity of FXS neurons. Astrocytes alter the microenvironment at a short time scale (trauma) or longer time scales (neurodegeneration, neurodevelopmental diseases) by secreting signaling molecules like cytokines. One such important signaling molecule is S100β. S100β is a calcium sensing protein, expressed primarily in the astrocytes. It exerts both intracellular and extracellular functions (reviewed in Donato *et al*., 2009; Donato *et al*., 2013; Van Eldik & Wainwright, 2003).

Recent studies have shown that the plasma concentration of S100β is elevated in children suffering from Autism Spectrum Disorders (Al-Ayadhi & Mostafa, 2012; Guloksuz *et al*., 2017). Studies on Down's syndrome using iPSC's have shown elevated levels of S100β in the ACM extracted from Down's astrocytes and this high concentration of S100β led to impaired neuronal excitability (Mizuno *et al.,* 2018). Extracellular S100β also modulates neuronal bursting by altering the persistent sodium conductance (I_{NaP}) (Morquette *et al.,* 2015). Our results have shown that astrocytes and the ACM determine neuronal bursting by modulating the I_{NaP}. This result combined with multiple lines of evidence of the role of extracellular S100β in modulating the neuronal function, led us to investigate if indeed S100β is the molecule in the ACM which rescued the aberrant network firing of the hPSC derived FXS neurons.

Because the function of S100β is dependent on the concentration, in this chapter we have studied the effect of two concentrations of exogenous S100β – 100 µM and 1mM on the network activity of hPSC derived neurons. The lines used for the study are: CON2, FXS, FXS3 (iPSC) and $FMR1^{+/y,}$ $FMR1^{-/y}$ (ESC). We found that 100 µM S100β could rescue the aberrant FXS bursting phenotype. However, 1 mM S100β altered the control bursting phenotype to the aberrant FXS bursting phenotype. From the study by Morquette *et al.,* it is known that S100β alters the I_{NaP} and thereby affects the bursting of neurons. In this chapter have also investigated if S100β modulates the I_{NaP} of hPSC derived neurons.

Results

6.1 Exogenous S100β in low concentration (100 µM) can rescue the aberrant bursting phenotype of hPSC derived FXS neurons co-cultured with FXS astrocytes

In the last chapter, we saw that the genotype of the human astrocytes determined the bursting phenotype of neurons. Interestingly, conditioned media from the astrocytes also recapitulated the same result – genotype of ACM determined the phenotype of neuronal network activity. Thus control astrocytes and ACM rescued the aberrant bursting of FXS neurons. This result suggested that the control astrocytes and ACM had a factor or factors "X" that could rescue the burst firing of FXS neurons. The calcium binding protein S100β is actively released into the extracellular space by the astrocytes (Shashoua *et al.,* 1984; Van Eldik & Zimmer, 1987). The extracellular S100β chelates calcium and modulates the bursting activity of the neurons by increasing the conductance of the persistence sodium channel (Morquette *et al.,* 2015). Thus, we hypothesized that the factor "X" released by the hPSC astrocytes that modulated the neuronal bursting activity was S100β and addition of exogenous S100β to the FXS neurons would rescue their aberrant network activity. To test this, we used human-astrocyte co-cultures – control neurons with control astrocytes and FXS neurons with FXS astrocytes. The spontaneous burst activity of the neurons was recorded when the neurons were 8 weeks *in vitro* (Fig 6.1). The baseline burst activity was recorded for 10 mins and 100 µM S100β was the added to the recording chamber. After 20 mins, the burst activity of the neuron was measured with the S100β in the bath (Fig 6.1A). Recordings from a CON2 neurons co-cultured with CON2 astrocytes revealed that addition of S100β did not have any significant effect on the bursting activity of the CON2 neuron even after 20 mins (Fig 6.1B). The number of bursts and burst duration (Fig 6.2C, D) in the *absence* and *presence* of S100β was not significantly different across the control iPSC and ESC line. Next, we recorded the baseline spontaneous network activity from a FXS3 neuron co-cultured with FXS3 astrocytes (Fig 6.1E, *left*, *red trace*). The burst activity of FXS3 neuron was the characteristic aberrant firing – high number of bursts, short burst duration. S100β was added and the burst activity was recorded in its presence. We found that the burst activity of the FXS3 neurons is slowly altered (Fig 6.1E, *middle, red trace*) and after 20 min of S100β, the burst activity is significantly altered to resemble that of the control neurons (Fig 6.1E, *right, grey trace*). The number of bursts of the FXS neurons was significantly less *after* addition of S100β (Fig. 6.1F). Similarly, the burst duration of the FXS neurons was increased *after* addition of S100β (Fig 6.1G) across the iPSC and ESC lines. This result suggests that 100 µM S100β can rescue the aberrant burst firing of the FXS neurons even when they are co-cultured with FXS astrocytes.

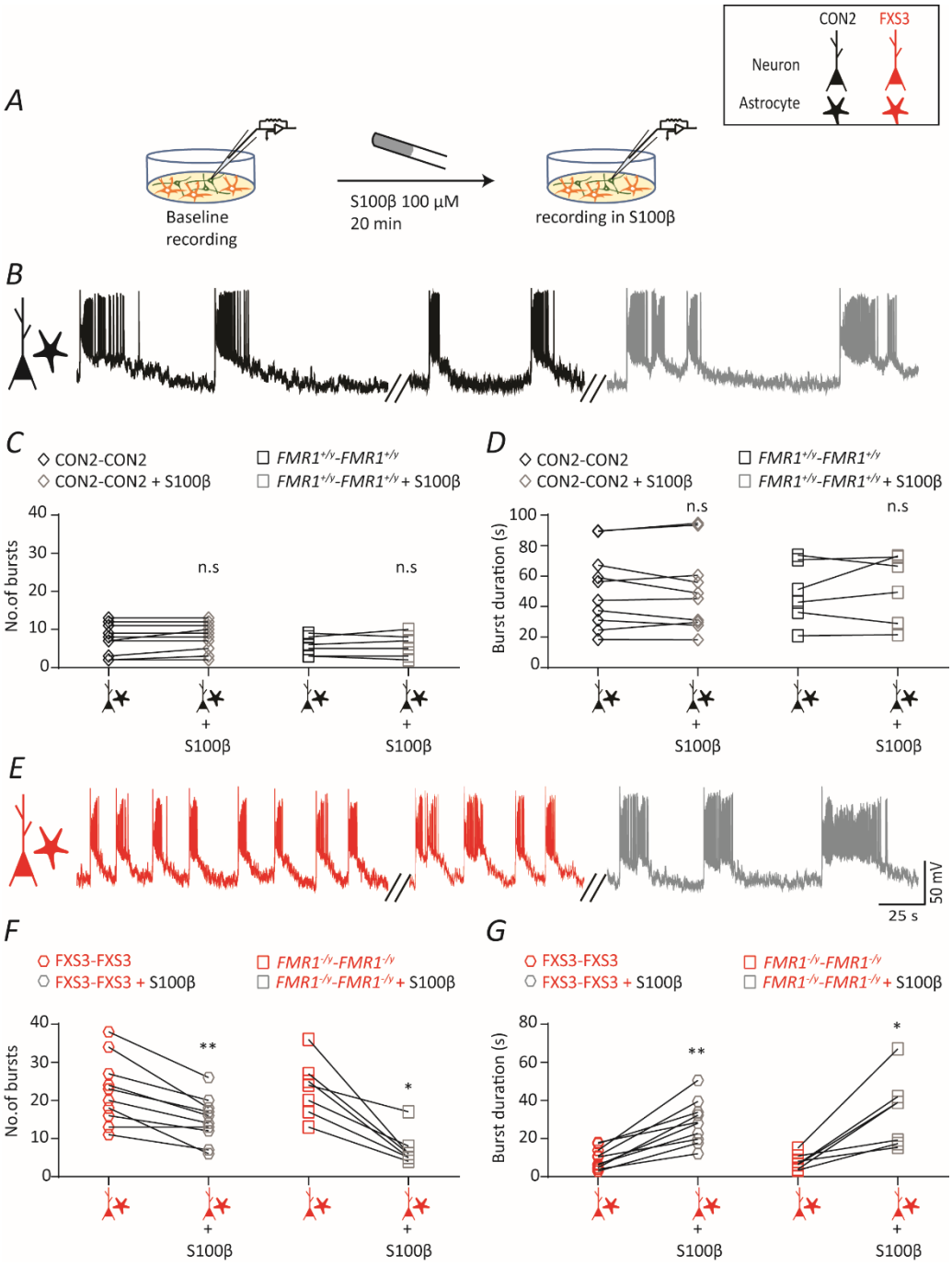

Figure 6.1 100 µM S100β rescues the aberrant bursting phenotype of FXS neurons co-cultured with FXS astrocytes.

(A) Schematic showing the protocol. The baseline spontaneous bursting activity is recorded for 10 min. S100β (100 µM) is added to the bath and burst activity is recorded for a further 20 min. **(B)** Representative current-clamp recording from a CON2 neuron co-cultured with CON2 astrocyte displaying the control bursting activity (*left trace*) – low burst number, longer burst duration. Addition of S100β does not alter the burst activity (*middle trace*) after 20 min (*right trace*). **(C)** Quantification of the number of bursts of control neurons (iPSC and ESC-derived) *before* and *after* addition of S100β. Overall the mean values are:

7.4 ± 1.27 (CON2 neurons co-cultured with CON2 astrocytes, n = 10, N = 3); 8 ± 1.18 (CON2 neurons co-cultured with CON2 astrocytes + S100β); 5.667 ± 1.022 (*FMR1*$^{+/y}$ neurons co-cultured with *FMR1*$^{+/y}$ astrocytes, n = 6, N = 2); 5.833 ± 1.25 (*FMR1*$^{+/y}$ neurons co-cultured with *FMR1*$^{+/y}$ astrocytes + S100β). **(D)** Quantification of the burst durations of control neurons *before* and *after* addition of S100β. Overall the mean burst durations (in seconds) are: 51.74 ± 7.97 (CON2 neurons co-cultured with CON2 astrocytes); 50.56 ± 8.39 (CON2 neurons co-cultured with CON2 astrocytes + S100β); 49.31 ± 8.33 (*FMR1*$^{+/y}$ neurons co-cultured with *FMR1*$^{+/y}$ astrocytes); 52.05 ± 9.22 (*FMR1*$^{+/y}$ neurons co-cultured with *FMR1*$^{+/y}$ astrocytes + S100β). **(E)** Representative trace from a FXS3 neuron co-cultured with FXS3 astrocytes displaying the FXS bursting - high number of bursts, shorter durations (*left trace*). Addition of S100β alters the bursting profile (middle trace) and after 20 min in presence of S100β FXS3 neuron displays a control bursting activity – low number of bursts, longer durations (right trace). **(F)** Quantification of the number of bursts of FXS neurons (iPSC and ESC-derived) *before* and *after* addition of S100β. Overall the mean values are: 22.4 ± 2.76 (FXS3 neurons co-cultured with FXS3 astrocytes, n = 10, N = 3); 14.9 ± 1.88 (FXS3 neurons co-cultured with FXS3 astrocytes + S100β); 23.14 ± 2.82 (*FMR1*$^{-/y}$ neurons co-cultured with *FMR1*$^{-/y}$ astrocytes, n = 7, N = 2); 7.286 ± 1.68 (*FMR1*$^{-/y}$ neurons co-cultured with *FMR1*$^{-/y}$ astrocytes + S100β). **(G)** Quantification of the burst durations of FXS neurons *before* and *after* addition of S100β. Overall the mean burst durations (in seconds) are: 9.45 ± 1.74 (FXS3 neurons co-cultured with FXS3 astrocytes); 28.52 ± 3.58 (FXS3 neurons co-cultured with FXS3 astrocytes + S100β); 7.73 ± 1.528 (*FMR1*$^{-/y}$ neurons co-cultured with *FMR1*$^{-/y}$ astrocytes); 34.18 ± 7 (*FMR1*$^{-/y}$ neurons co-cultured with *FMR1*$^{-/y}$ astrocytes + S100β). All values are ± SEM. $^{**}p < 0.01$, $^{*}p < 0.05$, Paired t-test, Wilcoxon matched – signed rank test.

6.2 The aberrant burst firing of control neurons co-cultured with FXS astrocytes is rescued by 100 µM S100β

As seen in chapter 5 (section 5.3), the astrocyte of the hPSC derived astrocyte determined the bursting phenotype of the neurons in a human neuron-astrocyte co-culture. Thus, control neurons when co-

cultured with FXS astrocytes displayed the aberrant FXS bursting phenotype – high number of bursts, short burst durations while FXS neurons co-cultured with control astrocytes displayed the control burst phenotype – low number of bursts, longer burst durations. Low concentrations of S100β (100 µM) rescued the aberrant bursting activity of FXS neurons co-cultured with FXS astrocytes, but had no effect on the burst profile of control neurons co-cultured with control astrocytes. We hypothesized that 100 µM S100β would also rescue the aberrant burst activity of control neurons co-cultured with FXS astrocytes but will not alter the bursting activity of FXS neurons co-cultured with control astrocytes. To test this, we used the same protocol as described in section 6.1. Neurons were co-cultured in two combinations – control neurons with FXS astrocytes and FXS neurons with control astrocytes. Baseline spontaneous bursting activity of the neurons (8 week *in vitro*) were recorded for 10 min and S100β (100 µM) was added to the recording chamber and the burst activity of the neuron was recorded in *presence* of S100β for further 20 min (Fig 6.2). CON2 neurons co-cultured with FXS3 astrocytes displayed the characteristic FXS bursting (Fig 6.2A, *left, black trace*). As hypothesized, addition of 100 µM S100β altered the bursting profile (Fig 6.2A, *middle, black trace*) to resemble the control bursting type (Fig 6.2A, *right, grey trace*). Analysis of the burst number and duration revealed that after addition of S100β to control neurons co-cultured with FXS astrocytes, there was a significant decrease in number of bursts (Fig 6.2B) and an increase in the burst durations (Fig 6.2C) across the iPSC and ESC lines. Next, we recorded bursting activity from FXS3 neuron co-cultured with CON2 astrocytes. The FXS3 neurons displayed the control bursting activity (Fig 6.2D, *left, red trace*). Addition of 100 µM S100β had no significant effect on the burst activity (Fig 6.2D, *middle, red trace*) even after 20 min (Fig 6.2D, *right, grey trace*). The burst number and duration (Fig 6E, F) of FXS neurons co-cultured with control astrocytes were not altered in *presence* of S100β. Thus addition of exogenous S100β rescued FXS bursting phenotype of hPSC derived neurons even in the presence of FXS astrocytes. This novel finding is in agreement with studies that have shown that S100β in low concentrations has a protective role.

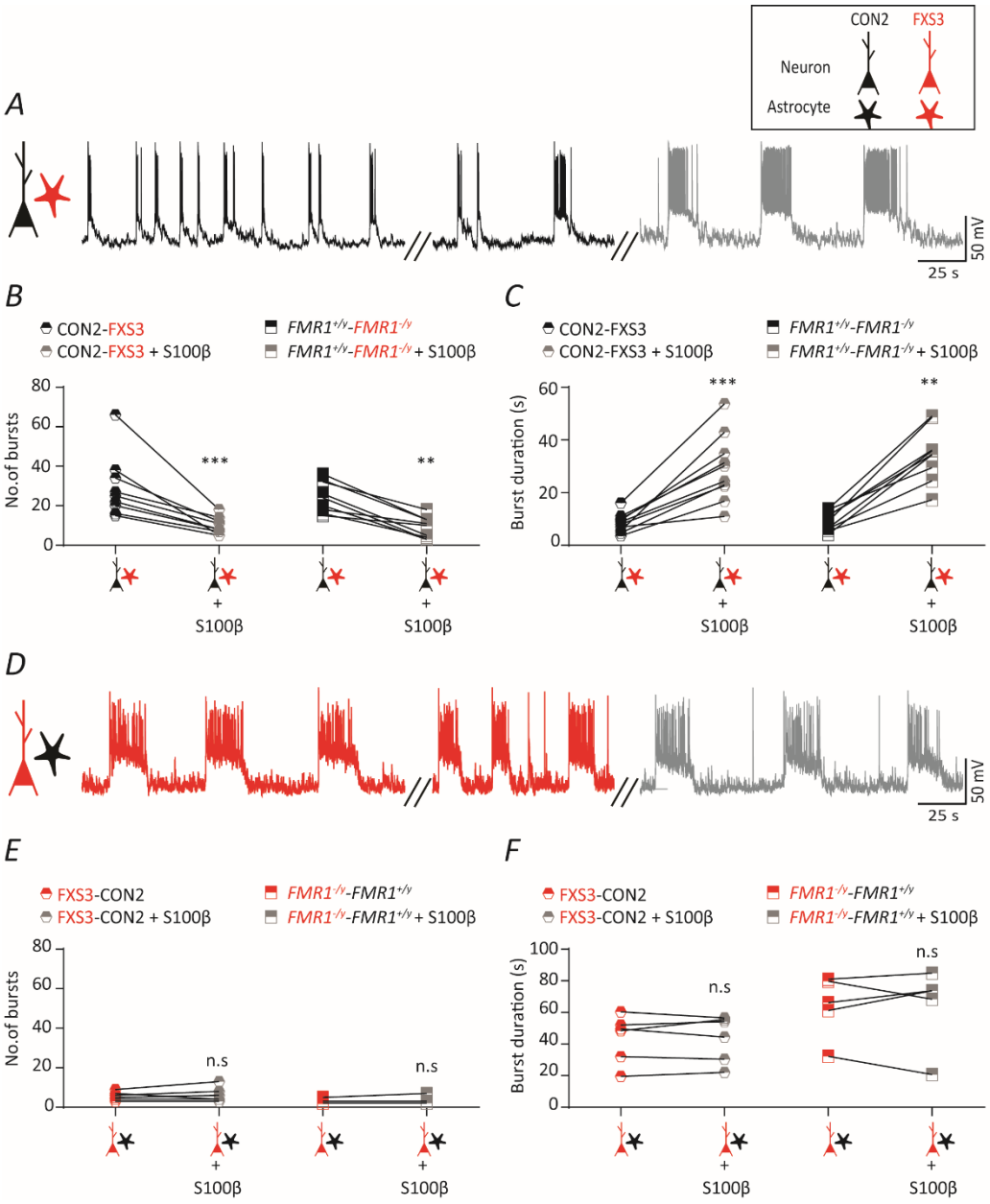

Figure 6.2 100 µM S100β corrects the aberrant network firing of control neurons co-cultured with FXS astrocytes.

(A) Representative trace from a CON2 neuron co-cultured with FXS3 astrocytes displaying the FXS bursting phenotype (*left trace*). In *presence* of S100β (100 µM) the burst activity is altered (*middle trace*) to resemble the control burst firing (*right trace*). **(B)** Quantification of the number of bursts of control neurons co-cultured with FXS astrocytes (iPSC and ESC) *before* and *after* addition of S100β. Overall the mean values are: 28.8 ± 4.72 (CON2 neurons co-cultured with FXS3 astrocytes, n = 10, N = 3); 9.9 ± 1.303 (CON2 neurons co-cultured with FXS3 astrocytes + S100β); 24.44 ± 2.6 (*FMR1*$^{+/y}$ neurons co-cultured with *FMR1*$^{-/y}$ astrocytes, n = 9, N = 3); 8.89 ± 1.8 (*FMR1*$^{+/y}$ neurons co-cultured with *FMR1*$^{-/y}$ astrocytes + S100β). **(C)** Quantification of the burst durations *before* and *after* addition of S100β. Overall the mean burst durations (in seconds) are: 8.42 ± 1.14 (CON2 neurons co-cultured with FXS3 astrocytes); 29.05 ± 3.97

(CON2 neurons co-cultured with FXS3 astrocytes + S100β); 9.055 ± 1.186 (*FMR1*$^{+/y}$ neurons co-cultured with *FMR1*$^{-/y}$ astrocytes); 34.4 ± 3.412 (*FMR1*$^{+/y}$ neurons co-cultured with *FMR1*$^{-/y}$ astrocytes + S100β). **(D)** Representative trace from a FXS3 neurons co-cultured with CON2 astrocytes bursting like the control (left trace). Addition of S100β does not alter the bursting profile (middle trace) after 20 min (right trace). **(E)** Quantification of the number of bursts of FXS neurons co-cultured with control astrocytes (iPSC and ESC – derived). Overall the mean numbers are: 5.66 ± 0.88 (FXS3 neurons co-cultured with CON2 astrocytes, n = 6, N = 2); 6.33 ± 1.52 (FXS3 neurons co-cultured with CON2 astrocytes + S100β); 3 ± 0.54 (*FMR1*$^{-/y}$ neurons co-cultured with *FMR1*$^{+/y}$ astrocytes, n = 7, N = 2); 3.4 ± 0.92 (*FMR1*$^{-/y}$ neurons co-cultured with *FMR1*$^{+/y}$ astrocytes + S100β). **(F)** Quantification of the burst durations. Overall the mean burst durations (in seconds) are: 43.72 ± 6.19 (FXS3 neurons co-cultured with CON2 astrocytes); 43.88 ± 5.93 (FXS3 neurons co-cultured with CON2 astrocytes + S100β); 64.1 ± 8.83 (*FMR1*$^{-/y}$ neurons co-cultured with *FMR1*$^{+/y}$ astrocytes); 64.3 ± 11.22 (*FMR1*$^{-/y}$ neurons co-cultured with *FMR1*$^{+/y}$ astrocytes + S100β).

6.3 High concentration of S100β (1 mM) alters the bursting profile of control neurons co-cultured with control astrocytes to resemble the FXS bursting

Several studies have shown that the children suffering from ASDs have an enhanced level of S100β in the serum (Al-Ayadhi & Mostafa, 2012; Guloksuz *et al.,* 2017). High levels of S100β are associated with neurotoxicity. This neurotoxicity is in part due to the interaction of S100β with the receptor for advanced glycation end products (RAGE) which leads to the transduction of several inflammatory stimuli (Donato *et al.,* 2001). The secretion of S100β from the astrocytes is also increased in response to metabolic stress (oxygen, serum and glucose deprivation) (Gerlach *et al.,* 2006). S100β is also elevated in another neurodevelopmental disorder, Down's syndrome (Yang *et al.,* 2005). Indeed, studies using iPSC neurons derived from DS patients have demonstrated aberrations in calcium signaling and neuronal excitability due to high S100β (Chen *et al*., 2014; Mizuno *et al.,* 2018). This led us to investigate the effect of high concentration of S100β on the hPSC derived neurons. Human neurons and astrocytes were co-cultured – control neurons with control astrocytes and FXS neurons with FXS astrocytes. 8 week old neurons were used for whole-cell patch clam recordings (Fig 6.3). The baseline spontaneous burst activity was recorded for 10 min and then 1 mM S100β was bath applied. Burst activity was recorded from the same neuron for an additional 20 min (Fig 6.3A). A CON2 neuron co-cultured with CON2 astrocytes displayed the characteristic control bursting phenotype (Fig 6.3B, *left, black trace*) – low number of bursts; longer durations. On addition of 1mM S100β, the bursting activity of the CON2 neuron is altered (Fig 6.3B, *middle, black trace*) and the CON2 neuron displays a FXS bursting phenotype – high number of bursts, shorter burst durations (Fig 6.3B, *right, pink trace*). There was a significant increase in the burst number (Fig 6.3C) and a significant decrease in the burst durations (Fig 6.3D) in control neurons co-cultured with control astrocytes across the iPSC and ESC lines. Next, we recorded the spontaneous network activity of FXS neurons co-cultured with FXS astrocytes. A FXS3 neuron co-cultured with FXS astrocyte displayed the characteristic FXS burst activity (Fig 6.3E, *left, red trace*). Addition of 1mM S100β did not change the bursting profile (Fig 6.3E, *middle, red trace*) even after 20 min (Fig 6.3E, *right, pink trace*). No significant changes in burst number (Fig 6.3F) or burst durations (Fig 6.3G) of FXS neurons co-cultured with FXS astrocytes was observed in the *presence* of 1mM S100β across the ESC and iPSC derived lines. Thus high concentration of S100β can change the bursting activity of control neurons to resemble the FXS, even when the culture contains control astrocytes. This result is especially interesting because 100 µM of S100β had no effect on the bursting activity of control neurons co-cultured with control astrocytes. This reiterates the role of dose dependent function of S100β.

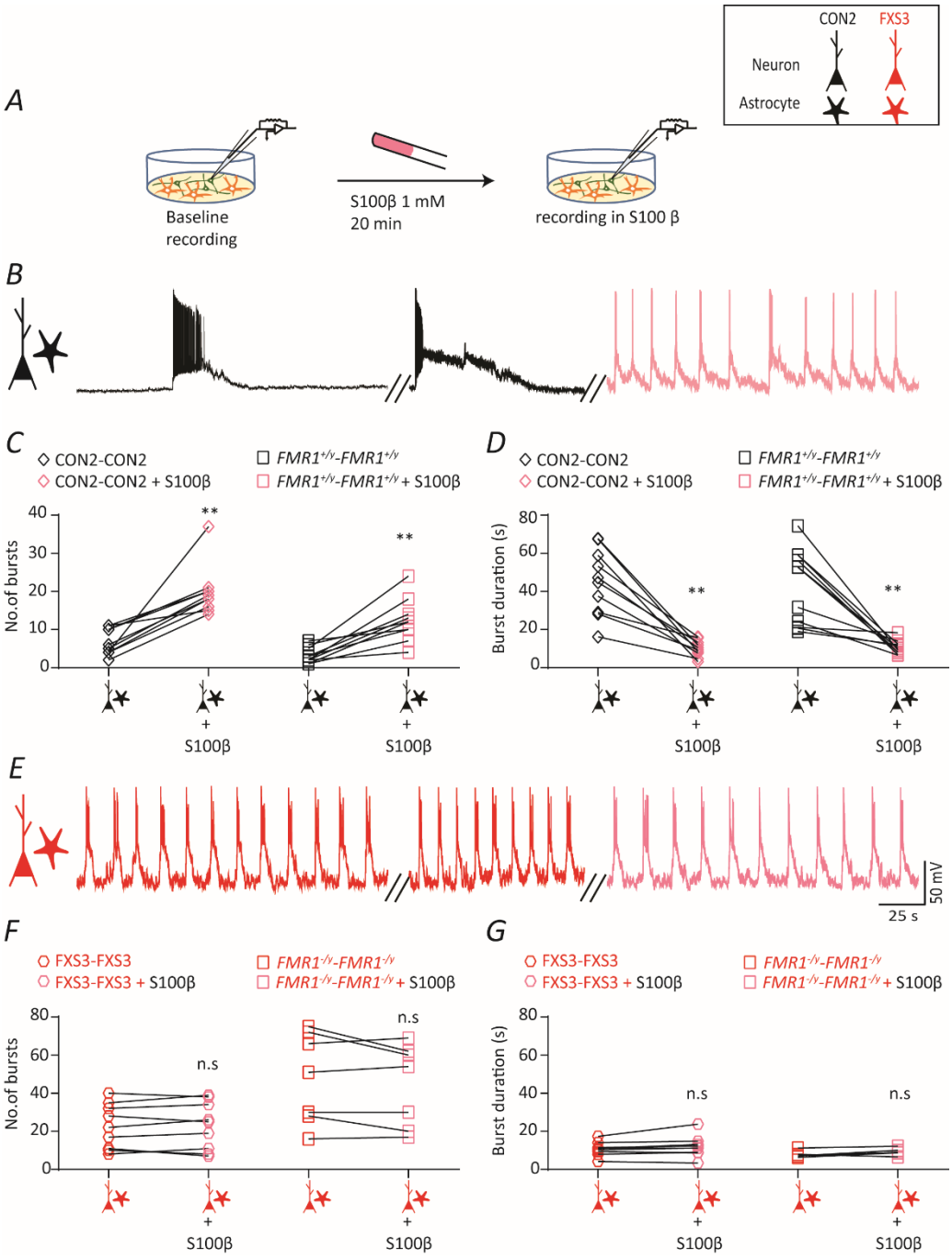

Figure 6.3 Control neurons co-cultured with control astrocytes display the aberrant FXS burst firing in presence of 1 mM S100β.

(A) Schematic showing the protocol. The baseline spontaneous bursting activity is recorded for 10 min. S100β (1 mM) is added to the bath and burst activity is recorded for a further 20 min. **(B)** Representative current-clamp recording from a CON2 neuron co-cultured with CON2 astrocyte displaying the control bursting activity (*left trace*) – low burst number, longer burst duration. Addition of S100β alters the burst profile (*middle trace*) and the CON2 neuron starts to burst like the FXS – higher number of bursts, shorter durations (*right trace*). **(C)** Quantification of the number of bursts of control neurons (iPSC and ESC-

derived) *before* and *after* addition of S100β. Overall the mean values are: 6.7 ± 1.08 (CON2 neurons co-cultured with CON2 astrocytes, n = 10, N = 3); 19.8 ± 2.04 (CON2 neurons co-cultured with CON2 astrocytes + S100β); 3.182 ± 0.6 (*FMR1*$^{+/y}$ neurons co-cultured with *FMR1*$^{+/y}$ astrocytes, n = 11, N = 3); 12.55 ± 1.6 (*FMR1*$^{+/y}$ neurons co-cultured with *FMR1*$^{+/y}$ astrocytes + S100β). **(D)** Quantification of the burst durations of control neurons *before* and *after* addition of S100β. Overall the mean burst durations (in seconds) are: 45.03 ± 5.49 (CON2 neurons co-cultured with CON2 astrocytes); 10.09 ± 1.36 (CON2 neurons co-cultured with CON2 astrocytes + S100β); 42.83 ± 5.96 (*FMR1*$^{+/y}$ neurons co-cultured with *FMR1*$^{+/y}$ astrocytes); 10.68 ± 1.051 (*FMR1*$^{+/y}$ neurons co-cultured with *FMR1*$^{+/y}$ astrocytes + S100β). **(E)** Representative trace from a FXS3 neuron co-cultured with FXS3 astrocytes displaying the FXS bursting - high number of bursts, shorter durations (*left trace*). Addition of S100β does not change the bursting profile (*middle trace*) after 20 min (*right trace*). **(F)** Quantification of the number of bursts of FXS neurons (iPSC and ESC-derived) *before* and *after* addition of S100β. Overall the mean values are: 22.56 ± 3.93 (FXS3 neurons co-cultured with FXS3 astrocytes, n = 9, N = 3); 23 ± 4.17 (FXS3 neurons co-cultured with FXS3 astrocytes + S100β); 48.29 ± 8.97 (*FMR1*$^{-/y}$ neurons co-cultured with *FMR1*$^{-/y}$ astrocytes, n = 7, N = 2); 44.57 ± 8.17 (*FMR1*$^{-/y}$ neurons co-cultured with *FMR1*$^{-/y}$ astrocytes + S100β). **(G)** Quantification of the burst durations of FXS neurons *before* and *after* addition of S100β. Overall the mean burst durations (in seconds) are: 10.79 ± 1.23 (FXS3 neurons co-cultured with FXS3 astrocytes); 11.96 ± 1.85 (FXS3 neurons co-cultured with FXS3 astrocytes + S100β); 7.62 ± 0.64 (*FMR1*$^{-/y}$ neurons co-cultured with *FMR1*$^{-/y}$ astrocytes); 9.31 ± 0.65 (*FMR1*$^{-/y}$ neurons co-cultured with *FMR1*$^{-/y}$ astrocytes + S100β). All values are ± SEM. ***p*< 0.01, Paired t-test, Wilcoxon matched – signed rank test.

6.4 FXS neurons co-cultured with control astrocytes display an aberrant FXS burst firing after addition of 1 mM S100β

In previous sections, we showed that low concentration of S100β did not alter the burst activity of hPSC derived neurons co-cultured with control astrocytes. However, the aberrant activity of neurons co-

cultured with FXS astrocytes was rescued by 100 µM S100β. Interestingly, high concentration of S100β (1 mM) altered the bursting activity of control neurons co-cultured with control astrocytes and had no effect on the bursting activity of FXS neurons co-cultured with FXS astrocytes. Thus we hypothesized that, 1 mM S100β would also alter the burst profile of FXS neurons co-cultured with control astrocytes and it will have no effect on the burst activity of control neurons co-cultured with FXS astrocytes. To test this, same protocol as described in section 6.3 was followed. Cells were co-cultured in two combinations – control neurons with FXS astrocytes and FXS neurons with control astrocytes. Spontaneous burst activity was recorded from 8 week old neurons. Baseline burst activity was recorded for 10 min. 1 mM S100β was bath applied and recordings were continued for a further 20 min (Fig. 6.4). CON2 neuron co-cultured with FXS3 astrocytes displayed the aberrant FXS burst firing (Fig 6.4A, *left, black trace*). Addition of 1 mM S100β did not have any effect on the burst firing (Fig 6.4A, *middle, black trace*) after 20 min (Fig 6.4A, *right, pink trace*). The burst number (Fig 6.4B) and duration (Fig 6.4C) were not significantly different in the *presence* of 1mM S100β across the iPSC and ESC line. Next we proceeded to record from FXS neurons co-cultured with control astrocytes. A FXS3 neuron co-cultured with CON2 astrocytes displayed the control bursting (Fig 6.4D, *left, black trace*). Upon addition of 1 mM S100β, the bursting profile changed (Fig 6.4D, *middle, black trace*) and the neuron started to display the aberrant FXS burst firing (Fig 6.4D, *right, pink trace*). Analysis of the burst number and duration (Fig 6.4E-F) revealed that across the iPSC and ESC lines, addition of 1 mM S100β significantly increased the number of bursts and decreased the burst duration. Together, the results from section 6.3 and 6.4 suggest that S100β in high concentration can alter the control burst firing of hPSC derived neurons to aberrant FXS burst firing even in the presence of control astrocytes.

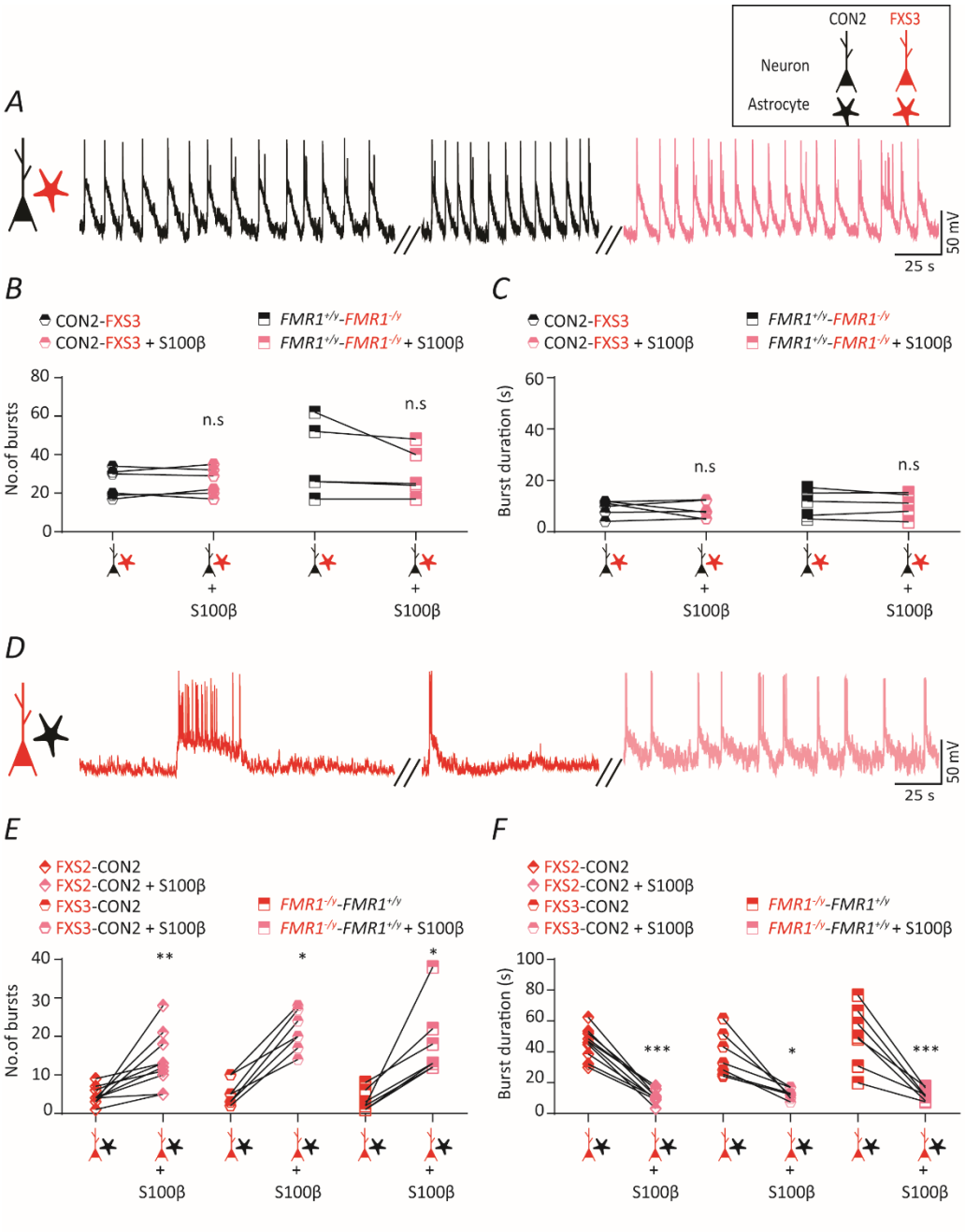

Figure 6.4 1 mM S100β alters the bursting profile of FXS neurons co-cultured with control astrocytes to resemble the aberrant FXS bursting.

(A) Representative trace from a CON2 neuron co-cultured with FXS3 astrocytes displaying the FXS bursting phenotype (*left trace*). In *presence* of S100β (1 mM) the burst activity is not altered (*middle trace*) even after 20 min (*right trace*). **(B)** Quantification of the number of bursts of control neurons co-cultured with FXS astrocytes (iPSC and ESC) *before* and *after* addition of S100β. Overall the mean values are: 25.17 ± 2.98 (CON2 neurons co-cultured with FXS3 astrocytes, n = 6, N = 2); 25.83 ± 2.93 (CON2 neurons co-cultured with FXS3 astrocytes + S100β); 36.6 ± 8.63 (*FMR1*$^{+/y}$ neurons co-cultured with *FMR1*$^{-/y}$ astrocytes, n = 9, N = 3); 30.8 ± 5.7 (*FMR1*$^{+/y}$ neurons co-cultured with *FMR1*$^{-/y}$ astrocytes + S100β). **(C)** Quantification

of the burst durations *before* and *after* addition of S100β. Overall the mean burst durations (in seconds) are: 9.34 ± 1.25 (CON2 neurons co-cultured with FXS3 astrocytes); 8.37 ± 1.36 (CON2 neurons co-cultured with FXS3 astrocytes + S100β); 11.08 ± 2.38 (*FMR1*$^{+/y}$ neurons co-cultured with *FMR1*$^{-/y}$ astrocytes); 10.5 ± 2.1 (*FMR1*$^{+/y}$ neurons co-cultured with *FMR1*$^{-/y}$ astrocytes + S100β). **(D)** Representative trace from a FXS3 neuron co-cultured with CON2 astrocytes bursting like the control (*left trace*). Addition of S100β alters the bursting profile (*middle trace*) and the neuron starts to display the control bursting (*right trace*). **(E)** Quantification of the number of bursts of FXS neurons co-cultured with control astrocytes (iPSC and ESC – derived). Overall the mean numbers are: 4.5 ± 0.71 (FXS2 neurons co-cultured with CON2 astrocytes, n = 10, N = 3); 13.6 ± 2.24 (FXS2 neurons co-cultured with CON2 astrocytes + S100β); 5.43 ± 1.25 (FXS3 neurons co-cultured with CON2 astrocytes, n = 7, N = 2); 21.43 ± 1.95 (FXS3 neurons co-cultured with CON2 astrocytes + S100β); 3.286 ± 1.01 (*FMR1*$^{-/y}$ neurons co-cultured with *FMR1*$^{+/y}$ astrocytes, n = 7, N = 2); 18.29 ± 3.57 (*FMR1*$^{-/y}$ neurons co-cultured with *FMR1*$^{+/y}$ astrocytes + S100β). **(F)** Quantification of the burst durations. Overall the mean burst durations (in seconds) are: 45.44 ± 3.1 (FXS2 neurons co-cultured with CON2 astrocytes); 11.34 ± 1.34 (FXS2 neurons co-cultured with CON2 astrocytes + S100β); 38.13 ± 5.41 (FXS3 neurons co-cultured with CON2 astrocytes); 12.65 ± 1.34 (FXS3 neurons co-cultured with CON2 astrocytes + S100β); 49.98 ± 7.44 (*FMR1*$^{-/y}$ neurons co-cultured with *FMR1*$^{+/y}$ astrocytes); 12.09 ± 1.43 (*FMR1*$^{-/y}$ neurons co-cultured with *FMR1*$^{+/y}$ astrocytes + S100β). All values are ± SEM. ***P<0.001, **p< 0.01, *p< 0.05. Paired t-test, Wilcoxon matched – signed rank test.

6.5 100 µM S100β increases the persistent sodium current of FXS neurons co-cultured with FXS astrocytes

In chapter 5, we provided evidence of the hPSC derived neurons and ACM modulating the persistent sodium channel (NaP) conductance and thereby determining the bursting phenotype of the neurons. Control neurons co-cultured with control astrocytes displayed robust I_{NaP} whereas FXS neurons co-cultured with FXS astrocytes displayed reduced I_{NaP}. This result was also recaptilated with astrocyte derived ACM – control neurons cultured in presence of ACM displayed robust I_{NaP} while I_{NaP} from FXS neurons cultured in presence of FXS ACM was severely reduced. It has been shown that extracellular calcium plays a very important role in modulating the persistent sodium current dependent bursting of neurons. Lowering of external calcium concentration $[Ca^{2+}]_o$ induces bursting by potentiating the I_{NaP} whereas increasing $[Ca^{2+}]_o$ resulted in suppression of bursting by decreasing the I_{NaP} (Hailing *et al.,* 2001). Astrocytes secrete S100β into the extracellular space, and S100β chelates the $[Ca^{2+}]_o$. The chelation of $[Ca^{2+}]_o$ results in an increase in the I_{NaP} of the neurons (Morquette *et al.,* 2015; Kadala *et al.,* 2015). Exogenous S100β also exerts the same function, thereby regulating bursting of neurons (Morquette *et al.,* 2015). In previous sections, we have discussed the dual role exhibited by S100β on the bursting activity of hPSC derived neurons co-cultured with human astrocytes. 100 µM S100β rescued the aberrant bursting phenotype of FXS neurons co-cultured with FXS astrocytes. We hypothesized that the rescue of the aberrant burst behaviour by 100 µM S100β was due to potentiation of I_{NaP} of FXS neurons co-cultured with FXS astrocytes. To test this we isolated the I_{NaP} from control neurons co-cultured with control astrocytes and FXS neurons co-cultured with FXS astrocytes. Depolarizing voltage ramp (-100 to -20 mV, 20 mV/s) was injected to the 8 week old neurons in the *absence* and *presence* of 1 µM TTX. The two traces were subtracted, to reveal the TTX-sensitive I_{NaP}. 100 µM S100β was applied to the recording chamber and after 20 min I_{NaP} was recorded with the S100β in the chamber (Fig 6.5). CON2 neuron co-cultured with CON2 astrocytes exhibited robust I_{NaP} (Fig 6.5A, *black trace*). The I_{NaP} was not significantly altered in presence of 100 µM S100β (Fig 6.5A, *grey trace*). Analysis of the current densities (Fig 6.5B-C) across the iPSC and ESC lines showed the same – in presence of 100 µM S100β there was no significant change in the I_{NaP} of control neurons co-cultured with control astrocytes. Next we proceeded to record from FXS neurons with FXS astrocytes. FXS3 neuron co-cultured with FXS3 astrocytes displayed reduced I_{NaP} (Fig 6.5D, *red trace*). Upon addition of 100 µM S100β there was an increase in the I_{NaP} of the FXS3 neuron (Fig 6.5D, *grey trace*). The I_{NaP} current densities across iPSC and ESC lines (Fig 6.5E-F) also showed a significant increase in the presence of 100 µM S100β. Thus exogenous S100β indeed modulated the NaP and it is this modulation that led to the rescue of burst activity in FXS neurons co-cultured with FXS astrocytes.

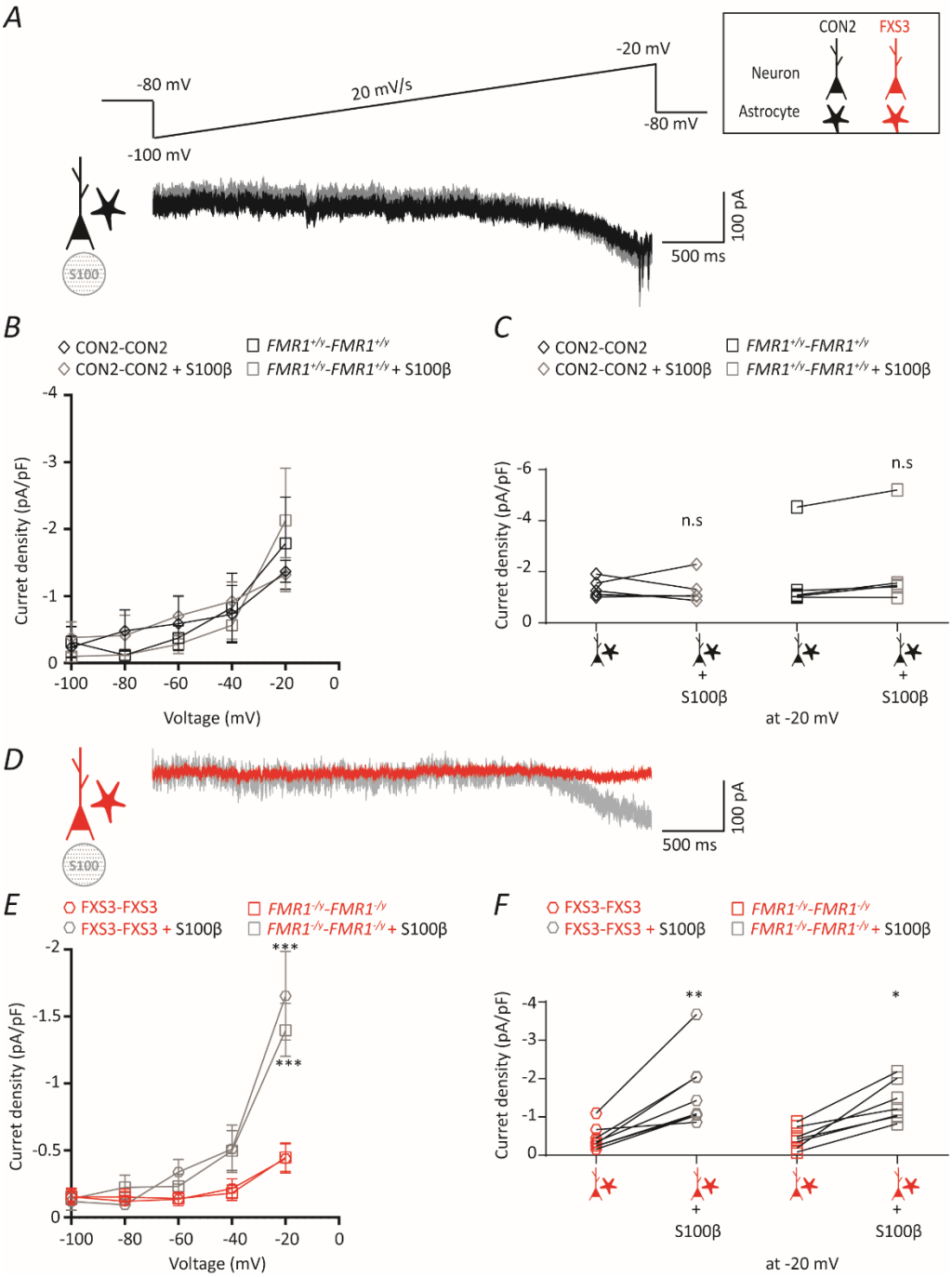

Figure 6.5 100 µM S100β increases the I_{NaP} in FXS neurons co-cultured with FXS astrocytes.

(A) A CON2 neuron co-cultured with CON2 astrocytes shows the characteristic robust I_{NaP} in response to depolarizing voltage ramp (-100 to -20 mV, 20 mV/s). Addition of 100 µM S100β has no effect on the I_{NaP} magnitude **(B)** I -V curves plotted from the ramp-evoked $I_{NaP,}$ showing the robust I_{NaP} of control neurons co-cultured with control astrocytes across the iPSC and ES lines in the *presence* and *absence* of S100β. Currents are normalized to the corresponding cell capacitance. **(C)** Current density at -20 mV showing no significant effect of 100 µM S100β on I_{NaP} current densities of control neurons co-cultured with control astrocytes. Overall the mean current densities (pA/pF) are: -1.368 ± 0.16 (CON2 neurons co-cultured with

CON2 astrocytes, n = 5, N = 2); -1.318 ± 0.25 (CON2 neurons co-cultured with CON2 astrocytes + S100β); -1.78 ± 0.68 (*FMR1*$^{+/y}$ neurons co-cultured with *FMR1*$^{+/y}$ astrocytes, n = 11, N = 3); -2.13 ± 0.77 (*FMR1*$^{+/y}$ neurons co-cultured with *FMR1*$^{+/y}$ astrocytes + S100β). **(D)** A FXS3 neuron co-cultured with FXS3 astrocytes shows reduced I_{NaP}. Addition of 100 µM S100β increases the $I_{NaP.}$ **(E)** I -V curves plotted from the ramp-evoked $I_{NaP,}$ showing the significant increase in I_{NaP} in the presence of S100β across the iPSC and ESC derived lines. (F) Current density at -20 mV shows the significant increase of I_{NaP} current densities in presence of 100 µM S100β in FXS neurons co-cultured with FXS astrocytes. Overall the mean current densities (pA/pF) are: -0.438 ± 0.1 (FXS3 neurons co-cultured with FXS3 astrocytes, n = 8, N = 3); -1.65 ± 0.33 (FXS3 neurons co-cultured with FXS3 astrocytes + S100β); -0.44 ± 0.1 (*FMR1*$^{-/y}$ neurons co-cultured with *FMR1*$^{-/y}$ astrocytes, n = 7, N = 3); -1.4 ± 0.19 (*FMR1*$^{-/y}$ neurons co-cultured with *FMR1*$^{-/y}$ astrocytes + S100β). All values are ± SEM. ***p< 0.001, **p< 0.01, *p<0.05, Two-way ANOVA - RM, Paired t-test, Wilcoxon matched – signed rank test.

6.6 Reduced I_{NaP} of control neurons co-cultured with FXS astrocytes is rescued following addition of 100 µM S100β

Control neurons when co-cultured with FXS astrocytes displayed similar persistent sodium channel dysfunction as FXS neurons co-cultured with FXS astrocytes evidenced by the significantly reduced I_{NaP} (chapter 5, section 5.8). In the previous section we discussed the modulation of NaP in FXS neurons co-

cultured with FXS astrocytes by S100β. Presence of 100 µM S100β potentiated the NaP channel thereby increasing the magnitude of I_{NaP}. We hypothesized that the reduced I_{NaP} of control neurons co-cultured with FXS astrocytes will be rescued to control levels by 100 µM S100β. To test this we followed the same protocol as decribed in section 6.5. Briefly, after isolation of I_{NaP} from the neuron, 100 µM S100β was added into the recording chamber and the I_{NaP} was recorded from the same neuron after 20 min. Recordings from a CON2 neuron co-cultured with FXS3 astrocytes, revealed the characteristic reduced I_{NaP} (Fig 6.6A, *black trace*) . Following addition of S100β, there is an increase in the I_{NaP} magnitude (Fig 6.6A, *grey trace*). Analysis of current densities across iPSC and ESC lines (Fig. 6B-C) revealed significant increase in the current density post application of 100 µM S100β. Next, we recorded the I_{NaP} from FXS neurons co-cultured with control astrocytes. We hypothesized that similar to control neurons co-cultured with control astrocytes, S100β would have no effect on the I_{NaP} magnitude in FXS neurons co-cultured with control astrocytes. Indeed, recordings from FXS3 neuron co-cultured with CON2 astrocytes showed that robust I_{NaP} (Fig 6.6D, *red trace*) which was not significantly altered after addition of 100 µM S100β (Fig 6.6D, *grey trace*). Analysis of the I_{NaP} current densities across the iPSC and ESC derived lines revealed the same – 100 µM S100β did not alter the I_{NaP} current densities of FXS neurons co-cultured with control astrocytes. Thus, these results together with section 6.5, suggest that exogenous S100β rectified the aberrant burst activity of neurons co-cultured with FXS astrocytes through modulating the NaP conductance. As many studies suggest, this S100β most likely chelates the external calcium and potentiates the already dysfunctional NaP in neurons co-cultured with FXS astrocytes thereby correcting the aberrant network activity.

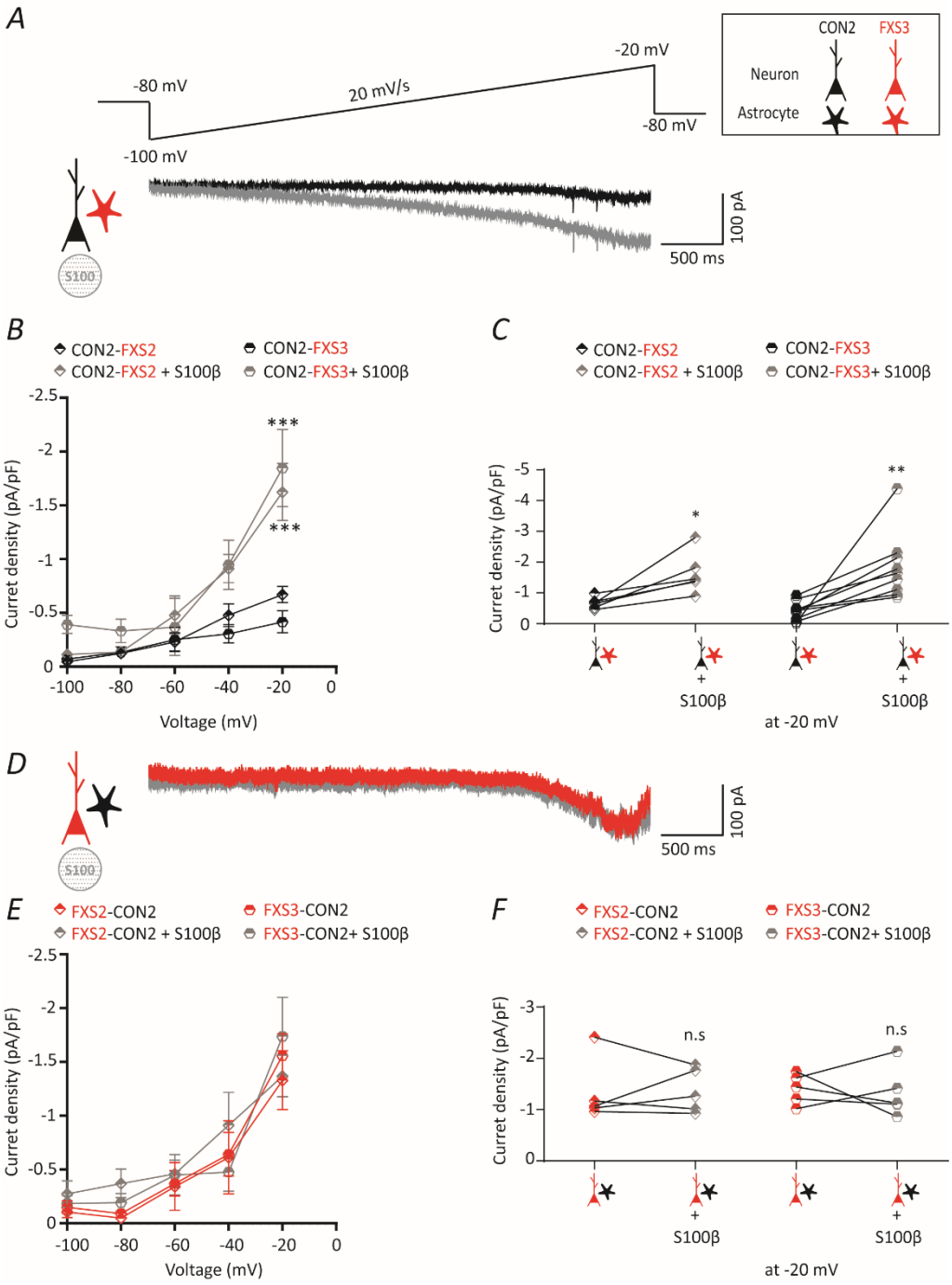

Figure 6.6 100 µM S100β increases the I_{NaP} in control neurons co-cultured with FXS astrocytes.

(A) I_{NaP} magnitude from a CON2 neuron co-cultured with FXS3 astrocytes (black trace) increases after application of 100 µM S100β (grey trace). **(B)** I -V curves plotted from the ramp-evoked $I_{NaP,}$ showing the significant increase in I_{NaP} in the presence of S100β across the iPSC lines. Current is normalized to capacitance. **(C)** Current density at -20 mV shows the significant increase of I_{NaP} current densities in presence of 100 µM S100β in control neurons co-cultured with FXS astrocytes. Overall the mean current densities (pA/pF) are: -0.67 ± 0.07 (CON2 neurons co-cultured with FXS2 astrocytes, n = 6, N = 2); -1.62 ±

0.26 (CON2 neurons co-cultured with FXS2 astrocytes + S100β); -0.41 ± 0.1 (CON2 neurons co-cultured with FXS3 astrocytes, n = 9, N = 3); -1.84 ± 0.35 (CON2 neurons co-cultured with FXS3 astrocytes + S100β); (D) FXS3 neuron co-cultured with CON2 astrocytes displayed robust I_{NaP} (red trace) which is unaltered after application of 100 µM S100β (red trace). (E) I -V curves plotted from the ramp-evoked $I_{NaP,}$ showing the robust I_{NaP} of FXS neurons co-cultured with control astrocytes across the iPSC lines in the *presence* and *absence* of S100β. Currents are normalized to the corresponding cell capacitance. **(C)** Current density at -20 mV showing no significant effect of 100 µM S100β on I_{NaP} current densities of FXS neurons co-cultured with control astrocytes. Overall the mean current densities (pA/pF) are: -1.329 ± 0.27 (FXS2 neurons co-cultured with CON2 astrocytes, n = 5, N = 2); -1.368 ± 0.19 (FXS2 neurons co-cultured with CON2 astrocytes + S100β); -1.406 ± 0.13 (FXS3 neurons co-cultured with CON2 astrocytes, n = 5, N = 2); -1.33 ± 0.21 (FXS3 neurons co-cultured with CON2 astrocytes + S100β). All values are ± SEM. ***p< 0.001, **p< 0.01, *p<0.05, Two-way ANOVA - RM, Paired t-test, Wilcoxon matched – signed rank test.

6.7 Veratridine rescues the aberrant network activity of FXS neurons co-cultured with FXS astrocytes

In chapter 4 (section 4.9) the aberrant burst firing of FXS neurons co-cultured with primary mouse astrocytes was rescued by the voltage-gated sodium channel activator, veratridine. Several studies have shown the increase or induction of burst activity by micromolar concentrations of veratridine (Tian *et al*., 1995; Fekete *et al.*, 2009). Indeed, 0.5 µM veratridine increased the burst duration and decreased the number of bursts significantly of FXS neurons in a human-rodent co-culture. This propelled us to investigate the effect of veratridine on the bursting of human neurons co-cultured with human astrocytes. Co-cultures of control neurons with control astrocytes and FXS neurons with FXS astrocytes were used for this experiment. Spontaneous network activity was recorded from the 8 week old neurons. After recording baseline activity (10 min), 0.5 µM veratridine was added to the bath chamber and the recordings were continued for 20 min, similar to S100β experiments (Fig 6.7A). The bursting activity of CON2 neuron co-cultured with CON2 astrocytes (Fig 6.7B, *left, black trace*) is not altered after addition of veratridine (Fig 6.7B, *middle, black trace*) even after 20 min (Fig 6.7B, *right, grey trace*). Next, we proceeded to study the effect of veratridine on the network activity of FXS neurons co-cultured with FXS astrocytes. The bursting profile of a FXS3 neuron co-cultured with FXS3 astrocytes (Fig 6.7C, *left, red trace*) changes after addition of 0.5 µM veratridine (Fig 6.7C, *middle, red trace*). After 20 min the bursting profile of the FXS3 neuron resembles that of the control (Fig 6.7C, *right, grey trace*). The number of bursts decreases significantly (Fig 6.7D) and there is a significant increase in the burst duration (Fig 6.7E) of FXS neurons co-cultured with FXS astrocytes whereas the burst number and duration of control neurons co-cultured with control astrocytes was not significantly altered by veratridine. Thus similar to rodent co-culture, veratridine can also rescue the aberrant burst firing of FXS neurons co-cultured with FXS human astrocytes.

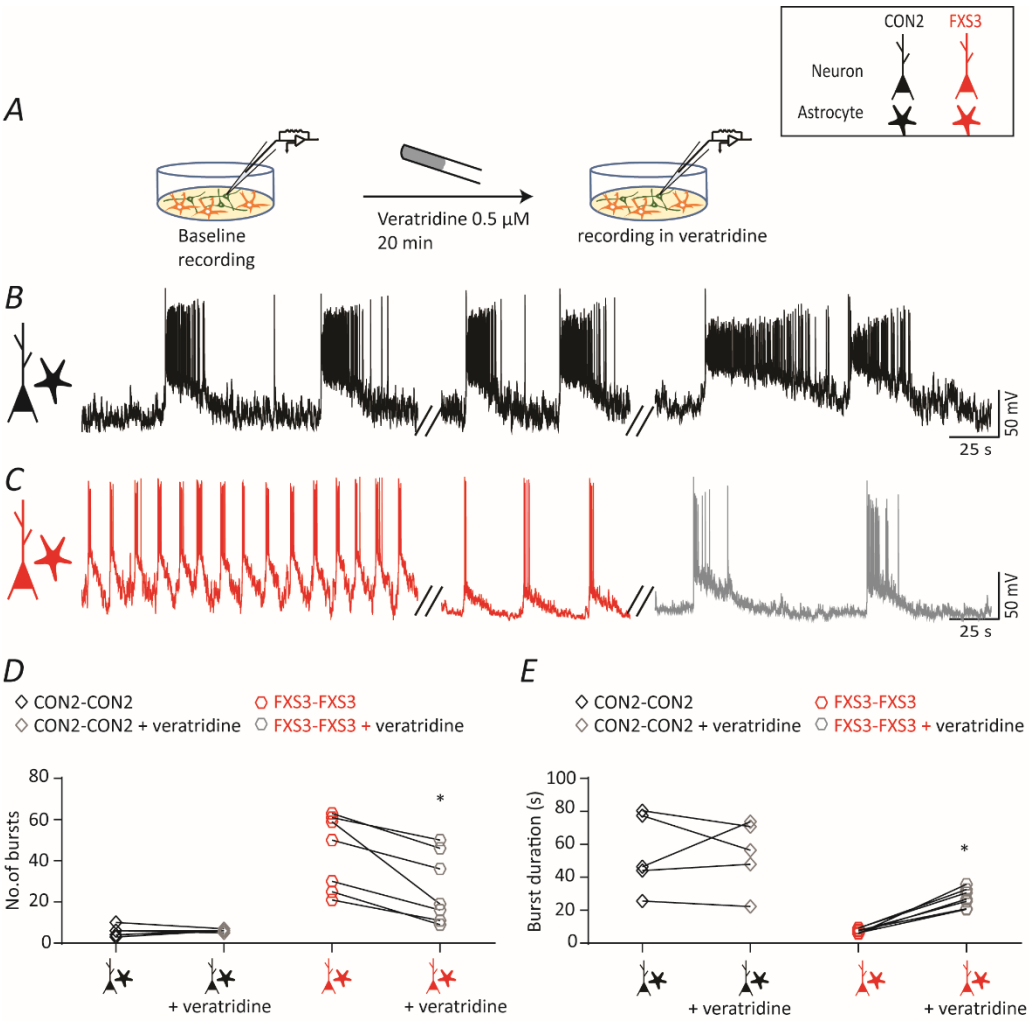

Figure 6.7 Veratridine corrects the aberrant burst firing of FXS neurons co-cultured with FXS astrocytes.

(A) Schematic showing the protocol for recording the effect of veratridine on the burst activity of hPSC derived neurons. **(B)** Representative trace showing the burst activity of a CON2 neuron co-cultured with CON2 astrocytes (*left trace*). Addition of veratridine does not alter the bursting profile (middle trace) even after 20 min (right trace). **(C)** A FXS3 neuron co-cultured with FXS3 astrocytes shows the characteristic aberrant burst firing (*left trace*). After addition of veratridine the bursting profile changes (*middle trace*) and starts to resemble the control bursting profile (*right trace*). (D) The number of bursts of FXS3 neurons co-cultured with FXS3 astrocytes decreases significantly in *presence* of veratridine. Overall the mean burst numbers are: 5.8 ± 1.2 (CON2 neurons co-cultured with CON2 astrocytes, n = 5, N = 2); 6 ± 0.31 (CON2 neurons co-cultured with CON2 astrocytes + veratridine); 44.14 ± 6.89 (FXS3 neurons co-cultured with FXS3 astrocytes, n = 7, N = 2); 26.71 ± 6.48 (FXS3 neurons co-cultured with FXS3 astrocytes + veratridine). **(D)** The burst durations of FXS neurons co-cultured with FXS astrocytes significantly increases after addition of veratridine. Overall the burst durations (in seconds) are: 54.78 ± 10.5 (CON2 neurons co-cultured with CON2 astrocytes); 54.24 ± 9.27 (CON2 neurons co-cultured with CON2 astrocytes + veratridine); 7.4 ± 0.51 (FXS3 neurons co-cultured with FXS3 astrocytes); 27.5 ± 2.18 (FXS3 neurons co-cultured with FXS3 astrocytes + veratridine). All values are ± SEM. *p< 0.05. Paired t-test, Wilcoxon matched – signed rank test.

6.8 Veratridine rescues the aberrant network activity of control neurons co-cultured with FXS astrocytes.

As seen in section 6.7, in *presence* of veratridine, the aberrant network activity of FXS neurons co-cultured with FXS astrocytes was corrected. We hypothesized that veratridine could also rescue the aberrant burst activity of control neurons co-cultured with FXS astrocytes. To test this, we followed the same protocol outlined in section 6.7. The spontaneous network activity of a CON2 neuron co-cultured with FXS3 astrocytes (Fig 6.8A, left, black trace) was altered after addition of 0.5 µM veratrdine to the bath chamber (Fig 6.8A, middle, black trace). After 20 min, the bursting profile resembled that of the control (Fig 6.8A, right, grey trace). There was a significant decrease of the number of bursts (Fig 6.8B) and significant increase in the burst duration (Fig 6.8C) following addition of veratridine. As a next step we checked if the spontaneous network activity of FXS neurons co-cultured with control astrocytes was affected by veratridine. Burst activity was recorded from FXS3 neuron co-cultured with CON2 astrocytes (Fig 6.8D, *left, red trace*). Addition of 0.5 µM veratridine did not alter the burst profile (Fig 6.8D, *middle, red trace*) even after 20 min (Fig 6.8D, *right, grey trace*). There was no significant change in the burst number (Fig 6.8E) or the burst duration (6.8F) in the *presence* of veratridine. The results of section 6.7 and 6.8 together suggest that veratridine rescues the aberrant burst activity of the neurons co-cultured with FXS astrocytes. This is similar to the effect mediated by S100β. As discussed in 6.5 and 6.6, the effect of S100β on the burst activity of neurons is primarily through the potentiation of persistent sodium channel, in the last set of experiments, we proceeded to study the effect of veratridine on I_{NaP}.

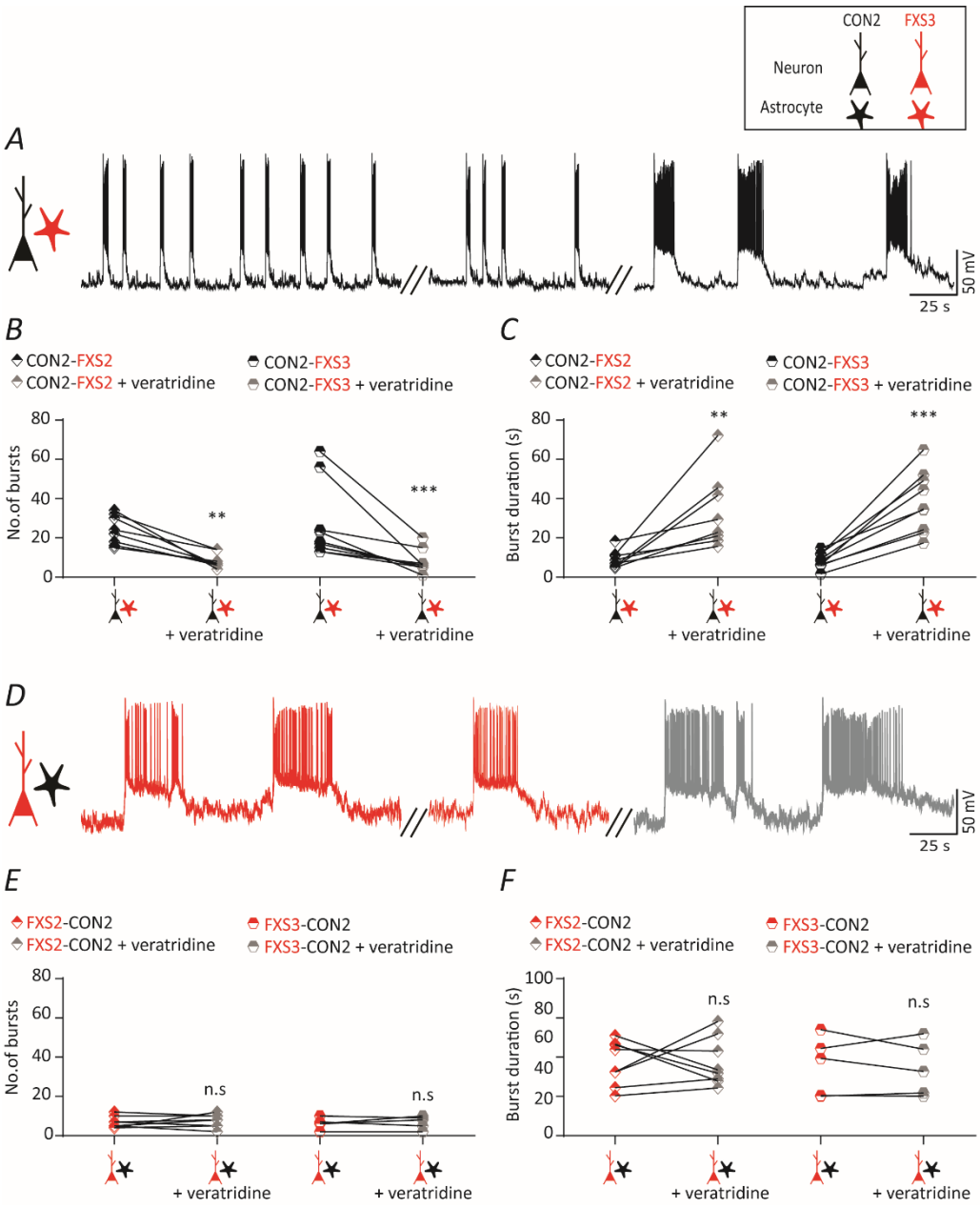

Figure 6.8 Aberrant network activity of control neurons co-cultured with FXS astrocytes is rescued by veratridine.

(A) Representative trace from a CON2 neuron co-cultured with FXS3 astrocytes shows the aberrant bursting profile (*left trace*) which is altered after the addition of veratridine (*middle trace*). The bursting profile starts to resemble the control bursting in presence of veratridine (*right trace*). **(B)** Quantification of the number of bursts across the iPSC lines shows a significant decrease in the burst number of control neurons co-cultured with FXS astrocytes in the *presence* of veratridine. Overall the mean number of bursts are: 23.88 ± 2.6 (CON2 neurons co-cultured with FXS2 astrocytes, n = 8, N = 2); 8.25 ± 1.31 (CON2 neurons co-cultured with FXS2 astrocytes + veratridine); 24 ± 4.98 (CON2 neurons co-cultured with FXS3 astrocytes, n = 12, N = 3); 7.33 ± 1.47 (CON2 neurons co-cultured with FXS3 astrocytes + veratridine). **(C)** Quantification of the burst durations shows a significant increase in the presence of veratridine. Overall

the mean burst durations (in seconds) are: 8.96 ± 1.62 (CON2 neurons co-cultured with FXS2 astrocytes); 33.39 ± 6.73 (CON2 neurons co-cultured with FXS2 astrocytes + veratridine); 8.64 ± 1.13 (CON2 neurons co-cultured with FXS3 astrocytes); 35.39 ± 4.184 (CON2 neurons co-cultured with FXS3 astrocytes + veratridine). **(D)** The bursting profile of FXS3 neuron co-cultured with CON2 astrocytes (*left trace*) does not change after application of veratridine *(middle trace*). 20 min of veratridine does not alter the burst profile of the neuron (*right trace*). **(E)** Quantification of the number of bursts of the iPSC lines in the *presence* and *absence* of veratridine. Overall the mean number of bursts are: 6.75 ± 1.03 (FXS2 neurons co-cultured with CON2 astrocytes, n = 8, N = 2); 7.5 ± 1.16 (FXS2 neurons co-cultured with CON2 astrocytes + veratridine); 6.2 ± 1.28 (FXS3 neurons co-cultured with CON2 astrocytes, n = 5, N = 2); 6.8 ± 1.46 (FXS3 neurons co-cultured with CON2 astrocytes + veratridine). All values are ± SEM. ***P<0.001, **p< 0.01. Paired t-test, Wilcoxon matched – signed rank test.

6.9 Veratridine increases the I_{NaP} in neurons co-cultured with FXS astrocytes

Experiments with S100β suggested that the correction of aberrant FXS firing by 0.5 µM S100β was by increasing the current through the NaP. So we hypothesized that veratridine's action on the NaP would be similar. Indeed several studies have shown that veratridine increases the I_{NaP} in neurons (Morquette *et al.,* 2015; Tazerart *et al.,* 2008). As reported in the previous sections, veratridine did not alter the bursting profile of neurons co-cultured with control astrocytes. So, in the last step of experiments, we selectively analysed the effect of veratridine on the I_{NaP} of neurons co-cultured with FXS astrocytes. Using the same depolarizing voltage ramp (-100 to -20 mV, 20 mV/s) I_{NaP} was evoked from the neurons. Veratridine was added to the recording chamber and the I_{NaP} was recorded from the same neuron after 20 min (Fig 6.9). A FXS2 neuron co-cultured with FXS2 astrocytes displays the characteristic reduced I_{NaP} (Fig 6.9A, *red trace*). As expected, veratridine increased the I_{NaP} magnitude of the FXS2 neuron (Fig 6.9A, *grey trace*). Analysis of the I_{NaP} current densities revealed that across the FXS iPSC lines, veratridine increased the I_{NaP} current density (Fig 6.9B-C). Similarly, a CON2 neuron co-cultured with FXS2 astrocytes, displays reduced I_{NaP} in response to the depolarizing voltage ramp (Fig 6.9D, *black trace*). Addition of veratridine resulted in an increase in the I_{NaP} magnitude of the CON2 neuron (Fig 6.9D, *grey trace*). There was a significant increase in the I_{NaP} current densities after addition of veratridine across the iPSC lines (Fig 6.9E-F). Together these results suggest that both S100β and veratridine correct the aberrant FXS firing by reversing the deficits in the neuronal I_{NaP} despite the presence of FXS astrocytes in the culture.

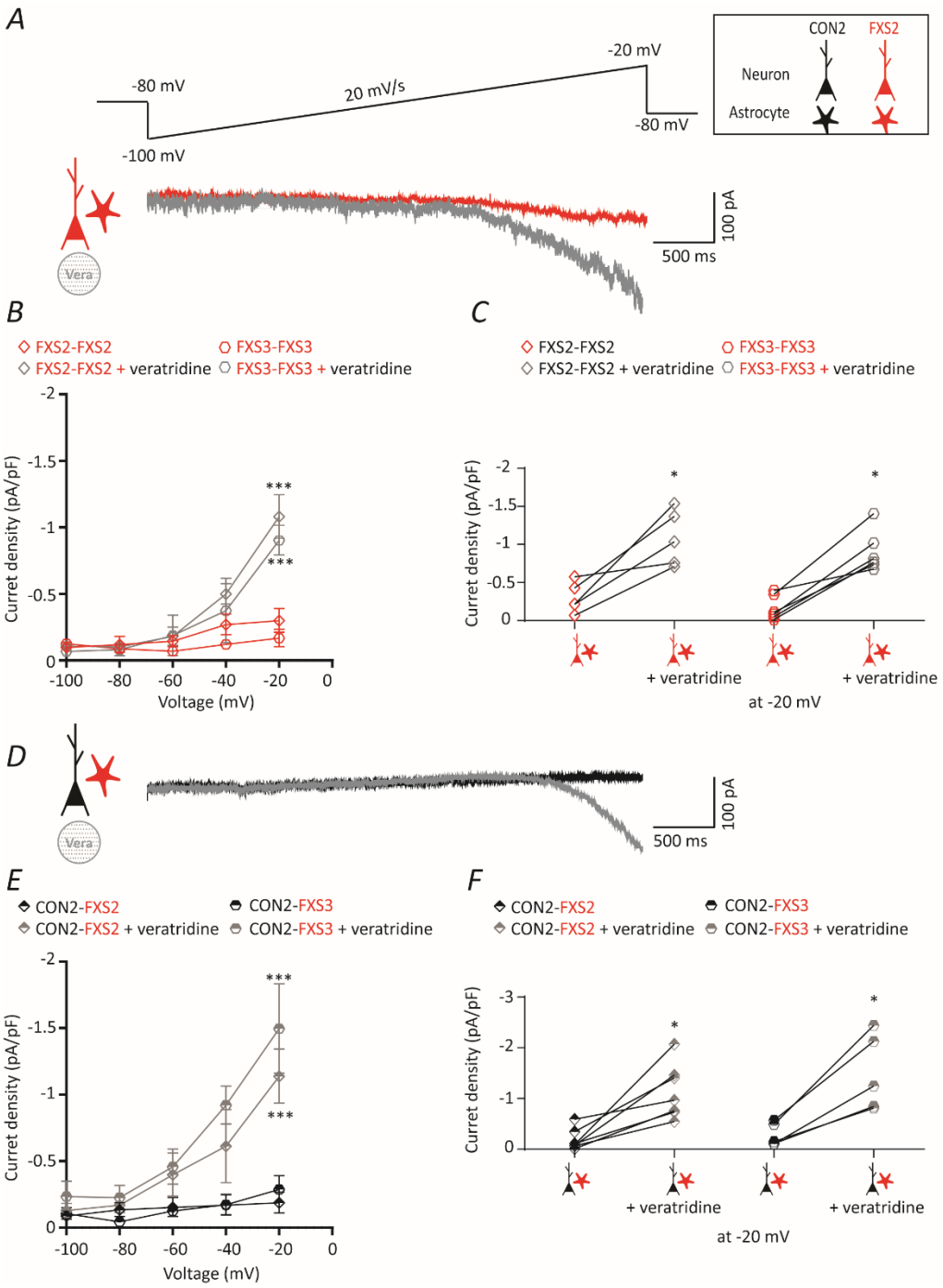

Figure 6.9 Veratridine corrects the I_{NaP} deficits in neurons co-cultured with FXS astrocytes.

(A) A FXS2 neuron co-cultured with FXS2 astrocytes shows reduced I_{NaP} (*red trace*). Addition of 0.5 µM veratridine increases the I_{NaP} (*grey trace*). **(B)** I -V curves plotted from the ramp-evoked $I_{NaP,}$ showing the significant increase in I_{NaP} in the presence of veratridine across the iPSC lines. Current is normalized to capacitance. **(C)** Current density at -20 mV shows the significant increase of I_{NaP} current densities in presence of 0.5 µM veratridine in FXS neurons co-cultured with FXS astrocytes. Overall mean current densities (pA/pF) are: -0.3 ± 0.09 (FXS2 neurons co-cultured with FXS2 astrocytes, n = 5, N = 2); -1.081 ±

0.16 (FXS2 neurons co-cultured with FXS2 astrocytes + veratridine); -0.17 ± 0.06 (FXS3 neurons co-cultured with FXS3 astrocytes, n = 9, N = 3); -0.9 ± 0.11 (FXS3 neurons co-cultured with FXS3 astrocytes + veratridine). **(D)** Reduced I_{NaP} (*red trace*) of a CON2 neuron co-cultured with FXS2 astrocytes is corrected after in the *presence* of veratridine (*grey trace*). **(E))** I -V curves showing a significant increase in the I_{NaP} current densities post application of veratridine in control neurons co-cultured with FXS astrocytes. **(F)** Current densities at -20 mV are significantly increased after addition of veratridine. Overall the mean current densities (pA/pF) are: -0.18 ± 0.07 (CON2 neurons co-cultured with FXS2 astrocytes, n = 7, N = 2); -1.13 ± 0.2 (CON2 neurons co-cultured with FXS2 astrocytes + veratridine); -0.28 ± 0.1 (CON2 neurons co-cultured with FXS3 astrocytes, n = 9, N = 3); -1.49 ± 0.33 (CON2 neurons co-cultured with FXS3 astrocytes + veratridine). All values are ± SEM. ***p< 0.001, *p<0.05, Two-way ANOVA - RM, Paired t-test, Wilcoxon matched – signed rank test.

Discussion

The pathophysiology of FXS though studied extensively, has been exclusively neurocentric for the past decades. The role of astrocytes and their secretome has rarely been taken into consideration. Recent lines of evidence strongly suggest the active role of astrocytes in the FXS pathophysiology. Studies using *Fmr1* KO mouse models have shown that lack of FMRP leads to hyperthrophy of astrocytes (Lee *et al.,* 2019). Interestingly, presence of healthy astrocytes is enough to correct the dendritic dysmorphogenesis in the absence of FMRP (Cheng *et al.,* 2012). Astrocytes influence the neural network firing in mice (Deemyad *et al.,* 2018) and abnormal astrocyte feedback could result in epileptic seizures (Yu *et al.,* 2020). Indeed, in Chapter 5, we have provided evidence of how astrocytes modulate the network activity of hPSC derived neurons. We saw that the presence of healthy astrocytes rescued the aberrant network firing of FXS neurons and this effect was also recapitulated by the conditioned media derived from astrocytes. We also reported that presence of FXS astrocytes/ACM drove the control neurons to fire aberrant bursts suggesting that it is the secretions from the astrocytes which modulate the hPSC derived neuronal network firing.

Astrocytes secrete a number of chemokines, cytokines and growth factors which mediate the neuron-glia communication. Some of the cytokines secreted by astrocytes in culture include interleukins like IL-6, IL-8, IL-1β (Choi *et al.,* 2014). Our results with the ACM led us to investigate the factors present in the ACM which could be responsible for the modulation of the neuronal network activity. We found that the molecule S100β was integral to the regulation of neuronal burst activity. Key findings emerging from our study are:

- S100β in low concentrations (100 µM) can correct the aberrant bursting phenotype of hPSC neurons co-cultured with FXS astrocytes.
- High concentrations of S100β (1 mM) converts the control bursting profile to a FXS bursting profile of neurons co-cultured with control astrocytes. Thus S100β modulation of the network burst firing depends on its concentration.
- S100β (100 µM) increases the persistent sodium current magnitude in neurons co-cultured with FXS astrocytes.
- Veratridine (0.5 µM) also corrects the aberrant bursting phenotype of hPSC neurons co-cultured with FXS astrocytes.
- The persistent sodium current magnitude of neurons co-cultured with FXS astrocytes increases in the *presence* of veratridine.

S100β is a calcium – chelating protein, released by the astrocytes into the extracellular space (reviewed in Donato *et al.,* 2013). It is involved in regulating the extracellular and intracellular calcium metabolism (Schafer & Heizmann, 1996). Depending on the concentration, S100β might have a trophic or a toxic effect. At nanomolar concentrations, it stimulates the growth of neurons and protects them during an injury or trauma (Rothermundt *et al.,* 2003; Gazzolo *et al.,* 2015). At micromolar concentrations S100β mediates apoptosis resulting in cell death (Sorci *et al*., 2004; Rothermundt *et al.,* 2003). S100β acts a damage – associated molecular pattern (DAMP) which is released by the cells under conditions of duress (Sorci *et al.,* 2010). A tight regulation of S100β takes place during neurogenesis, with an enhanced expression in neural progenitor cells (NPCs) when they are proliferating and migrating, followed by a decrease in S100β expression. This is concomitant with an increase in S100β expression in glial precursor cells and differentiated astrocytes (Raponi *et al.,* 2007).

The plasma concentration of S100β is enhanced in children with autism (Al-Ayadhi & Mostafa, 2012; Guloksuz *et al*., 2017). In the cerebellum of *Fmr1* KO mice, there was an increase in the expression of S100β (Pacey *et al.,* 2015). Recent studies have shown that S100β modulates the neuronal bursting. External addition of S100β led to rhythmic burst firing of neurons (Morquette *et al.,* 2015). In primary cortical and hippocampal neuronal culture, incubation of the neurons with nanomolar concentrations of S100β protected the neurons from excitotoxicity (Ahlemeyer *et al.,* 2000; Kogel *et al.,* 2004). Cortical neurons already exposed to excitoxicity, S100β promoted the survival of neurons (Villarreal *et al.,* 2011). Indeed, our results suggest a similar protective action of S100β. Exogenous S100β in low concentrations when added to the recording chamber, was able to rescue the aberrant burst firing of the neurons co-cultured with FXS astrocytes. The modulation of burst activity by S100β is primarily through the chelation of external calcium ions. The decrease in external calcium concentration increases the current through the persistent sodium channels resulting in an increase in the burst firing (Morquette *et al.,* 2015; Su *et al.,* 2001). This led us to investigate if S100β indeed modulated I_{NaP} in the hPSC derived neurons. 100 µM S100β indeed increased the I_{NaP} magnitude in neurons co-cultured with FXS astrocytes. Thus similar to other studies, S100β was able to rescue the aberrant burst firing of the neurons co-cultured with FXS astrocytes by increasing the current through persistent sodium channels.

To further corroborate the results obtained using 100 µM S100β, we performed similar experiments with a sodium channel opener, veratridine. The action of veratridine on the network activity of neurons is well established. Veratridine alters the sodium channel function and leads to induction of neuronal bursting (Tian *et al.,* 1995). The bursting activity elicited by veratridine is also dependent on calcium. Studies have

shown that in presence of calcium antagonists like cobalt and verampil, veratridine is unable to induce rhythmic bursting in neurons (Link *et al.,* 2008). In Chapter 4, we had reported the rescue of aberrant burst firing of FXS neurons by veratridine when the human neurons were co-cultured with rodent astrocytes. Here, we report that veratridine also corrects the aberrant burst activity of human neurons co-cultured with human FXS astrocytes. Several studies have shown that veratridine enhances the I_{NaP} thereby modulating neuronal networks (Tazerart *et al.,* 2008; Morquette *et al.,* 2015). Indeed, we found that veratridine increased the I_{NaP} magnitude of neurons co-cultured with FXS astrocytes. The results obtained using veratridine and S100β suggests that the modulation of I_{NaP} is criticial for proper burst firing.

The function of S100β is intimately associated with its concentration. Brain trauma induces S100β release from the astrocytes. Enhanced levels of S100β is found in the CSF and peripheral blood in a number of neurodegenerative and neurodevelopmental diseases (Van Eldik & Griffin, 1994; Braga *et al.,* 2006). iPSC studies using neurons from Down's Syndrome patients have shown an elevation in the S100β expression. Moreover this heightened S100β expression led to aberrant calcium signaling and dirsuptions in neuronal excitability (Chen *et al.,* 2014; Mizuno *et al.,* 2019). Several studies point towards an increase in S100β levels in the cortex of patients suffering from Alzheimer's and in the AD mouse models (Simpson *et al.,* 2010; Yeh *et al.,* 2015). Hence, an abnormal increase in the S100β levels is a common outcome of several diseases of the CNS. Here, we have confirmed the dual role of S100β on the neuronal network activity. High concentration of S100β converted the control bursting activity of neurons co-cultured with control astrocytes into aberrant FXS bursting. The mechanistic basis of this result is not very clear, however a probable mechanism was outlined in a study by Kispersky *et al.,* 2012, which suggested that a very high increase in the sodium conductance could lead to a decrease in the firing rate of neurons.

In Chapter 5, we had reported that astrocytes and ACM modulated the I_{NaP} and neuronal burst firing and in this chapter, we provide a potential molecule released by the astrocytes, S100β that modulated the $I_{NaP.}$ Different levels of S100B elicited bidirectional modulation of burst firing in neurons to achieve both protective (switching FXS firing to control) and injurious effects (control to FXS). It is worth nothing that the correction of burst activity by S100β though statistically significant, was not back to the exact same levels as the controls (Figure 6.1-6.2). This raises the possibility that other factors besides S100β may also contribute to this process. Our results provide a framework to investigate other potential molecules in the future. In conclusion, our study offers new dimension in understanding the FXS pathophysiology by focusing on neurons and astrocytes and their interactions. This may represent a new target for potential therapeutic strategies against this disorder.

7.1 AP firing is not impaired in hPSC derived cortical neurons in the absence of FMRP

In this study, we have attempted to comprehensively study the function of FMRP in maintaining proper neuronal activity. For this we have used human stem cell derived neurons and looked at the intrinsic, synaptic and network activity in the presence and absence of FMRP. The FXS pathophysiology in cortex has been extensively studied in mouse models and while these insights have been invaluable, recent studies have shown that the FXS pathophysiology in human cortical neurons can be very different. The cortical hyperexcitability phenotype was not found in ESC and iPSC derived human neurons .The human cortical neurons were either hypoexcitable or didn't exhibit any change in firing frequency in the absence of FMRP (Telias *et al.,* 2015; Zhang *et al.,* 2018). We have generated both human ESC and iPSC derived cortical neurons in this study. We found that generating neuron-only cultures led to the neurons developing diminished AP firing and synaptic activity. In a neuron-only culture, loss of FMRP did not alter the AP firing activity. The FXS neurons similar to control neurons were capable of firing sustained albeit immature action potentials in response to depolarizing current steps.

7.2 FXS neurons co-cultured with mouse astrocytes display aberrant network activity, due to decreased I_{NaP} and I_{BKCa}

Since we found that human cortical neurons in a neuron-only culture did not develop considerable synaptic activity, we generated co-cultures of human neurons with mouse astrocytes. We found that in this rodent co-culture, the human neurons fired mature APs and had robust synaptic activity. Similar to Zhang *et al.,* loss of FMRP did not lead to any change in the neuron's firing and synaptic activity. The human neurons in the rodent co-culture, also developed robust network activity, evidenced by spontaneous bursts of action potentials. This network activity was tightly regulated by FMRP. The FXS neurons displayed an aberrant network activity characterized by more frequent bursts that lasted for shorter durations. Studies in *Fmr1* KO mice have shown that in the entorhinal cortex the persistent sodium current (I_{NaP}) is enhanced (Deng & Klyachko, 2016). However we found that in hPSC derived cortical neurons, loss of FMRP led to diminished $I_{NaP..}$ This dysregulated I_{NaP} was responsible for the shorter burst durations of FXS neurons. The aberrant burst activity of the FXS neurons could be partially rectified by veratridine, a sodium channel opener. Another channel known to be affected in FXS is the BK channel (Deng *et al.,* 2013; Deng & Klyachko, 2016). Similar to *Fmr1* KO mice, hPSC derived FXS neurons also displayed diminished current through the BK channels. This diminished I_{BKCa} was responsible for the increase in the burst frequency of FXS neurons. Thus our study for the first time

shows the aberrant network firing in FXS neurons and the underlying channels which are dysregulated by the absence of FMRP.

7.3 hPSC derived astrocytes modulate the network activity of human cortical neurons

One of the key aspects of this study was to understand the glia-neuron crosstalk and how it influences neuronal function. Co-cultures of human neurons with human astrocytes were generated and we found that the astrocytes had a profound impact on the neuronal network activity. Control neurons co-cultured with control astrocytes displayed the characteristic control burst profile – low burst frequency, longer burst durations and FXS neurons co-cultured with FXS astrocytes displayed the aberrant burst profile – high burst frequency, shorter burst durations. However when control neurons were co-cultured with FXS astrocytes, the control neurons displayed the aberrant FXS burst firing. FXS neurons co-cultured with control astrocytes displayed the control bursting profile. Thus, presence of FMRP in the astrocytes was enough to correct the impaired bursting activity of FXS neurons. Consequently, absence of FMRP in the astrocytes led to impaired network activity in control neurons. We found that astrocytes influenced the network activity by modulation of the NaP channel. Control neurons when co-cultured with FXS astrocytes displayed diminished I_{NaP} whereas FXS neurons co-cultured with control astrocytes displayed robust $I_{NaP.}$ To determine whether the astrocytic modulation was contact dependent or independent we conducted a series of experiments wherein hPSC derived neurons were cultured in the presence of astrocyte conditioned media (ACM). We found that even in the absence of astrocytes, ACM was able to mediate similar effects on the neuronal network activity. We also demonstrated that like the astrocytes, the ACM regulated the NaP. This result suggests that the astrocytes release factor/s which in turn influence the neuronal persistent sodium channel and regulate bursting activity.

7.4 S100β released by the astrocytes modulate the neuronal bursting activity

Down's syndrome (DS) studies have demonstrated that hPSC derived DS astrocytes expressed high levels of the calcium chelating molecule, S100β (Chen *et al.,* 2014; Mizuno *et al.,* 2018). S100β has been known to regulate synaptic and rhythmic neuronal activity (Morquette *et al.,* 2015; Nishiyama *et al.,* 2002). We studied the effect of exogenous S100β on the network activity of the neurons in human neuron – astrocyte co-cultures. Low concentration of S100β (100 µM) was able to correct the aberrant bursting activity of the neurons co-cultured with FXS astrocytes. Further we also studied the effect of 100 µM S100β on the I_{NaP} and found that it enhances the I_{NaP} in cortical neurons co-cultured with FXS astrocytes. Thus despite the presence of FXS astrocytes in the culture, addition of exogenous S100β was able to

rescue the network deficits by increasing the current through the NaP channel. Intriguingly, high concentration of S100β (1 mM) exerted an opposite effect i.e. 1 mM S100β altered the bursting profile of neurons co-cultured with control astrocytes to resemble the FXS burst profile. Though S100β has been known to have neurotoxic effects at high concentration, the mechanism is relatively unknown.

Thus we conclude that in human cortical neurons, FMRP is crucial for proper network activity. Our study shows that the FMRP targets which have been found in rodent models are also potential targets in human neurons. The robust network activity demonstrated in this study can be exploited to study other neurodevelopmental and neurodegenerative diseases in the human stem cell model. One of the goals of this study was to understand the complexities of FXS pathophysiology and to do this we included human astrocytes. The crosstalk between neurons and glial cells has been long overlooked. Here, we show how astrocytes and its secretions are critical for the maintenance of proper neuronal network activity. Our study reveals a new role for astrocytes, and their interactions with neurons, in the pathogenesis of FXS, and may represent a new target for potential therapeutic strategies against this disorder.

Synopsis

Fragile X Syndrome (FXS) is an X-linked disorder and the most common form of inherited intellectual disability and autism. It is caused by an increased cytosine-guanine-guanine (CGG) triplet repeat mutation in the 5' UTR of the Fragile X mental retardation one (FMR1) gene, thereby silencing the gene and subsequent loss of its product. Clinical symptoms of FXS include, impaired cognition, anxiety, hyperactivity and repetitive behaviors (Pimentel, 1999; Bagni & Oostra, 2013).

The most well characterized animal model for studying FXS is the *Fmr1* knockout (*Fmr1* KO) mouse, which lacks the FMRP protein due to disruption in the *Fmr1* gene expression. Studies from the *Fmr1* KO mice have implied on how the loss of FMRP might be affecting several neuronal functions, including altered synaptic plasticity and cellular excitability in different brain regions (Huber *et al.,* 2002; Li *et al.,* 2002). In contrast, the amygdala from the same mouse model shows impairment in mGluR dependent long-term potentiation (LTP) (Suvrathan *et al.,* 2010). In a recent study by Zhang *et al.,* 2014, authors have shown increased neuronal and dendritic excitability, following tactile stimulus, in the somatosensory cortex of the *Fmr1* KO mice. Taken together, these data suggest that FMRP expression is necessary for proper neuronal development and normal synaptic physiology. Clinical investigations to develop FXS specific treatments based on the above preclinical findings have limited success (Berry-Kravis *et al.,* 2016; Mullard, 2016).

Thus, it is imperative to look into more human-based FXS *in vitro* models using neural progenitor cells and compare them with the existing mouse models of FXS.

The basic techniques to derive neurons from stem cells are now established (Benninger *et al.,* 2003; Wernig *et al.,* 2004). Increase in the refinement of culture protocols now make it possible to generate region specific neurons from embryonic or induced pluripotent stem cells (ESC/iPSC). The neurons thus generated are not only able to fire sustained action potentials, but they also establish normal synaptic connections (Moody & Bosma, 2005; Livesey *et al.,* 2014). The neurons derived from the human stem cells of patients suffering from FXS can therefore serve as an invaluable model to study the progression of the symptoms of FXS in vitro and subsequently help in developing new therapies. In my PhD study, I will be focusing on studying the functional properties of human stem cell derived FXS neurons and rescuing the defects, if any.

Aims and Objectives:

- Functional characterization of hPSC derived neurons in a pure neuronal culture
  - Intrinsic
  - Synaptic
- Functional characterization of hPSC derived FXS neurons in a rodent astrocyte co-culture.
  - Intrinsic
  - Synaptic
  - Network
- Effect of hPSC derived astrocytes on the electrophysiological "phenotype" of the hPSC derived neurons.

Results:

- Action potential properties of cortical neurons lacking FMRP are similar to controls in a neuron-only culture.
- Neurons lacking FMRP exhibit aberrant network activity when co-cultured with primary mouse astrocytes – high frequency bursts but shorter duration than control neurons.
- Neurons lacking FMRP display reduced persistent sodium channel current (I_{NaP}) and
- Neurons lacking FMRP display reduced persistent big conductance calcium-activated potassium (BKCa) current.
- Human astrocytes derived from pluripotent stem cells modulate the network activity of hPSC derived cortical neurons.
- Astrocyte conditioned media (ACM) derived from the human astrocytes can modulate the network activity of hPSC cortical neurons.
- A potential mechanism of how the ACM mediates these effects is through the molecule S100β, which potentiates the persistent sodium channel.

Conclusion:

- In this study, cortical neurons were derived from human pluripotent stem cells. To understand the FXS pathophysiology in humans, cortical neurons were derived from fibroblasts of FXS patients. An isogenic embryo stem cell line (*FMR1*$^{+/y}$, *FMR1*$^{-/y}$) wherein, FMR1 gene has been knocked out using CRISPR-Cas9 was also included.
- Culturing the neurons in a pure neuronal culture, the intrinsic and firing properties of the neurons are unaffected by the loss of FMRP
- The neurons in a purely neuronal culture failed to develop robust synaptic activity.
- Co-culturing the hPSC derived cortical neurons with primary mouse astrocytes led to the development of spontaneous neuronal network activity.
- Loss of FMRP led to aberrant network activity of neurons characterized by high frequency, short duration bursts.
- The persistent sodium current magnitude is reduced in neurons lacking FMRP. Potentiating the current with veratridine, “rescues” the aberrant network activity of FMRP-lacking neurons.
- Astrocytes modulate the neuronal network activity as shown by co-culturing the hPSC derived cortical neurons with hPSC derived astrocytes. The genotype of astrocytes determines the electrophysiological phenotype of neurons. This effect is mediated by the astrocyte conditioned media. The genotype of the ACM determines the type of bursting activity of the neurons.
- The ACM could be modulating the neuronal activity via the S100β molecule which is secreted by the astrocytes.

References

Ahlemeyer, B., Beier, H., Semkova, I., Schaper, C., & Krieglstein, J. (2000). S-100beta protects cultured neurons against glutamate- and staurosporine-induced damage and is involved in the antiapoptotic action of the 5 HT(1A)-receptor agonist, Bay x 3702. *Brain research*, *858*(1), 121–128. https://doi.org/10.1016/s0006-8993(99)02438-5

Al-Ayadhi, L. Y., & Mostafa, G. A. (2012). A lack of association between elevated serum levels of S100B protein and autoimmunity in autistic children. *Journal of neuroinflammation*, *9*, 54. https://doi.org/10.1186/1742-2094-9-54

Allen N. J. (2014). Astrocyte regulation of synaptic behavior. *Annual review of cell and developmental biology*, *30*, 439–463. https://doi.org/10.1146/annurev-cellbio-100913-013053

Anthony G. Boghdadi, Joshua Spurrier, Leon Teo, Mingfeng Li, Mario Skarica, Benjamin Cao, William Kwan, Tobias D. Merson, Susie K. Nilsson, Nenad Sestan, Stephen M. Strittmatter, James A. Bourne (2020). Primate-specific response of astrocytes to stroke limits peripheral macrophage infiltration. bioRxiv 2020.05.08.083501; doi: https://doi.org/10.1101/2020.05.08.083501

Araque, A., & Perea, G. (2004). Glial modulation of synaptic transmission in culture. *Glia*, *47*(3), 241–248. https://doi.org/10.1002/glia.20026

Araque, A., Carmignoto, G., Haydon, P. G., Oliet, S. H., Robitaille, R., & Volterra, A. (2014). Gliotransmitters travel in time and space. *Neuron*, *81*(4), 728–739. https://doi.org/10.1016/j.neuron.2014.02.007

Ascano, M., Jr, Mukherjee, N., Bandaru, P., Miller, J. B., Nusbaum, J. D., Corcoran, D. L., Langlois, C., Munschauer, M., Dewell, S., Hafner, M., Williams, Z., Ohler, U., & Tuschl, T. (2012). FMRP targets distinct mRNA sequence elements to regulate protein expression. *Nature*, *492*(7429), 382–386. https://doi.org/10.1038/nature11737

Ashley, C. T., Jr, Wilkinson, K. D., Reines, D., & Warren, S. T. (1993). FMR1 protein: conserved RNP family domains and selective RNA binding. *Science (New York, N.Y.)*, *262*(5133), 563–566. https://doi.org/10.1126/science.7692601

Astman, N., Gutnick, M. J., & Fleidervish, I. A. (2006). Persistent sodium current in layer 5 neocortical neurons is primarily generated in the proximal axon. *The Journal of neuroscience : the official journal of the Society for Neuroscience*, *26*(13), 3465–3473. https://doi.org/10.1523/JNEUROSCI.4907-05.2006

Avitzour, M., Mor-Shaked, H., Yanovsky-Dagan, S., Aharoni, S., Altarescu, G., Renbaum, P., Eldar-Geva, T., Schonberger, O., Levy-Lahad, E., Epsztejn-Litman, S., & Eiges, R. (2014). FMR1 epigenetic silencing commonly occurs in undifferentiated fragile X-affected embryonic stem cells. *Stem cell reports*, *3*(5), 699–706. https://doi.org/10.1016/j.stemcr.2014.09.001

Ayaydın, H., Kirmit, A., Çelik, H., Akaltun, İ., Koyuncu, İ., & Bilgen Ulgar, Ş. (2020). High Serum Levels of Serum 100 Beta Protein, Neuron-specific Enolase, Tau, Active Caspase-3, M30 and M65 in Children with Autism Spectrum Disorders. *Clinical psychopharmacology and neuroscience : the official scientific journal of the Korean College of Neuropsychopharmacology*, *18*(2), 270–278. https://doi.org/10.9758/cpn.2020.18.2.270

Azzarelli, R., Kerloch, T., & Pacary, E. (2015). Regulation of cerebral cortex development by Rho GTPases: insights from in vivo studies. *Frontiers in cellular neuroscience*, *8*, 445. https://doi.org/10.3389/fncel.2014.00445

Bagni, C., & Greenough, W. T. (2005). From mRNP trafficking to spine dysmorphogenesis: the roots of fragile X syndrome. *Nature reviews. Neuroscience*, *6*(5), 376–387. https://doi.org/10.1038/nrn1667

Bagni, C., Tassone, F., Neri, G., & Hagerman, R. (2012). Fragile X syndrome: causes, diagnosis, mechanisms, and therapeutics. *The Journal of clinical investigation*, *122*(12), 4314–4322. https://doi.org/10.1172/JCI63141

Baird, P. A., & Sadovnick, A. D. (1985). Mental retardation in over half-a-million consecutive livebirths: an epidemiological study. *American journal of mental deficiency*, *89*(4), 323–330.

Bakker, C. E., de Diego Otero, Y., Bontekoe, C., Raghoe, P., Luteijn, T., Hoogeveen, A. T., Oostra, B. A., & Willemsen, R. (2000). Immunocytochemical and biochemical characterization of FMRP, FXR1P, and FXR2P in the mouse. *Experimental cell research*, *258*(1), 162–170. https://doi.org/10.1006/excr.2000.4932

Bakker, C. E., Verheij, C., Willemsen, R., Van der Helm, R., Bygrave, A., Hoogeveen, A. T., … Willems, P. J. (1994). Fmr1 Knockout Mice : A Model to Study Fragile X Mental Retardation. *Cell*, *78*, 23–33.

Barbeito L. (2018). Astrocyte-based cell therapy: new hope for amyotrophic lateral sclerosis patients?. *Stem cell research & therapy*, *9*(1), 241. https://doi.org/10.1186/s13287-018-1006-y

Barger, S. W., & Van Eldik, L. J. (1992). S100 beta stimulates calcium fluxes in glial and neuronal cells. *The Journal of biological chemistry*, *267*(14), 9689–9694.

Barres B. A. (2008). The mystery and magic of glia: a perspective on their roles in health and disease. *Neuron*, *60*(3), 430–440. https://doi.org/10.1016/j.neuron.2008.10.013

Barres, B. A., Chun, L. L., & Corey, D. P. (1988). Ion channel expression by white matter glia: I. Type 2 astrocytes and oligodendrocytes. *Glia*, *1*(1), 10–30. https://doi.org/10.1002/glia.440010104

Barres, B. A., Chun, L. L., & Corey, D. P. (1989). Glial and neuronal forms of the voltage-dependent sodium channel: characteristics and cell-type distribution. *Neuron*, *2*(4), 1375–1388. https://doi.org/10.1016/0896-6273(89)90076-7

Barres, B. A., Koroshetz, W. J., Chun, L. L., & Corey, D. P. (1990). Ion channel expression by white matter glia: the type-1 astrocyte. *Neuron*, *5*(4), 527–544. https://doi.org/10.1016/0896-6273(90)90091-s

Bear, M. F., Huber, K. M., & Warren, S. T. (2004). The mGluR theory of fragile X mental retardation. *Trends in neurosciences*, *27*(7), 370–377. https://doi.org/10.1016/j.tins.2004.04.009

Bell, M. V., Hirst, M. C., Nakahori, Y., MacKinnon, R. N., Roche, A., Flint, T. J., Jacobs, P. A., Tommerup, N., Tranebjaerg, L., & Froster-Iskenius, U. (1991). Physical mapping across the fragile X: hypermethylation and clinical expression of the fragile X syndrome. *Cell*, *64*(4), 861–866. https://doi.org/10.1016/0092-8674(91)90514-y

Ben-Ari Y. (2001). Developing networks play a similar melody. *Trends in neurosciences*, *24*(6), 353–360. https://doi.org/10.1016/s0166-2236(00)01813-0

Benninger, F., Beck, H., Wernig, M., Tucker, K. L., Brüstle, O., & Scheffler, B. (2003). Functional integration of embryonic stem cell-derived neurons in hippocampal slice cultures. *The Journal of neuroscience : the official journal of the Society for Neuroscience*, *23*(18), 7075–7083. https://doi.org/10.1523/JNEUROSCI.23-18-07075.2003

Berry-Kravis, E., Des Portes, V., Hagerman, R., Jacquemont, S., Charles, P., Visootsak, J., Brinkman, M., Rerat, K., Koumaras, B., Zhu, L., Barth, G. M., Jaecklin, T., Apostol, G., & von Raison, F. (2016). Mavoglurant in fragile X syndrome: Results of two randomized, double-blind, placebo-controlled trials. *Science translational medicine*, *8*(321), 321ra5. https://doi.org/10.1126/scitranslmed.aab4109

Berry-Kravis, E., Hessl, D., Coffey, S., Hervey, C., Schneider, A., Yuhas, J., Hutchison, J., Snape, M., Tranfaglia, M., Nguyen, D. V., & Hagerman, R. (2009). A pilot open label, single dose trial of fenobam in adults with fragile X syndrome. *Journal of medical genetics*, *46*(4), 266–271. https://doi.org/10.1136/jmg.2008.063701

Berzhanskaya, J., Phillips, M. A., Shen, J., & Colonnese, M. T. (2016). Sensory hypo-excitability in a rat model of fetal development in Fragile X Syndrome. *Scientific reports*, *6*, 30769. https://doi.org/10.1038/srep30769

Bevan, S., Chiu, S. Y., Gray, P. T., & Ritchie, J. M. (1985). The presence of voltage-gated sodium, potassium and chloride channels in rat cultured astrocytes. *Proceedings of the Royal Society of London. Series B, Biological sciences*, *225*(1240), 299–313. https://doi.org/10.1098/rspb.1985.0063

Bhattacharyya, A., & Zhao, X. (2016). Human pluripotent stem cell models of Fragile X syndrome. *Molecular and cellular neurosciences*, *73*, 43–51. https://doi.org/10.1016/j.mcn.2015.11.011

Bhattacharyya, A., McMillan, E., Wallace, K., Tubon, T. C., Jr, Capowski, E. E., & Svendsen, C. N. (2008). Normal Neurogenesis but Abnormal Gene Expression in Human Fragile X Cortical Progenitor Cells. *Stem cells and development*, *17*(1), 107–117. https://doi.org/10.1089/scd.2007.0073

Bilican, B., Livesey, M. R., Haghi, G., Qiu, J., Burr, K., Siller, R., Hardingham, G. E., Wyllie, D. J., & Chandran, S. (2014). Physiological normoxia and absence of EGF is required for the long-term propagation of anterior neural precursors from human pluripotent cells. *PloS one*, *9*(1), e85932. https://doi.org/10.1371/journal.pone.0085932

Booker, S. A., Domanski, A., Dando, O. R., Jackson, A. D., Isaac, J., Hardingham, G. E., Wyllie, D., & Kind, P. C. (2019). Altered dendritic spine function and integration in a mouse model of fragile X syndrome. *Nature communications*, *10*(1), 4813. https://doi.org/10.1038/s41467-019-11891-6

Bosma, G. C., Custer, R. P., & Bosma, M. J. (1983). A severe combined immunodeficiency mutation in the mouse. *Nature*, *301*(5900), 527–530. https://doi.org/10.1038/301527a0

Bouhon, I. A., Joannides, A., Kato, H., Chandran, S., & Allen, N. D. (2006). Embryonic stem cell-derived neural progenitors display temporal restriction to neural patterning. *Stem cells (Dayton, Ohio)*, *24*(8), 1908–1913. https://doi.org/10.1634/stemcells.2006-0031

Braat, S., D'Hulst, C., Heulens, I., De Rubeis, S., Mientjes, E., Nelson, D. L., Willemsen, R., Bagni, C., Van Dam, D., De Deyn, P. P., & Kooy, R. F. (2015). The GABAA receptor is an FMRP target with therapeutic

potential in fragile X syndrome. *Cell cycle (Georgetown, Tex.)*, *14*(18), 2985–2995. https://doi.org/10.4161/15384101.2014.989114

Braga, C. W., Martinez, D., Wofchuk, S., Portela, L. V., & Souza, D. O. (2006). S100B and NSE serum levels in obstructive sleep apnea syndrome. *Sleep medicine*, *7*(5), 431–435. https://doi.org/10.1016/j.sleep.2005.12.012

Brager, D. H., Akhavan, A. R., & Johnston, D. (2012). Impaired dendritic expression and plasticity of h-channels in the fmr1(-/y) mouse model of fragile X syndrome. *Cell reports*, *1*(3), 225–233. https://doi.org/10.1016/j.celrep.2012.02.002

Brouwer, J. R., Mientjes, E. J., Bakker, C. E., Nieuwenhuizen, I. M., Severijnen, L. A., Van der Linde, H. C., Nelson, D. L., Oostra, B. A., & Willemsen, R. (2007). Elevated Fmr1 mRNA levels and reduced protein expression in a mouse model with an unmethylated Fragile X full mutation. *Experimental cell research*, *313*(2), 244–253. https://doi.org/10.1016/j.yexcr.2006.10.002

Brown, M. R., Kronengold, J., Gazula, V. R., Chen, Y., Strumbos, J. G., Sigworth, F. J., Navaratnam, D., & Kaczmarek, L. K. (2010). Fragile X mental retardation protein controls gating of the sodium-activated potassium channel Slack. *Nature neuroscience*, *13*(7), 819–821. https://doi.org/10.1038/nn.2563

Brozzi, F., Arcuri, C., Giambanco, I., & Donato, R. (2009). S100B Protein Regulates Astrocyte Shape and Migration via Interaction with Src Kinase: IMPLICATIONS FOR ASTROCYTE DEVELOPMENT, ACTIVATION, AND TUMOR GROWTH. *The Journal of biological chemistry*, *284*(13), 8797–8811. https://doi.org/10.1074/jbc.M805897200

Brumberg, J. C., Nowak, L. G., & McCormick, D. A. (2000). Ionic mechanisms underlying repetitive high-frequency burst firing in supragranular cortical neurons. *The Journal of neuroscience : the official journal of the Society for Neuroscience*, *20*(13), 4829–4843. https://doi.org/10.1523/JNEUROSCI.20-13-04829.2000

Bülow, P., Murphy, T. J., Bassell, G. J., & Wenner, P. (2019). Homeostatic Intrinsic Plasticity Is Functionally Altered in Fmr1 KO Cortical Neurons. *Cell reports*, *26*(6), 1378–1388.e3. https://doi.org/10.1016/j.celrep.2019.01.035

Bureau, I., Shepherd, G. M., & Svoboda, K. (2008). Circuit and plasticity defects in the developing somatosensory cortex of FMR1 knock-out mice. *The Journal of neuroscience : the official journal of the Society for Neuroscience*, *28*(20), 5178–5188. https://doi.org/10.1523/JNEUROSCI.1076-08.2008

Bushong, E. A., Martone, M. E., Jones, Y. Z., & Ellisman, M. H. (2002). Protoplasmic astrocytes in CA1 stratum radiatum occupy separate anatomical domains. *The Journal of neuroscience : the official journal of the Society for Neuroscience*, *22*(1), 183–192. https://doi.org/10.1523/JNEUROSCI.22-01-00183.2002

Butt, A., & Verkhratsky, A. (2018). Neuroglia: Realising their true potential. *Brain and neuroscience advances*, *2*, 2398212818817495. https://doi.org/10.1177/2398212818817495

Cahoy, J. D., Emery, B., Kaushal, A., Foo, L. C., Zamanian, J. L., Christopherson, K. S., Xing, Y., Lubischer, J. L., Krieg, P. A., Krupenko, S. A., Thompson, W. J., & Barres, B. A. (2008). A transcriptome database for astrocytes, neurons, and oligodendrocytes: a new resource for understanding brain development and

function. *The Journal of neuroscience : the official journal of the Society for Neuroscience*, *28*(1), 264–278. https://doi.org/10.1523/JNEUROSCI.4178-07.2008

Castrén, M., Tervonen, T., Kärkkäinen, V., Heinonen, S., Castrén, E., Larsson, K., Bakker, C. E., Oostra, B. A., & Akerman, K. (2005). Altered differentiation of neural stem cells in fragile X syndrome. *Proceedings of the National Academy of Sciences of the United States of America*, *102*(49), 17834–17839. https://doi.org/10.1073/pnas.0508995102

Cepeda, C., André, V. M., Wu, N., Yamazaki, I., Uzgil, B., Vinters, H. V., Levine, M. S., & Mathern, G. W. (2007). Immature neurons and GABA networks may contribute to epileptogenesis in pediatric cortical dysplasia. *Epilepsia*, *48 Suppl 5*, 79–85. https://doi.org/10.1111/j.1528-1167.2007.01293.x

Chambers, S. M., Fasano, C. A., Papapetrou, E. P., Tomishima, M., Sadelain, M., & Studer, L. (2009). Highly efficient neural conversion of human ES and iPS cells by dual inhibition of SMAD signaling. *Nature biotechnology*, *27*(3), 275–280. https://doi.org/10.1038/nbt.1529

Charles, A. C., Merrill, J. E., Dirksen, E. R., & Sanderson, M. J. (1991). Intercellular signaling in glial cells: calcium waves and oscillations in response to mechanical stimulation and glutamate. *Neuron*, *6*(6), 983–992. https://doi.org/10.1016/0896-6273(91)90238-u

Chen, C., Jiang, P., Xue, H., Peterson, S. E., Tran, H. T., McCann, A. E., Parast, M. M., Li, S., Pleasure, D. E., Laurent, L. C., Loring, J. F., Liu, Y., & Deng, W. (2014). Role of astroglia in Down's syndrome revealed by patient-derived human-induced pluripotent stem cells. *Nature communications*, *5*, 4430. https://doi.org/10.1038/ncomms5430

Cheng, C., Lau, S. K., & Doering, L. C. (2016). Astrocyte-secreted thrombospondin-1 modulates synapse and spine defects in the fragile X mouse model. *Molecular brain*, *9*(1), 74. https://doi.org/10.1186/s13041-016-0256-9

Cheng, C., Sourial, M., & Doering, L. C. (2012). Astrocytes and developmental plasticity in fragile X. *Neural plasticity*, *2012*, 197491. https://doi.org/10.1155/2012/197491

Choi, S. S., Lee, H. J., Lim, I., Satoh, J., & Kim, S. U. (2014). Human astrocytes: secretome profiles of cytokines and chemokines. *PloS one*, *9*(4), e92325. https://doi.org/10.1371/journal.pone.0092325

Christopherson, K. S., Ullian, E. M., Stokes, C. C., Mullowney, C. E., Hell, J. W., Agah, A., Lawler, J., Mosher, D. F., Bornstein, P., & Barres, B. A. (2005). Thrombospondins are astrocyte-secreted proteins that promote CNS synaptogenesis. *Cell*, *120*(3), 421–433. https://doi.org/10.1016/j.cell.2004.12.020

Chung, R. S., Hidalgo, J., & West, A. K. (2008). New insight into the molecular pathways of metallothionein-mediated neuroprotection and regeneration. *Journal of neurochemistry*, *104*(1), 14–20. https://doi.org/10.1111/j.1471-4159.2007.05026.x

Chung, R. S., Penkowa, M., Dittmann, J., King, C. E., Bartlett, C., Asmussen, J. W., Hidalgo, J., Carrasco, J., Leung, Y. K., Walker, A. K., Fung, S. J., Dunlop, S. A., Fitzgerald, M., Beazley, L. D., Chuah, M. I., Vickers, J. C., & West, A. K. (2008). Redefining the role of metallothionein within the injured brain: extracellular metallothioneins play an important role in the astrocyte-neuron response to injury. *The Journal of biological chemistry*, *283*(22), 15349–15358. https://doi.org/10.1074/jbc.M708446200

Churchill, J. D., Grossman, A. W., Irwin, S. A., Galvez, R., Klintsova, A. Y., Weiler, I. J., & Greenough, W. T. (2002). A converging-methods approach to fragile X syndrome. *Developmental psychobiology*, *40*(3), 323–338. https://doi.org/10.1002/dev.10036

Ciaccio, C., Fontana, L., Milani, D., Tabano, S., Miozzo, M., & Esposito, S. (2017). Fragile X syndrome: a review of clinical and molecular diagnoses. *Italian journal of pediatrics*, *43*(1), 39. https://doi.org/10.1186/s13052-017-0355-y

Contractor, A., Klyachko, V. A., & Portera-Cailliau, C. (2015). Altered Neuronal and Circuit Excitability in Fragile X Syndrome. *Neuron*, *87*(4), 699–715. https://doi.org/10.1016/j.neuron.2015.06.017

Corbin, F., Bouillon, M., Fortin, A., Morin, S., Rousseau, F., & Khandjian, E. W. (1997). The fragile X mental retardation protein is associated with poly(A)+ mRNA in actively translating polyribosomes. *Human molecular genetics*, *6*(9), 1465–1472. https://doi.org/10.1093/hmg/6.9.1465

Cornell-Bell, A. H., Finkbeiner, S. M., Cooper, M. S., & Smith, S. J. (1990). Glutamate induces calcium waves in cultured astrocytes: long-range glial signaling. *Science (New York, N.Y.)*, *247*(4941), 470–473. https://doi.org/10.1126/science.1967852

Crawford, D. C., Acuña, J. M., & Sherman, S. L. (2001). FMR1 and the fragile X syndrome: human genome epidemiology review. *Genetics in medicine : official journal of the American College of Medical Genetics*, *3*(5), 359–371. https://doi.org/10.1097/00125817-200109000-00006

Darnell, J. C., Van Driesche, S. J., Zhang, C., Hung, K. Y., Mele, A., Fraser, C. E., Stone, E. F., Chen, C., Fak, J. J., Chi, S. W., Licatalosi, D. D., Richter, J. D., & Darnell, R. B. (2011). FMRP stalls ribosomal translocation on mRNAs linked to synaptic function and autism. *Cell*, *146*(2), 247–261. https://doi.org/10.1016/j.cell.2011.06.013

Das Sharma, S., Pal, R., Reddy, B. K., Selvaraj, B. T., Raj, N., Samaga, K. K., Srinivasan, D. J., Ornelas, L., Sareen, D., Livesey, M. R., Bassell, G. J., Svendsen, C. N., Kind, P. C., Chandran, S., Chattarji, S., & Wyllie, D. (2020). Cortical neurons derived from human pluripotent stem cells lacking FMRP display altered spontaneous firing patterns. *Molecular autism*, *11*(1), 52. https://doi.org/10.1186/s13229-020-00351-4

De Boulle, K., Verkerk, A. J., Reyniers, E., Vits, L., Hendrickx, J., Van Roy, B., Van den Bos, F., de Graaff, E., Oostra, B. A., & Willems, P. J. (1993). A point mutation in the FMR-1 gene associated with fragile X mental retardation. *Nature genetics*, *3*(1), 31–35. https://doi.org/10.1038/ng0193-31

Deemyad, T., Lüthi, J., & Spruston, N. (2018). Astrocytes integrate and drive action potential firing in inhibitory subnetworks. *Nature communications*, *9*(1), 4336. https://doi.org/10.1038/s41467-018-06338-3

Defelipe J. (2011). The evolution of the brain, the human nature of cortical circuits, and intellectual creativity. *Frontiers in neuroanatomy*, *5*, 29. https://doi.org/10.3389/fnana.2011.00029

Delcourt, N., Jouin, P., Poncet, J., Demey, E., Mauger, E., Bockaert, J., Marin, P., & Galéotti, N. (2005). Difference in mass analysis using labeled lysines (DIMAL-K): a new, efficient proteomic quantification method applied to the analysis of astrocytic secretomes. *Molecular & cellular proteomics : MCP*, *4*(8), 1085–1094. https://doi.org/10.1074/mcp.M500040-MCP200

Deng, P. Y., & Klyachko, V. A. (2016). Genetic upregulation of BK channel activity normalizes multiple synaptic and circuit defects in a mouse model of fragile X syndrome. *The Journal of physiology*, *594*(1), 83–97. https://doi.org/10.1113/JP271031

Deng, P. Y., & Klyachko, V. A. (2016). Increased Persistent Sodium Current Causes Neuronal Hyperexcitability in the Entorhinal Cortex of Fmr1 Knockout Mice. *Cell reports*, *16*(12), 3157–3166. https://doi.org/10.1016/j.celrep.2016.08.046

Deng, P. Y., Carlin, D., Oh, Y. M., Myrick, L. K., Warren, S. T., Cavalli, V., & Klyachko, V. A. (2019). Voltage-Independent SK-Channel Dysfunction Causes Neuronal Hyperexcitability in the Hippocampus of *Fmr1* Knock-Out Mice. *The Journal of neuroscience : the official journal of the Society for Neuroscience*, *39*(1), 28–43. https://doi.org/10.1523/JNEUROSCI.1593-18.2018

Deng, P. Y., Rotman, Z., Blundon, J. A., Cho, Y., Cui, J., Cavalli, V., Zakharenko, S. S., & Klyachko, V. A. (2013). FMRP regulates neurotransmitter release and synaptic information transmission by modulating action potential duration via BK channels. *Neuron*, *77*(4), 696–711. https://doi.org/10.1016/j.neuron.2012.12.018

Devys, D., Lutz, Y., Rouyer, N., Bellocq, J. P., & Mandel, J. L. (1993). The FMR-1 protein is cytoplasmic, most abundant in neurons and appears normal in carriers of a fragile X premutation. *Nature genetics*, *4*(4), 335–340. https://doi.org/10.1038/ng0893-335

Dhandapani, K. M., & Brann, D. W. (2003). Transforming growth factor-beta: a neuroprotective factor in cerebral ischemia. *Cell biochemistry and biophysics*, *39*(1), 13–22. https://doi.org/10.1385/CBB:39:1:13

D'Hulst, C., De Geest, N., Reeve, S. P., Van Dam, D., De Deyn, P. P., Hassan, B. A., & Kooy, R. F. (2006). Decreased expression of the GABAA receptor in fragile X syndrome. *Brain research*, *1121*(1), 238–245. https://doi.org/10.1016/j.brainres.2006.08.115

D'Hulst, C., Heulens, I., Van der Aa, N., Goffin, K., Koole, M., Porke, K., Van De Velde, M., Rooms, L., Van Paesschen, W., Van Esch, H., Van Laere, K., & Kooy, R. F. (2015). Positron Emission Tomography (PET) Quantification of GABAA Receptors in the Brain of Fragile X Patients. *PloS one*, *10*(7), e0131486. https://doi.org/10.1371/journal.pone.0131486

Doers, M. E., Musser, M. T., Nichol, R., Berndt, E. R., Baker, M., Gomez, T. M., Zhang, S. C., Abbeduto, L., & Bhattacharyya, A. (2014). iPSC-derived forebrain neurons from FXS individuals show defects in initial neurite outgrowth. *Stem cells and development*, *23*(15), 1777–1787. https://doi.org/10.1089/scd.2014.0030

Domanski, A., Booker, S. A., Wyllie, D., Isaac, J., & Kind, P. C. (2019). Cellular and synaptic phenotypes lead to disrupted information processing in Fmr1-KO mouse layer 4 barrel cortex. *Nature communications*, *10*(1), 4814. https://doi.org/10.1038/s41467-019-12736-y

Donato R. (2001). S100: a multigenic family of calcium-modulated proteins of the EF-hand type with intracellular and extracellular functional roles. *The international journal of biochemistry & cell biology*, *33*(7), 637–668. https://doi.org/10.1016/s1357-2725(01)00046-2

Donato, R., Cannon, B. R., Sorci, G., Riuzzi, F., Hsu, K., Weber, D. J., & Geczy, C. L. (2013). Functions of S100 proteins. *Current molecular medicine*, *13*(1), 24–57.

Donato, R., Sorci, G., Riuzzi, F., Arcuri, C., Bianchi, R., Brozzi, F., Tubaro, C., & Giambanco, I. (2009). S100B's double life: intracellular regulator and extracellular signal. *Biochimica et biophysica acta*, *1793*(6), 1008–1022. https://doi.org/10.1016/j.bbamcr.2008.11.009

D'Souza, M. N., Gowda, N., Tiwari, V., Babu, R. O., Anand, P., Dastidar, S. G., Singh, R., James, O. G., Selvaraj, B., Pal, R., Ramesh, A., Chattarji, S., Chandran, S., Gulyani, A., Palakodeti, D., & Muddashetty, R. S. (2018). FMRP Interacts with C/D Box snoRNA in the Nucleus and Regulates Ribosomal RNA Methylation. *iScience*, *9*, 399–411. https://doi.org/10.1016/j.isci.2018.11.007

Eiges, R., Urbach, A., Malcov, M., Frumkin, T., Schwartz, T., Amit, A., Yaron, Y., Eden, A., Yanuka, O., Benvenisty, N., & Ben-Yosef, D. (2007). Developmental study of fragile X syndrome using human embryonic stem cells derived from preimplantation genetically diagnosed embryos. *Cell stem cell*, *1*(5), 568–577. https://doi.org/10.1016/j.stem.2007.09.001

Elkabetz, Y., Panagiotakos, G., Al Shamy, G., Socci, N. D., Tabar, V., & Studer, L. (2008). Human ES cell-derived neural rosettes reveal a functionally distinct early neural stem cell stage. *Genes & development*, *22*(2), 152–165. https://doi.org/10.1101/gad.1616208

Ennas, M. G., Cocchia, D., Silvetti, E., Sogos, V., Riva, A., Torelli, S., & Gremo, F. (1992). Immunocompetent cell markers in human fetal astrocytes and neurons in culture. *Journal of neuroscience research*, *32*(3), 424–436. https://doi.org/10.1002/jnr.490320314

Evans, M. J., & Kaufman, M. H. (1981). Establishment in culture of pluripotential cells from mouse embryos. *Nature*, *292*(5819), 154–156. https://doi.org/10.1038/292154a0

Fekete, A., Franklin, L., Ikemoto, T., Rózsa, B., Lendvai, B., Sylvester Vizi, E., & Zelles, T. (2009). Mechanism of the persistent sodium current activator veratridine-evoked Ca elevation: implication for epilepsy. *Journal of neurochemistry*, *111*(3), 745–756. https://doi.org/10.1111/j.1471-4159.2009.06368.x

Fellin T. (2009). Communication between neurons and astrocytes: relevance to the modulation of synaptic and network activity. *Journal of neurochemistry*, *108*(3), 533–544. https://doi.org/10.1111/j.1471-4159.2008.05830.x

Ferron L. (2016). Fragile X mental retardation protein controls ion channel expression and activity. *The Journal of physiology*, *594*(20), 5861–5867. https://doi.org/10.1113/JP270675

Franceschetti, S., Guatteo, E., Panzica, F., Sancini, G., Wanke, E., & Avanzini, G. (1995). Ionic mechanisms underlying burst firing in pyramidal neurons: intracellular study in rat sensorimotor cortex. *Brain research*, *696*(1-2), 127–139. https://doi.org/10.1016/0006-8993(95)00807-3

Freund, L. S., & Reiss, A. L. (1991). Cognitive profiles associated with the fra(X) syndrome in males and females. *American journal of medical genetics*, *38*(4), 542–547. https://doi.org/10.1002/ajmg.1320380409

Gan, L., & Kaczmarek, L. K. (1998). When, where, and how much? Expression of the Kv3.1 potassium channel in high-frequency firing neurons. *Journal of neurobiology*, *37*(1), 69–79. https://doi.org/10.1002/(sici)1097-4695(199810)37:1<69::aid-neu6>3.0.co;2-6

Gazzolo, D., Li Volti, G., Gavilanes, A. W., & Scapagnini, G. (2015). Biomarkers of Brain Function and Injury: Biological and Clinical Significance. *BioMed research international*, *2015*, 389023. https://doi.org/10.1155/2015/389023

Gerlach, R., Demel, G., König, H. G., Gross, U., Prehn, J. H., Raabe, A., Seifert, V., & Kögel, D. (2006). Active secretion of S100B from astrocytes during metabolic stress. *Neuroscience*, *141*(4), 1697–1701. https://doi.org/10.1016/j.neuroscience.2006.05.008

Gholizadeh, S., Halder, S. K., & Hampson, D. R. (2015). Expression of fragile X mental retardation protein in neurons and glia of the developing and adult mouse brain. *Brain research*, *1596*, 22–30. https://doi.org/10.1016/j.brainres.2014.11.023

Gholizadeh, S., Halder, S. K., & Hampson, D. R. (2015). Expression of fragile X mental retardation protein in neurons and glia of the developing and adult mouse brain. *Brain research*, *1596*, 22–30. https://doi.org/10.1016/j.brainres.2014.11.023

Gibson, J. R., Bartley, A. F., Hays, S. A., & Huber, K. M. (2008). Imbalance of neocortical excitation and inhibition and altered UP states reflect network hyperexcitability in the mouse model of fragile X syndrome. *Journal of neurophysiology*, *100*(5), 2615–2626. https://doi.org/10.1152/jn.90752.2008

Gocel, J., & Larson, J. (2012). Synaptic NMDA receptor-mediated currents in anterior piriform cortex are reduced in the adult fragile X mouse. *Neuroscience*, *221*, 170–181. https://doi.org/10.1016/j.neuroscience.2012.06.052

Gonçalves, J. T., Anstey, J. E., Golshani, P., & Portera-Cailliau, C. (2013). Circuit level defects in the developing neocortex of Fragile X mice. *Nature neuroscience*, *16*(7), 903–909. https://doi.org/10.1038/nn.3415

Gonçalves, J. T., Anstey, J. E., Golshani, P., & Portera-Cailliau, C. (2013). Circuit level defects in the developing neocortex of Fragile X mice. *Nature neuroscience*, *16*(7), 903–909. https://doi.org/10.1038/nn.3415

Gonzalez, L. L., Garrie, K., & Turner, M. D. (2020). Role of S100 proteins in health and disease. *Biochimica et biophysica acta. Molecular cell research*, *1867*(6), 118677. https://doi.org/10.1016/j.bbamcr.2020.118677

Graef, J. D., Wu, H., Ng, C., Sun, C., Villegas, V., Qadir, D., Jesseman, K., Warren, S. T., Jaenisch, R., Cacace, A., & Wallace, O. (2020). Partial FMRP expression is sufficient to normalize neuronal hyperactivity in Fragile X neurons. *The European journal of neuroscience*, *51*(10), 2143–2157. https://doi.org/10.1111/ejn.14660

Greco, C. M., Hagerman, R. J., Tassone, F., Chudley, A. E., Del Bigio, M. R., Jacquemont, S., Leehey, M., & Hagerman, P. J. (2002). Neuronal intranuclear inclusions in a new cerebellar tremor/ataxia syndrome among fragile X carriers. *Brain: a journal of neurology*, *125*(Pt 8), 1760–1771. https://doi.org/10.1093/brain/awf184

Gross, C., Raj, N., Molinaro, G., Allen, A. G., Whyte, A. J., Gibson, J. R., Huber, K. M., Gourley, S. L., & Bassell, G. J. (2015). Selective role of the catalytic PI3K subunit p110β in impaired higher order cognition in fragile X syndrome. *Cell reports*, *11*(5), 681–688. https://doi.org/10.1016/j.celrep.2015.03.065

Gross, C., Yao, X., Pong, D. L., Jeromin, A., & Bassell, G. J. (2011). Fragile X mental retardation protein regulates protein expression and mRNA translation of the potassium channel Kv4.2. *The Journal of neuroscience : the official journal of the Society for Neuroscience*, *31*(15), 5693–5698. https://doi.org/10.1523/JNEUROSCI.6661-10.2011

Grossman, A. W., Elisseou, N. M., McKinney, B. C., & Greenough, W. T. (2006). Hippocampal pyramidal cells in adult Fmr1 knockout mice exhibit an immature-appearing profile of dendritic spines. *Brain research*, *1084*(1), 158–164. https://doi.org/10.1016/j.brainres.2006.02.044

Guloksuz, S. A., Abali, O., Aktas Cetin, E., Bilgic Gazioglu, S., Deniz, G., Yildirim, A., Kawikova, I., Guloksuz, S., & Leckman, J. F. (2017). Elevated plasma concentrations of S100 calcium-binding protein B and tumor necrosis factor alpha in children with autism spectrum disorders. *Revista brasileira de psiquiatria (Sao Paulo, Brazil : 1999)*, *39*(3), 195–200. https://doi.org/10.1590/1516-4446-2015-1843

Gurdon J. B. (1962). The developmental capacity of nuclei taken from intestinal epithelium cells of feeding tadpoles. *Journal of embryology and experimental morphology*, *10*, 622–640.

Hagerman P. J. (2008). The fragile X prevalence paradox. *Journal of medical genetics*, *45*(8), 498–499. https://doi.org/10.1136/jmg.2008.059055

Hagerman, R. J., Jackson, A. W., 3rd, Levitas, A., Rimland, B., & Braden, M. (1986). An analysis of autism in fifty males with the fragile X syndrome. *American journal of medical genetics*, *23*(1-2), 359–374. https://doi.org/10.1002/ajmg.1320230128

Halevy, T., Czech, C., & Benvenisty, N. (2015). Molecular mechanisms regulating the defects in fragile X syndrome neurons derived from human pluripotent stem cells. *Stem cell reports*, *4*(1), 37–46. https://doi.org/10.1016/j.stemcr.2014.10.015

Hama, H., Hara, C., Yamaguchi, K., & Miyawaki, A. (2004). PKC signaling mediates global enhancement of excitatory synaptogenesis in neurons triggered by local contact with astrocytes. *Neuron*, *41*(3), 405–415. https://doi.org/10.1016/s0896-6273(04)00007-8

Hamilton, S. M., Green, J. R., Veeraragavan, S., Yuva, L., McCoy, A., Wu, Y., Warren, J., Little, L., Ji, D., Cui, X., Weinstein, E., & Paylor, R. (2014). Fmr1 and Nlgn3 knockout rats: novel tools for investigating autism spectrum disorders. *Behavioral neuroscience*, *128*(2), 103–109. https://doi.org/10.1037/a0035988

Han, X., Chen, M., Wang, F., Windrem, M., Wang, S., Shanz, S., Xu, Q., Oberheim, N. A., Bekar, L., Betstadt, S., Silva, A. J., Takano, T., Goldman, S. A., & Nedergaard, M. (2013). Forebrain engraftment by human glial progenitor cells enhances synaptic plasticity and learning in adult mice. *Cell stem cell*, *12*(3), 342–353. https://doi.org/10.1016/j.stem.2012.12.015

Harlow, E. G., Till, S. M., Russell, T. A., Wijetunge, L. S., Kind, P., & Contractor, A. (2010). Critical period plasticity is disrupted in the barrel cortex of FMR1 knockout mice. *Neuron*, *65*(3), 385–398. https://doi.org/10.1016/j.neuron.2010.01.024

Harrison, C. J., Jack, E. M., Allen, T. D., & Harris, R. (1983). The fragile X: a scanning electron microscope study. *Journal of medical genetics*, *20*(4), 280–285. https://doi.org/10.1136/jmg.20.4.280

Hays, S. A., Huber, K. M., & Gibson, J. R. (2011). Altered neocortical rhythmic activity states in Fmr1 KO mice are due to enhanced mGluR5 signaling and involve changes in excitatory circuitry. *The Journal of*

neuroscience : the official journal of the Society for Neuroscience, *31*(40), 14223–14234. https://doi.org/10.1523/JNEUROSCI.3157-11.2011

Heikkilä, T. J., Ylä-Outinen, L., Tanskanen, J. M., Lappalainen, R. S., Skottman, H., Suuronen, R., Mikkonen, J. E., Hyttinen, J. A., & Narkilahti, S. (2009). Human embryonic stem cell-derived neuronal cells form spontaneously active neuronal networks in vitro. *Experimental neurology*, *218*(1), 109–116. https://doi.org/10.1016/j.expneurol.2009.04.011

Heulens, I., D'Hulst, C., Van Dam, D., De Deyn, P. P., & Kooy, R. F. (2012). Pharmacological treatment of fragile X syndrome with GABAergic drugs in a knockout mouse model. *Behavioural brain research*, *229*(1), 244–249. https://doi.org/10.1016/j.bbr.2012.01.031

Higashimori, H., Schin, C. S., Chiang, M. S., Morel, L., Shoneye, T. A., Nelson, D. L., & Yang, Y. (2016). Selective Deletion of Astroglial FMRP Dysregulates Glutamate Transporter GLT1 and Contributes to Fragile X Syndrome Phenotypes In Vivo. *The Journal of neuroscience : the official journal of the Society for Neuroscience*, *36*(27), 7079–7094. https://doi.org/10.1523/JNEUROSCI.1069-16.2016

Hinton, V. J., Brown, W. T., Wisniewski, K., & Rudelli, R. D. (1991). Analysis of neocortex in three males with the fragile X syndrome. *American journal of medical genetics*, *41*(3), 289–294. https://doi.org/10.1002/ajmg.1320410306

Hodges, J. L., Yu, X., Gilmore, A., Bennett, H., Tjia, M., Perna, J. F., Chen, C. C., Li, X., Lu, J., & Zuo, Y. (2017). Astrocytic Contributions to Synaptic and Learning Abnormalities in a Mouse Model of Fragile X Syndrome. *Biological psychiatry*, *82*(2), 139–149. https://doi.org/10.1016/j.biopsych.2016.08.036

Irwin, S. A., Idupulapati, M., Gilbert, M. E., Harris, J. B., Chakravarti, A. B., Rogers, E. J., Crisostomo, R. A., Larsen, B. P., Mehta, A., Alcantara, C. J., Patel, B., Swain, R. A., Weiler, I. J., Oostra, B. A., & Greenough, W. T. (2002). Dendritic spine and dendritic field characteristics of layer V pyramidal neurons in the visual cortex of fragile-X knockout mice. *American journal of medical genetics*, *111*(2), 140–146. https://doi.org/10.1002/ajmg.10500

Irwin, S. A., Patel, B., Idupulapati, M., Harris, J. B., Crisostomo, R. A., Larsen, B. P., Kooy, F., Willems, P. J., Cras, P., Kozlowski, P. B., Swain, R. A., Weiler, I. J., & Greenough, W. T. (2001). Abnormal dendritic spine characteristics in the temporal and visual cortices of patients with fragile-X syndrome: a quantitative examination. *American journal of medical genetics*, *98*(2), 161–167. https://doi.org/10.1002/1096-8628(20010115)98:2<161::aid-ajmg1025>3.0.co;2-b

Jacobs, S., & Doering, L. C. (2010). Astrocytes prevent abnormal neuronal development in the fragile x mouse. *The Journal of neuroscience : the official journal of the Society for Neuroscience*, *30*(12), 4508–4514. https://doi.org/10.1523/JNEUROSCI.5027-09.2010

Jacquemont, S., Curie, A., des Portes, V., Torrioli, M. G., Berry-Kravis, E., Hagerman, R. J., Ramos, F. J., Cornish, K., He, Y., Paulding, C., Neri, G., Chen, F., Hadjikhani, N., Martinet, D., Meyer, J., Beckmann, J. S., Delange, K., Brun, A., Bussy, G., Gasparini, F., … Gomez-Mancilla, B. (2011). Epigenetic modification of the FMR1 gene in fragile X syndrome is associated with differential response to the mGluR5 antagonist AFQ056. *Science translational medicine*, *3*(64), 64ra1. https://doi.org/10.1126/scitranslmed.3001708

Johnson, M. A., Weick, J. P., Pearce, R. A., & Zhang, S. C. (2007). Functional neural development from human embryonic stem cells: accelerated synaptic activity via astrocyte coculture. *The Journal of*

neuroscience : the official journal of the Society for Neuroscience, *27*(12), 3069–3077. https://doi.org/10.1523/JNEUROSCI.4562-06.2007

Kadala, A., Verdier, D., Morquette, P., & Kolta, A. (2015). Ion Homeostasis in Rhythmogenesis: The Interplay Between Neurons and Astroglia. *Physiology (Bethesda, Md.)*, *30*(5), 371–388. https://doi.org/10.1152/physiol.00023.2014

Kalmbach, B. E., Johnston, D., & Brager, D. H. (2015). Cell-Type Specific Channelopathies in the Prefrontal Cortex of the fmr1-/y Mouse Model of Fragile X Syndrome. *eNeuro*, *2*(6), ENEURO.0114-15.2015. https://doi.org/10.1523/ENEURO.0114-15.2015

Keene, S. D., Greco, T. M., Parastatidis, I., Lee, S. H., Hughes, E. G., Balice-Gordon, R. J., Speicher, D. W., & Ischiropoulos, H. (2009). Mass spectrometric and computational analysis of cytokine-induced alterations in the astrocyte secretome. *Proteomics*, *9*(3), 768–782. https://doi.org/10.1002/pmic.200800385

Kettenmann, H., & Verkhratsky, A. (2008). Neuroglia: the 150 years after. *Trends in neurosciences*, *31*(12), 653–659. https://doi.org/10.1016/j.tins.2008.09.003

Kettenmann, H., Hanisch, U. K., Noda, M., & Verkhratsky, A. (2011). Physiology of microglia. *Physiological reviews*, *91*(2), 461–553. https://doi.org/10.1152/physrev.00011.2010

Khakh B. S. (2019). Astrocyte-Neuron Interactions in the Striatum: Insights on Identity, Form, and Function. *Trends in neurosciences*, *42*(9), 617–630. https://doi.org/10.1016/j.tins.2019.06.003

Kirwan, P., Turner-Bridger, B., Peter, M., Momoh, A., Arambepola, D., Robinson, H. P., & Livesey, F. J. (2015). Development and function of human cerebral cortex neural networks from pluripotent stem cells in vitro. *Development (Cambridge, England)*, *142*(18), 3178–3187. https://doi.org/10.1242/dev.123851

Kispersky, T. J., Caplan, J. S., & Marder, E. (2012). Increase in sodium conductance decreases firing rate and gain in model neurons. *The Journal of neuroscience : the official journal of the Society for Neuroscience*, *32*(32), 10995–11004. https://doi.org/10.1523/JNEUROSCI.2045-12.2012

Kiss T. (2008). Persistent Na-channels: origin and function. A review. *Acta biologica Hungarica*, *59 Suppl*, 1–12. https://doi.org/10.1556/ABiol.59.2008.Suppl.1

Kligman, D., & Marshak, D. R. (1985). Purification and characterization of a neurite extension factor from bovine brain. *Proceedings of the National Academy of Sciences of the United States of America*, *82*(20), 7136–7139. https://doi.org/10.1073/pnas.82.20.7136

Kogan, C. S., Bertone, A., Cornish, K., Boutet, I., Der Kaloustian, V. M., Andermann, E., Faubert, J., & Chaudhuri, A. (2004). Integrative cortical dysfunction and pervasive motion perception deficit in fragile X syndrome. *Neurology*, *63*(9), 1634–1639. https://doi.org/10.1212/01.wnl.0000142987.44035.3b

Kögel, D., Peters, M., König, H. G., Hashemi, S. M., Bui, N. T., Arolt, V., Rothermundt, M., & Prehn, J. H. (2004). S100B potently activates p65/c-Rel transcriptional complexes in hippocampal neurons: Clinical implications for the role of S100B in excitotoxic brain injury. *Neuroscience*, *127*(4), 913–920. https://doi.org/10.1016/j.neuroscience.2004.06.013

Krasovska, V., & Doering, L. C. (2018). Regulation of IL-6 Secretion by Astrocytes via TLR4 in the Fragile X Mouse Model. *Frontiers in molecular neuroscience*, *11*, 272. https://doi.org/10.3389/fnmol.2018.00272

Krencik, R., Weick, J. P., Liu, Y., Zhang, Z. J., & Zhang, S. C. (2011). Specification of transplantable astroglial subtypes from human pluripotent stem cells. *Nature biotechnology*, *29*(6), 528–534. https://doi.org/10.1038/nbt.1877

Krueger, D. D., Osterweil, E. K., Chen, S. P., Tye, L. D., & Bear, M. F. (2011). Cognitive dysfunction and prefrontal synaptic abnormalities in a mouse model of fragile X syndrome. *Proceedings of the National Academy of Sciences of the United States of America*, *108*(6), 2587–2592. https://doi.org/10.1073/pnas.1013855108

Lafon-Cazal, M., Adjali, O., Galéotti, N., Poncet, J., Jouin, P., Homburger, V., Bockaert, J., & Marin, P. (2003). Proteomic analysis of astrocytic secretion in the mouse. Comparison with the cerebrospinal fluid proteome. *The Journal of biological chemistry*, *278*(27), 24438–24448. https://doi.org/10.1074/jbc.M211980200

Lázaro, M. T., & Golshani, P. (2015). The utility of rodent models of autism spectrum disorders. *Current opinion in neurology*, *28*(2), 103–109. https://doi.org/10.1097/WCO.0000000000000183

Lee, F., Lai, T., Su, P., & Liu, F. (2019). Altered cortical Cytoarchitecture in the Fmr1 knockout mouse. *Molecular brain*, *12*(1), 56. https://doi.org/10.1186/s13041-019-0478-8

Lee, S. C., Liu, W., Dickson, D. W., Brosnan, C. F., & Berman, J. W. (1993). Cytokine production by human fetal microglia and astrocytes. Differential induction by lipopolysaccharide and IL-1 beta. *Journal of immunology (Baltimore, Md. : 1950)*, *150*(7), 2659–2667.

Li, M., Shin, J., Risgaard, R. D., Parries, M. J., Wang, J., Chasman, D., Liu, S., Roy, S., Bhattacharyya, A., & Zhao, X. (2020). Identification of FMR1-regulated molecular networks in human neurodevelopment. *Genome research*, *30*(3), 361–374. https://doi.org/10.1101/gr.251405.119

Ligsay, A., & Hagerman, R. J. (2016). Review of targeted treatments in fragile X syndrome. *Intractable & rare diseases research*, *5*(3), 158–167. https://doi.org/10.5582/irdr.2016.01045

Ligsay, A., Van Dijck, A., Nguyen, D. V., Lozano, R., Chen, Y., Bickel, E. S., Hessl, D., Schneider, A., Angkustsiri, K., Tassone, F., Ceulemans, B., Kooy, R. F., & Hagerman, R. J. (2017). A randomized double-blind, placebo-controlled trial of ganaxolone in children and adolescents with fragile X syndrome. *Journal of neurodevelopmental disorders*, *9*(1), 26. https://doi.org/10.1186/s11689-017-9207-8

Lines, J., Martin, E. D., Kofuji, P., Aguilar, J., & Araque, A. (2020). Astrocytes modulate sensory-evoked neuronal network activity. *Nature communications*, *11*(1), 3689. https://doi.org/10.1038/s41467-020-17536-3

Lines, J., Martin, E. D., Kofuji, P., Aguilar, J., & Araque, A. (2020). Astrocytes modulate sensory-evoked neuronal network activity. *Nature communications*, *11*(1), 3689. https://doi.org/10.1038/s41467-020-17536-3

Liu, T., Hospadaruk, L., Zhu, D. C., & Gardner, J. L. (2011). Feature-specific attentional priority signals in human cortex. *The Journal of neuroscience : the official journal of the Society for Neuroscience*, *31*(12), 4484–4495. https://doi.org/10.1523/JNEUROSCI.5745-10.2011

Livesey, M. R., Bilican, B., Qiu, J., Rzechorzek, N. M., Haghi, G., Burr, K., Hardingham, G. E., Chandran, S., & Wyllie, D. J. (2014). Maturation of AMPAR composition and the GABAAR reversal potential in hPSC-

derived cortical neurons. *The Journal of neuroscience : the official journal of the Society for Neuroscience*, *34*(11), 4070–4075. https://doi.org/10.1523/JNEUROSCI.5410-13.2014

Lubs H. A. (1969). A marker X chromosome. *American journal of human genetics*, *21*(3), 231–244.

MacVicar, B. A., & Newman, E. A. (2015). Astrocyte regulation of blood flow in the brain. *Cold Spring Harbor perspectives in biology*, *7*(5), a020388. https://doi.org/10.1101/cshperspect.a020388

Magistretti, J., & Alonso, A. (2002). Fine gating properties of channels responsible for persistent sodium current generation in entorhinal cortex neurons. *The Journal of general physiology*, *120*(6), 855–873. https://doi.org/10.1085/jgp.20028676

Magistretti, P. J., & Allaman, I. (2018). Lactate in the brain: from metabolic end-product to signalling molecule. *Nature reviews. Neuroscience*, *19*(4), 235–249. https://doi.org/10.1038/nrn.2018.19

Maroof, A. M., Keros, S., Tyson, J. A., Ying, S. W., Ganat, Y. M., Merkle, F. T., Liu, B., Goulburn, A., Stanley, E. G., Elefanty, A. G., Widmer, H. R., Eggan, K., Goldstein, P. A., Anderson, S. A., & Studer, L. (2013). Directed differentiation and functional maturation of cortical interneurons from human embryonic stem cells. *Cell stem cell*, *12*(5), 559–572. https://doi.org/10.1016/j.stem.2013.04.008

Martin G. R. (1981). Isolation of a pluripotent cell line from early mouse embryos cultured in medium conditioned by teratocarcinoma stem cells. *Proceedings of the National Academy of Sciences of the United States of America*, *78*(12), 7634–7638. https://doi.org/10.1073/pnas.78.12.7634

Martin, J. P., & Bell, J. (1943). A PEDIGREE OF MENTAL DEFECT SHOWING SEX-LINKAGE. *Journal of neurology and psychiatry*, *6*(3-4), 154–157. https://doi.org/10.1136/jnnp.6.3-4.154

Matsumura, H., Shiba, T., Inoue, T., Harada, S., & Kai, Y. (1998). A novel mode of target recognition suggested by the 2.0 A structure of holo S100B from bovine brain. *Structure (London, England : 1993)*, *6*(2), 233–241. https://doi.org/10.1016/s0969-2126(98)00024-0

McBride, S. M., Bell, A. J., & Jongens, T. A. (2012). Behavior in a Drosophila model of fragile X. *Results and problems in cell differentiation*, *54*, 83–117. https://doi.org/10.1007/978-3-642-21649-7_6

McCaughey-Chapman, A., & Connor, B. (2018). Human Cortical Neuron Generation Using Cell Reprogramming: A Review of Recent Advances. *Stem cells and development*, *27*(24), 1674–1692. https://doi.org/10.1089/scd.2018.0122

McKinney, B. C., Grossman, A. W., Elisseou, N. M., & Greenough, W. T. (2005). Dendritic spine abnormalities in the occipital cortex of C57BL/6 Fmr1 knockout mice. *American journal of medical genetics. Part B, Neuropsychiatric genetics : the official publication of the International Society of Psychiatric Genetics*, *136B*(1), 98–102. https://doi.org/10.1002/ajmg.b.30183

McLaren, J., & Bryson, S. E. (1987). Review of recent epidemiological studies of mental retardation: prevalence, associated disorders, and etiology. *American journal of mental retardation : AJMR*, *92*(3), 243–254.

Menendez, L., Yatskievych, T. A., Antin, P. B., & Dalton, S. (2011). Wnt signaling and a Smad pathway blockade direct the differentiation of human pluripotent stem cells to multipotent neural crest

cells. *Proceedings of the National Academy of Sciences of the United States of America*, *108*(48), 19240–19245. https://doi.org/10.1073/pnas.1113746108

Mica, Y., Lee, G., Chambers, S. M., Tomishima, M. J., & Studer, L. (2013). Modeling neural crest induction, melanocyte specification, and disease-related pigmentation defects in hESCs and patient-specific iPSCs. *Cell reports*, *3*(4), 1140–1152. https://doi.org/10.1016/j.celrep.2013.03.025

Michinaga, S., & Koyama, Y. (2019). Dual Roles of Astrocyte-Derived Factors in Regulation of Blood-Brain Barrier Function after Brain Damage. *International journal of molecular sciences*, *20*(3), 571. https://doi.org/10.3390/ijms20030571

Miles J. H. (2011). Autism spectrum disorders--a genetics review. *Genetics in medicine : official journal of the American College of Medical Genetics*, *13*(4), 278–294. https://doi.org/10.1097/GIM.0b013e3181ff67ba

Mizuno, G. O., Wang, Y., Shi, G., Wang, Y., Sun, J., Papadopoulos, S., Broussard, G. J., Unger, E. K., Deng, W., Weick, J., Bhattacharyya, A., Chen, C. Y., Yu, G., Looger, L. L., & Tian, L. (2018). Aberrant Calcium Signaling in Astrocytes Inhibits Neuronal Excitability in a Human Down Syndrome Stem Cell Model. *Cell reports*, *24*(2), 355–365. https://doi.org/10.1016/j.celrep.2018.06.033

Molyneaux, B. J., Arlotta, P., Menezes, J. R., & Macklis, J. D. (2007). Neuronal subtype specification in the cerebral cortex. *Nature reviews. Neuroscience*, *8*(6), 427–437. https://doi.org/10.1038/nrn2151

Mongiat, L. A., Espósito, M. S., Lombardi, G., & Schinder, A. F. (2009). Reliable activation of immature neurons in the adult hippocampus. *PloS one*, *4*(4), e5320. https://doi.org/10.1371/journal.pone.0005320

Moody, W. J., & Bosma, M. M. (2005). Ion channel development, spontaneous activity, and activity-dependent development in nerve and muscle cells. *Physiological reviews*, *85*(3), 883–941. https://doi.org/10.1152/physrev.00017.2004

Moore, N. H., Costa, L. G., Shaffer, S. A., Goodlett, D. R., & Guizzetti, M. (2009). Shotgun proteomics implicates extracellular matrix proteins and protease systems in neuronal development induced by astrocyte cholinergic stimulation. *Journal of neurochemistry*, *108*(4), 891–908. https://doi.org/10.1111/j.1471-4159.2008.05836.x

Morquette, P., Verdier, D., Kadala, A., Féthière, J., Philippe, A. G., Robitaille, R., & Kolta, A. (2015). An astrocyte-dependent mechanism for neuronal rhythmogenesis. *Nature neuroscience*, *18*(6), 844–854. https://doi.org/10.1038/nn.4013

Mor-Shaked, H., & Eiges, R. (2018). Reevaluation of *FMR1* Hypermethylation Timing in Fragile X Syndrome. *Frontiers in molecular neuroscience*, *11*, 31. https://doi.org/10.3389/fnmol.2018.00031

Moustakas, A., Souchelnytskyi, S., & Heldin, C. H. (2001). Smad regulation in TGF-beta signal transduction. *Journal of cell science*, *114*(Pt 24), 4359–4369.

Nägler, K., Mauch, D. H., & Pfrieger, F. W. (2001). Glia-derived signals induce synapse formation in neurones of the rat central nervous system. *The Journal of physiology*, *533*(Pt 3), 665–679. https://doi.org/10.1111/j.1469-7793.2001.00665.x

Navarrete, M., & Araque, A. (2014). The Cajal school and the physiological role of astrocytes: a way of thinking. *Frontiers in neuroanatomy*, *8*, 33. https://doi.org/10.3389/fnana.2014.00033

Nedergaard, M., Ransom, B., & Goldman, S. A. (2003). New roles for astrocytes: redefining the functional architecture of the brain. *Trends in neurosciences*, *26*(10), 523–530. https://doi.org/10.1016/j.tins.2003.08.008

Neves-Pereira, M., Müller, B., Massie, D., Williams, J. H., O'Brien, P. C., Hughes, A., Shen, S. B., Clair, D. S., & Miedzybrodzka, Z. (2009). Deregulation of EIF4E: a novel mechanism for autism. *Journal of medical genetics*, *46*(11), 759–765. https://doi.org/10.1136/jmg.2009.066852

Niedringhaus, M., Dumitru, R., Mabb, A. M., Wang, Y., Philpot, B. D., Allbritton, N. L., & Taylor, A. M. (2015). Transferable neuronal mini-cultures to accelerate screening in primary and induced pluripotent stem cell-derived neurons. *Scientific reports*, *5*, 8353. https://doi.org/10.1038/srep08353

Nishiyama, H., Knopfel, T., Endo, S., & Itohara, S. (2002). Glial protein S100B modulates long-term neuronal synaptic plasticity. *Proceedings of the National Academy of Sciences of the United States of America*, *99*(6), 4037–4042. https://doi.org/10.1073/pnas.052020999

Nussbaum, R. L., & Ledbetter, D. H. (1986). Fragile X syndrome: a unique mutation in man. *Annual review of genetics*, *20*, 109–145. https://doi.org/10.1146/annurev.ge.20.120186.000545

Oberheim, N. A., Takano, T., Han, X., He, W., Lin, J. H., Wang, F., Xu, Q., Wyatt, J. D., Pilcher, W., Ojemann, J. G., Ransom, B. R., Goldman, S. A., & Nedergaard, M. (2009). Uniquely hominid features of adult human astrocytes. *The Journal of neuroscience : the official journal of the Society for Neuroscience*, *29*(10), 3276–3287. https://doi.org/10.1523/JNEUROSCI.4707-08.2009

Oberman, L., Ifert-Miller, F., Najib, U., Bashir, S., Woollacott, I., Gonzalez-Heydrich, J., Picker, J., Rotenberg, A., & Pascual-Leone, A. (2010). Transcranial magnetic stimulation provides means to assess cortical plasticity and excitability in humans with fragile x syndrome and autism spectrum disorder. *Frontiers in synaptic neuroscience*, *2*, 26. https://doi.org/10.3389/fnsyn.2010.00026

Odawara, A., Katoh, H., Matsuda, N., & Suzuki, I. (2016). Physiological maturation and drug responses of human induced pluripotent stem cell-derived cortical neuronal networks in long-term culture. *Scientific reports*, *6*, 26181. https://doi.org/10.1038/srep26181

Odawara, A., Saitoh, Y., Alhebshi, A. H., Gotoh, M., & Suzuki, I. (2014). Long-term electrophysiological activity and pharmacological response of a human induced pluripotent stem cell-derived neuron and astrocyte co-culture. *Biochemical and biophysical research communications*, *443*(4), 1176–1181. https://doi.org/10.1016/j.bbrc.2013.12.142

O'Donovan M. J. (1999). The origin of spontaneous activity in developing networks of the vertebrate nervous system. *Current opinion in neurobiology*, *9*(1), 94–104. https://doi.org/10.1016/s0959-4388(99)80012-9

Olmos-Serrano, J. L., Paluszkiewicz, S. M., Martin, B. S., Kaufmann, W. E., Corbin, J. G., & Huntsman, M. M. (2010). Defective GABAergic neurotransmission and pharmacological rescue of neuronal hyperexcitability in the amygdala in a mouse model of fragile X syndrome. *The Journal of neuroscience :*

the official journal of the Society for Neuroscience, *30*(29), 9929–9938. https://doi.org/10.1523/JNEUROSCI.1714-10.2010

Omole, A. E., & Fakoya, A. (2018). Ten years of progress and promise of induced pluripotent stem cells: historical origins, characteristics, mechanisms, limitations, and potential applications. *PeerJ*, *6*, e4370. https://doi.org/10.7717/peerj.4370

Osumi, N., Shinohara, H., Numayama-Tsuruta, K., & Maekawa, M. (2008). Concise review: Pax6 transcription factor contributes to both embryonic and adult neurogenesis as a multifunctional regulator. *Stem cells (Dayton, Ohio)*, *26*(7), 1663–1672. https://doi.org/10.1634/stemcells.2007-0884

Paavilainen, T., Pelkonen, A., Mäkinen, M. E., Peltola, M., Huhtala, H., Fayuk, D., & Narkilahti, S. (2018). Effect of prolonged differentiation on functional maturation of human pluripotent stem cell-derived neuronal cultures. *Stem cell research*, *27*, 151–161. https://doi.org/10.1016/j.scr.2018.01.018

Pacey, L. K., & Doering, L. C. (2007). Developmental expression of FMRP in the astrocyte lineage: implications for fragile X syndrome. *Glia*, *55*(15), 1601–1609. https://doi.org/10.1002/glia.20573

Pacey, L. K., Guan, S., Tharmalingam, S., Thomsen, C., & Hampson, D. R. (2015). Persistent astrocyte activation in the fragile X mouse cerebellum. *Brain and behavior*, *5*(10), e00400. https://doi.org/10.1002/brb3.400

Pacey, L. K., Guan, S., Tharmalingam, S., Thomsen, C., & Hampson, D. R. (2015). Persistent astrocyte activation in the fragile X mouse cerebellum. *Brain and behavior*, *5*(10), e00400. https://doi.org/10.1002/brb3.400

Paluszkiewicz, S. M., Martin, B. S., & Huntsman, M. M. (2011). Fragile X syndrome: the GABAergic system and circuit dysfunction. *Developmental neuroscience*, *33*(5), 349–364. https://doi.org/10.1159/000329420

Pankratz, M. T., Li, X. J., Lavaute, T. M., Lyons, E. A., Chen, X., & Zhang, S. C. (2007). Directed neural differentiation of human embryonic stem cells via an obligated primitive anterior stage. *Stem cells (Dayton, Ohio)*, *25*(6), 1511–1520. https://doi.org/10.1634/stemcells.2006-0707

Parri, H. R., & Crunelli, V. (1998). Sodium current in rat and cat thalamocortical neurons: role of a non-inactivating component in tonic and burst firing. *The Journal of neuroscience : the official journal of the Society for Neuroscience*, *18*(3), 854–867. https://doi.org/10.1523/JNEUROSCI.18-03-00854.1998

Penrose, L. S. (1938). A Clinical and Genetic Study of 1280 Cases of Mental Defect. *Nature*, *141*(3570), 575–576.

Perea, G., & Araque, A. (2005). Properties of synaptically evoked astrocyte calcium signal reveal synaptic information processing by astrocytes. *The Journal of neuroscience : the official journal of the Society for Neuroscience*, *25*(9), 2192–2203. https://doi.org/10.1523/JNEUROSCI.3965-04.2005

Perea, G., Navarrete, M., & Araque, A. (2009). Tripartite synapses: astrocytes process and control synaptic information. *Trends in neurosciences*, *32*(8), 421–431. https://doi.org/10.1016/j.tins.2009.05.001

Pfeiffer, B. E., & Huber, K. M. (2007). Fragile X mental retardation protein induces synapse loss through acute postsynaptic translational regulation. *The Journal of neuroscience : the official journal of the Society for Neuroscience*, *27*(12), 3120–3130. https://doi.org/10.1523/JNEUROSCI.0054-07.2007

Pfrieger, F. W., & Barres, B. A. (1997). Synaptic efficacy enhanced by glial cells in vitro. *Science (New York, N.Y.)*, *277*(5332), 1684–1687. https://doi.org/10.1126/science.277.5332.1684

Pilpel, Y., Kolleker, A., Berberich, S., Ginger, M., Frick, A., Mientjes, E., Oostra, B. A., & Seeburg, P. H. (2009). Synaptic ionotropic glutamate receptors and plasticity are developmentally altered in the CA1 field of Fmr1 knockout mice. *The Journal of physiology*, *587*(Pt 4), 787–804. https://doi.org/10.1113/jphysiol.2008.160929

Qi, Y., Zhang, X. J., Renier, N., Wu, Z., Atkin, T., Sun, Z., Ozair, M. Z., Tchieu, J., Zimmer, B., Fattahi, F., Ganat, Y., Azevedo, R., Zeltner, N., Brivanlou, A. H., Karayiorgou, M., Gogos, J., Tomishima, M., Tessier-Lavigne, M., Shi, S. H., & Studer, L. (2017). Combined small-molecule inhibition accelerates the derivation of functional cortical neurons from human pluripotent stem cells. *Nature biotechnology*, *35*(2), 154–163. https://doi.org/10.1038/nbt.3777

Quiroz, J. A., Tamburri, P., Deptula, D., Banken, L., Beyer, U., Rabbia, M., Parkar, N., Fontoura, P., & Santarelli, L. (2016). Efficacy and Safety of Basimglurant as Adjunctive Therapy for Major Depression: A Randomized Clinical Trial. *JAMA psychiatry*, *73*(7), 675–684. https://doi.org/10.1001/jamapsychiatry.2016.0838

Raponi, E., Agenes, F., Delphin, C., Assard, N., Baudier, J., Legraverend, C., & Deloulme, J. C. (2007). S100B expression defines a state in which GFAP-expressing cells lose their neural stem cell potential and acquire a more mature developmental stage. *Glia*, *55*(2), 165–177. https://doi.org/10.1002/glia.20445

Raponi, E., Agenes, F., Delphin, C., Assard, N., Baudier, J., Legraverend, C., & Deloulme, J. C. (2007). S100B expression defines a state in which GFAP-expressing cells lose their neural stem cell potential and acquire a more mature developmental stage. *Glia*, *55*(2), 165–177. https://doi.org/10.1002/glia.20445

Rothermundt, M., Peters, M., Prehn, J. H., & Arolt, V. (2003). S100B in brain damage and neurodegeneration. *Microscopy research and technique*, *60*(6), 614–632. https://doi.org/10.1002/jemt.10303

Rothstein, J. D., Martin, L., Levey, A. I., Dykes-Hoberg, M., Jin, L., Wu, D., Nash, N., & Kuncl, R. W. (1994). Localization of neuronal and glial glutamate transporters. *Neuron*, *13*(3), 713–725. https://doi.org/10.1016/0896-6273(94)90038-8

Routh, B. N., Rathour, R. K., Baumgardner, M. E., Kalmbach, B. E., Johnston, D., & Brager, D. H. (2017). Increased transient Na^+ conductance and action potential output in layer 2/3 prefrontal cortex neurons of the $fmr1^{-/y}$ mouse. *The Journal of physiology*, *595*(13), 4431–4448. https://doi.org/10.1113/JP274258

Sakatani, S., Seto-Ohshima, A., Shinohara, Y., Yamamoto, Y., Yamamoto, H., Itohara, S., & Hirase, H. (2008). Neural-activity-dependent release of S100B from astrocytes enhances kainate-induced gamma oscillations in vivo. *The Journal of neuroscience : the official journal of the Society for Neuroscience*, *28*(43), 10928–10936. https://doi.org/10.1523/JNEUROSCI.3693-08.2008

Schäfer, B. W., & Heizmann, C. W. (1996). The S100 family of EF-hand calcium-binding proteins: functions and pathology. *Trends in biochemical sciences*, *21*(4), 134–140. https://doi.org/10.1016/s0968-0004(96)80167-8

Selinfreund, R. H., Barger, S. W., Pledger, W. J., & Van Eldik, L. J. (1991). Neurotrophic protein S100 beta stimulates glial cell proliferation. *Proceedings of the National Academy of Sciences of the United States of America*, *88*(9), 3554–3558. https://doi.org/10.1073/pnas.88.9.3554

Shashoua, V. E., Hesse, G. W., & Moore, B. W. (1984). Proteins of the brain extracellular fluid: evidence for release of S-100 protein. *Journal of neurochemistry*, *42*(6), 1536–1541. https://doi.org/10.1111/j.1471-4159.1984.tb12739.x

Sheridan, S. D., Theriault, K. M., Reis, S. A., Zhou, F., Madison, J. M., Daheron, L., Loring, J. F., & Haggarty, S. J. (2011). Epigenetic characterization of the FMR1 gene and aberrant neurodevelopment in human induced pluripotent stem cell models of fragile X syndrome. *PloS one*, *6*(10), e26203. https://doi.org/10.1371/journal.pone.0026203

Silva, L. R., Amitai, Y., & Connors, B. W. (1991). Intrinsic oscillations of neocortex generated by layer 5 pyramidal neurons. *Science (New York, N.Y.)*, *251*(4992), 432–435. https://doi.org/10.1126/science.1824881

Simpson, J. E., Ince, P. G., Lace, G., Forster, G., Shaw, P. J., Matthews, F., Savva, G., Brayne, C., Wharton, S. B., & MRC Cognitive Function and Ageing Neuropathology Study Group (2010). Astrocyte phenotype in relation to Alzheimer-type pathology in the ageing brain. *Neurobiology of aging*, *31*(4), 578–590. https://doi.org/10.1016/j.neurobiolaging.2008.05.015

Siomi, H., Siomi, M. C., Nussbaum, R. L., & Dreyfuss, G. (1993). The protein product of the fragile X gene, FMR1, has characteristics of an RNA-binding protein. *Cell*, *74*(2), 291–298. https://doi.org/10.1016/0092-8674(93)90420-u

Smith, W. C., & Harland, R. M. (1992). Expression cloning of noggin, a new dorsalizing factor localized to the Spemann organizer in Xenopus embryos. *Cell*, *70*(5), 829–840. https://doi.org/10.1016/0092-8674(92)90316-5

Smith, W. C., Knecht, A. K., Wu, M., & Harland, R. M. (1993). Secreted noggin protein mimics the Spemann organizer in dorsalizing Xenopus mesoderm. *Nature*, *361*(6412), 547–549. https://doi.org/10.1038/361547a0

Sofroniew, M. V., & Vinters, H. V. (2010). Astrocytes: biology and pathology. *Acta neuropathologica*, *119*(1), 7–35. https://doi.org/10.1007/s00401-009-0619-8

Sontheimer, H., Black, J. A., Ransom, B. R., & Waxman, S. G. (1992). Ion channels in spinal cord astrocytes in vitro. I. Transient expression of high levels of Na+ and K+ channels. *Journal of neurophysiology*, *68*(4), 985–1000. https://doi.org/10.1152/jn.1992.68.4.985

Sorci, G., Bianchi, R., Riuzzi, F., Tubaro, C., Arcuri, C., Giambanco, I., & Donato, R. (2010). S100B Protein, A Damage-Associated Molecular Pattern Protein in the Brain and Heart, and Beyond. *Cardiovascular psychiatry and neurology*, *2010*, 656481. https://doi.org/10.1155/2010/656481

Sorci, G., Riuzzi, F., Agneletti, A. L., Marchetti, C., & Donato, R. (2004). S100B causes apoptosis in a myoblast cell line in a RAGE-independent manner. *Journal of cellular physiology*, *199*(2), 274–283. https://doi.org/10.1002/jcp.10462

Sourial, M., & Doering, L. C. (2016). Astrocyte-Secreted Factors Selectively Alter Neural Stem and Progenitor Cell Proliferation in the Fragile X Mouse. *Frontiers in cellular neuroscience*, *10*, 126. https://doi.org/10.3389/fncel.2016.00126

Stefani, G., Fraser, C. E., Darnell, J. C., & Darnell, R. B. (2004). Fragile X mental retardation protein is associated with translating polyribosomes in neuronal cells. *The Journal of neuroscience : the official journal of the Society for Neuroscience*, *24*(33), 7272–7276. https://doi.org/10.1523/JNEUROSCI.2306-04.2004

Stevenson, R. E., Massey, P. S., Schroer, R. J., McDermott, S., & Richter, B. (1996). Preventable fraction of mental retardation: analysis based on individuals with severe mental retardation. *Mental retardation*, *34*(3), 182–188.

Strumbos, J. G., Brown, M. R., Kronengold, J., Polley, D. B., & Kaczmarek, L. K. (2010). Fragile X mental retardation protein is required for rapid experience-dependent regulation of the potassium channel Kv3.1b. *The Journal of neuroscience : the official journal of the Society for Neuroscience*, *30*(31), 10263–10271. https://doi.org/10.1523/JNEUROSCI.1125-10.2010

Su, H., Alroy, G., Kirson, E. D., & Yaari, Y. (2001). Extracellular calcium modulates persistent sodium current-dependent burst-firing in hippocampal pyramidal neurons. *The Journal of neuroscience : the official journal of the Society for Neuroscience*, *21*(12), 4173–4182. https://doi.org/10.1523/JNEUROSCI.21-12-04173.2001

Su, H., Alroy, G., Kirson, E. D., & Yaari, Y. (2001). Extracellular calcium modulates persistent sodium current-dependent burst-firing in hippocampal pyramidal neurons. *The Journal of neuroscience : the official journal of the Society for Neuroscience*, *21*(12), 4173–4182. https://doi.org/10.1523/JNEUROSCI.21-12-04173.2001

Sutherland, G. R., Gedeon, A., Kornman, L., Donnelly, A., Byard, R. W., Mulley, J. C., Kremer, E., Lynch, M., Pritchard, M., & Yu, S. (1991). Prenatal diagnosis of fragile X syndrome by direct detection of the unstable DNA sequence. *The New England journal of medicine*, *325*(24), 1720–1722. https://doi.org/10.1056/NEJM199112123252407

Suvrathan, A., Hoeffer, C. A., Wong, H., Klann, E., & Chattarji, S. (2010). Characterization and reversal of synaptic defects in the amygdala in a mouse model of fragile X syndrome. *Proceedings of the National Academy of Sciences of the United States of America*, *107*(25), 11591–11596. https://doi.org/10.1073/pnas.1002262107

Takahashi, K., & Yamanaka, S. (2006). Induction of pluripotent stem cells from mouse embryonic and adult fibroblast cultures by defined factors. *Cell*, *126*(4), 663–676. https://doi.org/10.1016/j.cell.2006.07.024

Takata, N., Mishima, T., Hisatsune, C., Nagai, T., Ebisui, E., Mikoshiba, K., & Hirase, H. (2011). Astrocyte calcium signaling transforms cholinergic modulation to cortical plasticity in vivo. *The Journal of neuroscience : the official journal of the Society for Neuroscience*, *31*(49), 18155–18165. https://doi.org/10.1523/JNEUROSCI.5289-11.2011

Tang, X., Zhou, L., Wagner, A. M., Marchetto, M. C., Muotri, A. R., Gage, F. H., & Chen, G. (2013). Astroglial cells regulate the developmental timeline of human neurons differentiated from induced pluripotent stem cells. *Stem cell research*, *11*(2), 743–757. https://doi.org/10.1016/j.scr.2013.05.002

Tazerart, S., Vinay, L., & Brocard, F. (2008). The persistent sodium current generates pacemaker activities in the central pattern generator for locomotion and regulates the locomotor rhythm. *The Journal of neuroscience : the official journal of the Society for Neuroscience*, *28*(34), 8577–8589. https://doi.org/10.1523/JNEUROSCI.1437-08.2008

Telias, M., Kuznitsov-Yanovsky, L., Segal, M., & Ben-Yosef, D. (2015). Functional Deficiencies in Fragile X Neurons Derived from Human Embryonic Stem Cells. *The Journal of neuroscience : the official journal of the Society for Neuroscience*, *35*(46), 15295–15306. https://doi.org/10.1523/JNEUROSCI.0317-15.2015

Telias, M., Segal, M., & Ben-Yosef, D. (2013). Neural differentiation of Fragile X human Embryonic Stem Cells reveals abnormal patterns of development despite successful neurogenesis. *Developmental biology*, *374*(1), 32–45. https://doi.org/10.1016/j.ydbio.2012.11.031

Testa-Silva, G., Loebel, A., Giugliano, M., de Kock, C. P., Mansvelder, H. D., & Meredith, R. M. (2012). Hyperconnectivity and slow synapses during early development of medial prefrontal cortex in a mouse model for mental retardation and autism. *Cerebral cortex (New York, N.Y. : 1991)*, *22*(6), 1333–1342. https://doi.org/10.1093/cercor/bhr224

Thomson, J. A., Itskovitz-Eldor, J., Shapiro, S. S., Waknitz, M. A., Swiergiel, J. J., Marshall, V. S., & Jones, J. M. (1998). Embryonic stem cell lines derived from human blastocysts. *Science (New York, N.Y.)*, *282*(5391), 1145–1147. https://doi.org/10.1126/science.282.5391.1145

Tian, L. M., Otoom, S., & Alkadhi, K. A. (1995). Endogenous bursting due to altered sodium channel function in rat hippocampal CA1 neurons. *Brain research*, *680*(1-2), 164–172. https://doi.org/10.1016/0006-8993(95)00258-r

Tucker, B., Richards, R., & Lardelli, M. (2004). Expression of three zebrafish orthologs of human FMR1-related genes and their phylogenetic relationships. *Development genes and evolution*, *214*(11), 567–574. https://doi.org/10.1007/s00427-004-0438-9

Tukker, A. M., Wijnolts, F., de Groot, A., & Westerink, R. (2018). Human iPSC-derived neuronal models for in vitro neurotoxicity assessment. *Neurotoxicology*, *67*, 215–225. https://doi.org/10.1016/j.neuro.2018.06.007

Uhlhaas P. J. (2011). High-frequency oscillations in schizophrenia. *Clinical EEG and neuroscience*, *42*(2), 77–82. https://doi.org/10.1177/155005941104200208

Ullian, E. M., Sapperstein, S. K., Christopherson, K. S., & Barres, B. A. (2001). Control of synapse number by glia. *Science (New York, N.Y.)*, *291*(5504), 657–661. https://doi.org/10.1126/science.291.5504.657

Vallier, L., Reynolds, D., & Pedersen, R. A. (2004). Nodal inhibits differentiation of human embryonic stem cells along the neuroectodermal default pathway. *Developmental biology*, *275*(2), 403–421. https://doi.org/10.1016/j.ydbio.2004.08.031

van der Molen, M. J., Stam, C. J., & van der Molen, M. W. (2014). Resting-state EEG oscillatory dynamics in fragile X syndrome: abnormal functional connectivity and brain network organization. *PloS one*, *9*(2), e88451. https://doi.org/10.1371/journal.pone.0088451

van Drongelen, W., Koch, H., Elsen, F. P., Lee, H. C., Mrejeru, A., Doren, E., Marcuccilli, C. J., Hereld, M., Stevens, R. L., & Ramirez, J. M. (2006). Role of persistent sodium current in bursting activity of mouse

neocortical networks in vitro. *Journal of neurophysiology*, *96*(5), 2564–2577. https://doi.org/10.1152/jn.00446.2006

Van Eldik, L. J., & Griffin, W. S. (1994). S100 beta expression in Alzheimer's disease: relation to neuropathology in brain regions. *Biochimica et biophysica acta*, *1223*(3), 398–403. https://doi.org/10.1016/0167-4889(94)90101-5

Van Eldik, L. J., & Wainwright, M. S. (2003). The Janus face of glial-derived S100B: beneficial and detrimental functions in the brain. *Restorative neurology and neuroscience*, *21*(3-4), 97–108.

Van Eldik, L. J., & Zimmer, D. B. (1987). Secretion of S-100 from rat C6 glioma cells. *Brain research*, *436*(2), 367–370. https://doi.org/10.1016/0006-8993(87)91681-7

Vasile, F., Dossi, E., & Rouach, N. (2017). Human astrocytes: structure and functions in the healthy brain. *Brain structure & function*, *222*(5), 2017–2029. https://doi.org/10.1007/s00429-017-1383-5

Vazin, T., & Freed, W. J. (2010). Human embryonic stem cells: derivation, culture, and differentiation: a review. *Restorative neurology and neuroscience*, *28*(4), 589–603. https://doi.org/10.3233/RNN-2010-0543

Verkerk, A. J., Pieretti, M., Sutcliffe, J. S., Fu, Y. H., Kuhl, D. P., Pizzuti, A., Reiner, O., Richards, S., Victoria, M. F., & Zhang, F. P. (1991). Identification of a gene (FMR-1) containing a CGG repeat coincident with a breakpoint cluster region exhibiting length variation in fragile X syndrome. *Cell*, *65*(5), 905–914. https://doi.org/10.1016/0092-8674(91)90397-h

Verkhratsky, A., & Nedergaard, M. (2014). Astroglial cradle in the life of the synapse. *Philosophical transactions of the Royal Society of London. Series B, Biological sciences*, *369*(1654), 20130595. https://doi.org/10.1098/rstb.2013.0595

Verlinsky, Y., Strelchenko, N., Kukharenko, V., Rechitsky, S., Verlinsky, O., Galat, V., & Kuliev, A. (2005). Human embryonic stem cell lines with genetic disorders. *Reproductive biomedicine online*, *10*(1), 105–110. https://doi.org/10.1016/s1472-6483(10)60810-3

Villarreal, A., Aviles Reyes, R. X., Angelo, M. F., Reines, A. G., & Ramos, A. J. (2011). S100B alters neuronal survival and dendrite extension via RAGE-mediated NF-κB signaling. *Journal of neurochemistry*, *117*(2), 321–332. https://doi.org/10.1111/j.1471-4159.2011.07207.x

Viviano, J., Krishnan, A., Wu, H., & Venkataraman, V. (2016). Electrophoretic mobility shift in native gels indicates calcium-dependent structural changes of neuronal calcium sensor proteins. *Analytical biochemistry*, *494*, 93–100. https://doi.org/10.1016/j.ab.2015.11.005

Volterra, A., & Meldolesi, J. (2005). Astrocytes, from brain glue to communication elements: the revolution continues. *Nature reviews. Neuroscience*, *6*(8), 626–640. https://doi.org/10.1038/nrn1722

Wallingford, J., Scott, A. L., Rodrigues, K., & Doering, L. C. (2017). Altered Developmental Expression of the Astrocyte-Secreted Factors Hevin and SPARC in the Fragile X Mouse Model. *Frontiers in molecular neuroscience*, *10*, 268. https://doi.org/10.3389/fnmol.2017.00268

Wang X. J. (1999). Synaptic basis of cortical persistent activity: the importance of NMDA receptors to working memory. *The Journal of neuroscience : the official journal of the Society for Neuroscience*, *19*(21), 9587–9603. https://doi.org/10.1523/JNEUROSCI.19-21-09587.1999

Wang, H., Ku, L., Osterhout, D. J., Li, W., Ahmadian, A., Liang, Z., & Feng, Y. (2004). Developmentally-programmed FMRP expression in oligodendrocytes: a potential role of FMRP in regulating translation in oligodendroglia progenitors. *Human molecular genetics*, *13*(1), 79–89. https://doi.org/10.1093/hmg/ddh009

Wang, L., Wang, Y., Zhou, S., Yang, L., Shi, Q., Li, Y., Zhang, K., Yang, L., Zhao, M., & Yang, Q. (2016). Imbalance between Glutamate and GABA in Fmr1 Knockout Astrocytes Influences Neuronal Development. *Genes*, *7*(8), 45. https://doi.org/10.3390/genes7080045

Wang, X., Lou, N., Xu, Q., Tian, G. F., Peng, W. G., Han, X., Kang, J., Takano, T., & Nedergaard, M. (2006). Astrocytic Ca2+ signaling evoked by sensory stimulation in vivo. *Nature neuroscience*, *9*(6), 816–823. https://doi.org/10.1038/nn1703

Weick, J. P., Liu, Y., & Zhang, S. C. (2011). Human embryonic stem cell-derived neurons adopt and regulate the activity of an established neural network. *Proceedings of the National Academy of Sciences of the United States of America*, *108*(50), 20189–20194. https://doi.org/10.1073/pnas.1108487108

Willemsen, R., Bontekoe, C. J., Severijnen, L. A., & Oostra, B. A. (2002). Timing of the absence of FMR1 expression in full mutation chorionic villi. *Human genetics*, *110*(6), 601–605. https://doi.org/10.1007/s00439-002-0723-5

Williams, S. R., & Stuart, G. J. (1999). Mechanisms and consequences of action potential burst firing in rat neocortical pyramidal neurons. *The Journal of physiology*, *521 Pt 2*(Pt 2), 467–482. https://doi.org/10.1111/j.1469-7793.1999.00467.x

Wilson, S. W., & Houart, C. (2004). Early steps in the development of the forebrain. *Developmental cell*, *6*(2), 167–181. https://doi.org/10.1016/s1534-5807(04)00027-9

Wilson, S. W., & Rubenstein, J. L. (2000). Induction and dorsoventral patterning of the telencephalon. *Neuron*, *28*(3), 641–651. https://doi.org/10.1016/s0896-6273(00)00171-9

Winningham-Major, F., Staecker, J. L., Barger, S. W., Coats, S., & Van Eldik, L. J. (1989). Neurite extension and neuronal survival activities of recombinant S100 beta proteins that differ in the content and position of cysteine residues. *The Journal of cell biology*, *109*(6 Pt 1), 3063–3071. https://doi.org/10.1083/jcb.109.6.3063

Wright, N. T., Inman, K. G., Levine, J. A., Cannon, B. R., Varney, K. M., & Weber, D. J. (2008). Refinement of the solution structure and dynamic properties of Ca(2+)-bound rat S100B. *Journal of biomolecular NMR*, *42*(4), 279–286. https://doi.org/10.1007/s10858-008-9282-y

Wu, S. H., & Oertel, D. (1987). Maturation of synapses and electrical properties of cells in the cochlear nuclei. *Hearing research*, *30*(1), 99–110. https://doi.org/10.1016/0378-5955(87)90187-0

Yan, Q. J., Asafo-Adjei, P. K., Arnold, H. M., Brown, R. E., & Bauchwitz, R. P. (2004). A phenotypic and molecular characterization of the fmr1-tm1Cgr fragile X mouse. *Genes, brain, and behavior*, *3*(6), 337–359. https://doi.org/10.1111/j.1601-183X.2004.00087.x

Yang, Y. H., Nam, M. S., & Yang, E. S. (2005). Rapid prenatal diagnosis of trisomy 21 by real-time quantitative polymerase chain reaction with amplification of small tandem repeats and S100B in chromosome 21. *Yonsei medical journal*, *46*(2), 193–197. https://doi.org/10.3349/ymj.2005.46.2.193

Yap, C. C., & Winckler, B. (2015). Adapting for endocytosis: roles for endocytic sorting adaptors in directing neural development. *Frontiers in cellular neuroscience*, *9*, 119. https://doi.org/10.3389/fncel.2015.00119

Yeh, C. W., Yeh, S. H., Shie, F. S., Lai, W. S., Liu, H. K., Tzeng, T. T., Tsay, H. J., & Shiao, Y. J. (2015). Impaired cognition and cerebral glucose regulation are associated with astrocyte activation in the parenchyma of metabolically stressed APPswe/PS1dE9 mice. *Neurobiology of aging*, *36*(11), 2984–2994. https://doi.org/10.1016/j.neurobiolaging.2015.07.022

You, Y., Borgmann, K., Edara, V. V., Stacy, S., Ghorpade, A., & Ikezu, T. (2019). Activated human astrocyte-derived extracellular vesicles modulate neuronal uptake, differentiation and firing. *Journal of extracellular vesicles*, *9*(1), 1706801. https://doi.org/10.1080/20013078.2019.1706801

Yu, Y., Yuan, Z., Fan, Y., Li, J., & Wu, Y. (2020). Dynamic Transitions in Neuronal Network Firing Sustained by Abnormal Astrocyte Feedback. *Neural plasticity*, *2020*, 8864246. https://doi.org/10.1155/2020/8864246

Zakrzewski, W., Dobrzyński, M., Szymonowicz, M., & Rybak, Z. (2019). Stem cells: past, present, and future. *Stem cell research & therapy*, *10*(1), 68. https://doi.org/10.1186/s13287-019-1165-5

Zalfa, F., Adinolfi, S., Napoli, I., Kühn-Hölsken, E., Urlaub, H., Achsel, T., Pastore, A., & Bagni, C. (2005). Fragile X mental retardation protein (FMRP) binds specifically to the brain cytoplasmic RNAs BC1/BC200 via a novel RNA-binding motif. *The Journal of biological chemistry*, *280*(39), 33403–33410. https://doi.org/10.1074/jbc.M504286200

Zalfa, F., Giorgi, M., Primerano, B., Moro, A., Di Penta, A., Reis, S., Oostra, B., & Bagni, C. (2003). The fragile X syndrome protein FMRP associates with BC1 RNA and regulates the translation of specific mRNAs at synapses. *Cell*, *112*(3), 317–327. https://doi.org/10.1016/s0092-8674(03)00079-5

Zhang, S. C., Wernig, M., Duncan, I. D., Brüstle, O., & Thomson, J. A. (2001). In vitro differentiation of transplantable neural precursors from human embryonic stem cells. *Nature biotechnology*, *19*(12), 1129–1133. https://doi.org/10.1038/nbt1201-1129

Zhang, Y., Bonnan, A., Bony, G., Ferezou, I., Pietropaolo, S., Ginger, M., Sans, N., Rossier, J., Oostra, B., LeMasson, G., & Frick, A. (2014). Dendritic channelopathies contribute to neocortical and sensory hyperexcitability in Fmr1(-/y) mice. *Nature neuroscience*, *17*(12), 1701–1709. https://doi.org/10.1038/nn.3864

Zhang, Y., Brown, M. R., Hyland, C., Chen, Y., Kronengold, J., Fleming, M. R., Kohn, A. B., Moroz, L. L., & Kaczmarek, L. K. (2012). Regulation of neuronal excitability by interaction of fragile X mental retardation protein with slack potassium channels. *The Journal of neuroscience : the official journal of the Society for Neuroscience*, *32*(44), 15318–15327. https://doi.org/10.1523/JNEUROSCI.2162-12.2012

Zhang, Y., Sloan, S. A., Clarke, L. E., Caneda, C., Plaza, C. A., Blumenthal, P. D., Vogel, H., Steinberg, G. K., Edwards, M. S., Li, G., Duncan, J. A., 3rd, Cheshier, S. H., Shuer, L. M., Chang, E. F., Grant, G. A., Gephart, M. G., & Barres, B. A. (2016). Purification and Characterization of Progenitor and Mature Human

Astrocytes Reveals Transcriptional and Functional Differences with Mouse. *Neuron*, *89*(1), 37–53. https://doi.org/10.1016/j.neuron.2015.11.013

Zhang, Z., Marro, S. G., Zhang, Y., Arendt, K. L., Patzke, C., Zhou, B., Fair, T., Yang, N., Südhof, T. C., Wernig, M., & Chen, L. (2018). The fragile X mutation impairs homeostatic plasticity in human neurons by blocking synaptic retinoic acid signaling. *Science translational medicine*, *10*(452), eaar4338. https://doi.org/10.1126/scitranslmed.aar4338

Appendix

Neurons	Astrocytes	Bursting phenotype of neurons
Control (iPSC and ESC)	Control (iPSC and ESC) and iPSC gene corrected FXS2Δ	Control bursting – lesser number of bursts, longer duration
FXS (iPSC and ESC)	FXS (iPSC and ESC)	FXS bursting – more number of bursts, shorter duration
Control	FXS	FXS bursting
FXS	Control (iPSC and ESC) and iPSC gene corrected FXS2Δ	Control bursting

Appendix 1.1 Effect of astrocyte genotype on the neuronal network phenotype

Neurons	ACM	Bursting phenotype of neurons
Control (iPSC and ESC)	Control (iPSC and ESC)	Control bursting – lesser number of bursts, longer duration
FXS (iPSC and ESC)	FXS (iPSC and ESC)	FXS bursting – more number of bursts, shorter duration
Control	FXS	FXS bursting
FXS	Control	Control bursting

Appendix 1.2 Effect of ACM genotype on the neuronal network phenotype